Absence of the dystrophin protein in Duchenne muscular dystrophy: effects on transcriptome, proteome and microRNA secretome



Tirsa Lucia Esther van Westering

Department of Physiology, Anatomy and Genetics

Somerville College, University of Oxford

Thesis submitted for the degree of

Doctor of Philosophy

Michaelmas term 2018

Declaration

The work presented in this thesis was undertaken in Professor Matthew Wood's laboratory at the Department of Physiology, Anatomy and Genetics, University of Oxford, between 2014 and 2018. I, Tirsa van Westering, hereby declare that all work presented is my own with the following exceptions. Synthesis of peptide conjugates in Chapters 3 and 5 was performed by Dr Liz O'Donovan and Dr Andrey Arzumanov, respectively, in the laboratory of Prof Mike Gait at the MRC Laboratory of Molecular Biology, Cambridge. Injection of PPMOs in Chapters 3 and 5 was performed by Dr Corinne Betts at the University of Oxford. The Affymetrix microarrays in Chapter 3 were performed by the Bioinformatics and Expression core facility at the Karolinska Institutet in Stockholm, Sweden. Transcriptomic data mining of the second Affymetrix array in Chapter 3 was performed by Dr Viola Volpato in the laboratory of Dr Caleb Webber at the University of Oxford. Data analysis and interpretation was performed by myself. Animal serum and tissues collected in Chapter 4 were performed by Dr Jun Tanihata in the laboratory of Prof Shin'ichi Takeda at the NCNP, Tokyo, Japan. Mass spectrometry and protein identification in Chapter 4 was performed by Dr Henrik Johansson in the laboratory of Prof Janne Lehtiö at the Karolinska Institutet in Stockholm, Sweden. Western blots for dataset validation and *Mvp* knockdown in H2K-*mdx52* cells in Chapter 4 were performed by Ms Miyako Seto in the laboratory of Prof Yoshitsugu Aoki at the NCNP, Tokyo, Japan, with subsequent (image) processing and analysis performed by myself. Dr Anna Coenen-Stass aided with the extracellular miRNA RT-qPCR in Chapter 4 and aliquoting of serum samples for the FirePlex assay in Chapter 5. Tissue and serum samples from *mdx-Xist*$^{\Delta hs}$ mice in Chapter 5 were collected by Dr Maaike van Putten in the laboratory of Prof Annemieke Aartsma-Rus at the LUMC, Leiden, the Netherlands. The FirePlex miRNA multiplex assays in chapter 5 were performed by Abcam, Cambridge. This work has not been submitted for any other degree at this university or any other institute of learning. This thesis includes text excerpts written by me from my first-author review paper published in 2015 (see Appendix 8.4), with necessary permission obtained where required.

Acknowledgements

Firstly, I would like to thank Professor Matthew Wood for giving me the opportunity to work in his lab, the freedom to pursue my ideas and interests during my DPhil and support during difficult periods. His advice throughout the years have given me a greater understanding of research itself and the scientific community. Secondly, I would like to thank Prof Nicola Smart for her intelligence and compassion, whose expertise helped me in a time when I was less sure. Especially, I am extremely grateful to Dr Corinne Betts and Dr Thomas Roberts. Corinne's technical expertise refined my own technical competence, and it is with her guidance that I learned independence and to pro-actively pursue research avenues of interest. Tom has given considerable support and guidance, without fail. His scientific knowledge, creativity and attention to detail know no bounds. He has shown me the possibilities of research and inspired me to keep cultivating my skills.

I would like to express my gratitude to the Muscular Dystrophy UK for kindly providing the funding for this research. Furthermore, I am grateful for the guidance and friendships I received in the Wood lab throughout the years. Specifically, I would like to thank Yoshi Aoki for giving me an opportunity to widen my scientific horizons, setting our collaboration in motion; Graham McClorey for his (scientific) advice and critical assessments, improving my work; Amarjit Bhomra for the incredible technical and emotional support; Suzan Hammond for all advice relating to animal experiments; Melissa Bowerman for showing me compassion, determination and scientific success for women; and Carlo Rinaldi for answering my desperate questions about my scientific career over a beer and diet-coke. Particularly, I am also grateful for the amazing company, support, laughter and of course food in the student office. A special thanks to my science sister Karin Meijboom, who was always ready to listen to my ups and downs, and experienced them with me. Thanks to Fiona Lee and Sabrina Heman-Ackah for the great company and exploration of Oxford's restaurants. I am

also grateful for the great friendships given by Britt Hanson, Larissa Goli, Loïc Roux and Marie Pauwels. The last year of my DPhil was infinitely improved by your presence.

Outside of work, I would like to express my gratitude to those people closest to me. Firstly, I am extremely grateful for having met my non-relative cousin Lorena Becerra Valdivia, who was always there for serious and fun moments alike. I wish the best in the world for you. I would also like to thank my family for loving me unconditionally. My brother Stefan, sister in law Michelle and their children for providing necessary distractions during visits to the Netherlands. My sister Tania, Michael Bright and their daughter Aria for providing a respite away from my thoughts of Oxford and support when times were hard. Most importantly, I would like to thank Thomas Jacob, who has been there to support me, always. You laughed and cried with me, and took care of me during the hardest times of my life. You truly are special, and I am so grateful you are there for me. Lastly, I would like to express my gratitude to my parents. I would not be here without your love and support. I could not ask for a better mother in the world, whose wisdom and affection are endless, even when I am breaking down. The advice of my father knew no bounds, encouraging my pursuit of a PhD at Oxford. I am heartbroken that you are not here anymore to see me complete the journey, but I hope I made you proud.

Abstract

Duchenne muscular dystrophy (DMD) is a classical monogenic disorder characterised by severe muscle weakness. Progressive muscle loss ultimately culminates in fatality due to failure of the heart and diaphragm muscles, typically in the 2nd-4th decade of life. The genetic cause of DMD is disruption of the *DMD* gene encoding for the dystrophin protein. Dystrophin is important for cytoskeletal structure and normal muscle function, and it plays a vital role in maintaining membrane stability and signalling functions. However, the downstream molecular events that follow dystrophin loss are incompletely understood. Moreover, pharmacodynamic biomarkers that can inform on disease progression are severely lacking. This thesis aimed to identify the effects of the dystrophin protein absence on the cardiac transcriptome, skeletal muscle proteome and extracellular microRNA (miRNA) secretome with pathological progression.

To improve the understanding of the dystrophic cardiomyopathic advancement in the various anatomical regions of the heart, transcriptomic arrays were performed on RNA taken from the distinct chambers to identify novel pathways involved in pathology. Analysis identified early molecular changes in the right atrium and ventricle, mostly related to cell migration and cardiac remodelling. Furthermore, *Sfrp2* (secreted Frizzled-related protein 2), a major regulator of the Wnt signalling pathway, was found to be highly differentially expressed between control and dystrophic hearts. It was observed that expression of the non-canonical c-Jun N-terminal kinase (JNK)-arm of the Wnt cascade was reduced. Interestingly, cellular fractionation demonstrated decreased levels in the cytoplasmic/extracellular region and increased expression surrounding the nucleus, which suggests a potential mislocalisation of the sFRP2 protein in dystrophic hearts.

Protein expression in skeletal muscle was characterised by high-resolution mass spectrometry-based proteomics in two dystrophic mouse models over time. Analysis of the two models at different time points allowed for protein identification irrespective of mutation or age. The results highlighted the involvement of many proteins in DMD, such as Rho GTPases, SLC25A24,

RICTOR, CAV3 and MVP. Expression of major vault protein (MVP) increased during differentiation of myoblasts *in vitro* and interestingly, *Mvp* knockdown was observed to potentially influence *Dmd* expression levels, suggesting a novel role for MVP in DMD pathology.

The miRNA secretome was examined to investigate the relationship between skeletal muscle dystrophin expression and extracellular miRNA abundance. Interestingly, while muscle-related miRNAs (myomiRs, indicative of muscle turnover) were not restored to wild-type levels in *mdx-Xist*$^{\Delta hs}$ mice, which express low levels of dystrophin from birth (~8-44%), other miRNAs such as miR-193b-3p, miR-370-3p and miR-483-3p did exhibit a decrease in extracellular abundance. In contrast, exon skipping treatment achieving similar dystrophin re-expression levels was able to completely restore serum miRNA levels. The disparity between the *mdx-Xist*$^{\Delta hs}$ and *mdx* mice treated with exon skipping was attributed to uneven dystrophin distribution at the sarcolemma in the former. The observed patchy, within-fibre mosaicism was unable to restore extracellular myomiR abundance, and by extension muscle turnover. These results are directly relevant to the development of therapeutic strategies for dystrophin re-expression.

In conclusion, this work has identified novel molecular pathways involved in cardiac and skeletal muscle dystrophic pathology. Furthermore, the results have demonstrated the importance of uniform dystrophin distribution at the sarcolemma for pathological correction. Together, these findings provide new insights into the molecular pathology of DMD with implications for therapy.

Table of contents

Declaration ii

Acknowledgements iii

Abstract v

Table of contents vii

List of figures xiii

List of tables xv

List of abbreviations xvi

1. Introduction 1

1.1 Duchenne muscular dystrophy 1

1.1.1 Clinical manifestation 1

1.1.2 The *DMD* gene 3

1.1.3 Dystrophin and its associated protein complex (DAPC) 4

1.1.4 Animal models for DMD 8

1.1.4.1 Mouse models 8

1.1.4.2 Canine models 10

1.2 Early pathological processes in DMD 11

1.2.1 Aberrant calcium signalling 11

1.2.1.1 Membrane tears 12

1.2.1.2 Stretched-activated channels (SACs) 12

1.2.1.3 Voltage-gated Ca^{2+} channels (VGCC) – L-type 14

1.2.1.4 Store-operated Ca^{2+} release 14

1.2.2 Oxidative stress and mitochondrial dysfunction 16

1.2.3 NO and NOS 16

1.3 Muscle progenitor cells 19

1.3.1 Satellite cells 19

1.3.2 Fibro-adipogenic progenitor cells 21

1.3.3 Other muscle-resident progenitor cells 22

1.4 Fibrosis 23

1.5 Therapeutic interventions for DMD 26
1.5.1 Current clinical disease management 26
1.5.2 Novel therapeutic strategies targeting dystrophin absence 27
1.5.2.1 Exon skipping 28
1.5.2.2 Stop codon read-through therapy 30
1.5.2.3 Cell-based therapy 31
1.5.2.4 Viral gene therapy for dystrophin transgene delivery 32
1.5.2.5 CRISPR-Cas9 34
1.5.2.6 Utrophin upregulation 35
1.6 miRNAs 45
1.6.1 miRNA biogenesis 45
1.6.2 Muscle-specific miRNAs 47
1.6.3 miRNAs in DMD 48
1.6.4 Extracellular miRNAs for DMD biomarkers 50
1.7 Thesis hypotheses and aims 54
2. General materials and methods 55
2.1 Animal studies 55
2.2 Cell culture 56
2.3 RNA extraction 57
2.3.1. Cells and tissues 57
2.3.2. Serum 57
2.4. Reverse transcription-quantitative polymerase chain reaction (RT-qPCR) 59
2.4.1. mRNA 59
2.4.2. miRNA 59
2.5. Western blotting 61
2.6. Myosin heavy chain immunofluorescence 63
3. Results I: Transcriptomic analysis identifies *Sfrp2* expression changes and its protein mislocalisation in dystrophic cardiomyopathy 64
3.1 Introduction 64

3.2 Materials and methods 68
3.2.1 Animals 68
3.2.2 Pip6a-PMO treatment 68
3.2.3 H2K-*mdx52* differentiation 69
3.2.4 H&E staining 70
3.2.5 RNA extraction 70
3.2.6 RT-qPCR 71
3.2.7 Microarray analysis 72
3.2.8 Western blotting 74
3.2.9 Immunofluorescence 75
3.2.10 Statistical analysis 76
3.3 Results 77
3.3.1 Heart morphology in control and diseased hearts 77
3.3.2 Transcriptomic analysis for pathway discovery 79
3.3.3 Involvement of *Sfrp2* and Wnt-related genes in the dystrophic heart 89
3.3.4 Identification of Wnt pathway protein involvement 97
3.3.5 Cellular translocation of sFRP2 99
3.3.6 Effect of *Sfrp2* on myoblast differentiation 104
3.4 Discussion 106
3.4.1 Global heart pathology 106
3.4.2 Treatment was unable to restore global transcriptomic expression 107
3.4.2 Sfrp2 divergence in dystrophic hearts 107
3.4.4 Study limitations and future directions 110
3.4.5 Conclusions 113
4. Results II: Utilisation of high-resolution proteomics analysis to identify novel differentially expressed proteins associated with disease progression in the skeletal muscle of two DMD mouse models 114
4.1 Introduction 114
4.2 Materials and methods 118
4.2.1. Animals 118
4.2.2. RNA extraction and RT-qPCR 118
4.2.3. Proteomic LC-MS/MS 120

4.2.4. Protein extraction and Western blotting 120
4.2.5. *Mvp* knockdown in C2C12 cells 121
4.2.6. Statistical analysis 122
4.3 Results 123
4.3.1. Experimental design 123
4.3.2 Proteomic analysis in healthy and dystrophic muscle over time 125
4.3.3 Dystrophin-associated protein complex 127
4.3.4 Comparison of *mdx* and *mdx52* dystrophic mouse models 129
4.3.5 Protein expression comparisons between WT versus *mdx* or WT versus *mdx52*. 130
4.3.6 Mutation-independent dystrophic proteome signature 133
4.3.7 Aging protein expression pattern between WT and Dystrophic 134
4.3.8 Validation of proteomics dataset 138
4.3.9 MVP is not required for myogenic differentiation, but may influence *Dmd* expression 140
4.4 Discussion 142
4.4.1 Comparing protein signatures of *mdx* and *mdx52* 142
4.4.2 Mutation-independent and/or age-related dystrophic proteome 143
4.4.3 Dystrophic involvement of MVP 145
4.4.4 Study limitations and future directions 146
4.4.5 Conclusions 147
5. Results III: Uniform dystrophin distribution at the sarcolemma is required to stabilise ex-miRNA release from dystrophic muscle 148
5.1 Introduction 148
5.2 Materials and methods 151
5.2.1 Animals 151
5.2.2 Exon skipping utilising PPMO 152
5.2.3 FirePlex serum miRNA profiling 152
5.2.4 RNA extraction and RT-qPCR 154
5.2.5 Western blotting 155
5.2.6 Cell culture 155
5.2.7 Statistical analysis 156
5.3 Results 157

5.3.1 Ex-miRNA abundance is not elevated in heterozygote *mdx* mice 157
5.3.2 Skewed X-chromosome inactivation induces variable skeletal muscle dystrophin protein levels in *mdx* mice 160
5.3.3 Identification of novel candidate biomarkers by serum miRNA profiling 161
5.3.4 Longitudinal analysis of serum miRNAs in *mdx* mice expressing varying levels of dystrophin protein 164
5.3.4 Orthogonal methodology RT-qPCR exhibits similar miRNA patterns as FirePlex 177
5.3.5 Uniform dystrophin expression is associated with serum miRNA restoration 182
5.3.6 Ex-miRNA abundance levels are influenced by gender 185
5.3.7 RT-qPCR fails to measure several low abundant miRNAs detected by FirePlex 186
5.3.8 Measured miRNAs decrease abundance with age 188
5.3.9 myomiRs, miR-193b-3p and miR-483-3p are released from myoblasts upon differentiation 190
5.4 Discussion 192
5.4.1 The relationship between skeletal muscle dystrophin expression and ex-miRNA abundance 192
5.4.2 Gender-specific miRNA abundance 195
5.4.3 Therapeutic implications 195
5.4.4 Study limitations and future directions 197
5.4.5 Conclusions 198
6. Discussion and conclusion 199
6.1 Summary of results 199
6.2 High-throughput methodologies in DMD 202
6.3 Mouse models for DMD research 204
6.4 Circulating biomarkers in DMD 205
6.5 Concluding remarks 207
7. References 208
8. Appendix 253
8.1 Differentially expressed *Fzd* receptors, *Sfrp* and *Wnt* ligands in all anatomical areas of the heart at all ages. 253
8.2 Selected miRNAs for initial FirePlex screen 254
8.3 Selected miRNAs for longitudinal FirePlex analysis 256

8.4 Publications 257
8.4.1 First author publications 257
8.4.2 Co-authored publications 257

List of figures

Figure 1.1 Dystrophin isoforms 6
Figure 1.2 Dystrophin and its associated proteins 7
Figure 3.1 Simplified schematic of the three main Wnt signalling arms. 66
Figure 3.2 Heart morphology of male and female C57BL/10 and *mdx* at 10, 24 and 52 weeks of age. 78
Figure 3.3 Dystrophin protein restoration in *mdx* hearts treated with Pip6a-PMO. 80
Figure 3.4 Comparison of heart cell type specific markers between C57BL/10 and *mdx* for all chambers. 82
Figure 3.5 Clustering of differentially expressed genes between C57BL/10 and *mdx* at 24 weeks. 83
Figure 3.6 Clustering of differentially expressed genes between C57BL/10, *mdx* and Pip6a-PMO at 10, 24 and 52 weeks. 87
Figure 3.7 mRNA expression of *Sfrp2* in female mice as measured by Affymetrix arrays. 91
Figure 3.8 GeNorm analysis identifying stable expression of 12 common housekeeping genes. ... 92
Figure 3.9 mRNA expression of *Sfrp2* in male and female mice. 93
Figure 3.10 mRNA expression of *Fzd1* and *Fzd3* in male and female mice. 95
Figure 3.11 mRNA expression of *Bambi* and *Tle2* in male and female mice. 96
Figure 3.12 Protein expression of sFRP2, β-catenin, JNK and NFAT. 99
Figure 3.13 Cytoplasmic and nuclear localisation of sFRP2 protein. 103
Figure 3.14 Effect of *Sfrp2* RNAi on rate of differentiation. 105
Figure 4.1 Mutation differences between *mdx* and *mdx52* mouse models. 116
Figure 4.2 Ex-miRNA abundance in WT, *mdx* and *mdx52* serum samples. 124
Figure 4.3 Cumulative protein frequency distribution of all proteins identified with HiRIEF-LC-MS/MS. 126
Figure 4.4 Clustering of differentially expressed proteins between WT, *mdx* and *mdx52* samples at 8, 16 and 80 weeks of age. 127
Figure 4.5 Relative protein expression of important proteins involved in the DAPC. 128
Figure 4.6 Differential protein expression between *mdx* and *mdx52* at 8, 16 and 80 weeks of age 130
Figure 4.7 Differentially expressed proteins between *mdx* vs WT and *mdx52* vs WT. 132
Figure 4.8 Most significant proteins and pathways in DMD pathology, irrespective of age or mutation. 134
Figure 4.9 Proteomic aging signature in WT and Dystrophic samples. 137
Figure 4.10 Proteins contributing to aging of WT and Dystrophic samples. 137

Figure 4.11 Validation of selected protein targets. 139
Figure 4.12 *Mvp* siRNA knockdown in C2C12 myoblasts does not affect differentiation, but may influence *Dmd* expression in dystrophin-deficient H2K-*mdx52* myoblasts. 141
Figure 5.1 Goodness of fit for calibrator values from two FirePlex measurements. 153
Figure 5.2 Serum miRNA levels and dystrophin expression in *mdx* heterozygote animals. 158
Figure 5.3 Experimental design of longitudinal miRNA profiling study. 161
Figure 5.4 Screen for differentially abundant ex-miRNAs in dystrophic serum. 163
Figure 5.5 Serum miRNA screening quality control analyses. 165
Figure 5.6 Longitudinal analysis of serum miRNA levels in mice expressing various levels of dystrophin protein. 167
Figure 5.7 Serum myomiRs are elevated irrespective of dystrophin protein levels in *mdx-Xist*$^{\Delta hs}$ mice. 170
Figure 5.8 Area under the curve (AUC) values from the ROC curve analysis. 170
Figure 5.9 Dystrophin-dependent reductions in serum levels of miR-193b-3p, miR-370-3p, and miR-483-3p in *mdx-Xist*$^{\Delta hs}$ mice. 173
Figure 5.10 Analysis of individual serum miRNAs – miR-208-3p, miR-378a-3p and miR-539-5p in *mdx-Xist*$^{\Delta hs}$ mice. 175
Figure 5.11 Analysis of individual serum miRNAs - miR-133b-3p, miR-22-3p and miR-30a-5p in *mdx-Xist*$^{\Delta hs}$ mice. 177
Figure 5.12 RT-qPCR validation of serum miRNA abundance at 16 weeks of age. 180
Figure 5.13 RT-qPCR validation of serum miRNA abundance at 24 weeks of age. 182
Figure 5.14 Uniform dystrophin protein expression is required for restoration of ex-miRNA levels. 184
Figure 5.15 Comparison of differential miRNA abundance in serum from male and female mice. 186
Figure 5.16 miRNAs exhibiting low abundance in FirePlex fail to validate with RT-qPCR. 187
Figure 5.17 Differentially expressed miRNAs at 80 weeks of age. 189
Figure 5.18 C2C12 myoblast differentiation induces release of miRNAs of interest. 191

List of tables

Table 1.1 Expression of dystrophin splice variants 4

Table 1.2 DMD (pre-clinical) therapies targeting the absence of dystrophin 37

Table 2.1 Antibodies for dystrophin protein detection by Western blot 62

Table 3.1 Overview of H2K-*mdx52* treatment with RNA interference 69

Table 3.2 Primer sequences utilised in qPCR for genes of interest. 72

Table 3.3 List of antibodies utilised for protein detection in Western blot. 75

Table 3.4 Gene ontology enrichment analysis in female C57BL/10 vs mdx heart samples 85

Table 3.5 Summary of theme compilation from REVIGO for RA, RV and LV at 10, 24 and 52 weeks of age 89

Table 4.1 miRNA assays utilised in RT-qPCR. 118

Table 4.2 Forward and reverse primer sequences utilised for mRNA detection. 119

Table 4.3 Antibodies used for protein detection by Western blot. 121

Table 4.4 Percentiles, mean, standard deviation and standard error of HiRIEF-LC-MS/MC. 125

Table 5.1 miRNA primers utilised for RT-qPCR validation. 154

Table 5.2 Primers and probes utilised for mRNA detection by qPCR. 155

List of abbreviations

2'OMePS	2'O methyl phosphorothioate
6MWT	6 minute walk test
rAAV	Recombinant adeno-associated virus
Ab/am	Antibiotics/antimycotics
ABD	Actin binding domain
ACE	Angiotensin-converting enzyme
Acta2	Actin, aortic smooth muscle
AGO	Argonaute
Ang-II	Angiotensin II
AON	Antisense oligonucleotide
AUC	Area under the curve
Bambi	BMP and activin membrane-bound inhibitor homolog
Bayley III	Bayley III scales of infant and toddler development
BMD	Becker muscular dystrophy
BMP	Bone morphogenic protein
BP	Biological processes
BSA	Bovine serum albumin
CaM	Calmodulin
CardiomiR	Cardiac-related miRNA
CAV3	Caveolin-3
CDF	Cumulative distribution function
CK	Creatine kinase
Ckm	Creatine kinase M-type
Cmah	Cytidine monophosphate-sialic acid hydroxylase
Cnn	Calponin-1
Cntn2	Contactin-2
CPP	Cell penetrating peptides
Cq	Quantitation cycle
CRD	Cysteine-rich domain
CRISPR-cas9	Clustered regularly interspaced short palindromic repeats-CRISPR associated 9
CTGF	Connective tissue growth factor

$CXMD_J$	Canine X-linked muscular dystrophy dog in Japan
DAPC	Dystrophin associated protein complex
DCM	Dilated cardiomyopathy
Ddr2	Discoidin domain-containing receptor 2
DGCR8	DiGeorge critical region 8
Dko	Double knockout mouse; negative for dystrophin and utrophin
DM	Differentiation medium
DMD	Duchenne muscular dystrophy
DMEM	Dulbecco's modified eagle medium
DTT	Dithiothreitol
DVL	Dishevelled-1
E-C	Excitation-contraction
ECG	Electrocardiogram
ECM	Extracellular matrix
EF	Ejection fraction
EMA	European Medicines Agency
eMHC	Embryonic MHC
eNOS	Endothelial nitric oxide synthase
ERK	Extracellular signal–regulated kinase
Ex-miRNA	Extracellular miRNA
F-actin	Polymerised actin
FAP	Fibro-adipogenic progenitor
FC	Fold change
FDA	US Federal Drug Administration
Fzd	Frizzled receptor
GC	Guanylyl cyclase
GM	Growth medium
GO	Gene ontology
GRMD	Golden retriever muscular dystrophy
GSK-3β	Glycogen synthase kinase 3-β
H&E	Haematoxylin and eosin
HDAC	Histone deacetylase
Het	Heterozygote *mdx*

HiRIEF-LC-MS/MS	High-resolution isoelectric focusing-liquid chromatography-tandem mass spectrometry
iNOS	Inducible nitric oxide synthase
IP_3	1,4,5-triphosphate
IP_3R	IP_3 receptor
IPA	Ingenuity pathway analysis
IVS	Interventricular septum
JNK	c-Jun N-terminal kinase
kD	Kilodaltons
LA	Left atrium
LRP	Lipoprotein-related receptor
LV	Left ventricle
MHC	Myosin heavy chain
miR	miRNA
miRNA	MicroRNA
MMP	Matrix metalloproteinase
MVP	Major vault protein
Myf5	Myogenic factor 5
Myh1	Myosin heavy chain 1
MyoD	Myoblast determination protein 1
MyoG	Myogenin
myomiR	Muscle-related miRNA
NCX	Na^+-Ca^{2+}-exchanger
NFAT	Nuclear factor of activated T-cells
Nkx2.5	Homeobox protein Nkx-2.5
nNOS	Neuronal nitric oxide synthase
NO	Nitric oxide
NOS1	Neuronal nitric oxide synthase
NOX	NADPH oxidase
NSAA	North star ambulatory assessment
PAK1	Serine/threonine-protein kinase PAK1
Pax7	Paired-box 7
PBS	Phosphate buffered saline
PCA	Principal component analysis

PCP	Planar cell polarity
Pecam1	Platelet endothelial cell adhesion molecule
Pip	Peptide nucleic acid (PNA)/PMO internalisation peptide
PKA	Protein kinase A
PLC	Phospholipase C
PMO	Phosphorodiamidate morpholino oligomers
PPMO	Peptide-conjugated PMO
Pre-miRNA	Precursor miRNA
Pri-miRNA	Primary miRNA
PTP	Permeability transition pore
PVDF	Polyvinylidene fluoride
RA	Right atrium
RER	Rough endoplasmic reticulum
REVIGO	Reduce and visualise gene ontology
RFU	Relative fluorescence unit
RISC	RNA-inducing silencing complex
RNAi	RNA interference
ROC	Receiver operating characteristic
ROCK	Rho-associated kinase
ROS	Reactive oxygen species
RT-qPCR	Reverse transcription-quantitative polymerase chain reaction
RV	Right ventricle
RyR	Ryanodine receptor
SAC	Stretch-activated channel
SERCA	Sarcoplasmic/endoplasmic reticulum Ca^{2+} ATPase
sFRP	Secreted frizzled-related protein
SR	Sarcoplasmic reticulum
SV	Stroke volume
TA	Tibialis anterior
TBST	Tris-buffered saline with 0.1% Tween
TGFβ	Transforming growth factor β
Tle2	Transducin-like enhancer protein 2
TMT	Tandem mass tags
Tnni3	Cardiac Troponin I

TRPC	Transient receptor potential cation
TRPV	Transient receptor potential vanilloid
UTR	Untranslated region
Utrn	Utrophin
VCL	Vinculin
VGCC	Voltage-gated Ca^{2+} channel
Wnt	Wingless/integrated
WT	Wild-type
Wt1	Wilms tumour protein homolog
XCI	X-chromosome inactivation

1. Introduction

1.1 Duchenne muscular dystrophy

1.1.1 Clinical manifestation

Duchenne muscular dystrophy (DMD) is a fatal, X-linked muscle degenerative disorder affecting ~1:5,000-10,000 live male births [1]. The disease is caused by a mutation in the *DMD* gene, encoding for the dystrophin protein. Dystrophin is a structural and signalling protein which is localised at the sarcolemma and acts as an organising centre for the dystrophin-associated protein complex (DAPC) [2]. This protein forms a mechanical link between the actin cytoskeleton and the extracellular matrix via the DAPC [3], and functions as a 'shock absorber' which protects myofibres from contractile damage [4]. Clinicians test for DMD when young males present with delays in major motor milestones. Several studies have been performed to assess disease severity, using various muscle function assessment scales (e.g. Bayley III scales of infant and toddler development (Bayley III), North star ambulatory assessment (NSAA)). These indicated that boys with DMD generally present with delayed motor skills, such as walking and climbing stairs, and exhibit below average language comprehension and cognitive function [5–8], although clinical manifestations vary considerably between patients [9]. Another typical feature is the Gowers' sign, whereby a child transitions from a sitting to a standing position while pushing their hands on their legs for support, which is indicative of proximal muscle weakness [10]. DMD diagnosis is then confirmed by elevated serum levels of the muscle-specific creatine kinase (CK; thought to leak of out fragile muscle membranes and elevated in patients with neuromuscular disorders), followed by identification of DMD-associated mutations [11]. Muscle biopsy and dystrophin immunostaining may also be used for diagnosis, although these are more invasive [11]. Recognition of disease pathology and testing has significantly advanced throughout the years, but the age of diagnosis remains around 5 years, even though symptoms are often noticed much earlier by parents [12,13]. Pathology subsequently progresses dramatically, and most patients

are wheelchair-bound by the age of 10-13 [14]. Aside from the early skeletal muscle phenotype, patients may also experience intellectual disability and impairment of cognitive functions such as working memory and multitasking [6,15–17]. The most common causes of death are respiratory problems and dilated cardiomyopathy (DCM), typically in the third decade of life. Generally, patients with stronger proximal muscles are more likely to succumb to cardiomyopathy, whereas patients with weaker muscles pass away due to respiratory failure [9]. With the advancements of therapeutic interventions, life expectancy has increased from ~14 years to over 25 years of age [18,19] and improved pulmonary assistance and care has reduced mortality caused by respiratory failure. However, since 1980, cardiac-related deaths have become more prevalent and have therefore received increased attention [18].

Cardiac dysfunction varies between patients but is often recognised by the presence of sinus tachycardia at a young age. Cardiomyopathic progression is coupled with left ventricular dysfunction, fibrosis, and changes in fractional shortening and electrocardiogram (ECG) measurements [20]. These ECG abnormalities are associated with morphological changes to cardiac muscle [21], myocardial fibrosis and conduction defects [22]. For instance, deep Q wave abnormalities have been associated with lateral wall scarring [23]. Interestingly, right ventricular wall function is relatively spared, which is thought to occur because of improved respiratory intervention strategies [24]. Cardiomyopathic progression is characterised by replacement of cardiomyocytes with fat and fibrosis, and these histological features are associated with a rapid decline in heart function. Fibrotic deposition first occurs at the postero-basal myocardium of the left ventricular free wall, after which the septum and rest of the outer ventricular wall are affected [20,25]. Fibrosis is present in some young patients (17% under 10 years of age) and increases in frequency with age (34% between 10–15 years and 59% older than 15 years of age) [26].

By 18 years of age all patients have developed cardiomyopathy [27] although 43% is asymptomatic, most likely due to reduced mobility thereby imposing less stress on the heart [20].

Wang *et al.*, discovered that survival rates dramatically decreased if the age of onset for left ventricular dysfunction was before 18 years, which was unrelated to *DMD* mutation [28]. Many patients also exhibit decreased heart rate variability, which can be correlated with disease progression, potentially making it a useful non-invasive tool to monitor cardiomyopathic progression [29].

1.1.2 The *DMD* gene

The *DMD* gene is located on the short arm of the X-chromosome (Xp21.2-p21.1) [30], spans ~2.4 megabases and consists of 79 exons. Mutations in the *DMD* gene can cause complete absence of the dystrophin protein (in DMD), or a truncated, partially functional protein, as is the case in Becker muscular dystrophy (BMD). Clinical disease presentation is highly variable but generally less severe in BMD compared to DMD, where 50% of BMD patients experience muscle weakness by 10 years of age, with most patients being symptomatic from age 20, although many preserve ambulation until their fourth decade of life [31,32].

Whether a mutation induces a BMD or DMD phenotype is dependent on the reading frame rule for ~90% of the cases [33]. This defines that out-of-frame mutations shift the reading frame such that they induce a disrupted translation reading frame and, by extension, a dysfunctional protein. In contrast, BMD patients retain an in-frame mutation which allows for the generation of a truncated dystrophin protein [34]. A comprehensive analysis of a mutation database containing 7,149 entries from DMD patients illustrated that most mutations occurred at the proximal (exon 2-20) and distal (exon 45-55) end of the gene, whereby the majority involved 1 or more exon deletions [35]. Due to the high number of mutations in exon 45-55, this area is often called the 'hot-spot' in DMD [35].

Interestingly, around 7% of DMD patients do not follow this reading frame rule. This may be due to large deletions or specific mutations causing instability or dysfunctionality of the protein. Indeed, the majority of the patients with in-frame duplications that do not follow the rule exhibit mutations in the actin binding domain [33]. Similarly, disease severity in BMD patients with at least 10% dystrophin protein and a mutation in exon 45-47 correlated with the location of the mutation,

rather than levels of dystrophin protein expression [36]. Indeed, many BMD patients with mutations in hinge III of the rod domain experience a mild disease phenotype and have a good prognosis [37], whereas patients with an exon 48-49 deletion experience a more severe cardiac pathology [31]. These studies suggest that the location of a given mutation is important for determining the degree of protein stability and structure, and by extension disease severity.

1.1.3 Dystrophin and its associated protein complex (DAPC)

At least six different tissue-specific dystrophin promoters exist which give rise to several splice variants (where the protein names are derived from their molecular mass in kilodaltons (kD)) (**Table 1.1** and **Figure 1.1**). Their expression varies between tissues, and the genomic locations of DMD-causing mutations may differentially affect the expression of these various protein isoforms. Therefore, many studies have attempted to link dystrophin variant to disease phenotype. For instance, Connelly *et al.* identified a correlation between reduced language and cognition, and absence of the Dp140 protein [6]. Similarly, loss of the Dp71 variant has been associated with cognitive impairment [15,16]. Hyperactivity has been observed in ~24% of the patients and linked to mutations in the 3' end [38]. Notably, the presence of multiple splice variants in any given tissue and the endogenous expression of dystrophin in a small number of fibres (called revertant fibres) mean that sporadic expression of the dystrophin protein in dystrophic muscle is expected.

Table 1.1 Expression of dystrophin splice variants

Isoform	Promoter Location	Main Tissue Expression	Included Exons	Reference
Dp427 brain (B)	5' end	Cortex and hippocampal neurons	1-79	[39]
Dp427 muscle (M)	5' end	Skeletal and cardiac muscle	1-79	[40]
Dp427 Purkinje (P)	5' end	Purkinje fibres	1-79	[41]
Dp260	Intron 29	Retina	30-79	[42,43]
Dp140	Intron 44	Brain, retina, kidney	45-79	[44]
Dp116	Intron 55	Peripheral Nerve	56-79	[45]
Dp71	Intron 62	Ubiquitous	63-79	[46,47]
Dp40	Intron 62	Brain	63-69	[48,49]

The full-length dystrophin protein (Dp427), expressed in skeletal and cardiac muscle, consists of a N-terminal domain (exons 1-8), a central rod domain (exons 9-63), a cysteine-rich domain (exons 64-69) and a C-terminal domain (exons 70-79) (**Figure 1.1**). The N-terminal domain includes a calponin 2 homology domain which directly binds to polymerised actin (F-actin) [50] and the intermediate filament protein cytokeratin [51]. These interactions link dystrophin to the contractile apparatus of the cell. Another actin binding area exists in the rod domain [52] and together these two different areas strengthen actin binding to dystrophin [53]. Conversely, the C-terminus consists of two α-helical coiled coil motifs which facilitate binding to β-dystroglycan [54], dystrobrevin [55] and the syntrophins (although recent evidence suggests additional syntrophin binding occurs within the rod domain [56]). By connecting to actin at the N-terminus and the dystroglycan complex on the other end of the protein, dystrophin provides a mechanical link between the actin cytoskeleton and the extracellular matrix, thereby preventing damage from muscle contraction [57,58]. The centre of the protein (rod and cysteine-rich domains) also plays important structural and signalling roles. The rod domain consists of 24 spectrin-like repeat regions, which are triple α-helices consisting of around 110 amino acids each [59–61]. Four proline-rich hinges are located at several intervals between the repeats which allow for flexibility of the protein. Through the spectrin-like repeats, dystrophin binds to microtubules [62], phospholipids [63] and indirectly to neuronal nitric oxide synthase (nNOS) [56]. The fourth hinge is stabilised by EF-hand motifs in the cysteine-rich domain [64].

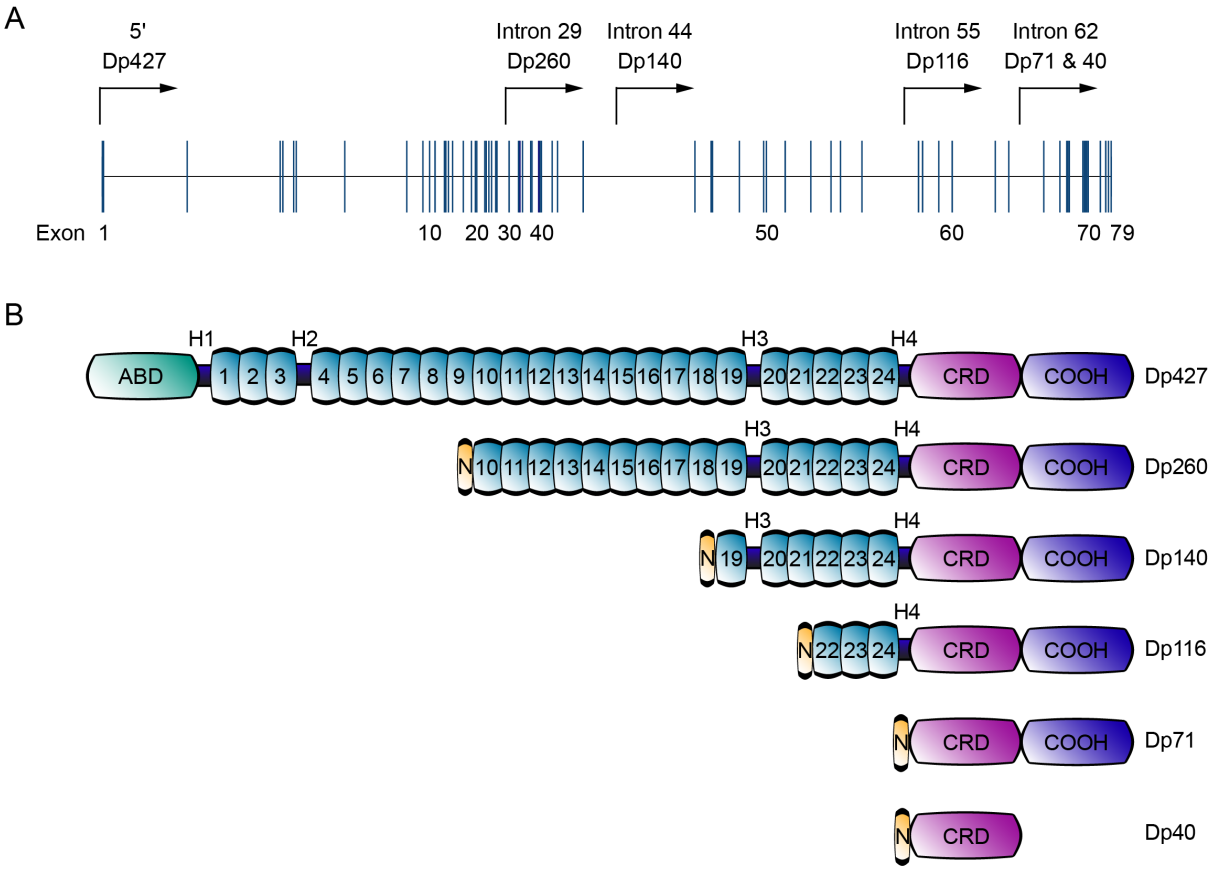

Figure 1.1 Dystrophin isoforms
A *DMD* gene identifying the splice sites for generation of the dystrophin isoforms. **B** Protein domains for the different isoforms. The full-length protein contains an actin-binding domain (ABD), the 24 spectrin-like repeats (1-24), the cysteine-rich domain (CRD; containing the WW, EF-hand and ZZ domains) and the C-terminal domain. Hinge regions (H1-4) are spread throughout the protein. Several domains are absent in the shorter isoforms and these proteins carry an alternative N-terminus (N).

To properly execute its stability function, dystrophin binds and acts as a scaffold for the DAPC (**Figure 1.2**). On the intracellular side, this complex consists of dystrophin, dystrobrevin, α- and β-syntrophin and nNOS (whereby syntrophin mediates nNOS binding) [56]. Dystrophin associates with dystroglycan, which is composed of the transmembrane β subunit and the extracellular α subunit. The extracellular subunit binds laminin, while β-dystroglycan is associated with biglycan and by extension the sarcoglycans (α, β, γ and δ) [65]. Through its connection with the dystroglycans, dystrophin is connected to laminin, thereby linking the cytoskeleton with the extracellular matrix. The individual components of the DAPC also play important structural and signalling roles and their genetic

disruption is associated with a plethora of other muscular disorders. Absence of dystrophin induces mislocalisation and/or reduction in dystrophin-associated proteins, such as nNOS. The cycles of muscle necrosis and regeneration due to the absence of dystrophin is also observed to cause morphological changes at the neuromuscular junction [66], which are absent in animals with ~50% dystrophin expression from birth [67].

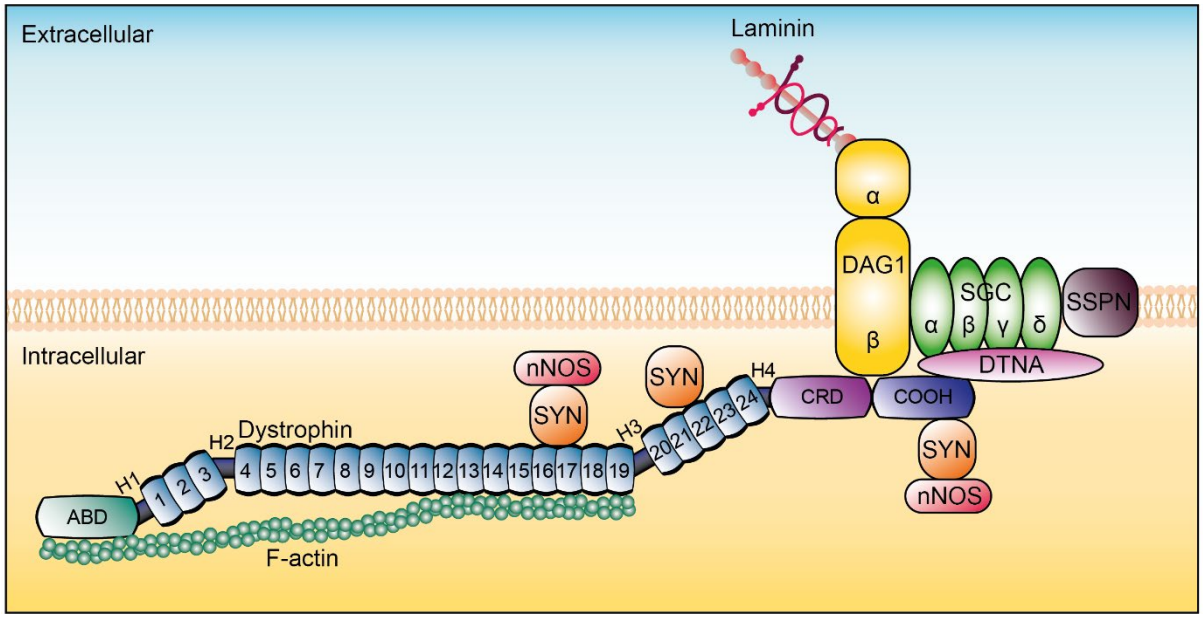

Figure 1.2 Dystrophin and its associated proteins
Dystrophin binds F-actin at the actin-binding domain on the N-terminal and at spectrin-like repeats 12-19. At the cysteine-rich and C-terminal domain it links to the α- and β-dystroglycans, dystrobrevin and syntrophins, indirectly linking dystrophin to laminin, sarcoglycans, sarcospan and nNOS. These connections enable dystrophin to form a mechanical link between the cytoskeleton and the extracellular matrix. ABD: actin-binding domain; COOH: C-terminal domain; CRD: cysteine-rich domain; DAG1: dystroglycan; DTNA: dystrobrevin; H1-4: hinge region; nNOS: neuronal nitric oxide synthase; SGC: sarcoglycan; SSPN: sarcospan; SYN: syntrophin.

In the adult myogenic lineage, a homolog of dystrophin, utrophin (UTRN), is mainly found in regenerating cells [68,69] and at the neuromuscular and myotendinous junctions [70,71]. Utrophin has a molecular weight of 395 kDa and a similar amino acid composition to dystrophin, although the rod domain is significantly shorter [71]. Despite some functional and expression differences, utrophin appears to have many of the same binding proteins, including certain components of the DAPC and F-actin [72,73] and it is thought that it could partially compensate for the loss of dystrophin.

1.1.4 Animal models for DMD

Since the discovery of the *DMD* gene in 1986 by Monaco *et al.* [30], ~60 different animal models of DMD have been established to investigate disease pathology [74]. Here, focus is given only to the most commonly used models, i.e. the *mdx* mouse, some of its derivatives and two dog models.

1.1.4.1 Mouse models

A single point mutation in exon 23 prevents the production of a stable dystrophin protein in the *mdx* mouse [75,76]. This model exhibits an obvious skeletal phenotype including elevated CK plasma levels, myofibre size variation and central nucleation [75], muscle necrosis [77], and a decline in specific muscle force and power with age [78]. Between 3 and 10 weeks of age, skeletal muscle undergoes a phase of myofibre necrosis and regeneration, after which pathology slowly progresses [74]. Respiratory function also deteriorates and correlates with the diaphragmatic degeneration observed in patients [79,80]. In addition, *mdx* mice display a cardiac phenotype, although this is not as severe as in patients. Increased right ventricle (RV) systolic volume and subsequent reduction in RV ejection fraction (EF) is observed at 3 months of age [81]. An increase in myocardial fibrosis and deterioration in left ventricle (LV) cardiac output (CO) is apparent from 6 months of age. By 9 months, stroke volume (SV) is decreased followed by a reduction in LV EF at 12 months of age. As with DMD patients, ECG recordings in conscious *mdx* mice revealed tachycardia, decreased heart rate variability [82], deep Q waves, diminished S:R ratios, polyphasic R-waves and shorter QT and PR intervals [83] compared to control animals.

Despite the presence of a pathological phenotype in the *mdx*, there is a large disparity in disease progression between these mice and DMD patients. For instance, *mdx* mice exhibit a relatively small reduction in life span [84] and they only experience a mild cardiomyopathy [81]. Therefore, other models have been generated with the aim of inducing a worsened pathology for DMD investigation or for further understanding of the dystrophin isoforms. This includes a dystrophin-utrophin double

knockout mouse (dko), which exhibits a severe general pathology and death occurs after 2-3 months [73,85]. Other models aimed to 'humanise' the *mdx* mouse. For instance, Chandrasekharan *et al.* developed the Cmah$^{-/-}$*mdx* mouse which contains a deletion in the cytidine monophosphate-sialic acid hydroxylase (*Cmah*) gene. This gene is inactivated in humans and alters the expression of sialic acids found on glycans (by preventing conversion of N-acetylneuraminic acid to N-glycolylneuraminic acid). The authors observed a decrease in life span and muscle function in the Cmah$^{-/-}$*mdx* compared to the *mdx* [86]. The Tyler, Wells and Wood labs further demonstrated an earlier cardiac deterioration in the Cmah$^{-/-}$*mdx* mice compared to the *mdx*, but the worsened skeletal muscle pathology observed in the original paper could not be corroborated [87].

Other models have investigated the influence of the genetic background on disease pathology. The most commonly used *mdx* mouse is bred on a C57BL/10 background, but Fukuda *et al.* showed that breeding on the DBA/2J background induced a more severe pathology [88]. These results have been corroborated by several other groups, which have shown atrophy at a younger age and reduced regeneration in muscle compared to the *mdx* on the C57BL/10 background [89,90]. Although cardiac inflammation and fibrosis occurred much earlier in *mdx* on the DBA/2 background (7-8 weeks), there are concerns with regards to normal cardiac functioning with these mice as wild-types exhibit calcifications in the heart [90,91]. Notably, wild-type DBA/2J mice exhibit signs of hypertrophic cardiomyopathy at four months of age [92]. Therefore, to what extent this model is superior to the *mdx* on the C57BL/10 background remains to be established.

Although progress has been made, it should be noted that all these models are limited by their inability to properly represent disease pathology in humans. The dko mouse most closely recapitulates DMD disease severity, but nevertheless comprises an extra protein deletion not present in human patients. Therefore, there remains a need to establish a representative model available for wide research use, given their usefulness for testing experimental therapies.

1.1.4.2 Canine models

The dystrophin-deficient dog model, golden retriever muscular dystrophy (GRMD), was first characterised in 1988 [93] and, unlike the *mdx* mouse, it better recapitulates the disease observed in human patients [94]. These dogs carry a point mutation in intron 6 of the *Dmd* gene, leading to a frameshift mutation and a premature stop codon. Since then, several other dog breeds were discovered to have mutations in the dystrophin gene [94]. Additionally, the GRMD dog was back-crossed with Beagles, establishing the canine X-linked muscular dystrophy dog in Japan ($CXMD_J$) [95], although this model is slightly less severe [96]. The GRMD and $CXMD_J$ breeds remain the most commonly used dog models for research into DMD [97]. Muscular dystrophy dogs exhibit fibrosis [98,99], reduced motor [99,100] and heart function [96,101], and often succumb to cardiorespiratory complications [97]. Even though dystrophic dogs provide a better model for studying DMD pathology than the *mdx* mouse, they exhibit high inter-litter variability, and their use is impeded at least partially due to high costs and ethical considerations [97,102]. As such, mice remain the most widely used animal model for DMD.

1.2 Early pathological processes in DMD

Since the discovery of the dystrophin gene and protein, much effort has focused on elucidating the mechanisms underlying DMD pathology. To this day, the process remains complex with the involvement of many aberrant pathways. The absence of dystrophin makes myofibres more vulnerable to contraction-induced damage and this increases the intracellular calcium concentration, thereby activating calcium-dependent proteases and calpains. Moreover, many other molecular changes ensue as a result of the calcium dysregulation and of the mislocalisation of nNOS and other members of the DAPC, such as changes in mitochondrial function, NF-κB, MAPK, PI3/AKT, and in nitric oxide (NO) and reactive oxygen species (ROS) production. Pro-inflammatory cytokines are also secreted, causing inflammation and immune cell infiltration, contributing to a cycle of muscle necrosis followed by regeneration. Throughout the disease course, muscle tissue exhibits chronic inflammation and myofibres are gradually replaced with adipose and connective tissue.

1.2.1 Aberrant calcium signalling

One of the first events thought to influence DMD molecular pathology is the increase in intracellular Ca^{2+}, which plays a vital role in excitation-contraction (E-C) coupling and intracellular signalling [103]. Elevated intracellular Ca^{2+} levels activate Ca^{2+}/calmodulin (CaM), CaM kinase II and protein kinase A (PKA), which hyper-phosphorylate Ca^{2+} channels inducing further Ca^{2+} influx and downstream pathological processes [104–107]. Increased Ca^{2+} also leads to mitochondrial dysregulation, protease calpain-mediated necrosis, and NF-κB activation, which results in inducible NOS (iNOS)-mediated inflammation [108,109].

It is currently unclear what the precise mechanisms are that trigger Ca^{2+} influx and release from Ca^{2+} stores. Several processes have been proposed and explored regarding initial entry of Ca^{2+} into the cell, which include (I) membrane tears, (II) stretch-activated channels (SACs), (III) the Na^{+}-Ca^{2+}-exchanger (NCX) and (IV) voltage-gated Ca^{2+} channels (VGCC). The initial intracellular Ca^{2+} increase

brings about the activation of store-operated channels such as sarcoplasmic/endoplasmic reticulum Ca^{2+} ATPase (SERCA), the ryanodine receptor (RyR) and the inositol 1,4,5-triphosphate (IP_3) receptor (IP_3R), thereby further increasing the intracellular Ca^{2+} concentration.

1.2.1.1 Membrane tears

Membrane fragility in dystrophic muscles was suggested to cause tears in the sarcolemma upon muscle contraction, allowing the passive influx and efflux of ions and proteins [4,103,110]. This theory was supported by studies utilising membrane sealants in *mdx* mice, whereby the membrane sealant poloxamer 188 lowered the Ca^{2+} influx and improved left ventricular end diastolic volume in hearts of *mdx* mice [111,112]. Interestingly, studies investigating the effect of the membrane sealant on skeletal muscle showed no improvement or even harmful results [113,114]. These studies would suggest that poloxamer 188 may be exerting other effects than membrane sealing and indeed, the contribution of membrane tears to the increased Ca^{2+} influx has been debated [103]. In an extensive review, Allen and Whitehead highlighted that the original papers normally cited as evidence for membrane tears only provided evidence for increased fragility of the sarcolemma [4,115]. Moreover, they showed that the time required for intracellular Ca^{2+} to increase (10-20 minutes after contraction) in *mdx* muscle did not correlate with membrane tears (in the order of seconds), and leakage of ions and proteins may be explained by other mechanisms such as SACs and lipid peroxidation [103]. Despite these contrasting results, a Phase II clinical trial has been initiated to study the safety and efficacy in heart and diaphragm of poloxamer 188 in DMD patients (Carmeseal-MD, clinical trials identifier: NCT03558958). Treatment in the first patient was well tolerated and serum CK and cardiac troponin were reduced. Ongoing results from the trial will hopefully provide more information regarding efficacy and mechanisms of the drug.

1.2.1.2 Stretched-activated channels (SACs)

SACs have also been investigated as a possible reason for the initial Ca^{2+} influx [110]. These channels open upon contraction induced by stretch and allow the influx of cations. Inhibition of SACs

following exposure to stretched contractions significantly diminished the rise of intracellular calcium in skeletal muscle myofibres and ventricular cardiomyocytes, and the blocking of protein kinase C (PKC) and phospholipase C (PLC) fully restored store-operated Ca^{2+} entry [116,117]. It should be noted that the SAC inhibitors utilised in these studies were non-specific and may have also blocked Na^{+} channels [116]. Therefore, the observed reduction of intracellular Ca^{2+} may (partially) be mediated by inhibition of the SACs and/or the NCX or VGCC that open due to Na^{+}-induced membrane depolarisation [116–120]. Given their properties, some of the channels and subunits of SACs have been implicated in DMD pathology. These channels include the mechano-sensitive transient receptor potential cation (TRPC) channels, specifically TRPC1, TRPC3 and TRPC6, and transient receptor potential vanilloid 2 (TRPV2).

TRPC1 channels translocate to the plasma membrane following co-localisation with caveolin-3 and are activated by the ROS-dependent Src kinase, leading to an influx of Ca^{2+}. Dystrophic muscles display increased expression levels of TRPC1 channels, caveolin-3 and Src kinase [121]. Importantly, TRPC1 associates with α-syntrophin and loss of the DAPC complex in DMD may therefore partially explain the changes in intracellular calcium [122]. The role of TRPC1 in the heart remains more elusive, but protein expression levels increase with age in the *mdx* mouse [116].

Genetically modified mice overexpressing TRPC3 exhibited increased calcium levels and a dystrophic phenotype in skeletal muscle [123]. Similarly, when a double-negative mutant for TRPC3 was crossed with the *mdx* mouse, dystrophic histology and CK levels were improved [123].

The TRPC6 channels have predominantly been investigated in relation to DMD heart pathology, although sarcolemmal expression has been observed in myofibres (in contrast to its normal intracellular localisation), suggesting their involvement in dystrophic skeletal muscle [124]. TRPC6 inhibition in the *mdx* heart resulted in reduced contractions and arrhythmias [125], and decreased S-nitrosylation of many proteins, thereby improving cardiac function and diminishing fibrosis [126].

These results suggest an important function for TRPC6 channels in cardiomyocytes, and potentially also in skeletal myofibres.

Finally, TRPV2 channels are observed to induce increased cellular calcium entry in primary myotubes from human DMD patients, but not controls [117]. *Mdx* mice negative for TRPV2 exhibited a smaller force drop after consecutive contractions in the extensor digitorum longus (EDL) muscle and reduced membrane damage [127]. Similarly, *mdx* cardiomyocytes exhibited an overexpression of TRPV2 channels at the sarcolemma (compared to its normal intracellular localisation) and these channels mediated the increase of cellular Ca^{2+} influx [128].

1.2.1.3 Voltage-gated Ca^{2+} channels (VGCC) – L-type

The voltage-dependent L-type Ca^{2+} channel also plays an important role in intracellular Ca^{2+} concentration. It is connected to F-actin by sub-sarcolemmal proteins, including dystrophin and α-actinin [129,130], and is thought to be involved in muscle contraction by determining the plateau phase of the action potential [131]. The channel exhibits a delayed inactivation rate in the *mdx* heart [132]. Viola *et al.* showed that communication between L-type Ca^{2+} channels and mitochondria was important for metabolic function in healthy cells and this communication was altered in *mdx* cardiomyocytes, although the exact proteins involved were unclear [133,134]. Interestingly, aged *mdx* cardiomyocytes exhibited similar L-type current properties compared to controls, suggesting no involvement or compensatory mechanisms mediated by this channel at later stages in the pathology [135].

1.2.1.4 Store-operated Ca^{2+} release

Three main channels on the sarcoplasmic reticulum (SR) are involved in regulating intracellular Ca^{2+} concentration: SERCA, RyR and IP_3R. Upon intracellular Ca^{2+} increase, SERCA pumps the ion into the SR for storage. In *mdx* mice, the fast-twitch EDL muscle exhibited increased SERCA levels and reduced Ca^{2+} uptake, although similar results were not observed in the slow-twitch soleus [136].

Reports on SERCA expression in the heart are contradictory, with some observing no changes and others a down-regulation in *mdx* SERCA protein levels [137,138]. Interestingly, the SERCA inhibitor sarcolipin is significantly upregulated in *mdx* mice and introduction of a truncated dystrophin in muscle was able to reduce sarcolipin levels [139]. Moreover, knockdown of sarcolipin in dko mice improved muscle regeneration, function and life span [140]. As such, these results suggest a direct link between dystrophin and regulation of SERCA through sarcolipin.

RyRs are activated by Ca^{2+} binding, thereby leading to Ca^{2+}-induced Ca^{2+} release stimulating E-C coupling [141,142]. There are three known isoforms, RyR1-3, which are generally expressed in skeletal muscle, heart and the brain, respectively [142]. RyR in *mdx* myocytes may be leaky due to hyperphosphorylation by PKA or CaMKII [104,142,143] which induces RyR dissociation from the stabilising protein calstabin-2 [144]. Interestingly, treatment with a RyR calcium release channel stabiliser improved muscle function and dystrophic histology in the *mdx* [145] and this compound is currently being investigated for its therapeutic potential in DMD (ARMGO Pharma, stabiliser compound: S48168/ARM210).

Lastly, the IP_3R is a calcium sensor and normally closes when the intracellular calcium crosses a high concentration threshold. It is activated by IP_3, a downstream protein of PLC, and expression levels of the receptor and its ligand were found to be significantly higher in dystrophic versus control myocytes [146]. Receptor inhibition led to improvement in muscle pathology and a reduction in autophagy of mitochondria (mitophagy) [147]. Moreover, inhibition of PLC reduced the Ca^{2+} concentration in *mdx* cardiomyocytes, whereby older *mdx* animals (9 and 12 months) showed a larger Ca^{2+} decrease upon inhibition [148]. These studies demonstrated that the effect of SERCA and IP_3R on intracellular Ca^{2+} concentration varies throughout life span, suggesting an important role for age in dystrophic Ca^{2+} homeostasis.

Many studies have been performed to elucidate the role of Ca^{2+} in DMD pathology, with results indicating the interaction of multiple complex mechanisms.

1.2.2 Oxidative stress and mitochondrial dysfunction

Another pivotal factor thought to be important in the early stages of DMD pathology is oxidative stress. This is caused by an overproduction of ROS, which has been shown to impair autophagy and lysosome formation, induce lipid peroxidation, sensitise SACs, and induce NF-κB-mediated inflammation and fibrosis in *mdx* mice [103,149,150]. Several clinical trials have addressed ROS overproduction through antioxidants, but none showed any clinical benefit, despite promising preclinical results [151–154]. One of the major producers of ROS is the NADPH oxidase (NOX) enzyme. The *mdx* mouse exhibits increased levels of NOX subunits and ROS production, whereby inhibition of NOX resulted in a reduction of ROS [155]. This in turn decreased stretch-induced membrane permeability and reduced intracellular calcium levels [156].

Mitochondria also contribute to ROS production and are additionally important for cell metabolism, muscle contraction [141], Ca^{2+} storage [157,158], and cell death [159]. It is thought that this functional oxidative capacity of the mitochondria is disturbed in the *mdx* model, whereby mild oxidative stress induces a reduction in oxidative phosphorylation, resulting in decreased ATP production [160]. The elevated intracellular Ca^{2+} concentration in dystrophin-deficient cells also induces a sudden increase in mitochondrial membrane permeability through the mitochondrial permeability transition pore (PTP). The PTP is a voltage-sensitive channel and an increase in the mitochondrial Ca^{2+} concentration results in the opening of this channel, which leads to mitochondrial swelling. Short-term opening of these channels is thought to be beneficial as it allows mitochondrial regulation of the intracellular Ca^{2+} and ROS balance [161,162], but their long-term opening is detrimental to the cell and induces necrosis of the mitochondria [163], thereby contributing to myofibre death [120].

1.2.3 NO and NOS

An important second messenger in cell physiology is the signalling molecule NO. It is produced by NOS of which there are three isoforms: nNOS, endothelial NOS (eNOS) and iNOS. nNOS and eNOS

are both constitutively expressed in muscle and heart, and activated by the Ca^{2+}-dependent calmodulin. eNOS is associated with caveolin-3 on the sarcolemma, whereas nNOS is associated with the dystroglycan complex and is in close proximity to SERCA and RyR [121,164–166]. Conversely, iNOS is only expressed in the cell during inflammation and is highly expressed in immune cells [164,165]. The localisation of NOS enzymes within the cell is crucial to their function as NO is only transiently active and thus needs to reach its target quickly [166].

In the healthy skeletal muscle and heart, NO is thought to play many functions including; (I) Activation of guanylyl cyclase (GC) which in turn generates cyclic GMP (cGMP). The downstream proteins, e.g. PKG, play a role in E-C coupling, although the extent of their function in heart and muscle remains to be established [160,166]; (II) Stimulation of ATP production in the mitochondrial respiratory chain and inhibition of mitochondrial cell death by binding to cytochrome c [164,167]; (III) Modulation of SERCA, RyR and histone deacetylase (HDAC) through cysteine S-nitrosylation [164,166]; (IV) Activation of satellite cells following muscle damage and assistance in normal mitochondrial development [164].

Due to its displacement from the sarcolemma, nNOS levels are considerably lower in DMD patients and the *mdx* mouse [168], and its vasodilator capacities are impaired [169]. Studies downregulating nNOS in *mdx* mice exacerbate muscle hypertrophy and inflammation [170]. In contrast, transgenic up-regulation of nNOS in the *mdx* mouse corrected the muscle and heart phenotypes, with a decrease in inflammatory markers, fibrosis and apoptosis. Some aspects of heart function also improved, such as SV and EF [171,172]. eNOS has been investigated less, but may also play an important role in DMD given its importance in cardiac function and its link to caveolin-3, which is also differentially expressed in dystrophic muscle [173,174].

Mitochondria are also a target of NO signalling and its downstream effectors. Overexpression of GC in 12 and 20 week old *mdx* mice improved muscle function and cardiac endurance, and led to enhanced mitochondrial function and reduced heart production of lactate dehydrogenase, a marker

of tissue damage [175]. The results suggest that absence of dystrophin disrupts cardiac metabolism, although the detailed mechanism(s) remain unclear [176].

Together these studies underscore the importance of ROS and NO function and their interaction with intracellular calcium and metabolism.

1.3 Muscle progenitor cells

An important aspect of DMD pathology is the regeneration process that ensues following myofibre necrosis. Several resident progenitor cells have been identified in skeletal muscle, which have been further investigated for their role in DMD. Adult heart progenitor cells will not be discussed here given the reservations concerning their existence [177].

1.3.1 Satellite cells

Satellite cells are a heterogeneous group of muscle-specific progenitor cells that reside in their niche between the sarcolemma and basal lamina of the muscle fibres. Satellite cells are kept in a quiescent state in healthy muscle, whereby over 500 genes are involved in inhibiting proliferation, preserving cell health and maintaining their anatomical positioning [178]. These cells are characterised by the expression of paired-box 7 (Pax7) which ensures its myogenic lineage [179]. Upon tissue injury, most satellite cells activate rapidly for repair [180], which induces expression of myoblast determination protein 1 (MyoD) and myogenic factor 5 (Myf5) [181–185] through the p38/β-MAPK pathway [186]. A subset of these cells [180] will reduce MyoD and Myf5 expression through Notch and Sprouty1 [185] and return to their quiescent state [186], whereas the majority will undergo further myogenic differentiation, characterised by myogenin (MyoG) expression and a decrease in Myf5 [187], and fuse with existing myotubes. Around 10% of satellite cells are negative for *Myf5* and studies have shown that these cells preferentially divide asymmetrically (one daughter cell self-renews, the other differentiates), thereby maintaining the stem cell pool. This is in contrast to myogenic differentiation observed in the remaining Myf5 positive cells [188]. The satellite cell population is also maintained through wingless/integrated (Wnt)7a signalling, which is an important factor for symmetric cell division [189]. In contrast, the canonical Wnt-β-catenin pathway has been shown to promote C2C12 myoblast differentiation, indicating multiple roles for this pathway in muscle satellite cell homeostasis [190].

Interestingly, Dumont *et al.* discovered that dystrophin is important in asymmetric cell division, where it aids the apicobasal polarisation of important markers of cell polarity, Mark2 and Pard3 [191]. The absence of dystrophin in *mdx* progenitor cells led to dysregulation of the apicobasal axis, thereby maintaining a higher number of satellite cells while impairing regeneration. In contrast, other studies have suggested a depletion of the satellite cell pool in DMD [192], although importantly, biopsies from patients in the early and advanced stages of the disease show an increase in satellite stem cells [193,194]. Given these findings, it is thought that satellite cells in DMD remain in a state of quiescence due to failure of passing the spindle assembly checkpoint [195,196], decreasing satellite cell functionality. Diametrically opposing results have been obtained regarding the regenerative potential of satellite cells. Boldrin *et al.* illustrated that satellite cells from young and old *mdx* mice contributed to regeneration *in vitro* [197], suggesting that the environment influences the regenerative capacity of satellite cells. Furthermore, stem cells obtained from patients that were corrected for dystrophin *ex vivo* were engrafted into *mdx* muscle and able to populate the myofibres [198]. In contrast, a recent study by Meng *et al.* demonstrated that CD133+ cells (a precursor of satellite cells) derived from DMD patient muscle (a heterogeneous mixture of satellite cells, myoendothelial cells, pericytes and fibroblasts) had a reduced regenerative capacity *in vitro* [199], and the differing results highlight the uncertainty as to what extent DMD satellite cells retain their regenerative potential.

Aside from myogenic differentiation, a small proportion of satellite cells are also able to commit to a fibrogenic lineage in aged mice [200]. This is thought to be mediated by an elevated canonical Wnt pathway due to transforming growth factor β (TGFβ) 2 activation, inducing loss of myogenic potential [201]. These results further highlight the importance of the environment on differentiation potential. However, many aspects remain unclear, especially given that the Wnt pathway has also been implicated in promotion of myoblast differentiation. This disparity may be caused by cell state (e.g. quiescent satellite cell or activated myoblast), involvement of various Wnt ligands inducing differing outcomes, or the relatively few cells undergoing fibrogenic differentiation

being overshadowed/not measured in other studies that focus on the myogenic lineage-committed satellite cells.

1.3.2 Fibro-adipogenic progenitor cells

More recently, the fibro-adipogenic progenitor (FAP) cell has been identified, demonstrating multipotent differentiation into fibroblasts and adipocytes, among other lineages [202–204], and is present in both skeletal muscle and heart [203,205]. These cells are positive for platelet-derived growth factor receptor α (PDGFRα) and are found in the interstitial space between myofibres. Following tissue injury they secrete fibroblast growth factors (e.g. FGF2 and 6) that induce myogenic differentiation in satellite cells [202,203,206] . Upon tissue repair, FAP cell numbers generally return to basal levels, although with chronic injury, they persist and differentiate into fibro-adipocytes [202,203].

FAP cells are activated in dystrophic muscle [207] and their regulation is at least partially influenced by NO [208]. NO increased miR-27b expression (microRNAs (miRNAs) detailed in **Chapter 1.6**), thereby downregulating peroxisome proliferator-activated receptor γ (*Pparγ*) and inducing inhibition of FAP differentiation in skeletal muscle [208]. The mislocalisation of nNOS and subsequent decrease in NO production in dystrophic muscle likely contributes to FAP differentiation and fibrotic pathology. Interestingly, the function of FAPs can be modulated by HDAC inhibitors in young *mdx* mice. Following HDAC inhibitor treatment, FAPs from young *mdx* mice preferentially differentiated into myotubes and promoted myogenic differentiation in satellite cells [209,210]. In contrast, HDAC inhibition had no effect on FAPs from old *mdx* mice, resulting in continued repression of satellite cell differentiation and FAPs forming adipocytes [209,210]. These striking results highlight the importance of the environment and early treatment. Moreover, it is clear that these cells are important for efficient muscle regeneration, with complex communication between FAP cells, fibroblasts and satellite cells [211].

1.3.3 Other muscle-resident progenitor cells

Other progenitor cells with multipotent differentiation capacities have also been identified, which include bone marrow-derived stem cells [212], muscle-derived stem cells [213–215], muscle side population cells [179,216], mesoangioblasts [217], pericytes [218,219], PW1 cells [220] and Twist2 cells [221]. Apart from the Twist2 cells that contribute to specific myofibre types, more recent research suggest that many of these progenitor cells may not contribute substantially to the myogenic lineage or they require specific cues from *Pax7*-positive satellite cells to differentiate into myotubes [222,223]. Whether this characteristic interferes with their therapeutic potential in DMD remains to be established, although several studies have demonstrated their ability to integrate and contribute to the muscles following muscle injury in healthy animals or upon their systemic delivery in DMD models [219,224,225].

1.4 Fibrosis

The extracellular matrix (ECM) is an important structure in muscle morphology and its functions include muscle maintenance and enhancing load bearing [226]. During muscle repair, ECM deposition is thought to provide a scaffold and is afterwards removed by factors inducing degradation, including serine proteases and matrix metalloproteinases [227]. However, in DMD, ECM deposition becomes abnormal and excessive, leading to the development of fibrosis, with changes in collagen subtype expression compared to controls [227–230]. This fibrotic damage persists and impedes muscle function. Fibrotic mechanisms are generally thought to be similar between tissues, although small differences may exist.

Several important pathways have been identified in DMD fibrosis, with perhaps the most important one being TGFβ1. This secreted cytokine has been linked to many functions, including cell proliferation and immune regulation [231]. It binds to the TGFβ receptor I and II complex and is able to activate several (non-)canonical downstream pathways. The canonical pathway phosphorylates transcription factors Smad2/3, which form a complex with Smad4 and translocate to the nucleus for activation of target genes involved in fibrosis. Other pathways that can be activated by TGFβ1 involve several arms of the MAPK pathway (JNK, p38 and ERK) and PI3/AKT, although it is unclear how these interact in detail. TGFβ1 exerts its fibrotic function through its communication with fibroblasts, which in turn secrete ECM components, such as collagen [231]. Its expression can be inhibited by an increase in insulin-like growth factor (IGF), which reduces Smad3 phosphorylation [232].

One of the downstream targets of TGFβ1 is connective tissue growth factor (CTGF) [233], and its decrease improves endurance and muscle strength, in addition to reducing fibrosis in the *mdx* [234]. Moreover, it is able to prevent myoblast differentiation through downregulation of desmin and MyoD [235]. Studies have shown that expression of TGFβ1 and CTGF positively correlated with *mdx* disease pathology and severity [236], and this pathway axis appeared very important for the presence of pathological fibrosis [237]. Interestingly, Morales *et al.* found a possible link between CTGF and the

renin-angiotensin system, which is important for blood pressure regulation. Angiotensin-converting enzyme (ACE) was shown to be upregulated in *mdx* regenerating fibres, fibroblasts and infiltrating macrophages [238]. Its inhibition improved fibrotic muscle phenotype by decreasing CTGF expression, without affecting TGFβ1 [239]. To what extent this system plays a role in DMD fibrosis remains to be established.

Another aspect of the increase in fibrosis is the dysfunctional regulation of degradation proteins. Matrix metalloproteinases (MMPs) comprise a large family of proteolytic, calcium-dependent, enzymes that are involved in the breakdown of the ECM. Transcripts from MMP-2 and tissue inhibitors of metalloproteinases (TIMP) 1 and 2, in addition to MMP-2 activity, were significantly upregulated in DMD patient muscle [240]. Several of these factors have been further investigated for their function (e.g. MMP-2 is involved in angiogenesis [241] and MMP-10 in muscle regeneration [242]), but most efforts have focused on MMP-9, a gelatinase important for collagen IV degradation. Upon tissue injury, this protein is rapidly expressed and enzymatically activated to aid ECM remodelling [243]. However, its functions become pathogenic upon chronic activation contributing to fibrosis, and high MMP-9 levels are observed in DMD patients, which increase over time [243,244]. Several studies have shown that MMP-9 was able to activate TGFβ1 [245] as well as cleave laminin [246] and β-dystroglycan [247]. These targets play an important role in DMD pathology and the development of fibrosis, and MMP-9 may be contributing to the dystrophic phenotype through these pathways. Overexpression of MMP-9 in control and *mdx* mice led to skeletal muscle hypertrophy [248]. In contrast, MMP-9 inhibition in the *mdx* mouse improved pathology and regeneration through stimulation of myogenesis, the Notch pathway (involved in satellite cell proliferation) and a preferential activation of canonical over non-canonical Wnt pathways (involved in muscle regeneration) [249–251].

Several other factors have been implicated in DMD fibrotic pathology, such as miR-21 (miRNAs detailed in **Chapter 1.6**) and plasminogen activators. The activation of the TGFβ1 pathway by

the urokinase-type plasminogen activator followed by translocation of Smad proteins, allowed Smad binding to the Drosha complex, thereby facilitating miRNA maturation [252,253]. miR-21 subsequently increased fibrosis. However, the accuracy of this model is unclear as TGFβ1 has also been observed to downregulate miR-29 and miR-206 expression in C2C12 myoblasts and primary muscle cells [254]. Together, the results illustrate a complex fibrotic pathology in DMD.

1.5 Therapeutic interventions for DMD

1.5.1 Current clinical disease management

There is currently no cure for DMD and so therapy has largely been limited to the management of symptoms. The three predominant treatment approaches include glucocorticoids, for amelioration of the skeletal muscle phenotype, mechanical respiratory support and cardiac management. Glucocorticoids significantly improve muscle strength and function [19,255] and more recent studies have implicated long-term corticosteroid use in the stabilisation of pulmonary function, prolonging ambulation, reducing the prevalence of scoliosis and delaying death [19,256,257]. Glucocorticoids have also been associated with delaying the onset of cardiomyopathy by 4% for each year of steroid treatment [258]. Commencement of treatment is recommended once motor function progression halts during the plateau phase around 4-8 years of age. Side effects include Cushing's syndrome and osteoporosis [259], and so treatment is administered on alternate days, although more recent evidence suggests an advantage for daily dosing [260,261].

Pulmonary function is carefully monitored in DMD patients and deterioration in respiratory muscles leads to respiratory insufficiency and pulmonary hypertension [260]. This pulmonary hypertension in turn influences cardiac function and contributes to DCM [262]. Therefore, assisted mechanical support is given as soon as nocturnal hypoventilation is apparent, with the aim of maintaining adequate ventilation and coughing reflex [263]. A non-invasive positive-pressure ventilation machine with a mechanical insufflation-exsufflation device is the preferred respiratory support device and has substantially reduced mortality in DMD patients [264]. As a last resort, tracheostomy is utilised if non-invasive ventilation is no longer effective [265].

Lastly, approaches to delay the decline in cardiac functionality include ACE inhibitors, β-blockers and diuretics, which appear to be cardioprotective [266,267]. ACE inhibitors prevent the conversion of angiotensin-I to angiotensin-II (Ang-II), reducing circulating levels of Ang-II. As Ang-II is

able to stimulate aldosterone, thereby activating fibroblasts, ACE inhibitors reduce myocardial fibrosis [268]. The inhibitors are generally implemented upon LV systolic functional decline [269], whereby treatment in DMD patients with an EF below 55% resulted in significant improvements in cardiac function and delayed the progression of cardiomyopathy [270].

Another cardiac intervention strategy includes beta-blockers, which are often prescribed to patients presenting with arrhythmia and systolic dysfunction [269]. They prevent the binding of catecholamines to adrenergic receptors, leading to a reduction in sympathetic nervous system activity. Cardiologists often prescribe a cocktail of ACE inhibitors, β-blockers and diuretics which significantly improves cardiac function and survival in DMD patients [270,271]. However, regular cardiac assessments are imperative to ensure the correct treatment regimen, as it has been observed that administration of the β-blocker metoprolol was detrimental to RV function when administered at early stages of cardiomyopathic progression [272].

Cardiac resynchronisation therapy may be considered in a subset of DMD patients who are unresponsive to pharmacological interventions [273]. Installation of a bi-ventricular pacemaker allows the synchronous pacing of the septal and lateral walls of the left ventricle. Other measures such as left ventricular assist devices HeartMate II and HeartWare, have also been employed in an effort to reduce heart failure [274,275]. In both cases these devices markedly improved cardiac function and quality of life, thus demonstrating their potential for DMD patients who do not respond to conventional interventions. However, they are generally more invasive methods and the long-term benefits should be more carefully examined [269].

1.5.2 Novel therapeutic strategies targeting dystrophin absence

A large proportion of the preclinical research has focused on finding novel treatment options to target the absence of the dystrophin protein. Several therapeutic strategies have made significant progress over the last decade and are summarised in **Table 1.2**. Importantly, an exon skipping phosphorodiamidate morpholino oligomer (PMO), eteplirsen (**Chapter 1.5.2.1**), and a stop-codon

read-through treatment, Translarna (**Chapter 1.5.2.2**), have been approved by the US Federal Drug Administration (FDA) and the European Medicines Agency (EMA), respectively. The current section summarises the development of the most notable strategies.

1.5.2.1 Exon skipping

A promising approach for treating DMD patients is the use of antisense oligonucleotides (AONs) to induce skipping of *DMD* exons so as to correct the aberrant reading frame [276]. AONs are short, single stranded nucleic acid sequences which are complementary to a target pre-mRNA splicing signal. For the *DMD* gene, AONs sterically block the binding of splicing factors (which normally facilitate intron removal), thereby skipping the desired exon and producing a functional, albeit shorter, dystrophin protein [277]. This therapy is capable of treating ~83% of DMD patients with dystrophin mutations, specifically 79% of patients with deletions, 91% with small mutations (mostly single nucleotide polymorphisms (SNPs)) and 73% with duplications [278]. A significant shortfall of this approach is that a single AON is only capable of targeting one exon at a time, focusing efforts on exons which would assist the greatest number of patients [278]. However, recent studies have demonstrated the possibility of using a multi-exon skipping cocktail in the *mdx52* and $CXMD_J$ models [279–281].

The predominant AON chemistries which have been undergoing clinical evaluation are PMOs [282] and 2'O methyl phosphorothioate RNA (2'OMePS) [282–285]. The backbone chemistry of the AON influences its affinity for serum proteins (which is higher for negatively charged backbones), and by extension affects efficacy due to filtering and excretion of the AON [286]. Of particular interest are the clinical developments of drisapersen (2'OMePS) and eteplirsen (PMO). Although drisapersen induced up to 15.6% of dystrophin protein re-expression in patient muscle following a 6 mg/kg dose (*n*=12) [287], long-term clinical benefit was not significant in this safety and efficacy trial after 49 weeks and a phase II trial failed to meet its primary endpoint (*N*=53, including placebo group) [285]. Interestingly, patients who were able to walk between 300-400 m in the 6-minute walk test (6MWT; assessing the distance walked by patients within 6 minutes) at baseline exhibited a significantly slower

decline in 6MWT distance following drisapersen treatment compared to placebo (*n*=80) [288]. Further studies, however, showed safety concerns with higher, and more efficacious, doses of the drug [289] and FDA approval was not received, resulting in the cessation of its development [290].

Eteplirsen exhibited safety and exon skipping ability in several clinical trials [291,292]. Even though the FDA advisory committee was ambivalent over the effectiveness of the drug, eteplirsen received provisional FDA approval in a controversial decision in 2016 [293]. Evidence from the clinical trials was limited to a modest dystrophin increase in patient biopsies [284], with only 12 patients included in the trial and progress measured against natural history controls. Nevertheless, long-term assessments showed significantly lower declines in 6 minute walk distance compared to the controls [292]. More recent evidence demonstrated exon skipping in all patients treated with eteplirsen and significant increases in dystrophin-positive fibres, although total protein levels were still low (~1-2%) [294]. Further functional evidence will be necessary to determine the clinical benefit of eteplirsen in patients and preserve FDA approval. Other exon skipping compounds, such as Viltolarsen (developed by Nippon Shinyaku) [295] and DS-5141b (developed by Daiichi Sankyo), are currently undergoing safety and efficacy assessments in clinical trials (NCT02740972 and NCT02667483, respectively).

Although PMOs and 2'OMePS have demonstrated potential for treating DMD in preclinical and clinical studies, the confounding issues are their relatively poor systemic delivery and low exon skipping efficiency, as observed with eteplirsen [282,283,296,297]. In an effort to overcome these obstacles, a new AON chemistry has demonstrated marked preclinical success and was capable of restoring dystrophin in skeletal muscle and heart, with low levels in the brain of DMD mouse models (tricyclo-DNA oligomers). However, it should be noted that these positive findings required multiple administrations and very high doses (200 mg/kg per week) [298].

Importantly, cell penetrating peptides (CPPs) have also been developed to improve systemic delivery. These short peptide sequences are chemically conjugated to neutral AONs, such as PMOs, to facilitate delivery across the plasma membrane. A multitude of studies have investigated peptide

conjugated AONs in the context of DMD and these AONs can broadly be classified into 3 distinct groups namely the Pips (peptide nucleic acid (PNA)/PMO internalisation peptide), the arginine rich, and the phage and chimeric peptides (latter two summarised in **Table 1.2**).

The Pips have undergone several development stages in an effort to improve systemic targeting [299–301]. These peptides have demonstrated skeletal muscle and cardiac dystrophin expression and arginine-rich CPPs conjugated to PMO were the first to show activity in the heart [302]. Development of the Pip6-series conjugated to PMOs (Pip6a, b, e and f) demonstrated enhanced cardiac targeting, while maintaining efficacy in skeletal muscles. Cardiac dystrophin restoration levels were between 12-57% of wild-type following a single 12.5 mg/kg administration [303]. Moreover, exercise-induced cardiomyopathy was prevented following long-term administrations of 10 mg/kg Pip6f-PMO [304]. It was found that the hydrophobic core was critical for targeting the heart. However, the high toxicity profile of these peptides is a concern and therefore efforts had been made to reduce the number of arginine residues (thought to contribute to toxicity) in further peptide iterations (Pip7, 8 and 9) [305]. Toxicity assessments are currently ongoing.

Overall, with the advancement and approval of several novel therapeutic strategies targeting the underlying dystrophin absence, it is clear the field is rapidly advancing, thereby hopefully resulting in a viable therapeutic option for all patients in the near future.

1.5.2.2 Stop codon read-through therapy

A small number of patients (~10-15%) have a nonsense mutation which leads to a premature stop-codon thereby disrupting the open reading frame [306,307]. Antibacterial drugs called aminoglycosides are able to induce ribosome ‘read-through’ of these premature stop codons without affecting normal stop codons, thereby restoring the reading frame and generating a functional dystrophin protein [306,308,309]. A high-throughput screen identified PTC124, a small molecule able to induce read-through of premature stop codons, which has shown significant promise both *in vitro* and *in vivo* [309]. Positive preclinical results have led to the development of Translarna, which received

conditional approval by the EMA as it induced stop codon read-through in patients able to walk between 300-400m at baseline in the 6MWT (*N*=99, including placebo group). Its efficacy will be closely monitored for several years to better understand functional outcomes and inform decisions on continued EMA approval [310,311]. However, Translarna failed to induce stop codon read through in stable and transient luciferase reporter systems [312], potentially suggesting other mechanisms behind this drug's activity.

Other studies have also identified the small molecules RTC13 and RTC14 capable of inducing stop codon read-through. These compounds were administered intramuscularly and intravenously in *mdx* mice, and RTC13 demonstrated better dystrophin restoration in skeletal and heart muscle compared to gentamicin (see **Table 1.2**), RTC14 and Translarna. In addition, muscle function was improved and serum CK levels were decreased in *mdx* mice treated with RTC13 [313]. RTC13 provides a promising new therapeutic molecule for patients with a premature stop codon and a patent for this drug has now been submitted [314].

1.5.2.3 Cell-based therapy

Cell-based therapy aims to transplant dystrophin-positive cells into DMD patient tissue, for integration with the myotubes and co-population of the satellite cells. These cells can be derived either from healthy precursor cells or from patient cells that are genetically modified *ex vivo* [315]. The first successful *in vivo* transplantation in a dystrophic mouse model was performed by Partridge *et al.* who showed that wild-type myoblasts were able to fuse with dystrophic muscle in congenic strains [316]. Since, several different muscle precursor cells have been explored for therapeutic purposes in DMD including myoblasts, fibroblasts, bone-marrow derived stem cells, CD133+ stem cells and mesoangioblasts (see **Table 1.2**) [316–325].

Several groups have aimed at utilising genetically modified patient precursor cells as treatment, as it allows for circumvention of immunological suppression normally required when introducing foreign material (although recent evidence suggests a 'pro-survival cocktail' may improve

engraftment as well [326]). This involves *in vitro*/*ex vivo* modification of the genome using nucleases [141,327–329]. One study assessed genetic modification of patient iPS cells *in vitro* and observed dystrophin expression following skeletal muscle cell differentiation [328]. More recently, Siemionow *et al.* generated chimeric myoblasts of dystrophin positive and negative cells *in vitro* and, following local administration, achieved around 37% patchy dystrophin expression in the gastrocnemius muscle of *mdx* mice [330]. This method may circumvent rejection of engraftment and provides a new avenue for cell therapy.

Overall, genetic modification of patient cells *ex vivo* followed by engraftment provides a valuable treatment option due to a reduced or non-existent immunological response. However, this technique is still challenged by the difficulty to induce and sustain adequate levels of dystrophin, and the high levels of progenitor cells necessary, especially for systemic delivery. Moreover, intramuscular progenitor cell delivery has achieved the most successful results, but this approach is unable to target the more difficult to reach tissues [307].

1.5.2.4 Viral gene therapy for dystrophin transgene delivery

Another therapeutic strategy undergoing development is the use of viral vectors to deliver a dystrophin transgene to the cell. Given the enormous size of the *DMD* gene, multiple studies have endeavoured to distinguish the integral components of the dystrophin protein to develop a shortened version that may be inserted into the viral genome (mini- or microdystrophin) [331]. Several viruses have been considered as a potential delivery vector, including lentivirus, adenovirus and adeno-associated virus (AAV; first two summarised in **Table 1.2**).

In order to safely apply the virus, AAV has been modified to exclude all viral genes, and leave only essential repeats for replication (recombinant AAV, rAAV) [307], whereby the AAV requires co-transfection of a vector carrying components necessary for replication. The various AAV serotypes exhibit different tropisms [332], with rAAV2/AAV8, rAAV6 and rAAV9 exhibiting particular promise in

the *mdx* heart for mini- or micro-dystrophin delivery [333,334]. This cardiac targeting is particularly important given the difficulty of efficiently restoring dystrophin in the heart.

IV administration of rAAV6 microdystrophin was successful at restoring dystrophin in tibialis anterior (TA) muscle, diaphragm and heart in young *mdx* mice [335]. Interestingly, heart function did not recover even though heart mass was normal [335]. Viral delivery in 20-month-old *mdx* mice also improved respiratory and skeletal muscle function [336], suggesting that even though *mdx* muscles have been significantly damaged by the disease, treatment may still be capable of improving some muscle pathology [336]. rAAV9 has shown the greatest promise in transfecting the heart [337]. Mini- and micro-dystrophin rAAV9 administration in young and adult *mdx* mice restored dystrophin expression and improved cardiac function [338–340]. Further studies utilising the GRMD dog model administrated intravenous mini-dystrophin using rAAV9 in neonatal dogs and revealed varied dystrophin expression (between 15% and 100% depending on the muscle analysed) [338].

Clinical trials using viral vectors for truncated dystrophin delivery are currently recruiting patients for Phase I trials (NCT03362502, NCT03368742 and NCT03375164). One phase I clinical trial has already been performed, which tested the safety of a chimeric vector of AAV1 and AAV2 (rAAV2.5) and discovered the virus was well tolerated by patients [341]. However, these patients produced T-cells specific to epitopes of dystrophin-positive cells [342]. This suggests complications for viral dystrophin delivery treatment as well as other therapeutic strategies aiming to restore dystrophin, and therefore should be considered in future advancements of treatment.

In addition to antibodies against dystrophin, immunological responses to the AAV virus have also been observed in humans, and utilisation of viral delivery may require immune suppression in some patients [343,344]. Viral delivery treatment is further confounded by the high titres of virus that are needed to reach all muscles. The latter factor has been addressed by the generation of chimeric vectors, such as rAAV2/8, containing microdystrophin. Lower titre levels resulted in almost 100%

transfection in 10 week old *mdx* mice, with effective dystrophin expression in skeletal muscles and heart, improved muscle function and no observed immune response [345].

The large number of investigations have resulted in significant progress in the field of a truncated dystrophin protein delivery using viral vectors. Nevertheless, special care should be taken regarding immunogenicity against prevalent viruses such as AAV [307,346], and also the dystrophin protein itself [342]. Moreover, repeat administration will be problematic due to the presence of neutralising antibodies arising from the first treatment [343]. Lastly, incorrect insertions of the virus into the host genome may occur with vectors such as lentiviruses [307]. Further research will be necessary to address these important concerns with regards to therapy.

1.5.2.5 CRISPR-Cas9

An exciting extension of the exon skipping approach has been the development of the clustered regularly interspaced short palindromic repeats-CRISPR associated 9 (CRISPR-Cas9) system to permanently excise *DMD* exons from the genome. The gene-specific guide RNA associates with the Cas9 enzyme, resulting in a break in the DNA which can be repaired through homologous or non-homologous end-joining. Since its discovery, many studies have utilised this system for dystrophin gene correction as it provides a relatively easy tool for gene editing. Virus-delivered CRISPR-Cas9 endonuclease and guide RNA administration was able to induce exon deletion in skeletal and heart muscle of *mdx* mice, which exhibited functional muscle improvement (dystrophin restoration ranging between 39-67% intramuscularly and 10-50% systemically) [347–349]. Furthermore, studies with a DMD dog model carrying a mutation in exon 50 showed extremely efficient exon skipping in skeletal (3-90%) and cardiac (92%) muscle with a high dose ($1x10^{14}$ viral genomes/kg) [350]. Although existing concerns for viral delivery of micro- and mini-dystrophin are also relevant for CRISPR-Cas9 treatment, the preclinical results are extremely promising given the high levels of dystrophin restoration achieved, and further studies will hopefully determine its efficacy in the clinic.

1.5.2.6 Utrophin upregulation

Utrophin upregulation was one of the first therapeutic strategies developed to compensate for the lack of dystrophin in the cell. The dko mouse model lacking dystrophin and utrophin (*mdx*/utrn$^{-/-}$) exhibits worsened skeletal muscle and cardiac pathology compared to the *mdx* and has a life span of only 2-3 months [73,85,351,352]. Overexpression of utrophin in *mdx* mice was able to prevent dystrophic muscle pathology [353], indicating that utrophin is able to compensate for the absence of dystrophin in the *mdx*. Therefore, several studies have investigated the effects of upregulation of utrophin, with recent results indicating the most effective outcomes if utrophin isoforms A' and F are targeted [354]. Several strategies of utrophin upregulation in *mdx* mice have shown positive improvement of skeletal muscle phenotype [353,355–359] and most recent viral delivery of a micro-utrophin transgene was able to target both heart and skeletal muscles, showing physiological improvement [360]. The preclinical data provide significant evidence that utrophin upregulation could be an effective therapy in DMD patients. Therefore, an oral drug targeting utrophin upregulation, SMT C1100 (Ezutromid), was developed. Preclinical studies identified increased utrophin RNA and protein levels, reduced pathology and improved muscle function in treated *mdx* mice [361]. Phase I clinical trials showed that the drug was well tolerated, leading to the progression into Phase II [362]. However, the Phase II trial failed to meet its primary and secondary endpoints after 48 weeks of treatment, and development of this drug has now been ceased (*N*=38). The results were quite surprising given that an interim report after 24 weeks of treatment indicated reduced inflammation and muscle damage in patients.

Negative findings in the clinical trial may be explained by many factors, including advanced disease pathology, inadequate endpoints or ineffective utrophin targeting of the drug. Another reason may be that the drug upregulated utrophin expression (as observed in Phase I) but was unable to localise it to the correct subcellular domain (as is shown to be effective with biglycan treatment; **Table 1.2**) [363]. Indeed, BMD and DMD patients naturally exhibit higher utrophin levels, which gradually

increase over time [364]. This may suggest that it is not utrophin expression *per se*, but also its location in the cell that may influence its efficacy in ameliorating DMD pathology. Perhaps the most effective strategy may be a combination of utrophin upregulation and localisation.

Table 1.2 DMD (pre-clinical) therapies targeting the absence of dystrophin (modified from own review paper [365]**).**

Treatment	Research stage	Results	Selected references
		Exon skipping	
2'O MePS AON	Preclinical: *mdx*	IM administration in *mdx* mice revealed low dystrophin restoration, even with multiple high doses. Repeated systemic delivery of the compound was able to induce ~5% dystrophin expression in skeletal muscle, though no expression could be detected in the heart.	[283,287–289,366]
	Clinical: Phase III trial	Clinically, 6mg/kg was the maximally tolerated dose in patients. Phase III trial did not meet 6MWT endpoint, although a subpopulation able to walk 300-400 m at the start of the trial showed significant improvement following treatment.	
CPP-AONs - Arginine rich	Preclinical: *mdx* and *mdx*/utrn$^{-/-}$	Multiple IP administrations of P007 produced ~100% dystrophin in diaphragm and low levels in skeletal muscles. Single IV restored dystrophin in skeletal muscle and diaphragm, and ~50% in the heart. Treatment in the *mdx*/utrn$^{-/--}$ mouse improved mortality rate and corrected kyphosis. In contrast B-peptide was less toxic, whereby repeat and high dose IV administration demonstrated impressive exon skipping, notably in heart (72%). Improvements in cardiac function, with preserved diastolic function after 6 months.	[73,302,367–373]
	Preclinical: $CXMD_J$	B-peptide PMO was also used for a multi exon skipping cocktail in $CXMD_J$ dogs, which restored dystrophin in the heart and improved electrocardiogram abnormalities.	
CPP-AONs - Phage Peptides	Preclinical: *mdx*	Several peptides have been discovered through a phage library: MSP enhanced *in vivo* skeletal and cardiac muscle binding capacity. B-MSP-PMO showed 2-5 fold improvement in skeletal muscle compared to B-PMO. A 12-	[374–379]

		mer phage resulted in ~25% dystrophin expression in skeletal muscle (75mg/kg). A 7-mer phage conjugated to 2'OMePS resulted in exon skipping in multiple tissues including heart and diaphragm. Muscle-specific cyclic peptide (cyPep10) conjugated to 2'OMePS AON resulted in improved muscle delivery and exon skipping in the *mdx*.	
CPP-AONs - Pips	Preclinical: *mdx*	Pip2a and Pip2b induced strong exon skipping following IM administration and IV injection of Pip5e resulted in systemic high dystrophin restoration. Pip6-PMO series: Pip6a, Pip6b and Pip6f exhibited best dystrophin expression in heart. Long-term IV administration prevented deterioration in heart function following exercise.	[301,303,304]
NS-065/NCNP-01	Preclinical: DMD patient cells	The compound NS-065/NCNP-01 restored dystrophin protein at 55-87% one week after the second weekly administration.	[295,380]
Viltolarsen	Clinical: Phase I	The preclinical data led to a Phase I study to assess the safety and pharmacokinetics. The drug was well tolerated and induced exon skipping of ~3 % in most patients. A phase II study has recently been completed with higher doses of NS-065/NCNP-01 (40 mg/kg and 80 mg/kg) to assess safety and efficacy. Identifier: NCT02740972	
Octa-guanidium conjugated PMO AON (vivo-morpholinos)	Preclinical: *mdx* and *mdx52* Preclinical: GRMD	Capable of restoring dystrophin in skeletal muscle and hearts of *mdx* and *mdx52* mice. Studies in the GRMD dog model demonstrated dystrophin restoration, although high doses led to adverse events.	[279,381–383]
PMO AON	Preclinical: *mdx*	Repeat IV administrations of a high dose restored dystrophin in multiple skeletal muscles of the *mdx* mouse, although <2% in the heart.	[282,284,291,292,294,384,385]

Eteplirsen	Clinical: Phase I, II and III trials	Clinically, eteplirsen was well tolerated and dystrophin was present after 48 weeks. At 84 weeks stabilisation in the 6MWT was observed and at 120 weeks eteplirsen stabilised pulmonary function. Eteplirsen received conditional FDA approval in 2016.	
Tricyclo-DNA AON	Preclinical: *mdx*	Multiple IV administrations at very high doses (200mg/kg per week) resulted in dystrophin in skeletal muscle and heart of *mdx* mice, with low levels in the brain and improvements in cardiac and pulmonary function. Further studies identified minimal adverse effects in *mdx* following treatment.	[298,386]
		Read-through therapy	
Gentamicin	Preclinical: *mdx*	Preclinical studies achieved low levels of dystrophin expression in skeletal muscles and heart, and protection against muscle damage in the EDL.	[387–390]
	Clinical: Phase I trials	Clinical trials exhibited an increase in dystrophin production but no clinical benefit. One individual showed functional stability. Lack of effect may be due to small amounts of active component for read-through present in the drug.	
Negamycin	Preclinical: *mdx*	Antibiotic drug to reduce side effects seen in gentamycin. Subcutaneous injections of negamycin were safer than gentamycin, but induced only low dystrophin expression in skeletal muscle and heart.	[391]
NPC-14/ Arbekacin sulfate	Clinical: Phase II trials	Investigation of safety and efficacy. NCT01918384	Clinical trials.gov
PTC124	Preclinical: HEK293 cells and *mdx*	Preclinical studies observed a 20-25% increase of dystrophin in TA, diaphragm and heart of *mdx*. Improved physiological function of EDL.	[309–311,392–394]
Ataluren/ Translarna	Clinical: Phase I, II and III trials	Clinically, the drug was generally well tolerated. Overall no significant improvement, but patients with a baseline between 300-400 m in the 6-minute-walk test responded well to treatment.	

		Translarna was conditionally approved by the EMA in 2014. EMEA/H/C/002720	
RTC13 and RTC14	Preclinical: *mdx*	RTC13 demonstrated better efficacy (restored dystrophin in skeletal muscle and heart) than gentamicin, PTC124 and RTC14 in *mdx*. Improved muscle function and decreased serum CK.	[313,314]
	Clinical	A patent has recently been submitted and issued.	
Cell-based therapy			
Bone marrow-derived stem cells	Preclinical: *mdx* and GRMD	The cells are observed to migrate to damaged muscle areas following injection where they differentiate into myogenic cells and aid regeneration. Substantial dystrophin restoration is seen in skeletal muscle of *mdx* mice, but no restoration observed in GRMD dogs.	[321,322]
CD133+ stem cells	Preclinical: *mdx*/SCID	Cells exhibited an ability to differentiate into myocytes and engraftment results in effective dystrophin restoration in *mdx*/SCID mice.	[323,324]
	Clinical: Phase I trial	Clinical trial demonstrated safety, without local or systemic side effects in 8 patients.	
Fibroblasts	Preclinical: *mdx*	These cells show an ability to differentiate into myotubes and exhibited effective transfection, resulting in dystrophin expression in immuno-compromised mice.	[319]
iPS cells	Preclinical: *mdx*/SCID	Differentiation of iPS cells into muscle precursor cells followed by injection into TA induced dystrophin expression. Cells integrated with muscle cells and settled in satellite cell population. Improved TA function.	[395–398]
	Preclinical: *mdx*	IM injection of myogenic progenitors derived from iPS cells into *mdx* mice with muscle injury induced by cardiotoxin improved histology.	
Mesangioblasts	Preclinical: *mdx*	Utilising the PiggyBac transposon system, *mdx* mesangioblast progenitor cells were transfected with full-length dystrophin *in vitro* and injected IM	[325,399,400]

		into *mdx*/SCID mice. Muscles exhibited increased dystrophin levels (11-44%) and improved muscle function.	
	Preclinical: GRMD	Improved functional mobility and partial dystrophin restoration in skeletal muscle.	
	Clinical: Phase II trial	IV transplantation of HLA-matched mesangioblasts in patients which showed no clinical benefit.	
Myoblasts	Preclinical: *mdx*	Older studies induced partial dystrophin expression in *mdx* mice. More recently, chimeric myoblasts were created that induced around 37% dystrophin expression and improved muscle function in *mdx* mice.	[316,317,330]
	Clinical: Phase II	Clinical trial performed in 1995 but showed no beneficial effects A new clinical trial is currently recruiting patients to assess efficacy of myoblast transplantation. Identifier: NCT02196467	
Viral delivery of mini- or microdystrophin			
'Gutted' adenovirus	Preclinical: *mdx*	IM with full dystrophin cDNA displayed dystrophin expression, improved muscle force and protected against muscle damage.	[401]
rAAV2/ AAV8	Preclinical: *mdx*	IV injection of this chimeric vector containing codon-optimised micro-dystrophin in *mdx* mice resulted in almost 100% transfection, effective dystrophin expression in skeletal muscle and heart, and improved muscle function. No immunological response was observed.	[345]
rAAV2.5	Clinical: Phase I	Intramuscular administration of a chimeric vector of AAV1 and AAV2 (rAAV2.5) was well tolerated by patients.	[341]
rAAV6	Preclinical: *mdx*/utrn$^{-/-}$	IV administration of rAAV6 microdystrophin to 1 month old *mdx*/utrn$^{-/-}$ restored dystrophin in skeletal, respiratory and cardiac muscles for at least one year. Mice exhibited improved life span and skeletal/respiratory muscle physiology. Although heart mass normalised, cardiac function did not recover.	[335,336]

	Preclinical: *mdx*	20 month old *mdx* mice exhibited dystrophin expression in skeletal muscle and heart, and improved pathology. Mice received an intravenous injection with rAAV6 microdystrophin 4 months before.	
AAV9	Preclinical: *mdx*	Micro-dystrophin administration in young *mdx* induced dystrophin expression and slowed progression of cardiac phenotype. 10 month old mice expressed dystrophin and cardiac function improved.	[337,338,340,402,403]
	Preclinical: DBA/2J-*mdx*	Intravenous administration of rAAV9 microdystrophin in 10 week old *mdx* mice resulted in skeletal and cardiac muscle dystrophin expression at 6 months. Muscle pathology and function was significantly improved in some but not all skeletal muscles.	
	Preclinical: GRMD	IV mini-dystrophin administration in neonatal GRMD dogs revealed varied dystrophin expression. Further studies demonstrated that micro-dystrophin administration in 2 month old dogs restored dystrophin expression and improved muscle histology.	
Lentivirus	Preclinical: myotubes, primary myoblasts and *mdx*	Transfection with mini- or microdystrophin: 20-25% dystrophin expression in TA muscles (for a 2 year period). Less central nucleation, but no protection from muscle injury. Able to transfect TA myogenic progenitor cells. Successful transfection of full-length dystrophin in myotubes.	[404–407]
		CRISPR-cas9	
CRISPR-cas9	Preclinical: *mdx*	Local and systemic administration of the CRISR-Cas system restored dystrophin between 39-67% locally and 10-50% body-wide, and functional muscle improvement was observed.	[347–350]
	Preclinical: ΔE50-MD dog	Studies utilising a DMD dog model, with a mutation in exon 50, showed extremely efficient exon skipping in skeletal (3-90%) and cardiac (92%) muscle with the high dose.	

Utrophin upregulation			
Artificial zinc finger transcription factor Jazz	Preclinical: cultured cells, *mdx* muscle	Transgenic models and viral delivery of ZFs regulated utrophin A promoter. It improved muscle function and reduced pathology in TA.	[357–359,408]
Biglycan protein anchoring	Preclinical: *mdx*	The non-glycanated isoform upregulates utrophin (among others) to the sarcolemma. Treatment with recombinant human biglycan reduced pathology in quadriceps and diaphragm and improved physiology in EDL. Intravenous human biglycan delivery to *mdx* improved muscle histology and physiology.	[65,363,409]
TVN-102	Clinical: pre-submission	Tivorsan Pharmaceuticals has received orphan drug status for TVN-102 and plans to initiate clinical trials in 2019.	
Let-7c interaction	Preclinical: *mdx*	Inhibition of the let-7c and utrophin interaction de-repressed utrophin production and improved muscle histology and function.	[410]
p38 MAPK activation	Preclinical: *mdx*	Treatment with a p38 MAPK activator (i.e. heparin or celecoxib) improved muscle fibre integrity and strength. It increased utrophin expression ~1.5-2 fold in TA, diaphragm and heart through translational activation.	[411,412]
SMT C1100/ Ezutromid	Preclinical: *mdx*	Increased RNA and protein of utrophin in skeletal and cardiac *mdx* muscle. Reduced pathology and improved muscle function in skeletal muscle.	[361,362,413]
	Clinical: Phase I	Summit Therapeutics performed a Phase I trial with mild side-effects at higher dose but generally well tolerated.	
	Clinical: Phase II	A Phase II trial did not meet its primary and secondary endpoints, and has been discontinued.	
SMT 022357	Preclinical: *mdx*	This second-generation compound following SMT C1100 increased utrophin in various skeletal muscles, diaphragm and heart. Improved myofibre stability and muscle physiology.	[414]

Utrophin transgene	Preclinical: *mdx/*utrn$^{-/-}$	Transgenic utrophin expression which improved pathology in skeletal muscle, but not heart.	[353,355,356]

A summary of therapeutic interventions (recently) under consideration for DMD, including specific strategies employed, models utilised and outcomes of treatment.

IV: Intravenous; IM: intramuscular; IP: intraperitoneal.

1.6 miRNAs

1.6.1 miRNA biogenesis

miRNAs are a class of short (~22 nucleotides), single stranded RNA molecules involved in the regulation of gene expression. They act as endogenous RNA interference (RNAi) effectors, whereby gene silencing is triggered through (partial) complementary binding to a target mRNA. Ambros *et al.* discovered that the temporal decrease of the LIN-14 protein, important for *Caenorhabditis elegans* (*C. elegans*) development, was not executed by a protein, but rather a short 22 and 61 nucleotide transcript, providing initial evidence for the endogenous RNAi function of miRNAs [415]. This class of RNA has since been identified in all eukaryotes and is involved in numerous functions and diseases, including cell proliferation, apoptosis and cancer [416–418], and novel miRNAs and functions continue to be discovered [418,419].

miRNAs are transcribed by RNA Polymerase II from introns in protein-coding genes or from their own promoters, among others [420], whereby most are generated through the canonical pathway. Polyadenylated and capped primary miRNA (pri-miRNA) [421] is transcribed in the nucleus, after which it associates with the microprocessor complex consisting of one ribonuclease III enzyme Drosha protein and two DiGeorge critical region 8 (DGCR8) proteins [422–424]. DGCR8 aids in target recognition of the miRNA and Drosha subsequently cleaves it at the base of the hairpin, resulting in a 60-70 nucleotide hairpin product [424,425]. This precursor miRNA (pre-miRNA) contains a 2 nucleotide 3' overhang [425] and is subsequently transported into the cytoplasm by binding the Ran-GTP dependent Exportin-5 (XPO5) [426], although other export routes may exist [427].

Once in the cytoplasm, the mature miRNA is produced when the RNase III-type enzyme Dicer cleaves the pre-miRNA, resulting in a double-stranded miRNA [428,429]. This process is aided by *trans*-activation-responsive RNA-binding protein (TRBP), whereby two of its double-stranded RNA-binding domains (dsRBD) interact with the pre-miRNA, and a third with Dicer [430,431]. The miRNA strand

that exhibits lower 5′ thermodynamic stability is typically the guide strand [432]. This guide strand is subsequently loaded into the RNA-inducing silencing complex (RISC), which has at its core a protein from the highly conserved Argonaute (AGO, 1-4) family [433]. The other strand is cleaved by AGO2 and subsequently degraded [434]. Many factors, including phosphorylation of Drosha and Dicer, and RNA binding proteins, further modulate miRNA biogenesis and activity [418]. Mature 3p/5p miRNA nomenclature is based on whether the chosen guide strand stems from the 3′ or 5′ end of the pre-miRNA hairpin.

Non-canonical miRNA biogenesis include a small class of miRNAs, mirtrons, which are derived from introns and structurally similar to pre-miRNAs, but do not get cleaved by Drosha [435], and rare Dicer-independent miRNAs which are cleaved by AGO proteins [436,437]. These appear to act similarly to canonically synthesised miRNAs [438].

The mature miRNA sequence that is loaded into the RISC complex then achieves gene silencing through binding to its target mRNA at miRNA response elements (MRE), often at the 3′ untranslated region (UTR) [439,440]. To enable target recognition, the ‘seed region’ of the miRNA should be complementary to the mRNA. This region consists of 2-8 nucleotides and is often found on the 5′ end of the miRNA [441]. miRNAs bind with imperfect complementarity and silence gene expression through a variety of mechanisms such as translational regulation, and mRNA cleavage and decay through de-adenylation and decapping [420,442,443].

Other aspects may assist in mRNA-miRNA binding and stability, such as proximity pairing of miRNA nucleotides 13-16 and a minimal distance of 15 nucleotides from the stop codon [439]. Additionally, trans-acting proteins binding to the mRNA UTRs can regulate miRNA site recognition by masking its binding site [444,445]. More recently, studies have identified direct and indirect roles for miRNAs in gene activation, and as such, they appear to be important for gene regulation in general rather than just silencing [446]. Together, these studies suggest a complex biogenesis and mechanism of action for miRNAs.

1.6.2 Muscle-specific miRNAs

Tissue-specific miRNA expression has been observed, and Lagos-Quintana *et al.* identified high levels of miRNA-1 (miR-1) in heart tissue from mice [447]. Since then, miR-133 and miR-206 have additionally been identified to exhibit high, muscle-specific expression and have been termed the 'myomiRs'. Whereas miR-1 and miR-133 are expressed by all muscles, miR-206 is skeletal muscle-specific [448,449]. The miRNA, miR-208, located in the muscle cell-specific myosin heavy chain gene [450], has been identified as cardiac-specific [448], with miR-208a and miR-208b expressed in the atria and ventricles respectively [451]. However, recent studies have identified a role for miR-208b in cell cycle regulation of myoblasts, promoting skeletal muscle cell proliferation, which suggests activity of miR-208 in skeletal muscle in addition to the heart [452].

The myomiRs, miR-1, miR-133 and miR-206, are induced by the myogenic transcription factors MyoG, MyoD and myocyte enhancer factor 2 (MEF2) [453–455], and several studies have identified their importance in muscle development and myogenesis. Even though miR-1 and miR-133 are transcribed together from the same chromosomal loci, they exhibit opposing roles. While miR-1 was found to promote differentiation in C2C12 myoblasts, miR-133 was observed to induce myoblast proliferation [456].

Many homology similarities and function can be identified between miR-1 and miR-206 and these two miRNAs differ by only 4 nucleotides outside of the seed region. Both miRNAs promote differentiation by inhibiting Pax7 expression, a key marker for quiescent satellite cells (detailed in **Chapter 1.4.1**) [457]. Interestingly, established targets of miR-206 include utrophin, the homolog of dystrophin, and oestrogen receptor α (ERα) [449].

Aside from the traditional myomiRs, several other non-muscle-specific miRNAs have been associated with muscle tissue. For instance, miR-664-5p plays a role in the proliferation of myoblasts by inhibiting serum response factor (SRF) during myoblast proliferation and the canonical Wnt-pathway effector Wnt1 during differentiation, thereby diminishing the differentiation of myoblasts

[458]. Other miRNAs involved in cardiac function include miR-34a, miR-199a and miR-590. Inhibition of miR-34a in C57BL/6 mice undergoing cardiac failure reduced cell death and fibrosis, and improved the recovery of cardiac function [459]. In contrast, exogenous addition of miR-199a and miR-590 was shown to promote cardiomyocyte proliferation and stimulate cardiac regeneration, thereby improving function following infarction in CD1 mice [460].

1.6.3 miRNAs in DMD

Since the discovery of miRNAs, many studies have explored the potential of miRNAs in diseases, including DMD. A large miRNA array comparing, among others, DMD patient muscle with controls identified 62 miRNAs out of 428 that were differentially expressed, including miR-146b, miR-29b, miR-368 and miR-486 [461]. Greco *et al.* built upon this work and identified miRNAs that were differentially expressed in both patient and *mdx* muscle [462]. Of the 189 miRNAs analysed by RT-qPCR, 36 were significantly different in dystrophic muscle. 13 miRNAs that exhibited high fold changes were further characterised, of which 3 were downregulated (miR-1, miR-29c and miR-135a) and 8 upregulated (miR-31, miR-34c, miR-206, miR-222, miR-223, miR-335, miR-449 and miR-494) in both patient and *mdx* muscle [462]. Despite overlapping results, some miRNAs were not observed to be differentially expressed in both studies (e.g. miR-31 and miR-146b) and one reason may be variability in miRNA expression between muscles (mixture vs quadriceps). Indeed, Roberts *et al.* identified that out of 188 miRNAs in quadriceps, 181 in diaphragm, and 64 in heart, only 18 miRNAs were commonly differentially expressed between the various muscles [463]. The high number of miRNAs analysed in these studies have allowed further identification and characterisation of the miRNA pattern in dystrophic muscle.

The mislocalisation of nNOS due to DAPC disruption results in decreased HDAC2 nitrosylation, which results in increased binding to the miR-1 and miR-29 promotors, thereby inducing downregulation of these miRNAs [464]. Interestingly, upon exon skipping treatment, expression levels of miR-1 and miR-29 are restored to wild-type (WT) levels, confirming the importance of dystrophin

expression on certain miRNAs [464]. Additionally, the downregulation of miR-29 promotes the differentiation of myoblasts into myofibroblasts, and is therefore thought to contribute to fibrosis observed in DMD [465]. *In vivo* restoration of miR-29 promoted muscle regeneration and inhibited fibrogenesis in the *mdx* [465]. *Mdx* and patient muscles also exhibit a reduction in miR-486, and this miRNA is known to play a role in hypertrophy, growth and apoptosis of the muscle. Its overexpression in *mdx*^{5cv} mice (containing several sequence deletions after exon 10) improved DMD pathology, including integrity of the sarcolemma and muscle physiology [466].

Other studies have identified *Dmd* mRNA as a direct target of several miRNAs, including miR-31, which is highly upregulated in *mdx* and patient muscle [467]. miR-31 binds directly to the 3' UTR of the *Dmd* mRNA, thereby repressing translation. Further mechanistic studies identified its main functional effect during early myoblast differentiation and suggested an important role for miR-31 in repressing late stage differentiation markers, such as dystrophin. This miRNA is consistently upregulated throughout differentiation in *mdx* myoblasts, indicating increased regeneration and a reduced differentiation potential in *mdx* myoblasts [467]. Inhibiting miR-31 expression during exon skipping treatment improved dystrophin restoration efficiency two-fold in dystrophin-deficient human myoblasts, suggesting a potential for therapeutic utility [467].

miR-340 is highly expressed in hearts exhibiting cardiac failure as a result of dilated cardiomyopathy and this miRNA is also able to bind to the 3' UTR of the *Dmd* mRNA and inhibit translation of the dystrophin protein. miR-340 expression is dependent on cardiac volume overload and is able to induce fibroblast activation, resulting in hypertrophy [468]. Although it is unclear why this miRNA downregulates dystrophin expression during heart failure, this pattern has also been observed in rats undergoing the transition from hypertrophy into heart failure [469], suggesting a targeted mechanism in dystrophin downregulation during this degenerative cardiac process.

Lastly, miR-448 has been implicated in DMD cardiomyopathy, with a dramatic decrease in expression in the *mdx* mouse heart. Kyrychenko *et al.* discovered that downregulation of miR-448

increased expression of the *Ncf1* gene, which is a regulatory subunit of the NOX2 protein (see **Chapter 1.2.2**). Inhibition of miR-448 increased ROS production and Ca^{2+} signalling pathways in cardiomyocytes, and chronic administration of a miR-448 inhibitor led to dilated cardiomyopathy in the *mdx mouse* [470]. The results suggest an important role for miR-448 in metabolic homeostasis of the heart and an involvement in DMD pathology.

1.6.4 Extracellular miRNAs for DMD biomarkers

Upon maturation, miRNAs can be exported into the extracellular space and extracellular miRNAs have been considered for biomarker purposes. In serum, they are found to be highly stable and are mostly (>97%) associated with ribonucleoprotein (RNP) complexes (with proteins such as AGO2 or in lipoprotein particles), although a small subset are contained within extracellular vesicles [471–473]. The function of this release remains a matter of contention as miRNAs have been shown to have a direct biological function by some, whereas others suggest that extracellular miRNAs (ex-miRNAs) are a by-product of cellular activity [474].

Several studies have demonstrated functional transfer of miRNAs from exosomes, which supports the argument that ex-miRNAs exert a function. Forterre *et al.* observed that many of the miRNAs expressed in myoblasts and myotubes (*n*=196 and *n*=208 respectively) were sorted into exosomes secreted by these cells (*n*=168 and *n*=180 respectively), suggesting that a large subset of miRNAs is exported into exosomes. The authors further demonstrated a reduction in expression of sirtuin1 at both the mRNA and protein level following incubation of myoblasts with exosomes derived from myotubes, but not from myoblasts [475]. Importantly, these results identify the potential of exosomes to have an effect on recipient cells and support a biological function for secreted miRNAs. Conversely, it should be noted that often the number of exosomes used in functional transfer studies is similar to the total number of exosomes found in serum [476], and exosome isolation techniques are often inappropriate, thereby possibly negating the biological relevance of these studies.

Ultimately, it seems probable that some ex-miRNAs are mere cellular waste, whereas others exert biological functions, most likely at the paracrine level [477].

Elevated levels of circulating miRNAs have been detected in DMD. Whereas low copy numbers of miR-1, miR-133 and miR-206 are normally found in serum from healthy controls, DMD patients exhibit significantly elevated ex-myomiRs in their serum, with abundance in BMD patients at intermediate levels [478]. The Morgan and Wood labs have shown that these secreted myomiRs are indicative of muscle turnover in male, 12 week old, *mdx* mice whereby extracellular expression levels peak at 4 and 12 weeks, consistent with necrosis and regeneration respectively [479]. It is thought that many of these miRNAs are passively released and/or leaked from damaged muscle. However, the same groups have shown that intra- and ex-miRNA levels are not differentially abundant with a similar directionality (e.g. high increase in tissue and serum) [463]. Moreover, myomiRs are selectively released upon C2C12 myoblast differentiation *in vitro* [480], suggestive of regulated release and a potential role for myomiRs in skeletal muscle differentiation.

Cacchiarelli *et al.* was the first to observe that the degree of miRNA abundance negatively correlated with the child's motor ability based on the NSAA assessment, whereby increased myomiR levels were observed in children with decreased motor ability, although it should be noted that these could only be correlated in ambulant children (n=10) [478]. This is likely due to higher physical activity in ambulant children and/or the pathological disease progression. Interestingly, after exon skipping treatment with eteplirsen there was a trend for myomiR reduction in patient serum, although this was not statistically significant [481]. This may be explained by the short duration of treatment or differences in corticosteroid treatments, which affects ex-miRNA abundance [481]. It may also be due to low efficacy of dystrophin restoration. Indeed, the Morgan and Wood labs, and others, has previously shown that effective skeletal muscle dystrophin restoration through exon skipping strategies is able to completely restore ex-myomiR to control levels [463] and peptide conjugated

PMOs (PPMO) of varying potencies for dystrophin re-expression (Pip6a-PMO and Pip6e-PMO) restore ex-miRNAs to different degrees [479].

Given these results, many studies have focused on utilising ex-miRNA abundance for biomarker purposes. Currently, outcome measurements to assess effectiveness in clinical trials include muscle biopsy, the levels of serum CK and the 6MWT, which evaluates the distance walked by patients within 6 minutes [477]. However, each method is subject to important limitations. Firstly, muscle biopsy is important to quantify dystrophin re-expression following dystrophin restoration therapies. However, this method is highly invasive and given that only a very small section is taken, it may not properly represent the re-expression efficacy in the whole musculature, or even within a single muscle [482]. Moreover, quantification is often performed by Western blot, which shows relatively low reproducibility [483]. Secondly, serum CK levels are significantly elevated in neuromuscular disorders, including DMD. Nevertheless, CK is not a reflection of dystrophin restoration [484]. Rather, it is passively released upon muscle membrane fragility [103] and therefore only an indirect marker of one aspect of DMD pathology. Moreover, serum levels decrease with age, thereby making measurement of treatment efficacy more difficult [484]. Lastly, the 6MWT is measured to assess muscle functionality, but is highly dependent on factors such as patient motivation and can by definition only be applied to ambulant patients. This excludes the non-ambulant population, losing information on the efficacy of treatment in a more advanced disease stage [477]. As such, there is an unmet need for new biomarkers to measure disease progression.

Therefore, studies have aimed to identify and characterise serum miRNAs in DMD mouse models and patients. For instance, the muscle-specific miR-1, miR-133, miR-206, miR-208 and miR-499 were differentially expressed in serum from DMD patients [485]. Other studies have aimed to identify cardiomyopathy-specific miRNAs. For example, worsened cardiac fibrosis was associated with upregulation of miR-222, miR-26 and miR-378a-5p in serum from BMD and DMD patients [486]. Further heart-related miRNAs identified in GRMD dog and patient serum are miR-208a, miR-208b,

miR-499, miR-539 and miR-95 [487]. It should be noted that ex-miRNA abundance and significance can vary between studies, possibly due to differences in miRNA measuring techniques. Moreover, ex-miRNA levels gradually decrease over time in patient serum, thereby complicating the assessment of treatment efficacy (which is also thought to decrease abundance of elevated miRNAs) [478].

Most recently, Catapano *et al.* investigated the secretion of miRNAs into patient urine. They divided patients into ambulant and non-ambulant, and found a significant downregulation of exosome-related miR-39c-3p, and miR-23b-3p and miR-21-5p compared to controls, respectively [488]. This non-invasive method provides a novel way to investigate ex-miRNA biomarker potential, though limitations with exosome isolation methods as discussed above need to be considered.

Overall, several miRNAs have been identified as significantly elevated in DMD patient serum, although a decrease in abundance with time is observed in *mdx* and patient serum. This may pose a limiting factor as this encumbers measurement of treatment efficacy in older patients. Ultimately, their biomarker potential remains to be established in further dystrophin-restoring clinical trials.

1.7 Thesis hypotheses and aims

This thesis investigates the influence of the absence of the dystrophin protein on the cardiac transcriptome, the skeletal muscle proteome and the miRNA secretome through the following aims:

1. Understanding of differentially expressed transcripts and molecular pathways implicated at the early stages of dystrophic cardiac pathology in five anatomical heart regions.
2. Identification of novel differentially expressed proteins associated with dystrophic disease progression in skeletal muscle.
3. Understanding the influence of varying levels of dystrophin protein in skeletal muscle on miRNA abundance in serum.

2. General materials and methods

2.1 Animal studies

All Oxford-based experiments housed animals at the Biomedical Services Building at the University of Oxford, under 12:12 hour light:dark conditions, with access to food and water *ad libitum*, in individually ventilated cages (IVC), kept specific pathogen free (SPF; testing for a large number of viruses, bacteria and parasites). All procedures were performed in accordance with the Animals Scientific Procedures Act 1986 with approval from the UK Home Office (project licenses 30/2907 and 30/2306). Animals were sacrificed through a rising concentration of CO_2 followed by exsanguination and cervical dislocation. For terminal serum collection, blood was obtained from the jugular vein of the mouse into clotting Microvette CB 300 collection tubes (16.440; Sarstedt, Nümbrecht, Germany). Blood was incubated at 4°C for 2-3 hours to enable clotting, after which serum was collected through centrifugation at 10,000 × *g* for 5 minutes and stored at -80°C. Generally, tissues were snap frozen in dry-ice-cooled isopentane and stored at -80°C.

2.2 Cell culture

C2C12 myoblasts were cultured at 37°C with 5% CO_2 in Dulbecco's modified eagle medium (DMEM) supplemented with 20% foetal bovine serum (FBS) and 1% antibiotics/antimycotics (ab/am) (growth medium: GM) (all Life Technologies, Carlsbad, USA). C2C12 myoblasts were differentiated in DMEM containing 2% horse serum (HS) and 1% ab/am (differentiation medium: DM) for 6 days to form multinucleated myotubes.

Cells collected for RNA or protein were detached from the plate through incubation with TrypLE Express Enzyme (Gibco, Waltham, MA, USA) for 5 minutes at 37°C. Supernatant was mixed with differentiation medium at a 1:1 ratio to inactivate the enzyme, collected into new tubes and centrifuged at 4,000 × *g* for 4 minutes. Supernatant was subsequently removed, and pellets were stored at -20°C.

Cells that were utilised for visualisation of protein expression localisation by immunofluorescence were washed two times with phosphate buffered saline (PBS), incubated with 200 µL of 4% paraformaldehyde (PFA) for 10 minutes to allow cell fixation and washed another three times with PBS before storage at 4°C.

2.3 RNA extraction

2.3.1. Cells and tissues

Most RNA extractions were performed utilising TRIzol Reagent (Invitrogen, Waltham, MA, USA) according to manufacturer's instructions. Briefly, cell samples were homogenised in TRIzol through vortexing. In contrast, tissue samples were lysed using the Precellys 24 Tissue Homogeniser (Bertin Technologies, Paris, France), which disrupts tissue sections by vigorously shaking re-enforced tubes containing metal ball bearings. Supernatant was transferred to new tubes, after which chloroform was added in a 1:5 ratio with TRIzol. Samples were vortexed for 10 seconds, incubated for 10 minutes at room temperature and centrifuged for 15 minutes at 12,000 × *g* to allow for phase separation. The aqueous phase containing nucleic acids was collected and mixed with 1 µL glycogen (20mg/mL stock; Roche, Dorset, UK and ThermoFisher Scientific, Waltham, USA) in fresh tubes, then mixed with 500 µL isopropanol, which allows for nucleic acid precipitation. Samples were subsequently incubated for 10 minutes at room temperature or overnight at -20°C and centrifuged for 10 minutes at 12,000 × *g*. Supernatant was discarded and the nucleic acid-containing pellets were washed with 75% ethanol to remove residual salts, followed by centrifugation for 5 minutes at 7,500 × *g* and discarding of the supernatant. Tubes were briefly centrifuged at room temperature for 30 seconds at 3,000 × *g* and residual liquid removed. Pellets were air-dried for 5-10 minutes at room temperature and dissolved in nuclease-free water. RNA was then incubated at 55°C for 5 minutes and RNA concentration determined using a Nanodrop Spectrophotometer (ThermoFisher Scientific). RNA was stored at -80°C. All centrifugation steps were performed at 4°C unless indicated otherwise.

2.3.2. Serum

25-50µL of serum was added to 600µL of TRIzolLS and incubated for 5 minutes at room temperature. A spike-in of a 5 nM exogenous cel-miR-39 (5'-UCACCGGGUGUAAAUCAGCUUG- 3') (Integrated DNA Technologies, Leuven, Belgium) was added to allow for RT-qPCR data normalisation (3 µL per sample). Samples were also supplemented with nuclease-free water to total 800 µL, to

ensure correct sample to TRIzol ratio. 160 µL chloroform was subsequently added, after which the samples were incubated for 10 minutes at room temperature and centrifuged for 15 minutes at 12,000 × *g* to allow phase separation. The nucleic acid-containing aqueous phase was transferred to new tubes containing 1 µL glycogen, after which the samples were vortexed and mixed with 400 µL isopropanol. Mixtures were incubated for 20 minutes at room temperature or overnight at -20°C, followed by centrifugation for 10 minutes at 10,000 × *g*. Supernatant was discarded and the nucleic acid-containing pellets washed with 1 mL of 75% ethanol to remove residual salts. Samples were then centrifuged for 5 minutes at 7,500 × *g*, after which the supernatant was discarded. Tubes were briefly centrifuged at room temperature for 30 seconds at 3,000 × *g* and residual supernatant was removed. Pellets were air-dried for 5-10 minutes and dissolved in 30 µL nuclease-free water. Lastly, samples were incubated for 10 minutes at 55°C and subsequently stored at -80°C. All centrifugation steps were performed at 4°C unless indicated otherwise.

2.4. Reverse transcription-quantitative polymerase chain reaction (RT-qPCR)

2.4.1. mRNA

RNA was reverse transcribed using the High-Capacity cDNA Reverse Transcription Kit (4368814; Applied Biosystems, Waltham, MA, USA) according to manufacturer's instruction. A master mix containing 2 µL of 10 × buffer, 0.8 µL dNTP mix, 2 µL 10 × random primers and 1 µL of reverse transcription reagent was added to 250-1,000 ng of total RNA. Nuclease-free water was also added to obtain a total volume of 20 µL per reaction. cDNA was synthesised using the following incubation conditions: 10 minutes at 25°C, 120 minutes at 37°C and 5 minutes at 85°C.

The cDNA template was amplified on a StepOne Plus real-time PCR Thermocycler (Life Technologies) using SYBR Green Gene Expression Master Mix (Life Technologies). Samples were measured in duplicate, whereby reactions consisted of 2 µL of 1:10 diluted cDNA, 10 µL SYBR green Assay, 1 µL 20 × primer probe and 7 µL nuclease-free water. Amplification was performed using universal cycling conditions (i.e. samples were heated for 10 minutes at 95°C followed by 40 cycles of 15 seconds at 95°C and 1 minute at 60°C). A melting stage was included at the end, whereby measurements were taken from 60°C to 95°C with incremental steps of 0.3°C or 0.8°C. The melt curve was utilised to identify the reaction specificity and the presence of a single melting peak, suggesting an absence of primer-dimer products. A control, negative for cDNA, was included with each gene target. RT-qPCR data were analysed using the Pfaffl method [489] and PCR efficiencies determined by LinRegPCR [490].

2.4.2. miRNA

RNA was reverse transcribed using TaqMan MicroRNA Reverse Transcription Kit (Applied Biosystems) according to manufacturer's instructions. A master mix was prepared, containing 2 µL miRNA RT buffer, 1 µL MultiScribe RT, 0.15 µL dNTP mix, 0.18 µL RNase Inhibitor, the miRNA primers

(2 µL for 5 × stock, 1 µL for 20 × stock or 0.33 µL for 60 ×) and the addition of water to a total of 15 µL. 5 µL RNA was added to the master mix and samples were incubated in a thermal cycler for cDNA synthesis under the following incubation conditions: 30 minutes at 16°C, 30 minutes at 42°C, 5 minutes at 85°C, then held at 4°C until stored at -20°C.

The cDNA template was amplified utilising TaqMan Gene Expression Master Mix (Applied Biosystems) on a StepOne Plus real-time PCR Thermocycler (Life Technologies) using cycling conditions as above (excluding the melt curve analysis stage). Samples were measured in duplicate, whereby reactions consisted of 1.29 µL of cDNA and a master mix of 10 µL TaqMan Assay, 0.33 µL (for 60 ×) or 1 µL (for 20 ×) of primer probe and reaction volume was made up with nuclease-free water to total 20 µL. A control, negative for cDNA, was included with each gene target. RT-qPCR data were analysed using the Pfaffl method and PCR efficiencies determined by LinRegPCR as described above.

2.5. Western blotting

Protein lysates were obtained utilising different extraction buffers, which are described in detail in their respective chapters. Lysates were then mixed with 10 × NuPAGE sample reducing agent (Invitrogen, Waltham, MA, USA) and 4 × NuPAGE LDS sample buffer (Invitrogen), heated at 70°C for 5 minutes and centrifuged for 5 minutes at 13,000 × *g*. Protein was subsequently size separated on a 10% Bis-Tris or 3-8% Tris-Acetate gradient gel (Invitrogen) using 20 × NuPAGE MOPS or 20 × NuPAGE Tris-acetate SDS Running buffer (Invitrogen) in ddH_2O, respectively. Proteins were transferred onto a 0.45 µm polyvinylidene fluoride (PVDF) membrane, with 20 × NuPAGE Transfer Buffer (Invitrogen) in ddH_2O supplemented with 10% Alcohol (methanol or ethanol). To prevent non-specific binding, membranes were blocked for 1 hour at room temperature in Tris-buffered saline (50 nM Tris pH 7.5, 150 mM NaCl with 0.1% Tween; TBST), supplemented with 5% non-fat dry milk or 5% bovine serum albumin (BSA) (the latter was utilised for detection of phospho-proteins). For detection of dystrophin, PBS-based Odyssey blocking buffer (LI-COR Biotechnology, Lincoln, USA) was utilised to block the membrane. Primary antibodies were incubated overnight at 4°C, followed by three washes for 3 minutes with TBST or PBST (corresponding to blocking buffer composition). Membranes were then probed with secondary antibody for 1 hour at room temperature, followed by three more washes. The Odyssey Fc Imager (LI-COR Biotechnology, Lincoln, OR, USA) was used for protein visualisation.

Dystrophin and vinculin primary antibodies are detailed in **Table 2.1**. Li-COR secondary antibodies were used for primary antibody detection at a 1:10,000-20,000 dilution: 800CW Goat anti-Mouse IgG (H+L; P/N 925-32210), 800CW Goat anti-Rabbit IgG (H+L; P/N 925-32211), 680RD Donkey anti-Mouse IgG (H+L; P/N 925-68072) and 680RD Goat anti-Rabbit IgG (H+L; P/N 925-68071; all Li-COR, Biotechnology, Lincoln, NE, USA).

Table 2.1 Antibodies for dystrophin protein detection by Western blot

Antibody	Dilution	Product Code	Company
Dystrophin	1:100	NCL-DYS1	Leica Biosystems
Vinculin	1:100,000	V9131	Sigma-Aldrich

2.6. Myosin heavy chain immunofluorescence

To allow staining of myosin heavy chain (MHC) in C2C12 myoblasts, cells were incubated with 200 µL of 0.2% Triton X-100 at room temperature for 15 minutes enabling membrane permeabilisation, followed by three PBS washes and a 30 minute block in 200 µL of 5% BSA at room temperature. The primary antibody for MHC (MF20, developed by D. A. Fischman, obtained from the Developmental Studies Hybridoma Bank (DSHB), created by the NICHD of the NIH and maintained at The University of Iowa, Department of Biology, Iowa City, IA, USA) was suspended in 200 µL of 5% BSA (1:200 dilution) and added to the cells for 2 hours at room temperature. After two PBS washes, 200 µL of the secondary goat anti-mouse AlexaFluor 488 antibody (1:500 dilution) and Hoechst33342 (1:5000 dilution) in 5% BSA was added for 1 hour at room temperature, before storage at 4°C until ready for imaging on the EVOS microscope (Life Technologies). All solutions were prepared in PBS.

Myogenic index was defined as the number of nuclei that were MHC-positive. Fusion index was defined as the number of MHC-positive cells containing two or more nuclei. Both counts were divided by the total number of nuclei and multiplied by 100 to obtain the percentage.

3. Results I

Transcriptomic analysis identifies *Sfrp2* expression changes and its protein mislocalisation in dystrophic cardiomyopathy

3.1 Introduction

Despite significant efforts to elucidate the mechanisms of DMD pathology, the role of the dystrophin protein is yet to be completely defined. Several transcriptomic studies have been performed with the aim of further understanding the underlying pathology of DMD. For instance, Tian *et al.* identified 74 aberrant pathways based on differentially expressed genes in patient skeletal muscle, including inflammatory pathways [491]. Furthermore, the EL Andaloussi, Lehtiö and Wood groups compared expression of the transcriptome with the proteome in *mdx* versus control muscle, where they identified changes in metabolism and axonal guidance signalling, and highlighted the well-described dystrophic feature Tgfβ1 as an important upstream regulator, among many others [492]. However, similar studies examining the transcriptomic signature in the dystrophic heart are severely lacking, and this remains an important avenue for further investigation.

Generally in DMD studies, analysis of the heart often comprised a lysate of the whole heart or the apex (includes the RV, LV and interventricular septum (IVS)), but evidence from transcriptomic arrays performed with cardiac samples from humans and mice has demonstrated large gene expression discrepancies between the atria and ventricles [493–495]. Moreover, Shimura *et al.* identified metabolic profiles that were chamber dependent in C57BL/6 mice. Total levels of many metabolites, such as ATP and lactate acetyl CoA, were higher in both ventricles compared to the atria, consistent with a higher energy demand required for the pumping of blood [496]. Together with the observation that pathology progresses differently through the heart in patients (e.g. fibrosis starts at

the postero-basal wall of the left ventricle), this suggests a requirement for future cardiac investigations to distinguish between the anatomical regions.

The highly conserved Wnt pathway (as mentioned in **Chapter 1.3**) has been implicated in several aspects of DMD pathology. The secreted Wnt ligands bind to Frizzled receptors, activating downstream processes. The pathway consists of three main arms, although other proteins have also been associated with Wnt regulation (e.g. GTPase activating YAP/TAZ leading to osteogenesis and migration activation [497]) (**Figure 3.1**). (I) The canonical β-catenin pathway relies on the activation of dishevelled-1 (DVL) and axin through Frizzled and lipoprotein-related receptors (LRP) 5 and 6 to disassemble the 'destruction complex', which normally phosphorylates β-catenin through glycogen synthase kinase 3-β (GSK-3β), targeting it for degradation. The disassembly of the complex prevents β-catenin phosphorylation, allowing the unphosphorylated protein to migrate to the nucleus and activate transcription. The activated genes are tissue- and environment-dependent [498]. (II) The non-canonical planar cell polarity (PCP) pathway activates the Rho-associated kinase (ROCK) and results in the phosphorylation of JNK through the Frizzled-mediated activation of Rho and Rac, respectively. This pathway is involved in cytoskeletal re-organisation and migration, among others. (III) The non-canonical Wnt/calcium pathway acts through G-proteins to activate PLC, which generates IP_3, thereby increasing the intracellular calcium concentration through IP_3 receptors. The resulting activation of calcineurin mediates the dephosphorylation of nuclear factor of activated T-cells (NFAT), allowing its translocation to the nucleus [498].

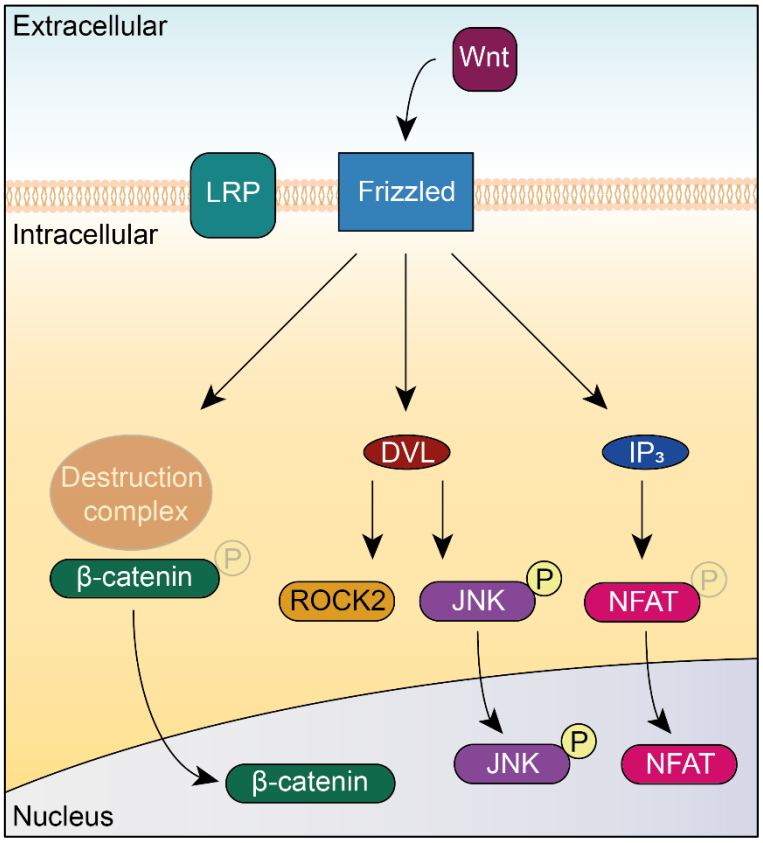

Figure 3.1 Simplified schematic of the three main Wnt signalling arms.
Through activation of the Wnt ligand, the Fzd (frizzled) and LRP receptors can activate the canonical β-catenin pathway through disassembly of the destruction complex, allowing the dephosphorylation of β-catenin and its translocation into the nucleus. DVL activation may also lead to the stimulation of ROCK2 and phosphorylation of JNK, which allows the displacement of the latter to the nucleus. Lastly, activated Fzd may also lead to an increase in IP_3-mediated intracellular Ca^{2+}, resulting in the dephosphorylation of NFAT and its translocation to the nucleus. P indicates phosphorylated protein.

Dysregulation of members of the Wnt signalling pathway have been observed in transcriptomic analyses in DMD patients [499]. Indeed, muscle biopsies from DMD patients (*n*=6) exhibited an increase of 223% and 371% of β-catenin and phosphorylated GSK-3β to GSK-3β ratio compared to controls, respectively [500]. Mouse studies identified that local application of the Wnt7a ligand induced satellite cell expansion and myofibre hypertrophy, improved muscle strength and reduced contractile damage in the *mdx* mouse [501]. The Wnt pathway is also targeted by MMP-9 (decreases and increases canonical and non-canonical arms, respectively) [251], miR-199a-5p [502]

and miR-664-5p [458], and has been shown to promote satellite cell population and precursor cell differentiation [189,190,503] in skeletal muscle of the *mdx* mouse.

Currently, no studies have been performed investigating the involvement of the Wnt signalling pathway in the dystrophic heart, but this pathway has been implicated in several aspects of the diseased heart in other contexts. For instance, several Wnt ligands are upregulated following myocardial infarction, located at the border of the infarction area. Wnt pathway upregulation occurs in a similar timeframe with angiogenesis, fibrosis and inflammation [504,505]. Furthermore, activation of β-catenin has been implicated in cardiac hypertrophy of mouse cardiomyocytes [506–508] and cardiomyocyte growth in the failing mouse heart [509]. The numerous studies implicating the Wnt pathway in several aberrant cardiac processes highlight its importance in the pathological heart.

Therefore, in this chapter, transcriptomic arrays were utilised to investigate cardiomyopathy at different stages of the disease (10 weeks: pre-cardiomyopathic; 24 weeks: start of cardiomyopathy; 52 weeks: cardiomyopathy [81]), with the aim of identifying novel pathways involved in the early cardiac pathology. By separating the heart into several anatomical regions (right atrium (RA), left atrium (LA), right ventricle (RV), left ventricle (LV) and interventricular septum (IVS)), pathology and its progression could be analysed in more detail, contributing to chamber-specific and whole-heart understanding. The results illustrated a highly differentially expressed secreted frizzled-related protein (sFRP) 2 protein (a regulator of the Wnt pathway) and demonstrated its potential cellular mislocalisation in dystrophic hearts.

3.2 Materials and methods

3.2.1 Animals

Tissues were collected from male and female C57BL/10ScSnJ and *mdx* (C57BL/10ScSn-*Dmd*^{mdx}/J) mice at 10, 24 and 52 weeks of age (*n*=4 per group). Collected hearts were either suspended in 4% PFA for fixation or in All Protect Tissue Reagent (Qiagen, Venlo, the Netherlands) to prevent degradation of RNA and protein (*n*=4 per group). Hearts left in 4% PFA were incubated at room temperature for 24 hours, after which they were equilibrated in PBS supplemented with 50% sucrose at 4°C for a minimum of 7 days (*n*=4 per group). Tissues were subsequently passed through a 1:1 solution of 50% sucrose/PBS and Tissue-Tek O.C.T Compound (VWR, Radnor, USA) and then through a 100% O.C.T. Compound solution, before being frozen in 100% O.C.T. Compound and stored at -80°C.

Hearts suspended in All Protect Tissue Reagent were immediately dissected to obtain the RA, LA, RV, LV IVS, and incubated overnight at 4°C. Tissues were subsequently removed, cleared of the reagent, and stored at -80°C. Tissues were cut and weighed (>0.3mg) for downstream RNA and protein analyses.

3.2.2 Pip6a-PMO treatment

The cell penetrating peptide Pip6a (RXRRBRRXR YQFLI RXRBRXRB, where X is aminohexanoic acid, and B is β-alanine) was conjugated to a Phosphorodiamidate Morpholino Oligonucleotide, PMO (5'-GGCCAAACCTCGGCTTACCTGAAAT-3'; Gene Tools LLC, Philomath, OR, USA) through an amide linkage between the C-terminus of the peptide and the amine of the morpholine heterocycle on the 3' end of the PMO [303]. The conjugate was then dissolved in sterile H_2O and filtered through a 0.22 µm cellulose acetate membrane. Subsequently, female *mdx* mice at 4, 18 and 48 weeks of age received 10 mg/kg Pip6a-PMO conjugate injections dissolved in 0.9% saline once per week for a period of 6 weeks (*n*=3 for each age). Synthesis and injection of the peptides were performed by Dr Liz O'Donovan and Dr Corinne Betts respectively. At 10, 24 and 52 weeks of age, *mdx* mice treated with

Pip6-PMO and their age- and sex-matched controls (C57BL/10 and *mdx*, both *n*=4) were sacrificed and tissues were collected.

3.2.3 H2K-*mdx52* differentiation

The H2K-*mdx52* cells are male murine myoblast cells containing a deletion of exon 52 in the *Dmd* gene [279,510]. To ensure cell attachment, flasks were coated with 0.1mg/mL matrigel diluted in DMEM, and cells were cultured in GM at 33°C. To induce cell differentiation, medium was changed to DM and cells incubated at 37°C. 6-well plates were coated with matrigel and cells were seeded at 70,000 cells per well in GM (**Table 3.1**). Two days after seeding,, a subset of cells was collected for RNA and protein (*n*=3). The remaining wells were treated with siRNA targeting *Sfrp2* or a non-targeting siRNA at a concentration of 25 nM and incubated at 37°C. siRNA compounds contained a pool of 4 different siRNAs specifically targeting the gene of interest (ON-TARGET *plus* siRNA, Dharmacon, Cambridge, UK). siRNAs were allowed to form complexes with RNAiMAX Lipofectamine (ThermoFisher Scientific) in low-serum Opti-MEM medium (Life Technologies) for 5 minutes. Cells were subsequently transfected twice with siRNA in an Optimem:DM ratio of 1:5 with two days' rest in between transfections. Cells were collected six days after differentiation (*n*=3 per group), whereby medium was replaced with TrypLE Express Enzyme, cells incubated for 5 minutes at 37°C and the supernatant mixed with DM at a 1:1 ratio for enzyme neutralisation. 250 µL and 1,250 µL of the cell suspension were centrifuged at 4,000 × *g* for 4 minutes for RNA and protein respectively, whereby supernatant was removed and pellets stored at -20°C.

Table 3.1 Overview of H2K-*mdx52* treatment with RNA interference

Medium	GM		DM						
Day	1	2	3	4	5	6	7	8	9
Treatment	Seed cells	Rest	siRNA	Rest		siRNA	Rest		Collect

3.2.4 H&E staining

Haematoxylin and eosin (H&E) allow for the staining of acidic (coloured blue) and basic (coloured pink) structures in tissue sections. As such, haematoxylin highlights the nuclei in blue/purple and eosin allows for visualisation of the cytoplasm in pink. Fixed hearts were cryosectioned longitudinally into 10 µm sections. Slides were then air dried, incubated in PBS for OCT removal and stained in haematoxylin for 10-12 minutes. Sections were subsequently washed in distilled H_2O and stained with eosin for 30 seconds. Following four H_2O washes, slides were air-dried for 10-12 minutes and mounted in DPX mountant (BDH Chemicals, VWR, Lutterworth, UK).

3.2.5 RNA extraction

To prevent phenol contamination (which influences microarray measurements), RNA for Affymetrix arrays was extracted utilising RNeasy Fibrous tissue mini kit (Qiagen) according to manufacturer's instructions. Briefly, tissue was homogenised in 300 µL RLT buffer, supplemented with 1% β-mercaptoethanol, using the Precellys 24 Tissue Homogeniser (4 × 5,000 rpm for 30s). Lysates were then transferred to fresh tubes, supplemented with 590 µL of RNase-free water and 10 µL proteinase K, and incubated at 55°C for 10 minutes. Samples were subsequently centrifuged at room temperature for 3 minutes at 10,000 × *g* and supernatant was transferred to a new tube. 450µL of 100% ethanol was mixed with the samples, after which 700 µL of the solution was transferred to a RNeasy Mini Spin Column and centrifuged at room temperature for 30 seconds at 10,000 × *g*. The flow-through was discarded. This step was repeated with the remainder of the sample. 350 µL of RW1 was then added to the columns and centrifuged for 30 seconds at 10,000 × *g*. Columns were incubated with a mixture of 70 µL RDD buffer and 10 µL DNase I for 15 minutes, followed by addition of 350 µL RW1 buffer and centrifugation for 30 seconds at 10,000 × *g*. 500 µL RPE buffer supplemented with 4 volumes of 100% ethanol was added to the columns, followed by centrifugation for 2 minutes at 10,000 × *g* and this step was repeated. Columns were subsequently centrifuged for 1 minute at 10,000 × *g* to eliminate any residual buffers in the column. Lastly, 30 µL nuclease-free water was added to the

columns, after which samples were centrifuged for 1 minute at 10,000 × *g*. The eluate was then used to repeat the previous centrifugation step to maximise RNA recovery yield. RNA concentration was subsequently determined using a Nanodrop Spectrophotometer (ThermoFisher Scientific) and samples were stored at -80°C. All steps were performed at room temperature unless indicated otherwise.

All other RNA extractions utilised TRIzol Reagent as described in Chapter 2.

3.2.6 RT-qPCR

RNA was reverse transcribed as indicated in Chapter 2. A stable reference gene was determined through geNorm analysis (ge-SY-12; Primer Design, Chandler's Ford, UK), which allows comparison of stable expression of 12 reference genes in the samples of interest. One sample from each group (i.e. RA, LA, RV, LV and IVS from C57BL/10, *mdx* and Pip6a-PMO treated *mdx* males and females at 10, 24 and 52 weeks of age) was selected and 4 µL of 250ng RNA was mixed with 196 µL nuclease-free water for 1:50 dilution (total samples *N*=75). The cDNA template was amplified on a StepOne Plus real-time PCR Thermocycler (Life Technologies, Waltham, MA, USA) using SYBR Green Gene Expression Master Mix (Life Technologies). Samples were measured in duplicate, whereby reactions consisted of 5 µL 1:50 diluted cDNA, 10 µL SYBR Green Master Mix, 1 µL Primer Mix and 4 µL of nuclease-free water. Two negative controls were included (nuclease-free water run with cDNA synthesis followed by qPCR and nuclease-free water run in qPCR). Results were subsequently analysed with qBase+ (Biogazelle, Ghent, Belgium) provided with the geNorm kit. Analysis was performed according to manufacturer's instructions, using the 'geNorm experiment' option in the software. Limitations of the software allowed the merging of 10 plates only. Given the high sample and plate numbers (*N*=75, 12 reference genes on 24 plates), analysis had to be split into 'male', 'female' and 'treated female *mdx*'. The most stable reference genes from these analyses were then compared between groups. The following reference genes were analysed: *18S rRNA*, *Actb*, *Atp5b*, *B2m*, *Canx*, *Cyc1*, *Eif4a2*, *Gapdh*, *Rpl13a*, *Sdha*, *Ubc* and *Ywhaz*.

mRNA from genes involved in the Wnt signalling pathway was subsequently measured using qPCR. Genes analysed are listed in **Table 3.1**. The cDNA was diluted 1:10 and amplified on a StepOne Plus real-time PCR Thermocycler (Life Technologies) using SYBR Green Gene Expression Master Mix (Life Technologies).

Table 3.2 Primer sequences utilised in qPCR for genes of interest.

Gene of interest	Primer	Sequence 5' to 3'
Bambi	Forward	CACTTTGGAATGCTGTCACG
	Reverse	GAAGTCAGCTCCTGCATCTTAG
Fosl1	Forward	CCCTACCGAACATCCAGC
	Reverse	TTGGCACAAGGTGGAACT
Fzd1	Forward	TCCGGCAAGACACTGAATTC
	Reverse	GCGATGGCTAGGATCAGG
Fzd3	Forward	CTCTACCTTGTGCCACTCTTG
	Reverse	TCTGAGTAACCTGGTACGGAC
Rpl13a	Forward	TCCCTCCACCCTATGACAAG
	Reverse	GTCACTGCCTGGTACTTCC
Sfrp2	Forward	GCCTGCAAAACCAAGAATGAG
	Reverse	GTCTTGCTCTTTGTCTCCAGG
Tle2	Forward	CAGAGTGGACAGAGCTGC
	Reverse	CTTCCTCACTGTCATAAGGCC
Wnt1	Forward	GATTTTGGTCGCCTCTTTGG
	Reverse	CGTGGCATTTGCACTCTTG

3.2.7 Microarray analysis

Following RNA extraction, 8µL of RNA from the female samples was utilised for Affymetrix genechip mouse 2.1 ST arrays, which were performed at the Karolinska Institutet in Stockholm, Sweden. Arrays were performed in two steps, whereby first all heart chambers from C57BL/10 and *mdx* samples at 24 weeks were analysed to identify chambers that are more important for disease progression at early stages. Multiple experiment Viewer (TMeV; the Institute for Genomic Research, Rockville, MD, USA) was utilised to investigate differential gene expression, whereby Student's *t*-tests were used to identify differentially expressed genes between C57BL/10 and *mdx* for each chamber.

The log_2 array values were imported into TMeV for hierarchical clustering analysis. ANOVA analysis comparing all groups was performed to identify the differentially expressed genes and visualised in a hierarchically clustered heatmap. Principal component analysis (PCA) was performed in R using the 'prcomp' function. Both the PANTHER and the DAVID database were utilised for gene ontology (GO) term identification. The following statistical filters were applied: (I) $P<0.05$ for the *t*-tests followed by Bonferroni correction in PANTHER; (II) ratio|1.5| on the significant data from the *t*-tests with a Bonferroni correction in PANTHER; (III) $P<0.05$ for the *t*-tests followed by Benjamini-Hochberg correction ($P<0.05$) in DAVID; (IV) FDR<0.2 on the significant data as identified by the *t*-tests and Benjamini-Hochberg correction ($P<0.05$) in DAVID. The PANTHER database only allowed the use of a Bonferroni correction, whereas the FDR-like Benjamini-Hochberg correction was available in DAVID.

Gene expression of all remaining samples was subsequently measured with Affymetrix microarrays and data merged with previous results (resulting in combined data from two microarrays). Probe-level intensities were obtained using the affy package in Bioconductor [511], whereby the robust multi-array average algorithm [512] was used to perform background correction, quantile normalisation, and summarisation by robust linear model fit (median polish) on log2 transformed intensities for each probe set and sample. Variation due to batch effect was removed using the function ComBat [513] from the "sva" R package. Differential gene expression analysis was then performed using the empirical Bayes (eBayes) method from the limma R package [514]. To define a large set of differential expressed genes a threshold of fold change (FC) |1.5| was applied. Classical enrichment analysis was subsequently performed by testing the over-representation of GO biological processes terms within the group of differentially expressed genes using a Fisher test by "TopGO" R package [515], with a $P<0.05$ correction applied. Finally, REVIGO [516] was used to obtain the most representative enriched GO terms based on semantic similarity (simRel score). Transcriptomic data mining of the combined Affymetrix arrays was performed by Dr Viola Volpato in the laboratory of Dr

Caleb Webber at the University of Oxford. Data analysis, interpretation and figure design was performed by myself.

The transformed and analysed data were then utilised to produce a heatmap with TMeV and a PCA in R using the 'prcomp' function, with differentially expressed genes between all samples as identified by a one-way ANOVA in TMeV (P<0.05).

3.2.8 Western blotting

Protein was extracted from the separate heart chambers using RIPA lysis buffer (ThermoFisher Scientific), supplemented with 5% SDS, 1% protease inhibitors (Sigma-Aldrich) and 1% phosphatase inhibitors (Sigma-Aldrich). Atrial and ventricular samples were suspended in 100 µL and 200 µL lysis buffer respectively, after which they were homogenised utilising the Precellys 24 Tissue Homogeniser (4 × 5,000 rpm for 30 seconds; Bertin). Following incubation at 4°C for 5 minutes, lysates were centrifuged at 4°C for 5 minutes at 14,000 × *g*, aliquoted into two new tubes per sample and placed at -20°C or -80°C for short- or long-term storage, respectively.

In addition, nuclear and cytoplasmic protein was extracted from C57BL/10 and *mdx* LV heart tissue at 52 weeks using a nuclear extraction kit (Abcam) according to manufacturer's instructions. Briefly, tissue was homogenised in pre-extraction buffer supplemented with 0.1% dithiothreitol (DTT), 0.1% protease inhibitors and 1% phosphatase inhibitors (Sigma-Aldrich). Samples were then transferred to new tubes, incubated on ice for 15 minutes and centrifuged at 4°C for 15 minutes at 12,000 × *g*. Supernatant was removed and stored as cytoplasmic fraction at -80°C. The remaining pellets were resuspended in Extraction buffer, supplemented with 0.1% DTT, 0.1% protease inhibitors and 0.1% phosphatase inhibitors, and incubated on ice for 15 minutes, vortexing every 3 minutes. Lysates were then centrifuged at 4°C for 10 minutes at 14,000 × *g* and supernatant stored as nuclear fraction at -80°C.

Protein concentration was subsequently measured using the Pierce BCA Protein Assay Kit (ThermoFisher Scientific). 2 µL of lysate was mixed with 98 µL of ddH_2O and aliquoted into a 96-well plate with 250 µL working solution (50:1 ratio for reagent A:B). The plate was subsequently shaken for 330 seconds and incubated at 37 °C for 30 minutes, before protein measurement. A BSA (New England Biolabs, Ipswich, MA, USA) standard prepared with a 1:50 dilution of lysis buffer was included to quantify protein concentrations (1 mg, 0.5 mg, 0.25 mg, 0.125 mg, 0). Absorbance was measured using a ClarioStar plate reader (BMG LabTech, Offenburg, Germany) and compared with a standard curve of serially diluted BSA, allowing for protein quantification.

30-50 µg of protein lysate was used for Western blotting. A list of measured proteins can be found in **Table 3.2.**

Table 3.3 List of antibodies utilised for protein detection in Western blot.

Antibody	Product code	Host species	Dilution used	Secondary antibody
sFRP2	PA5-50962	Rabbit	1:500	800CW
Phospho β-catenin	#9565	Rabbit	1:1000	800CW
β-catenin	#25362	Rabbit	1:1000	Conjugated to HRP
Phospho JNK	#9255	Rabbit	1:1000	800CW
JNK	#9252	Mouse	1:1000	680RD
Phospho NFAT	SAB4503947	Rabbit	1:500	800CW
NFAT	PA536101	Rabbit	1:500	800CW
Dystrophin	NCL-DYS1	Mouse	1:100	800CW
Vinculin	V9131	Mouse	1:100,000	680RD

3.2.9 Immunofluorescence

Fixed hearts were cryosectioned longitudinally into 10 µm sections. Slides were then air dried and incubated in PBS to remove OCT compound from the slides. Hydrophobic barriers were drawn around heart sections using a PAP pen (Sigma-Aldrich) and samples were incubated with PBS supplemented with 0.15% Triton X-100 for 10 minutes at room temperature, followed by two 5 minute washes with PBS. Sections were then blocked at room temperature for 1 hour in blocking solution (PBS supplemented with 10% goat serum and 1% BSA), after which they were incubated with primary

antibodies in blocking solution overnight at 4°C. Following three 5 minute washes, samples were incubated with secondary antibodies in blocking solution at room temperature for 1 hour. This was followed by three more 5 minutes washes with PBS, a 5 minute incubation of 1:5,000 dilution Hoechst33342 (ThermoFisher Scientific) in PBS at room temperature and two final rinses with PBS before mounting with a 1:1 glycerol:PBS mixture. Sections were incubated with sFRP2 antibody (PA5-76794; ThermoFischer Scientific) at a 1:100 dilution and a secondary AlexaFluor 555 (1:200), and subsequently imaged on the Olympus FV1000 (Olympus, Tokyo, Japan) for cellular localisation or Leica DM IRB (Leica, Wetzlar, Germany) for total sFRP2 intensity measurement.

All images were analysed using FIJI (NIH, Bethesda, MD, USA). Total sFRP2 protein was quantified through the Measure option. To ascertain nuclear localisation of sFRP2, Hoechst33342 channel was selected and made binary or adjusted to threshold, utilising the Otsu method. 'Fill holes' was selected for the binary image, particles analysed, and nuclei localisations saved to ROI manager. ROI selections were mapped to the sFRP2 channel and fluorescence intensity measured as above. Output is reflected as average of nuclei intensities.

3.2.10 Statistical analysis

The following analyses were performed in GraphPad Prism 7 (GraphPad Software Inc, La Jolla, CA): Student's *t*-test, one-way ANOVA and two-way ANOVA. ANOVA with Tukey *post hoc* correction was used for comparisons between 3 groups or more. GraphPad was also utilised for visualisation of PCA plots.

3.3 Results

3.3.1 Heart morphology in control and diseased hearts

Gender differences have been observed in relation to the heart, and indeed, studies investigating differences in heart failure between male and female patients have ascertained that women presenting with heart failure are often older and have a better prognosis [517]. In contrast, aged female *mdx* mice (~22 months) exhibit a more severe cardiomyopathy than males, with abnormalities in ECG among others, as discussed in **Chapter 1** [518]. To further elucidate global gender differences at earlier stages of the disease, H&E staining was performed on whole-mount C57BL/10 and *mdx* hearts from both genders. Samples were longitudinally sectioned so that a view of all chambers was visible. Different pathological stages were included to assess the progression, i.e. 10 weeks representing pre-cardiomyopathy, 24 weeks early cardiomyopathy and 52 weeks developing cardiomyopathy (n=4 per group), based on data from [81] investigating physiological cardiomyopathic progression utilising MRI (**Figure 3.2**).

Comparing control with dystrophic hearts revealed small changes present at 10 weeks in both genders. Overall muscle wall was markedly wider and the RV wall appeared less even, particularly in the males (see arrowheads **Figure 3.2**). In the early cardiomyopathic stage (24 weeks), *mdx* myocardium width was more similar to controls, although the uniformity of the right ventricular wall worsened. Moreover, myofibre morphological organisation appeared less structured in the atria and ventricles. By 52 weeks of age, dystrophic pathology was clearly visible in both male and female *mdx* hearts, with irregular cardiomyocyte morphology and presumptive collagen depositions. Males appeared hypertrophic and exhibited more distinct morphological changes as defined above, consistent with DMD cardiac literature [519,520]. As expected, few differences were observed between the hearts of C57BL/10 males and females, with what appears to be a smaller male myocardium at 10 weeks compared to a larger male myocardium at 24 weeks, although this may also

be due to plane of section. By 52 weeks of age no differences between the two C57BL/10 genders were observed.

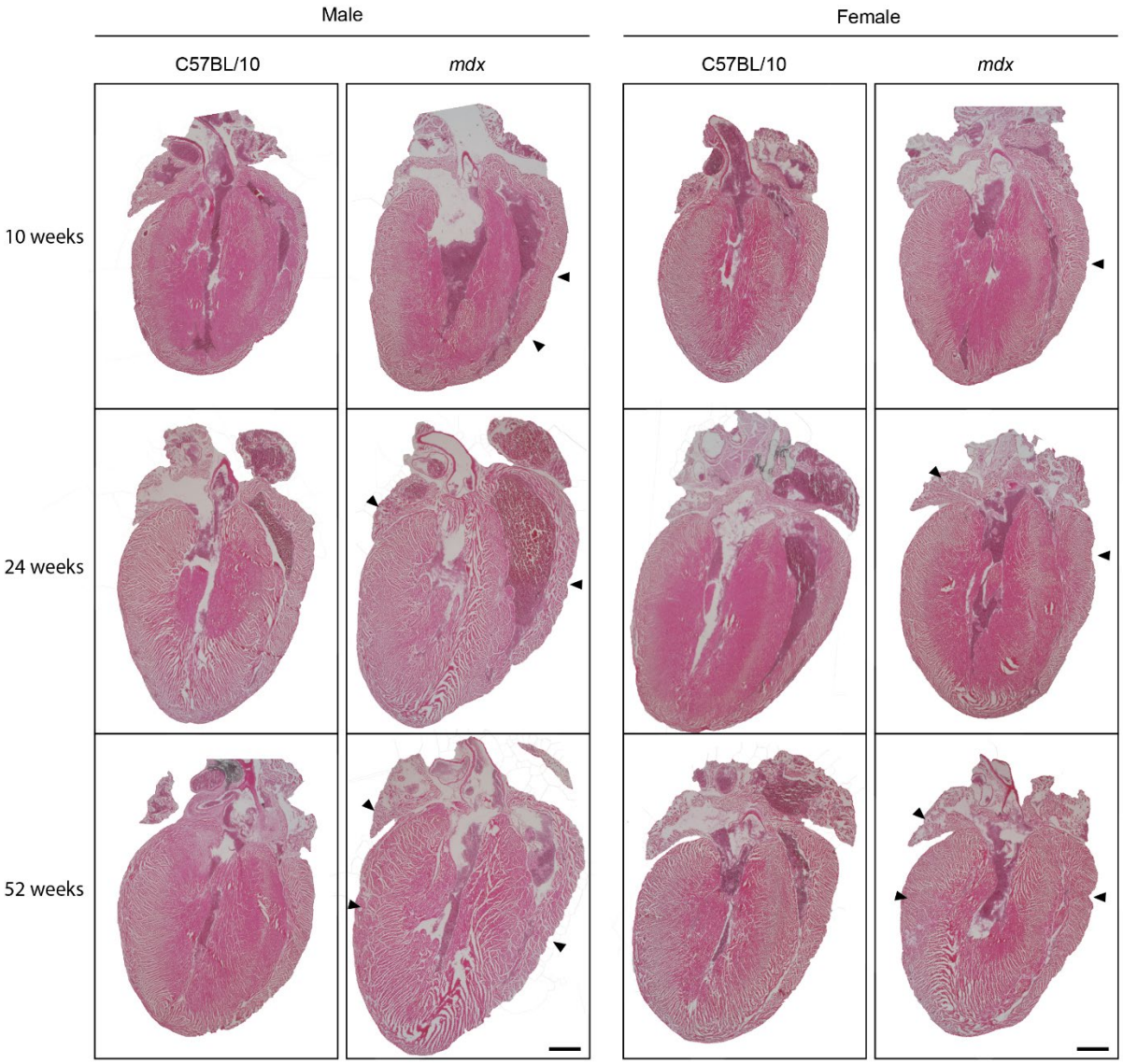

Figure 3.2 Heart morphology of male and female C57BL/10 and *mdx* at 10, 24 and 52 weeks of age. Male and female C57BL/10 and *mdx* hearts at 10, 24 and 52 weeks of age were fixed and stained with H&E to assess general morphology. Scale bars indicate 1 mm. Representative images of *n*=4.

3.3.2 Transcriptomic analysis for pathway discovery

At present, it is unclear what molecular processes are involved in the progression of cardiomyopathy over time. It is furthermore uncertain whether these processes differentially affect the various anatomical regions of the heart. Given that previous studies have demonstrated differences in physiological function and fibrotic progression between the two ventricles [25,81], this suggests the importance of individual chamber analysis. Additionally, whether these aberrant processes can be restored through long-term treatment with dystrophin re-expression at different stages of the disease remains an unanswered question. Therefore, transcriptomic arrays were utilised to assess transcript expression in C57BL/10, *mdx* and *mdx* mice treated with a peptide-conjugated PMO at different stages of the pathology (10, 24 and 52 weeks of age).

To ensure correction of aberrant pathways, *mdx* mice were given 6 weekly injections of 10mg/kg Pip6a-PMO, as the Gait and Wood labs have previously shown that this compound can efficiently restore dystrophin protein levels in the heart [303]. Mice age limitations allowed commencement of treatment at 4 weeks of age, resulting in cardiac transcript measurement at 10 weeks. Therefore, to ensure appropriate approximation of pre-cardiomyopathy, transcriptomic arrays were performed on female cardiac tissue. Although the heart is not completely devoid of a cardiac phenotype, the female pathology is less severe than males at 10 weeks, yet exhibits signs of cardiomyopathy at later ages (**Figure 3.2** and [518]).

To assess whether PPMO treatment resulted in adequate dystrophin restoration for downstream transcriptomic analysis, dystrophin levels were measured by Western blot in the RA, LA, RV, LV and IVS of female *mdx* mice at 10, 24 and 52 weeks of age (*n*=3 per group; **Figure 3.3A**). Successful dystrophin restoration was achieved in all anatomical regions of the heart for each time point. Dystrophin restoration was highest in the LA at 10 weeks (44%) and ranged between 19-31% in the other chambers (**Figure 3.3B**). By 24 weeks of age, dystrophin was similarly restored between the chambers and dystrophin protein expression ranged between 31-66% of WT levels. Although

dystrophin re-expression was less efficient at 52 weeks of age, significant protein restoration was still achieved, ranging between 13-34% of WT.

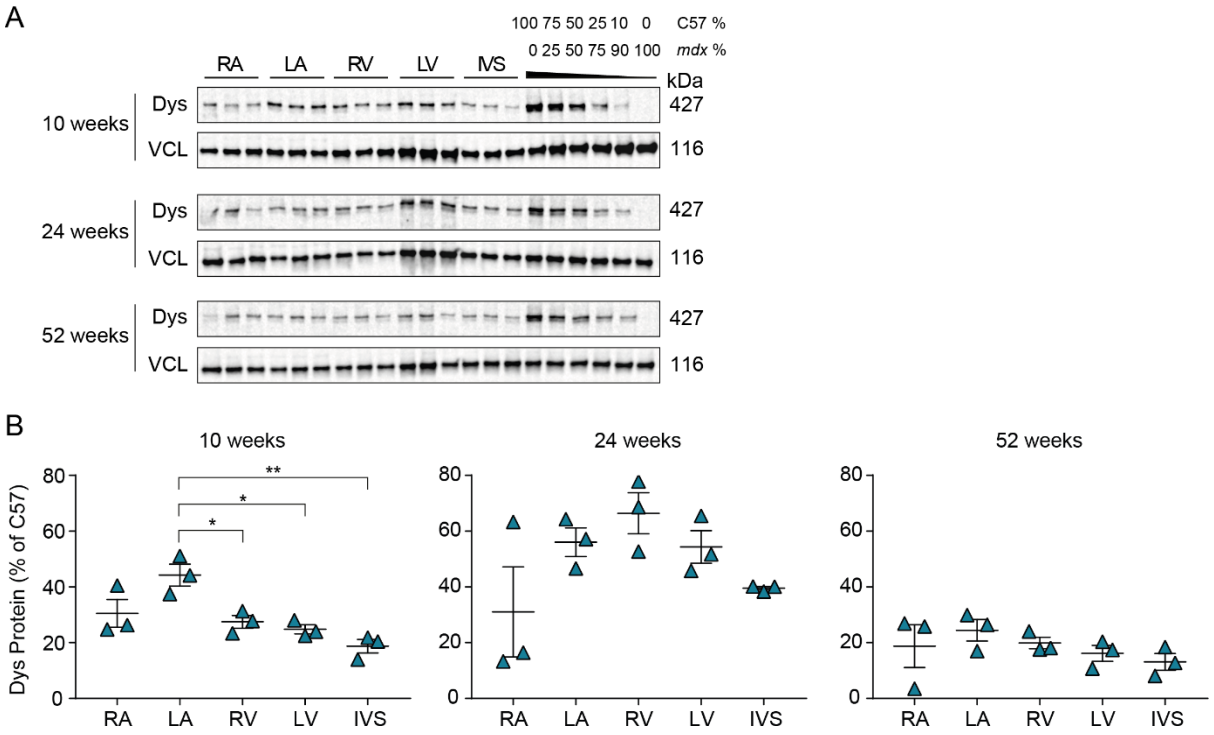

Figure 3.3 Dystrophin protein restoration in *mdx* hearts treated with Pip6a-PMO.
Female *mdx* mice at 4, 18 and 46 weeks of age were treated weekly with 10 mg/kg Pip6a-PMO until tissue collection at 10, 24 and 52 weeks of age. Hearts were dissected into RA, LA, RV, LV and IVS. **A** Protein was extracted and size separated on a 3-8% Tris-Acetate gel. A standard curve, consisting of mixtures of C57BL/10n and *mdx* protein lysates in ratios as indicated, was used to quantify dystrophin protein expression in the Pip6a-PMO-treated *mdx* hearts. **B** Protein quantification of Pip6a-PMO-treated *mdx* hearts (*n*=3). Dystrophin (Dys) protein expression was normalised to vinculin (VCL). All values are mean ± SEM. * P<0.05, ** P<0.01, one-way ANOVA with Tukey *post hoc* test.

Given the large number of samples when genotype, chambers and three ages were considered, an initial microarray analysis was performed in a subset of samples. RA, LA, RV, LV and IVS from female C57BL/10 and *mdx* at 24 weeks of age were dissected and equilibrated in a solution preserving RNA and protein, to prevent RNA degradation (*n*=4 per group). The intermediate age of 24 weeks was selected as it represents early cardiomyopathy, enabling identification of aberrant processes involved in primary chamber pathology. Following transcript microarray analysis, gene

markers for specific cardiac cell types were identified in the dataset to understand cell type composition within the samples.

Markers for cardiomyocytes (Homeobox protein Nkx-2.5, *Nkx2.5*; Cardiac Troponin I, *Tnni3*) [521–523], vascular smooth muscle cells (Calponin-1, *Cnn*; Actin, aortic smooth muscle, *Acta2*) [524], fibroblasts (Discoidin domain-containing receptor 2, *Ddr2*) [525], endothelial cells (Platelet endothelial cell adhesion molecule, *Pecam1*) [526], epicardial cells (Wilms tumour protein homolog, *Wt1*) [527] and Purkinje fibres (Contactin-2, *Cntn2*) [528] were analysed in the transcriptomic dataset (**Figure 3.4**). One-way ANOVA analysis indicated no significant differences between chamber comparison of C57BL/10 and *mdx* in any of the cell type markers ($P<0.05$). The results suggested that cell type composition in samples from the various strains (C57BL/10 and *mdx*) and chambers (RA, LA, RV, LV and IVS) were similar, thereby facilitating strain and chamber comparison.

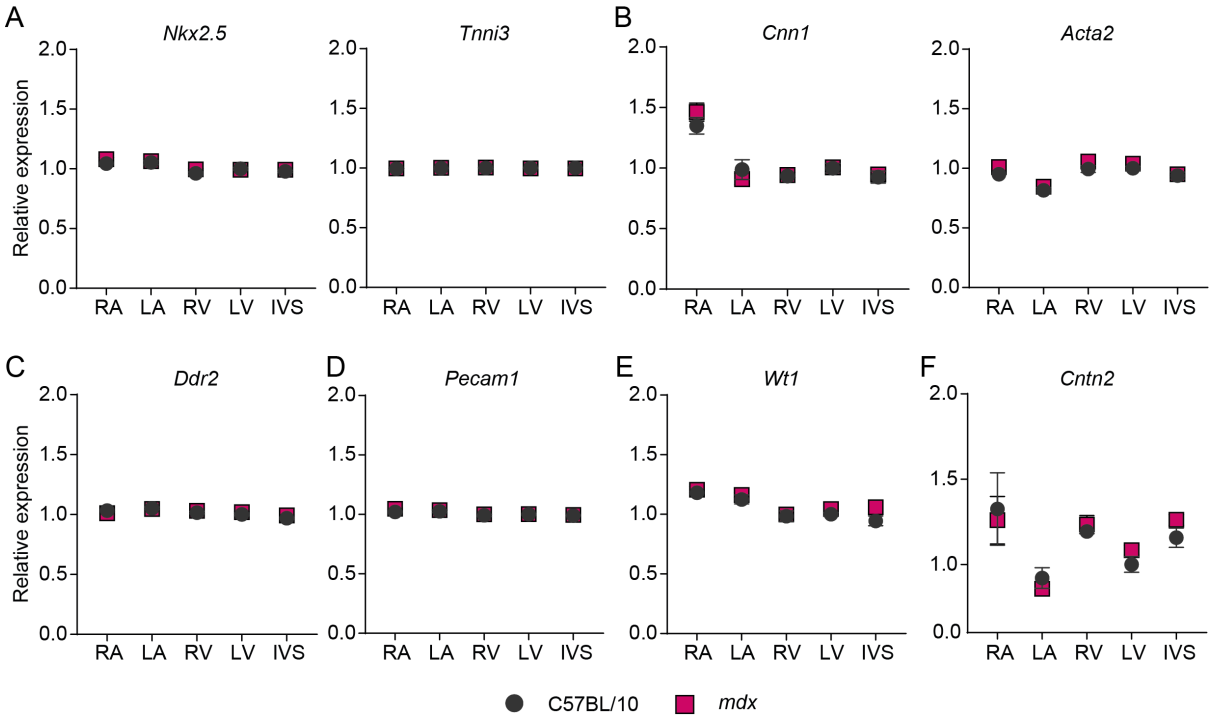

Figure 3.4 Comparison of heart cell type specific markers between C57BL/10 and *mdx* for all chambers.

Hearts from female C57BL/10 and *mdx* mice were collected at 24 weeks of age and dissected into RA, LA, RV, LV and IVS (*n*=4 per group). Gene expression levels of **A** cardiomyocyte-specific *Nkx2.5* and *Tnni3,* **B** vascular smooth-muscle cell-specific *Cnn1* and *Acta2,* **C** fibroblast-specific *Ddr2* **D** endothelial cell-specific *Pecam1*, **E** epicardial cell-specific *Wt1*, **F** Purkinje fibre-specific *Cntn2*. Batch-corrected $\log_2$ array signals were scaled such that the mean of the C57BL/10 LV was returned to a value of 1. All graphs are mean ± SEM. Two-way ANOVA identified no significant expression differences for any of the genes. mRNA expression levels acquired from transcriptomic dataset.

The data were then further analysed for a global overview (**Figure 3.5**). Differentially expressed genes (*n*=4,932) as identified through one-way ANOVA with Bonferroni correction (*P*<0.05) were visualised by heatmap (**Figure 3.5A**) and PCA (**Figure 3.5B**). The data showed a clear separation between the atrial and ventricular samples, indicating that the most samples cluster according to their anatomical location. Control and dystrophic samples cluster by anatomical region, with little intermingling between the strains as illustrated by the heatmap (e.g. RA 10 week *mdx* cluster together, next to RA C57BL/10 10 weeks). The C57BL/10 RA 3 does not cluster as clearly with remaining atrial samples from the group in the PCA plot (**Figure 3.5B**), although it generally exhibits a similar z-score directionality to the other atrial samples in the heatmap (**Figure 3.5A**). The results highlight clear

stratification between atrial and ventricular samples, but separation between each C57BL/10 and *mdx* chamber can be observed at this age.

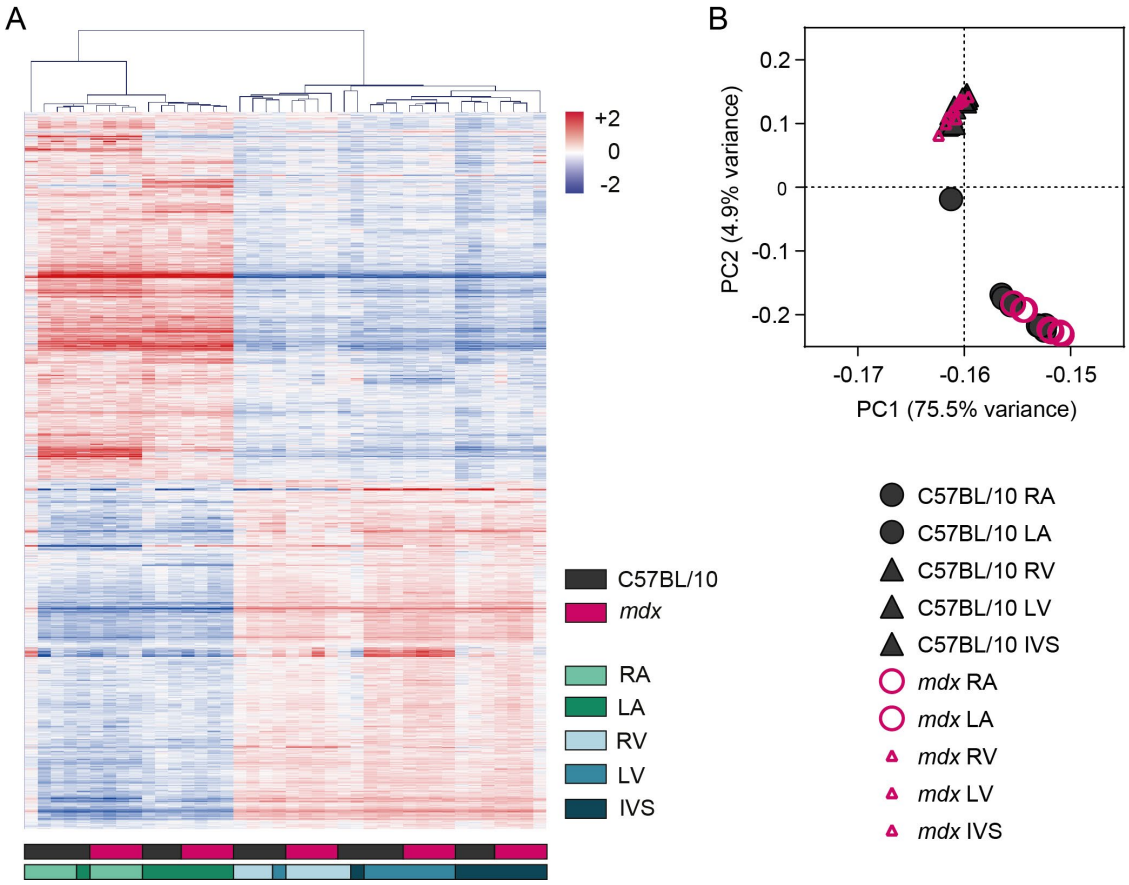

Figure 3.5 Clustering of differentially expressed genes between C57BL/10 and *mdx* at 24 weeks. Hearts from female C57BL/10 and *mdx* mice were collected at 24 weeks of age and dissected into RA, LA, RV, LV and IVS (n=4 per group). **A** Heatmap clustering of samples and genes identified as differentially expressed by one-way ANOVA (P<0.05) with Bonferroni correction. Scale bar represents row Z-scores, with red and blue indicating higher and lower than mean abundance respectively. Strain and chamber are indicated by colour below heatmap. **B** PCA clustering of samples. One-way ANOVA (P<0.05) with Bonferroni correction.

To further elucidate the transcriptomic differences between control and disease chambers, Student's *t*-tests were performed between C57BL/10 and *mdx* to identify differentially expressed genes for each chamber (P<0.05), which identified 590 significant genes in the RA, 598 in the LA, 1,065 in the RV, 1,156 in the LV and 1,068 in the IVS (**Table 3.3**). The data were subsequently filtered using

several statistical methods (as described in **Chapter 3.2**) and transcripts were analysed by GO. The GO classification system constitutes pathways characterised based on known clustering of genes and proteins as identified by experimental and inferential data. GO enrichment analysis is then performed with the dataset. Although this limits identification of novel connections, the method proves useful for ascertaining novel roles of established pathways in DMD.

Both the PANTHER and the DAVID database were utilised to search for genes matching to established GO terms (detailed in **Chapter 3.2**). Similar classification patterns were observed between the different analyses (e.g. fewer GO terms identified in LA, and a higher number in RA), and an overview of GO terms identified following DAVID database analysis is given as a representative in **Table 3.3**. Interestingly, even though the right and left atria comprised a comparable number of differentially expressed genes, many of the RA genes cluster within known GO terms, whereas those in the LA do not. This could indicate that the LA pathology is less organised (suggestive of lesser pathology) or it entails novel pathways not yet codified in GO classifications. A similar pattern is observed for the RV, LV and IVS, with the latter exhibiting fewer genes clustering to known GO terms than the RV or LV. Among the GO terms identified, many are related to the extracellular matrix composition and the immune system. Both themes are expected given the known pathology of DMD, whereby immune infiltration and changes in fibrosis-related matrix metalloproteases are observed (as detailed in **Chapter 1**). Together, the data suggest a more focused pathological progression at this age in the RA, RV, and LV based on GO term enrichment and therefore these chambers were further investigated at the other time points (10 and 52 weeks) from female C57BL/10 and *mdx,* and all ages from the treatment groups with transcriptomic microarrays (*n*=3 per group).

Table 3.4 Gene ontology enrichment analysis in female C57BL/10 vs *mdx* heart samples at 24 weeks of age.

	RA	LA	RV	LV	IVS
Differentially expressed transcripts	590	598	1065	1156	1068
GO terms	Extracellular matrix	N/A	Secreted	Immunoglobulin V region	N/A
	Proteinaceous extracellular matrix		Glycoprotein	Immunoglobulin-related groups	
	Extracellular region part		Cytoplasmic vesicle	Ribosome	
			Extracellular matrix	Signal	
				Heterotetramer	
				Secreted	
				Disulfide bond	
				Extracellular matrix	

Following Affymetrix analysis on the additional samples, the data were merged with the previous experiment and, because technical variations between the two microarray runs affected the measurements, data were batch-corrected. One-way ANOVA was subsequently performed with Bonferroni *post hoc* correction ($P<0.05$) and the data were visualised by hierarchical clustering heatmap and PCA (**Figure 3.6**). These clearly exhibit a divide between atrial and ventricular samples (**Figure 3.6A**). The PCA plot illustrates that at 10 weeks of age, C57BL/10 and *mdx* samples cluster quite closely together for all chambers. The later ages exhibit further segregation between the two strains, which is particularly visible in the ventricular samples at 52 weeks (**Figure 3.6B**). Careful consideration of the treatment shows that these cluster closely to the *mdx* samples for each chamber at 10 and 52 weeks of age. At the early cardiomyopathic stage (24 weeks), treatment is observed to partially restore gene expression as Pip6a-PMO treated *mdx* samples cluster in between the C57LB/10 and *mdx*. However, these differences may be due to the batch effect (treatment samples analysed in

different microarray). The results showed that treatment had little effect on the global gene expression pattern.

A

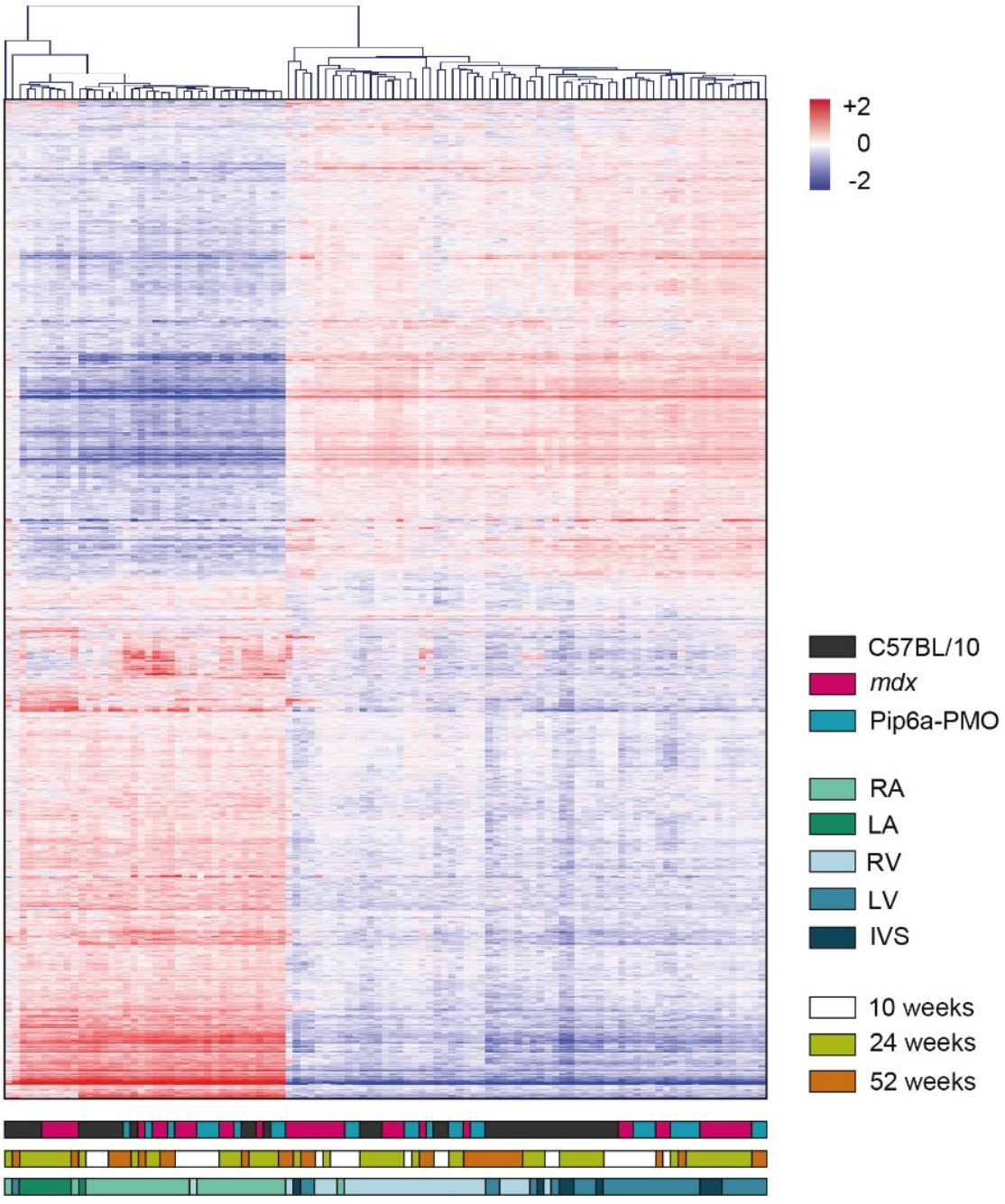

B

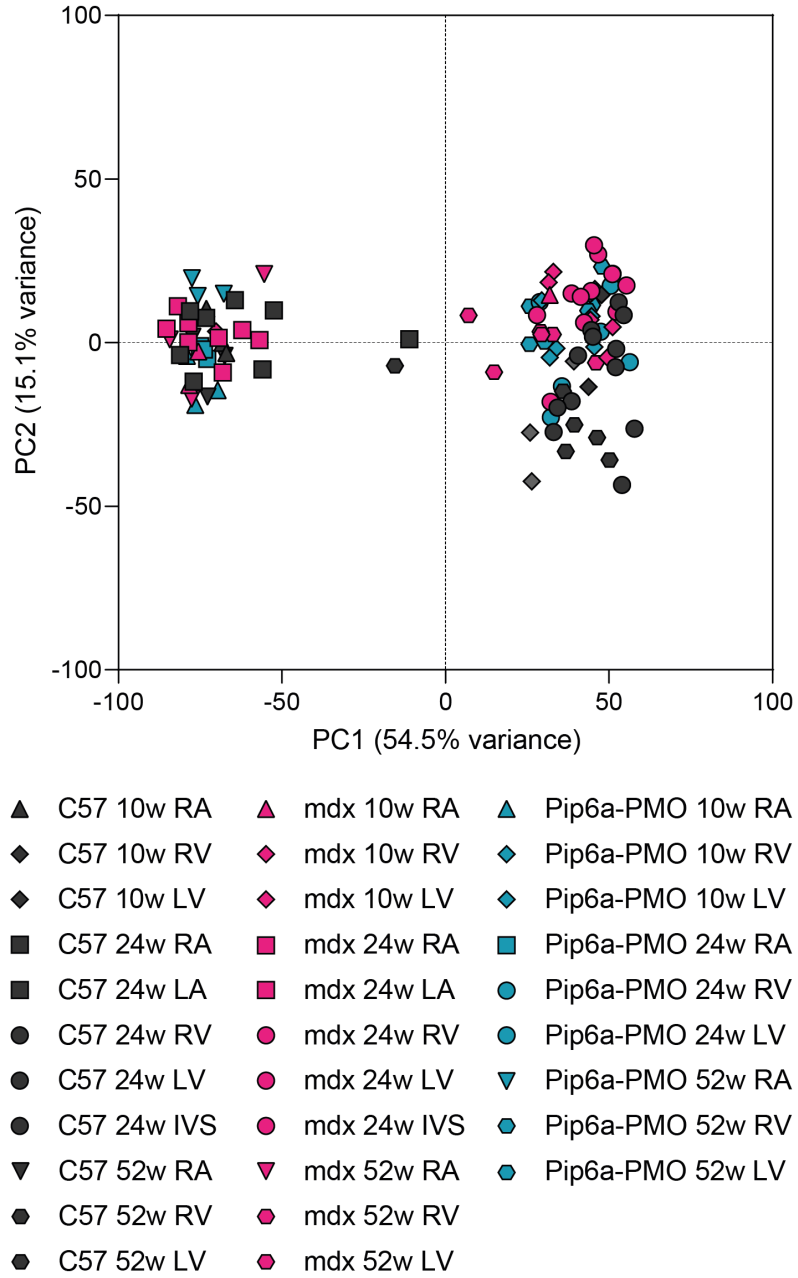

Figure 3.6 Clustering of differentially expressed genes between female C57BL/10, *mdx* and Pip6a-PMO at 10, 24 and 52 weeks.

Hearts from female C57BL/10, *mdx* and Pip6a-PMO-treated *mdx* mice were collected at 10, 24 and 52 weeks of age and dissected into RA, LA, RV, LV and IVS (n=3-4 per group). **A** Heatmap clustering of samples and genes identified as differentially expressed by one-way ANOVA (P<0.05) with Bonferroni correction. Scale bar represents row Z-scores, with red and blue indicating higher and lower than mean abundance respectively. Strain, age and chamber are indicated by colour below heatmap. **B** PCA clustering of samples. One-way ANOVA (P<0.05) with Bonferroni correction. Data generated based on analysis from Dr Viola Volpato.

Comparisons between C57BL/10 and *mdx* were subsequently made for each anatomical region at each time point (FC > |1.5|). Genes above the fold change threshold were utilised for GO enrichment analysis. As this resulted in the generation of several hundreds of GO terms, reduce and visualise gene ontology (REVIGO) was employed. This programme structures the data by grouping the GO terms into coherent themes based on semantic similarity, removing redundant GO terms. The themes obtained for C57BL/10 and *mdx* comparisons are illustrated in **Table 3.4**. Colours are utilised to indicate overlap in themes between the chambers and/or ages.

The REVIGO analysis demonstrated little similarity between the three ages for the RA and LV, suggestive of a dynamic pathological progression (**Table 3.4**). The two common themes, cell adhesion and locomotion, are indicative of heart remodelling. Interestingly, themes between the 10 week and 52 week RV are very similar (associated with cellular remodelling and inflammation), suggestive of similar aberrant processes at the early and later pathological stages. The REVIGO analysis highlights that the RA and LV exhibit transitions in processes contributing to pathology over time, whereas cardiomyopathy in the RV entails similar mechanisms with age.

Table 2.5 Summary of theme compilation from REVIGO for comparisons between female C57BL/10 and *mdx* RA, RV and LV at 10, 24 and 52 weeks of age. Colours indicate overlap between chambers and/or ages. Data generated based on analysis from Dr Viola Volpato.

RA	RV	LV
10 weeks		
Response to Endogenous Stimulus		Detection of Stimulus
Cell Adhesion	Cell Adhesion	
Biological Adhesion	Biological Adhesion	
Behaviour	Locomotion	
Movement of Cell or Subcellular Component	Extracellular Matrix Organisation	
Positive Regulation of Multicellular Organismal Process	Inflammatory Response	
Striated Muscle Tissue Development	Regulation of Cell Proliferation	
24 weeks		
Response to Mechanical Stimulus	Detection of Chemical Stimulus Involved in Sensory Perception of Smell	
Locomotion		
Cell-Cell Signalling		
Secretion		
Blood Circulation		
52 weeks		
Cell Adhesion	Cell Adhesion	Cell Adhesion
Biological Adhesion	Biological Adhesion	Biological Adhesion
Locomotion	Locomotion	Locomotion
Cell Activation	Extracellular Matrix Organisation	Extracellular Matrix Organisation
Response to Wounding	Defence Response	Circulatory System Development
Regulation of Body Fluid Levels	Positive Regulation of Multicellular Organismal Process	Cellular Response to Growth Factor Stimulus

3.3.3 Involvement of *Sfrp2* and Wnt-related genes in the dystrophic heart

Following further detailed investigation, the gene *Sfrp2* is shown to be associated with many of the common themes (locomotion, cell communication and regeneration) and was consistently upregulated (FC>2.5) in all chambers at almost every age (**Figure 3.7**). *Sfrp2* encodes the Secreted Frizzled-Related Protein 2 (sFRP2), which consist of a C-terminal Netrin domain and a Frizzled domain

[529,530]. It is a major regulator of the Wnt signalling pathway, where it is thought to exert its functions through several mechanisms; (I) Binding Wnt ligands at the Frizzled domain, thereby preventing association of the Wnt ligand with its receptor; (II) Binding Frizzled (FZD) receptors, inhibiting Wnt signalling; (III) Formation of sFRP2 dimers, preventing their binding to Wnt ligands, enabling Wnt signalling (III); Association of Wnt to the Netrin domain, enabling association of the Wnt ligand with its receptor through the CRD domain. It is unclear when each function is exerted [530,531]. Other non-Wnt-related functions include inhibition of apoptosis, BMP signalling and osteoclast formation [531]. sFRP2 has been shown to induce differentiation in C2C12 myoblast cells through the canonical β-catenin pathway [190] and in cardiac progenitor cells following cardiac ischaemia through the planar cell polarity arm acting on JNK [532]. Furthermore it activates cardiac fibroblasts through the canonical Wnt pathway [533]. Most importantly, its expression is increased in skeletal muscle from the *mdx* mouse, whereas patient biopsies exhibit a decrease compared to controls [534]. It is unclear why there is a discordance between mouse and patient data, but this may be due to stages and development of pathology.

In the current study, batch-corrected $\log_2$ array signal of *Sfrp2* mRNA, as measured by the Affymetrix arrays, illustrate significant *Sfrp2* upregulation in the RA at 10 and 24 weeks, the LV at 24 weeks and the RV at 52 weeks of age in female *mdx* mice compared to WT (*n*=3-4 per group; **Figure 3.7**). Pip6a-PMO treatment significantly restored *Sfrp2* expression in the RA at 24 weeks of age. The remaining anatomical areas and ages did not exhibit a significant difference in expression between Pip6a-PMO treated *mdx* and *mdx* or C57LB/10, although a trend towards *Sfrp2* restoration was observed. Other Wnt ligands and Frizzled receptors were observed to be differentially expressed (**Appendix 8.1**), suggesting Wnt pathway involvement in DMD, consistent with previous reports [201,501].

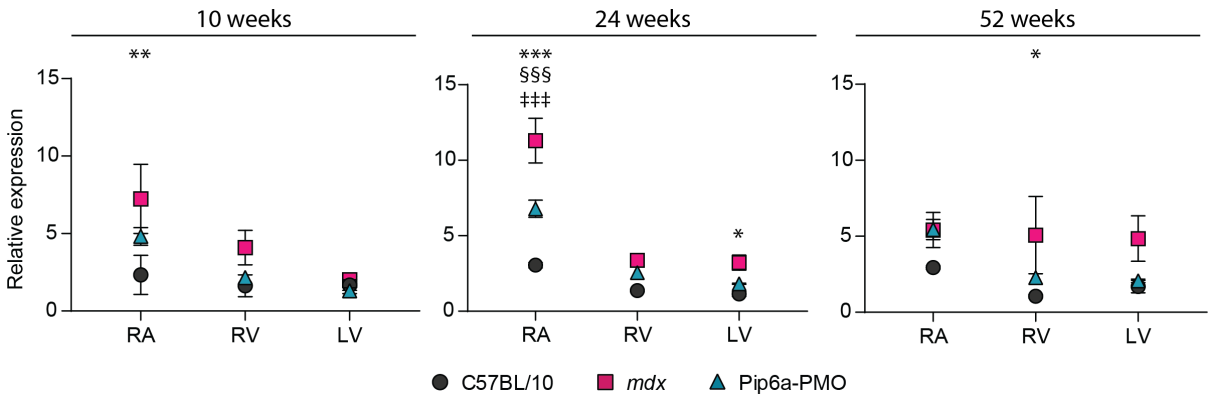

Figure 3.7 mRNA expression of *Sfrp2* in female mice as measured by Affymetrix arrays.
Affymetrix arrays were performed on RNA extracted from female C57BL/10, *mdx* and Pip6a-PMO-treated *mdx* mice at 10, 24 and 52 weeks (*n*=3-4 per group). Batch-corrected $\log_2$ array signals were scaled such that the mean of the C57BL/10 LV 10w was returned to a value of 1. Values are mean ± SEM. * *P*<0.05, ** *P*<0.01, *** *P*<0.001 for comparisons between C57BL/10 and *mdx*. §§§ *P*<0.001 for comparisons between C57BL/10 and Pip6a-PMO-treated *mdx*. ‡‡‡ *P*<0.001 for comparisons between *mdx* and Pip6a-PMO-treated *mdx*. Two-way ANOVA with Tukey *post hoc* correction, comparing groups within each chamber.

The transcriptomic results revealed an important role for the Wnt-signalling pathway related *Sfrp2*, with several Wnt ligands and Fzd-receptors differentially expressed between C57BL/10 and *mdx* (**Appendix 8.1**). *Sfrp2* was therefore further validated through orthogonal methodology, RT-qPCR, in the female samples utilised for the transcriptomic arrays and age-matched male C57BL/10 and *mdx* hearts. The latter were included to confirm findings in the male hearts. To enable accurate RT-qPCR analysis, GeNorm was utilised to identify a stable housekeeping gene. **Figure 3.8** illustrates expression stability measures of 12 commonly used reference genes, as assessed with male and female C57BL/10, *mdx* and Pip6a-PMO-treated *mdx* at 10, 24 and 52 weeks of age (1 representative from each group, *N*=75). All males and Pip6a-PMO treated females exhibit highest stability of *Rpl13a*, which is the second most stable reference gene in the other females. In accordance with other recent studies [535], the widely used reference gene *Gapdh* was one of the least stable of all assessed genes, suggesting it may be a poor choice for reference in RT-qPCR. The females illustrate a high stability for

Ywhaz, but as this gene did not perform as well in the males, *Rpl13a* was chosen for as a reference gene.

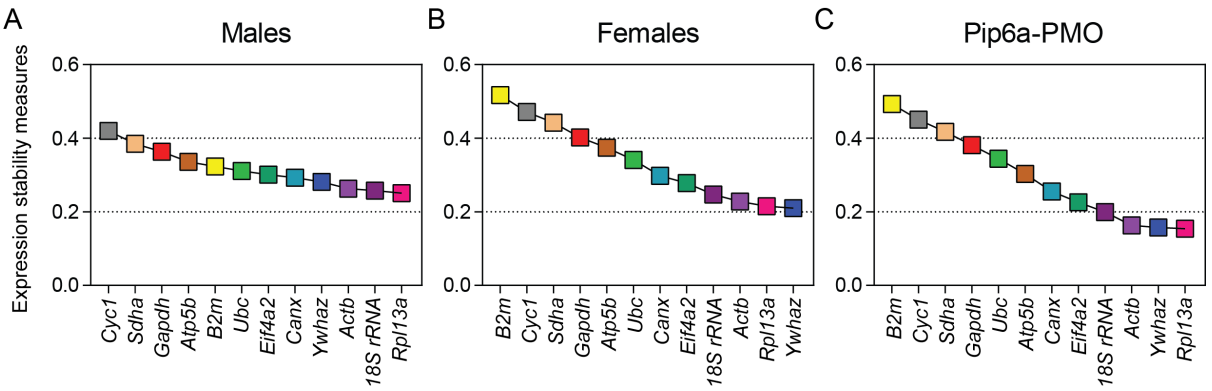

Figure 3.8 GeNorm analysis identifying stable expression of 12 common housekeeping genes. RT-qPCR was performed on RNA extracted from male and female C57BL/10 and *mdx* mice, and Pip6a-PMO-treated female *mdx* mice at 10, 24 and 52 weeks (*N*=75). Graphs illustrate the expression stability measures identified in **A** all male samples, **B** female C57BL/10 and *mdx* at all ages, and **C** all Pip6a-PMO treated *mdx* samples. Reference genes are sorted from low to high stability.

Following identification of a stable housekeeping gene, *Sfrp2* transcript was measured in all samples (male and female C57BL/10 and *mdx*, and Pip6a-PMO treated female *mdx* at 10, 24 and 52 weeks of age, *n*=4 per group; **Figure 3.9**). *Sfrp2* was significantly upregulated in the female RA, LA and RV at 10 weeks, the RA and RV at 24 weeks and the RA, LA, RV and IVS at 52 weeks of age. Similarly, the males exhibited differential expression of *Sfrp2* in the RA and RV at 10 weeks, and the RV, LV and IVS at 24 and 52 weeks. Differential expression increased with disease progression (i.e. between 10, 24 and 52 weeks), especially for the ventricular chambers. Interestingly, *mdx* to C57B/10 transcript ratios were larger in the males than in females at the two younger ages. These ratio differences may be explained by an earlier manifestation of cardiomyopathy in male *mdx* mice. Noticeably, *Sfrp2* expression in the left atrium of male *mdx* remained low across all ages, whereas it was consistently upregulated in the right atrium (although did not always reach significance). This suggests a difference between these two chambers, perhaps related to the cardiac physiological function, and therefore it is important to further understand the role of *Sfrp2* in the dystrophic heart. The RT-qPCR data

validated the Affymetrix arrays and illustrated upregulation of *Sfrp2* during early progression and later manifestation of the disease.

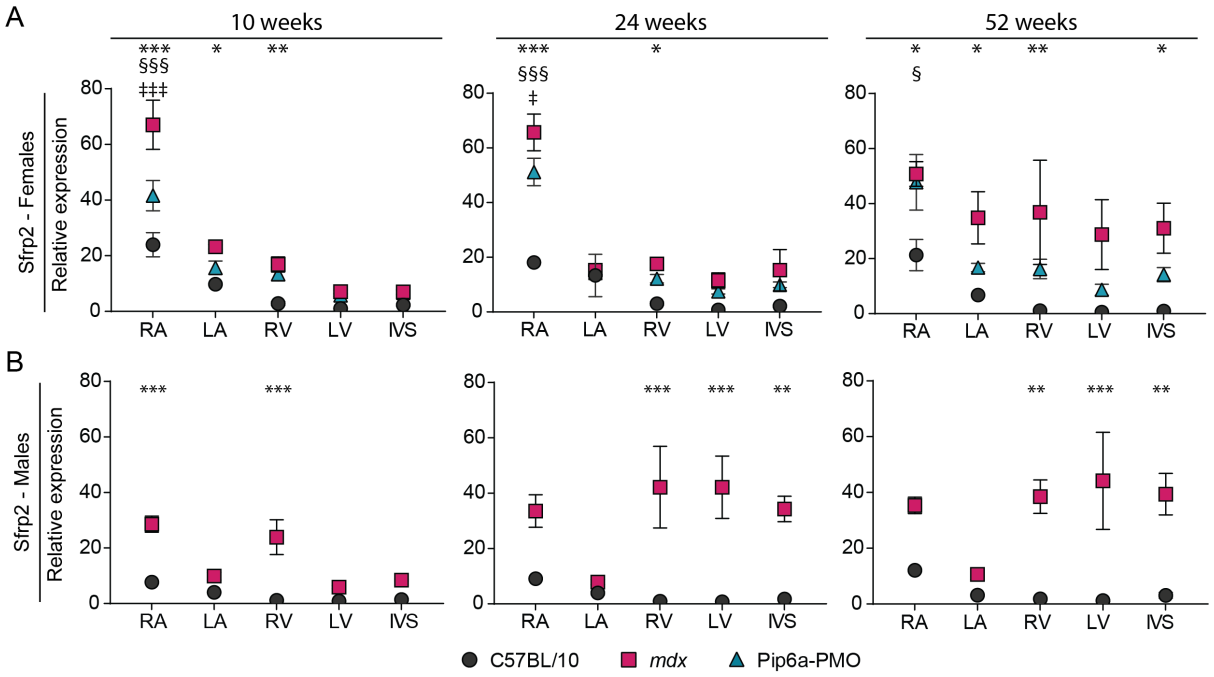

Figure 3.9 mRNA expression of *Sfrp2* in male and female mice.
RT-qPCR was performed on RNA extracted from male and female C57BL/10 and *mdx* mice, and Pip6a-PMO-treated female *mdx* mice at 10, 24 and 52 weeks. Graphs illustrate mRNA expression of *Sfrp2* identified in **A** all female samples and **B** all male samples (*n*=4 per group). Expression was normalised to *Rpl13a*. Expression ratios were scaled such that the mean of the female C57BL/10 LV 10w was returned to a value of 1. Values are mean ± SEM. * *P*<0.05, ** *P*<0.01, *** *P*<0.001 for comparisons between C57BL/10 and *mdx*. § *P*<0.05, §§§ *P*<0.001 for comparison between C57BL/10 and Pip6a-PMO-treated *mdx*. ‡ *P*<0.05, ‡‡‡ *P*<0.001 for comparisons between *mdx* and Pip6a-PMO-treated *mdx*. Two-way ANOVA with Tukey *post hoc* correction, comparing groups within each chamber.

In addition to *Sfrp2*, transcript levels of several differentially expressed genes in the transcriptomic dataset were selected for further validation by RT-qPCR in the same samples. *Bambi*, *Fzd1*, *Fzd3* and *Tle2* were analysed as these genes play roles in the different aspects of the Wnt-signalling pathway. *Fzd1* (Frizzled-1) and *Fzd3* (Frizzled-3) are members of the G-protein coupled receptor family [536] and contribute to the canonical [537] and non-canonical [538] arm of the Wnt-pathway, respectively (**Figure 3.10**). sFRP2 protein interacts with these receptors to modulate downstream effectors. Small differential expression changes were observed in both males and

females at different time points, but no consistent pattern was detected. Female *mdx* at 52 weeks expressed higher levels of *Fzd1* in the LA, RV and IVS, although these same changes were not seen in the males at the same age. It is possible that *Fzd1* plays a role in pathology in these chambers only at an older age in the female *mdx* heart. *Fzd3* expression was significantly lower in the LA of *mdx* male hearts at 24 weeks of age, while this was not observed at any of the other ages.

Expression levels of *Bambi* (BMP and activin membrane-bound inhibitor homolog) and *Tle2* (Transducin-like enhancer protein 2) were also determined (**Figure 3.11**). *Bambi* is a transmembrane glycoprotein and its downregulation reduces activation of the Wnt β-catenin pathway, thereby inhibiting myoblast differentiation [539]. *Tle2,* on the other hand, is a transcriptional repressor of downstream β-catenin targets *Tcf/Lef* transcription factors [540]. Apart from the C57LB/10 and Pip6a-PMO comparison at 52 weeks in the IVS, RT-qPCR data indicated no differential expression between male nor female C57BL/10 and *mdx* at any of the ages for *Bambi*. Female Pip6a-PMO treated LA at 10 weeks was significantly elevated compared to C57BL/10 and *mdx* for *Tle2*. Furthermore, *mdx* exhibited a reduction in *Tle2* expression in the RV at 52 weeks of age. No other comparison was significant.

The results illustrated large transcriptomic differences in *Sfrp2* expression between C57BL/10 and *mdx* in both genders. Interestingly, transcript level differences for other Wnt-pathway components (*Fzd1*, *Fzd3*, *Bambi* and *Tle2*; **Figures 3.10** and **3.11**) were negligible, although these genes may be activated at the translational or post-translational level [541]. Indeed, the effector proteins of the different arms of the Wnt signalling pathway require (de)phosphorylation for their translocation and subsequent gene transcription [498]. Therefore, assessing activation of this pathway requires downstream protein analysis to ascertain whether the different arms are affected in dystrophic hearts.

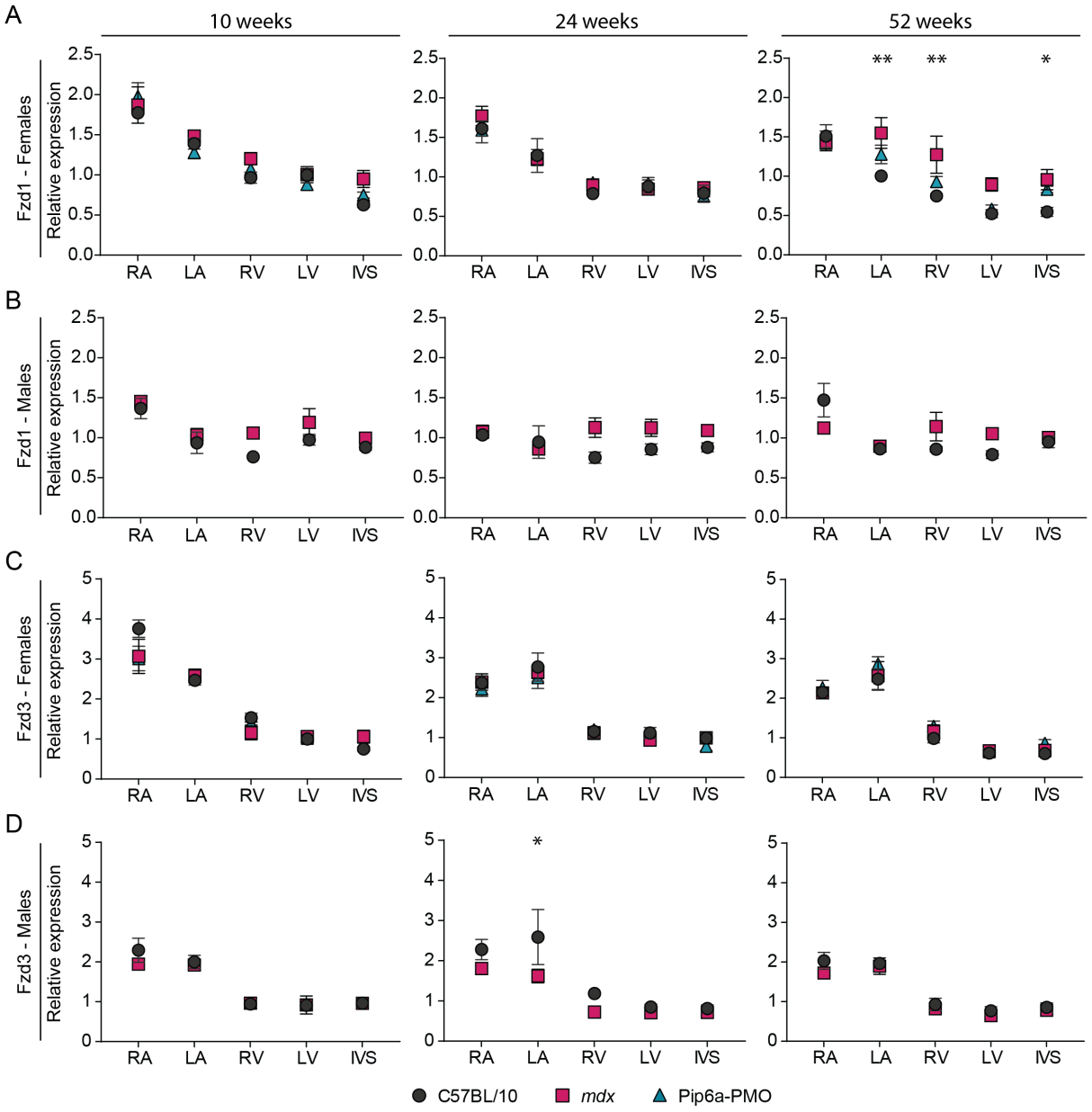

Figure 3.10 mRNA expression of *Fzd1* and *Fzd3* in male and female mice.

RT-qPCR was performed on RNA extracted from male and female C57BL/10 and *mdx* mice, and Pip6a-PMO-treated female *mdx* mice at 10, 24 and 52 weeks (*n*=4 per group). Graphs illustrate mRNA expression of *Fzd1* and *Fzd3* identified respectively in **A, C** all female samples and **B, D** all male samples. Expression was normalised to *Rpl13a*. Expression ratios were scaled such that the mean of the female C57 LV 10w was returned to a value of 1. Values are mean ± SEM. * $P<0.05$, ** $P<0.01$ for comparisons between C57BL/10 and *mdx*. Two-way ANOVA with Tukey *post hoc* correction, comparing groups within each chamber.

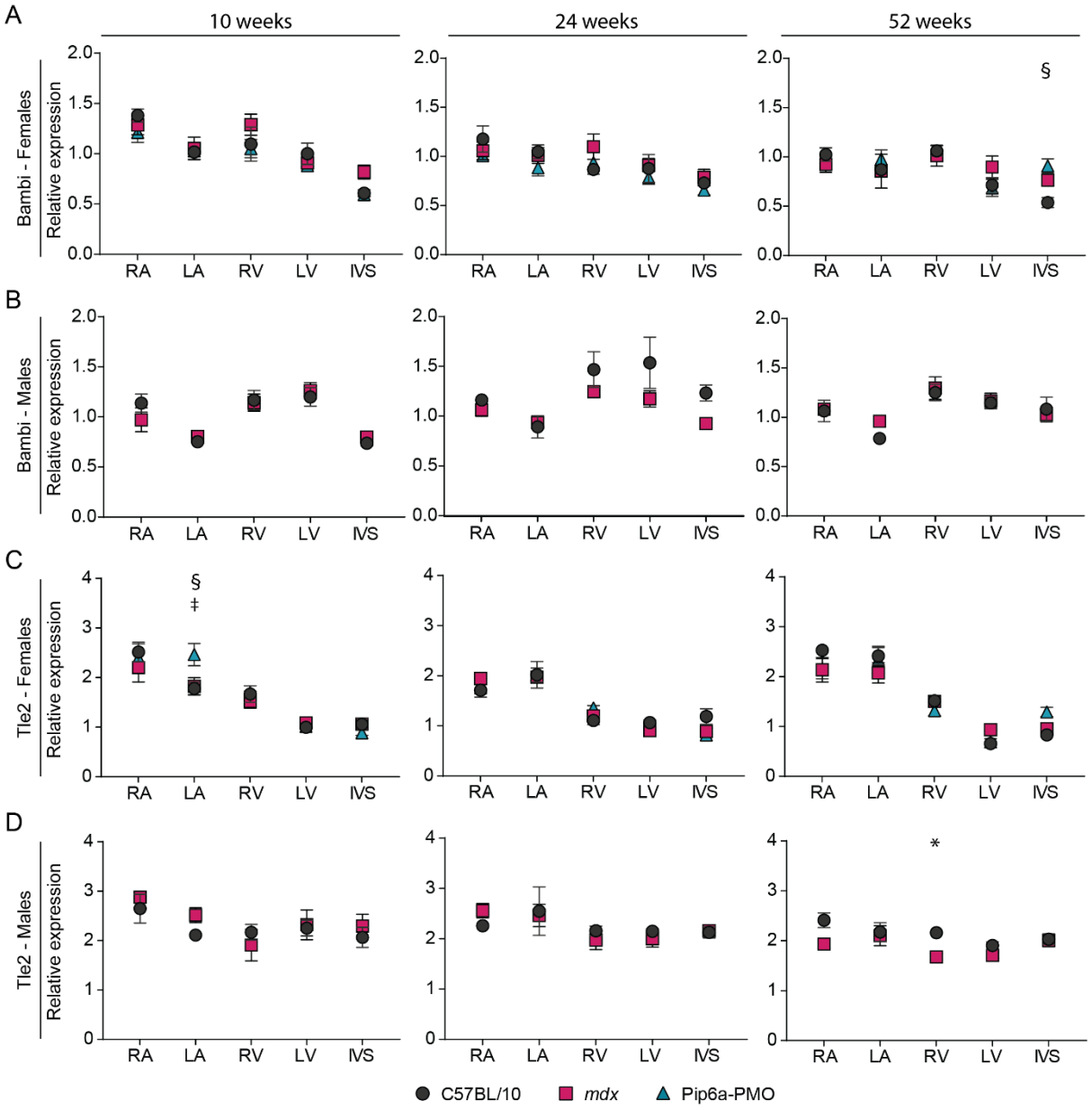

Figure 3.11 mRNA expression of *Bambi* and *Tle2* in male and female mice.

RT-qPCR was performed on RNA extracted from male and female C57BL/10 and *mdx* mice, and Pip6a-PMO-treated female *mdx* mice at 10, 24 and 52 weeks (*n*=4 per group). Graphs illustrate mRNA expression of *Bambi* and *Tle2* identified in **A, C** all female samples and **B, D** all male samples. Expression was normalised to *Rpl13a*. Expression ratios were scaled such that the mean of the female C57 LV 10w was returned to a value of 1. Values are mean ± SEM. * *P*<0.05 for comparison between C57BL/10 and *mdx*. § *P*<0.05 for comparison between C57BL/10 and Pip6a-PMO-treated *mdx*. ‡ *P*<0.05 for comparison between *mdx* and Pip6a-PMO-treated *mdx*, two-way ANOVA with Tukey *post hoc* correction.

3.3.4 Identification of Wnt pathway protein involvement

Transcriptomic arrays were performed on female control and disease mice as it better represented a pre-cardiomyopathic stage at 10 weeks (**Chapter 3.3.1**). This allowed the identification of the *Sfrp2* gene and Wnt signalling pathway involvement in the young dystrophic heart. Following the identification of this pathway, further experiments were performed in males to better extend the relevance of these findings to the DMD patient population. Given that protein phosphorylation is important for the activity of the effector proteins of the Wnt signalling pathway, phosphorylated and non-phosphorylated protein levels for β-catenin, JNK and NFAT were analysed. The phosphorylated/non-phosphorylated ratios were calculated to determine changes in protein activation.

First, sFRP2 protein levels were evaluated and quantified by Western blot in male C57BL/10 and *mdx* and 10, 24 and 52 weeks of age (*n*=3 per group; **Figure 3.12A**). Values were normalised to vinculin protein. Surprisingly, protein expression did not vary much between C57BL/10 and *mdx* mice at any of the ages, in contrast to what was observed by RT-qPCR. Western blot quantification of JNK illustrated large reductions in pJNK/JNK ratios were observed in the dystrophic samples at 24 and 52 weeks of age for both atria, although this only reached statistical significance for the RA (**Figure 3.12C**). The ventricles exhibited a small reduction in pJNK/JNK ratio in the *mdx* at 24 weeks of age, although not significant, and these were not present at 52 weeks of age. The reduction in the pJNK/JNK ratio in dystrophic muscles indicates a decrease in the JNK pathway activation. Analysis of β-catenin exhibited some differences in the phosphorylated to unphosphorylated ratio between C57BL/10 and *mdx* at 10 weeks of age for the RA, LA and IVS, even though this did not reach statistical significance (**Figure 3.12B**). No changes were observed at any of the other time points. Ratio values for NFAT did not exhibit any differential expression pattern (**Figure 3.12D**). The results indicate a potential involvement for JNK in the cardiomyopathy of DMD, and its function in planar cell polarity, specifically in the atria of the dystrophic heart.

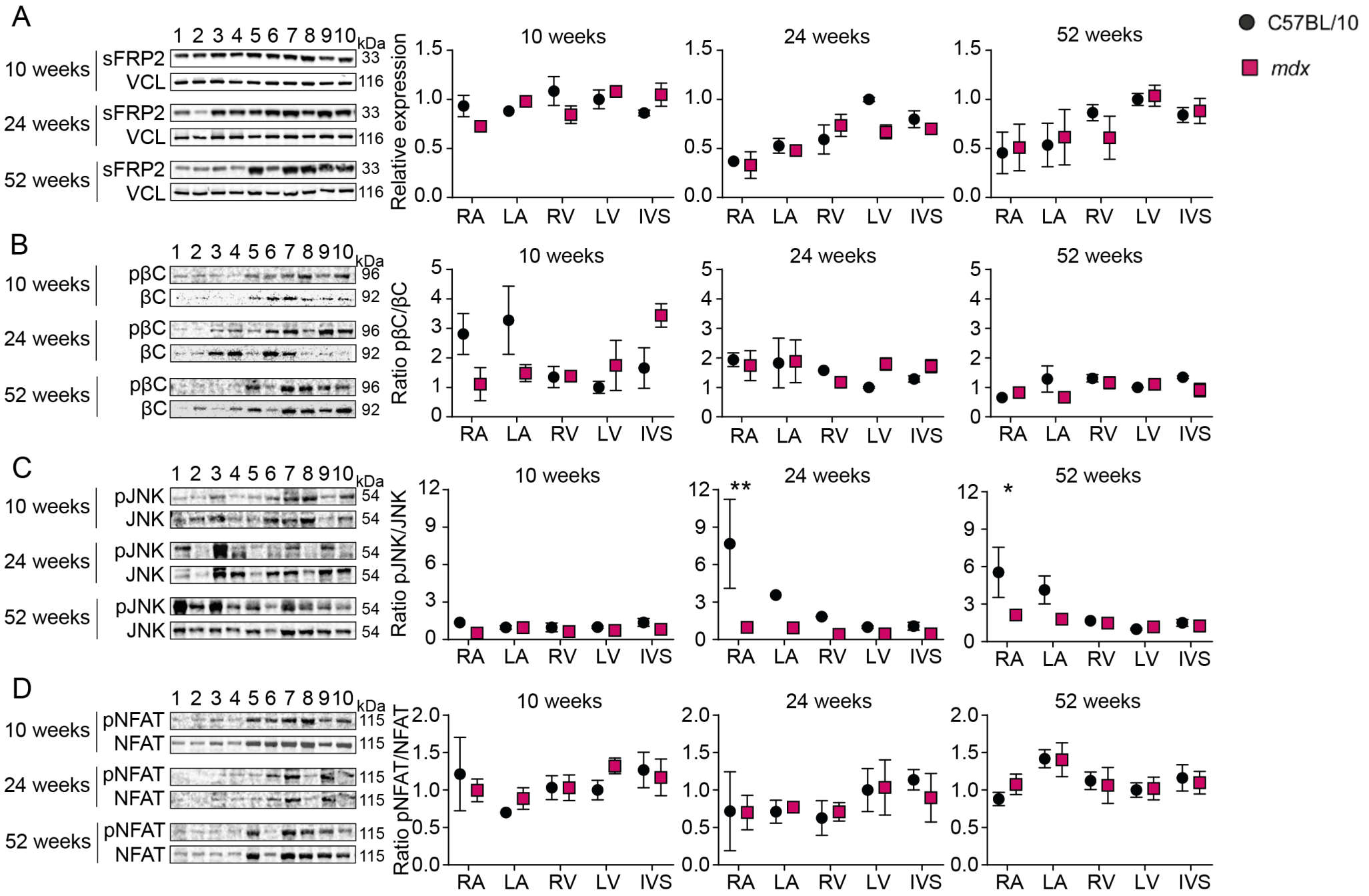
A
1 2 3 4 5 6 7 8 9 10 kDa
10 weeks
sFRP2
VCL
24 weeks
sFRP2
VCL
52 weeks
sFRP2
VCL
33
116
Relative expression
10 weeks
24 weeks
52 weeks
RA LA RV LV IVS
C57BL/10
mdx
B
pβC
βC
96
92
Ratio pβC/βC
C
pJNK
JNK
54
Ratio pJNK/JNK
**
*
D
pNFAT
NFAT
115
Ratio pNFAT/NFAT

Figure 3.12 Protein expression of sFRP2, β-catenin, JNK and NFAT.
Protein was extracted from male C57BL/10 and *mdx* mice at 10, 24 and 52 weeks, and size-separated on a 10% Bis-Tris gel (*n*=3 per group). Western blot bands illustrated for **A** sFRP2 and vinculin (VCL), **B** phospho-β-catenin (pβC) and β-catenin (βC), **C** phospho-JNK and JNK, and **D** phospho-NFAT and NFAT.

Sample order is as follows: 1. C57BL/10 RA, 2. *mdx* RA, 3. C57BL/10 LA, 4. *mdx* LA, 5. C57BL/10 RV, 6. *mdx* RV, 7. C57BL/10 LV, 8. *mdx* LV, 9. C57BL/10 IVS, 10. *mdx* IVS. sFRP2 was normalised to vinculin expression. β-catenin, JNK and NFAT were measured as the phosphorylated to non-phosphorylated ratio. Expression ratios were scaled such that the mean of the C57BL/10 LV at each time point was returned to a value of 1. Graphs illustrate mean ± SEM. * $P<0.05$, ** $P<0.01$ for comparisons between C57BL/10 and *mdx*. Two-way ANOVA with Tukey *post hoc* correction, comparing groups within each chamber.

3.3.5 Cellular translocation of sFRP2

The sFRP2 protein expression levels observed with the Western blot quantification were surprising given the large differential transcript expression. Therefore, to investigate whether reduced protein translocation may be inducing high *Sfrp2* levels, cytoplasmic and nuclear protein was extracted from male C57BL/10 and *mdx* LV at 52 weeks (*n*=3 per group). Western blot illustrated vinculin protein presence in the nuclear extract, suggesting sub-optimal extraction and some cytoplasmic carryover, a limitation of the technique (**Figure 3.13*A***). However, apart from one C57BL/10 sample, all nuclear extracts exhibited large reduction in vinculin protein compared to the cytoplasmic extracts. The deviating C57BL/10 sample displayed the opposite pattern, suggesting incorrect protein extraction and this sample was removed from further analysis. The sFRP2 protein was subsequently normalised to vinculin and quantified, indicating that cytoplasmic sFRP2 protein was significantly reduced in the *mdx* samples (**Figure 3.13*A***). Nuclear sFRP2 protein in *mdx* mice also exhibited a tendency to increase compared to C57BL/10 (*mdx* to C57BL/10 ratio is 3.2). These results suggest a reduction in cytoplasmic sFRP2 protein, but conflict with the sFRP2 protein levels detected by Western blot. These differences may be explained by the naturally high variations in the Western blot technique and/or sub-optimal nuclear and cytoplasmic fractionation [483]. Alternatively, total sFRP2 protein expression may not change (whole-cell lysate Western blot), but subcellular localisation of the protein may be altered.

To investigate whether the observed differences in sFRP2 level between whole cell lysates and cellular fractions could be attributed to technical variations or a biological finding, immunofluorescence was utilised to investigate sFRP2 protein localisation in the atria, RV, LV and IVS (**Figure 3.13*B***, ***C***, ***D*****,** ***E*** and ***F***). Total sFRP2 protein intensity per section was observed to be reduced in all dystrophic chambers (**Figure 3.13B**), whereas mean intensity of sFRP2 in the nuclear/rough endoplasmic reticulum (RER) regions increased in the RV, LV and IVS (**Figure 3.13C**, **D**, **E** and **F**). While preliminary, the Western blot fractionation and immunofluorescence data suggests reduced translocation of sFRP2 to the extracellular space in dystrophic hearts.

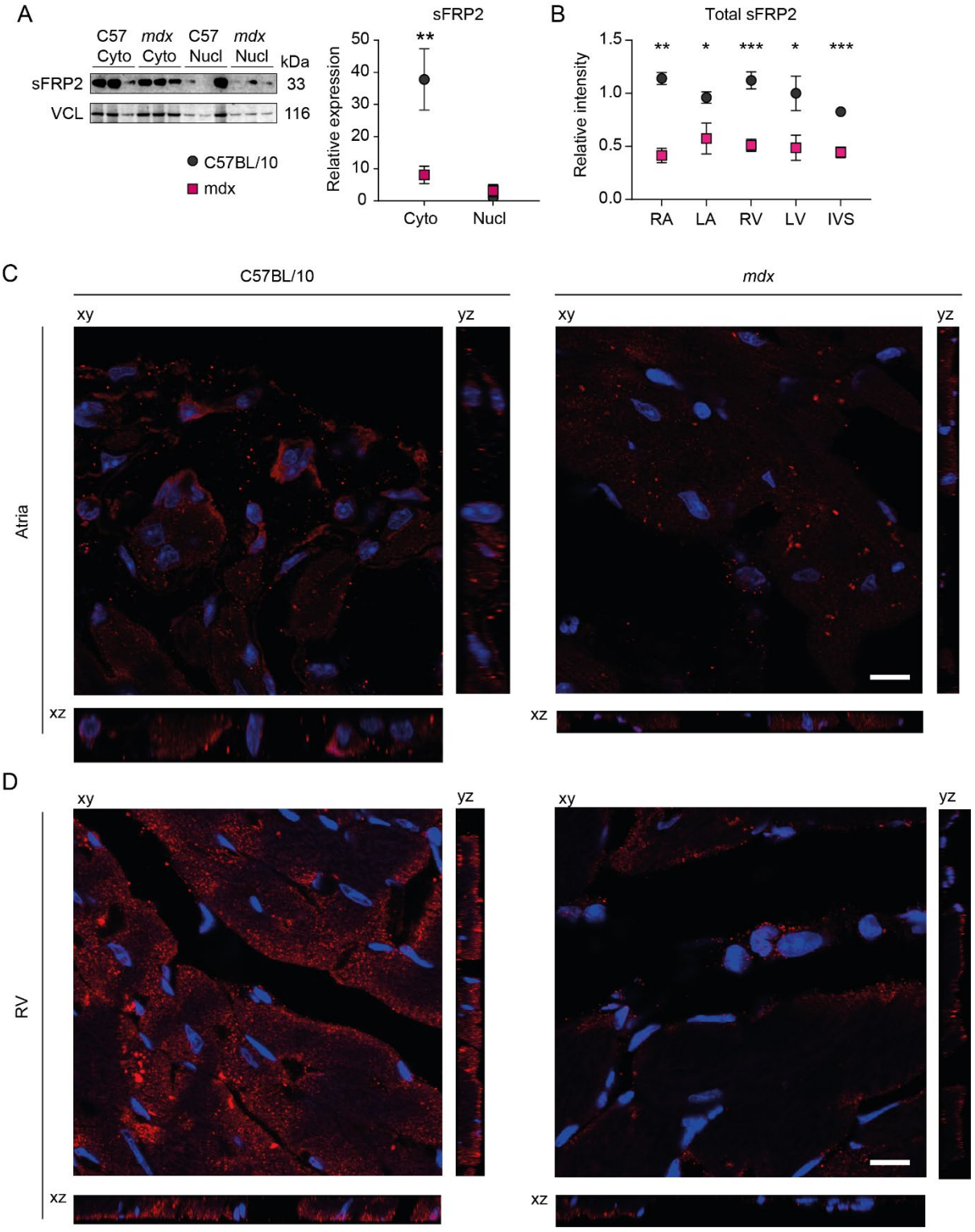
A
C57 Cyto
mdx Cyto
C57 Nucl
mdx Nucl
kDa
sFRP2
33
VCL
116
C57BL/10
mdx
sFRP2
Relative expression
50
40
30
20
10
0
**
Cyto
Nucl
B
Total sFRP2
Relative intensity
1.5
1.0
0.5
0.0
**
*
***
*
***
RA
LA
RV
LV
IVS
C
C57BL/10
mdx
xy
yz
xz
Atria
D
RV

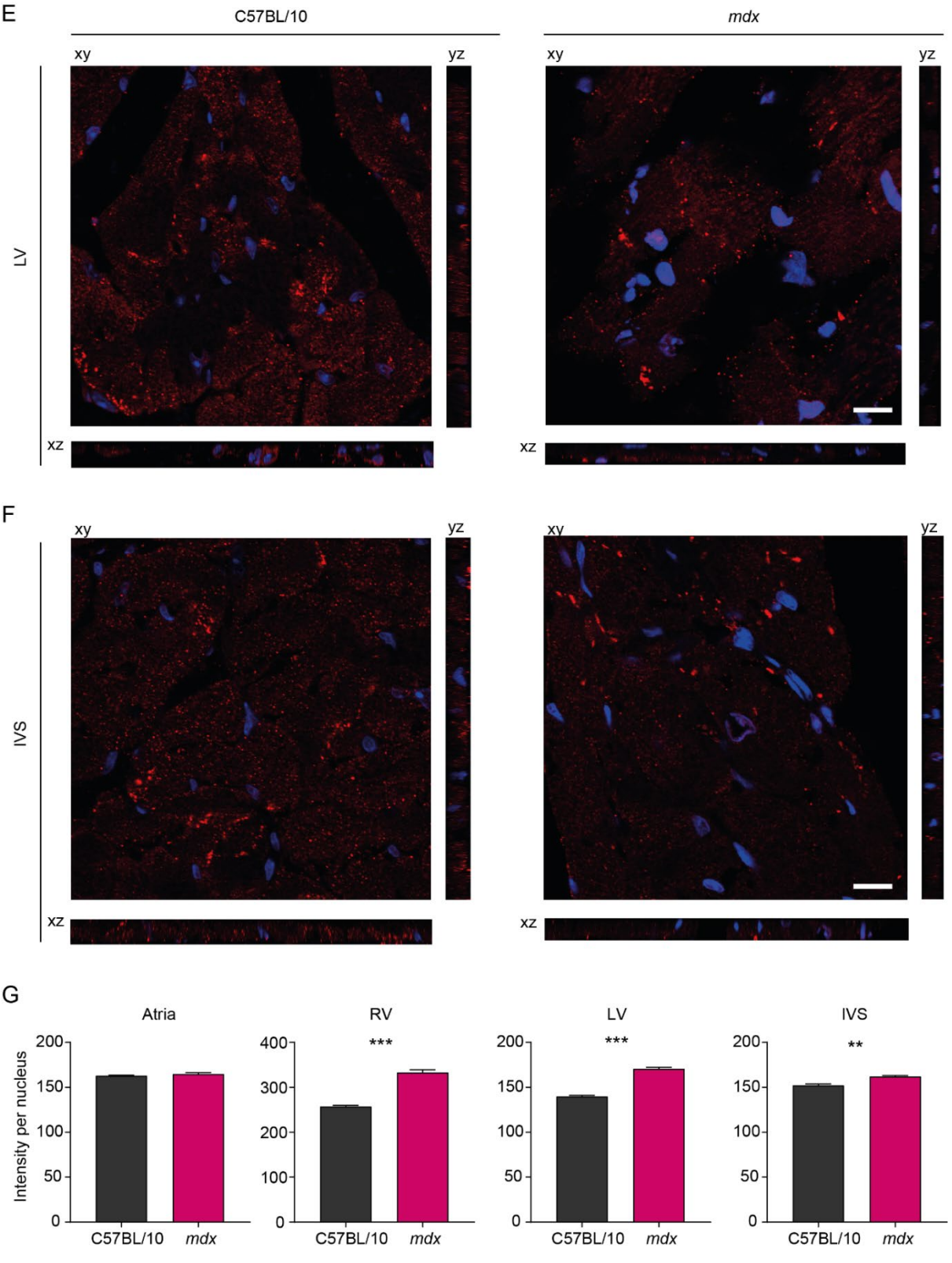
E
C57BL/10
mdx
xy
yz
xz
LV
F
IVS
G
Atria
RV
LV
IVS
Intensity per nucleus
200
150
100
50
0
400
300
***
**
C57BL/10
mdx

Figure 3.13 Cytoplasmic and perinuclear localisation of sFRP2 protein.
A Nuclear and cytoplasmic protein was extracted from the male C57BL/10 and *mdx* LV at 52 weeks of age and size separated on a 10% Bis-Tris gel (*n*=3 per group). Membranes were probed for sFRP2 with Vinculin (VCL) as loading control. Protein was quantified through normalisation to vinculin. Expression ratios were scaled such that the mean of the C57 cytoplasm was returned to a value of 1. Graph illustrates mean ± SEM. ** *P*<0.01 for comparison between C57BL/10 and *mdx*, two-way ANOVA with Tukey *post hoc* correction. **B** Total sFRP2 intensity in hearts from C57BL/10 and *mdx* at 52 weeks of age (*n*=4 per group). Expression ratios were scaled such that the mean of the C57 LV was returned to a value of 1. Graph illustrates mean ± SEM. * *P*<0.05, ** *P*<0.01 and *** *P*<0.001, Student's *t*-test for comparison of C57BL/10 and *mdx* in each chamber.
Fixed hearts from C57BL/10 and *mdx* mice 52 weeks of age were then stained for sFRP2 (red), and Hoechst (blue) to identify nuclei. Staining and sFRP2 mean intensity was performed for **C** atria, **D** RV, **E** LV and **F** IVS. Scale bars indicate 50 µm with 3x zoom. Images demonstrate sFRP2 and nuclei merged with three planes of section to illustrate sFRP2 nuclear localisation. Representative images for *n*=4. **G** Graphs are mean sFRP2 intensity per nucleus ± SEM. ** *P*<0.01 and *** *P*<0.001, Student's *t*-test for comparisons of C57BL/10 and *mdx* in each chamber.

3.3.6 Effect of *Sfrp2* on myoblast differentiation

The results so far indicated a potential role for sFRP2 in cardiomyocytes, perhaps reducing phosphorylated JNK levels thereby affecting the Wnt planar cell polarity pathway (**Figure 3.12**), but its exact function remains unclear. Previous studies have shown that addition of recombinant sFRP2 protein inhibits C2C12 myoblast differentiation, while maintaining a healthy cell population [542], indicating a role for this protein in cell proliferation and differentiation. To elucidate the function of sFRP2 in DMD, the effect of *Sfrp2* RNA interference on dystrophin-deficient cell differentiation was investigated. Given the reservations about the existence of cardiac progenitor cells [177], H2K-*mdx52* were utilised as proof of principle. Upon differentiation, cells were treated twice with siRNA *Sfrp2* or Ctrl over a period of 6 days (*n*=3 per group). RT-qPCR analysis illustrated extremely efficient knock-down with quantitation cycle (Cq) values detected for only one of three siSfrp2-treated replicates (**Figure 3.14*A***). Protein level quantification demonstrated a 50% reduction in sFRP2 protein expression for two of three samples (sample with high protein expression did not correlate to the sample with higher mRNA expression) (**Figure 3.14*B***). mRNA and protein discordance may be due to limited sample sizes and require experimental repeats. RT-qPCR for the common differentiation markers (*Myh1*, *Ckm* and *Myog*) exhibited little variation between replicates (**Figure 3.14*C***). *Myh1* (myosin heavy chain 1) normally increases with differentiation due to the formation of myotubes and is a late myogenic marker [543]. Interestingly, *Myh1* gene expression was significantly reduced in siSfrp2-treated samples relative to control. Its gene expression following RNA interference was significantly elevated in Ctrl versus *Sfrp2* siRNA. Another late myogenic stage marker, *Ckm* (creatine kinase M-type) [544], exhibited the same pattern, whereas an early myogenic marker, *MyoG* [543], was significantly elevated in cells treated with *Sfrp2* siRNA. Together, the results demonstrate that reduced levels of *Sfrp2* inhibit myogenic differentiation, although outcomes should be confirmed on the protein level by immunofluorescence for MYH1. They further exhibited that differentiation progresses more slowly in H2K-*mdx52* cells when treated with *Sfrp2* siRNA, which suggests low *Sfrp2* levels may potentially impede differentiation between the stage of *Myog* and *Myh1* expression. This suggests a role for

sFRP2 in myoblast differentiation in DMD. Whether these results can be directly translated to dystrophic cardiomyocytes remains to be established.

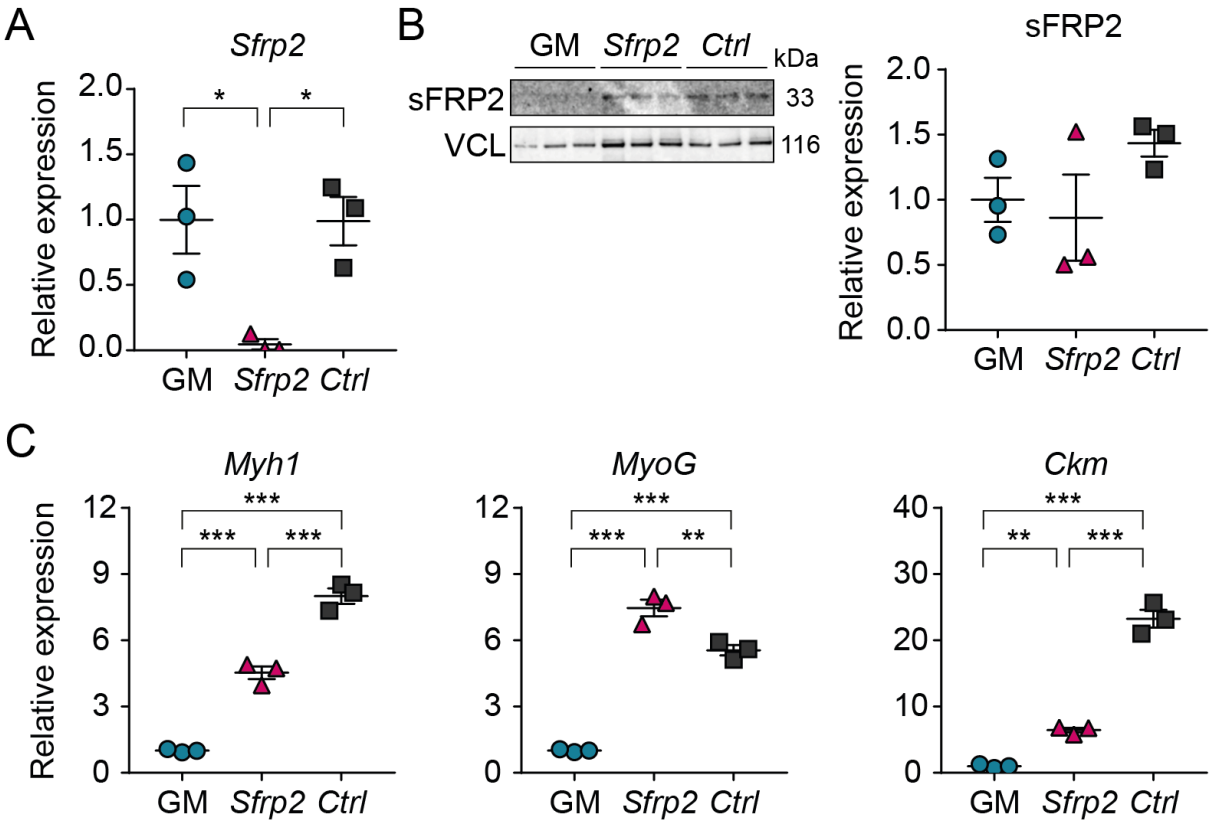

Figure 3.14 Effect of *Sfrp2* RNAi on rate of differentiation.
H2K-*mdx52* myoblasts cells were cultured for 2 days (GM) before being differentiated to form multinucleated myotubes. Upon differentiation, cells were transfected with *Sfrp2* or Ctrl siRNA. Cells were collected 6 days after differentiation (*Sfrp2* or Ctrl; *n*=3 per group). **A** mRNA transcripts of *Sfrp2* at GM and 6 days after differentiation when treated with siRNA for *Sfrp2* or Ctrl. **B** Protein was extracted and size separated by Western blot. Bands as indicated for sFRP2, with vinculin (VCL) as loading control. sFRP2 protein expression was subsequently quantified for all conditions. **C** RT-qPCR was utilised to detect mRNA transcripts for common differentiation markers *Myh1*, *MyoG* and *Ckm*. Values are mean ± SEM. * *P*<0.05, ** *P*<0.01 and *** *P*<0.001, one-way ANOVA with Tukey *post hoc* correction.

3.4 Discussion

3.4.1 Global heart pathology

Cardiomyopathy remains one of the major causes of death for DMD patients, yet it remains unclear how the disease progresses over time and how it affects each anatomical area of the heart. Therefore, this study utilised transcriptomic arrays on region-dissected heart tissue at different cardiomyopathic stages with the aim of elucidating some of these processes. Initially, global heart morphology was assessed in C57BL/10 and *mdx* mice and revealed evidence of pathology at all time points in both male and female *mdx* hearts. Pathology appeared less severe in the female *mdx*, although the heart does deteriorate over time and studies suggest a more drastic decline in female heart function compared to male *mdx* at 22 months of age [518]. This is likely attributed to hormonal changes and indeed, the incidence of cardiovascular disease increases significantly in post-menopausal women [545]. Utilising females for the transcriptomic arrays allowed for the identification of novel pathways in a less severe early cardiomyopathic state, which enabled analysis of primary cardiomyopathic processes occurring in the dystrophic heart. Many of these processes were related to cardiac remodelling and cell migration. This may be due to cardiomyocytes expanding in size and increasing protein production, contributing to cardiac hypertrophy [546], and to changes in the extracellular matrix and fibroblasts that activate and induce fibrosis [231]. The results also identified REVIGO theme differences between the chambers, which were indicative of a dynamic regulation of the cardiac anatomical areas. Contextually, the physiological nature of the heart requires different functionalities for the various anatomical regions. The receiving of blood in the atria versus the pumping of blood in the ventricles requires diverse activity and energy demand between these chambers [496]. Chamber function is further affected by the destination of circulation, i.e. lungs or the rest of the body containing (de)oxygenated blood. Previous studies have demonstrated a severe pathology of the diaphragm in *mdx* mice, and the observed pulmonary hypertension further contributes to right heart deterioration [304,547,548]. The RV deteriorates before the LV and this is

indeed visible on a molecular level, whereby the RV exhibited a more organised clustering of genes with the GO term enrichment, as identified by the higher number of themes compared to the LV at 10 weeks. In contrast, RA pathology appears to be affected at a similarly early stage as the RV, as is indicated by the prominent number of themes identified by the REVIGO analysis. Together, the results suggest a dynamic regulation of cardiomyopathic processes, whereby the right heart appears to be affected earlier by pathology, as is corroborated by physiological studies [81,304].

3.4.2 Treatment was unable to restore global transcriptomic expression

This study utilised peptide-conjugated PMOs to analyse the effect of long-term dystrophin treatment on amelioration of aberrant pathways. While effective dystrophin re-expression was confirmed, global transcript expression analysis revealed minimal differences between the untreated and PPMO-treated *mdx* mice. Several reasons could explain this effect. The *mdx* mouse only exhibits a relatively mild pathology compared to patients, especially at the early ages examined. Transcriptomic differences between C57BL/10 and *mdx* were relatively small, therefore obfuscating any transcript restoration following PPMO treatment. Another possibility may be due to the inherent inability of the heart to regenerate like skeletal muscle, which has shown improvement following PPMO treatment [492]. Thus, any benefit garnered from treatment is limited as there are no/few stem cells to repopulate and strengthen the cardiac muscle [177]. Lastly, the level of dystrophin restored may have been insufficient to correct pathology. While low levels of dystrophin re-expression are able to ameliorate pathology in skeletal muscle [492], the current study demonstrates that similar effects are not observed to the same degree within cardiac muscle. This is an important consideration for dystrophin restoration treatment in patients with more progressed cardiomyopathy.

3.4.3 Sfrp2 divergence in dystrophic hearts

Following analysis of GO terms associated with the progression of cardiomyopathy, *Sfrp2* expression exhibited significantly increased fold changes in the dystrophic heart at all time points and this pattern was confirmed by RT-qPCR. Nonetheless, other Wnt-related genes exhibited little

differences in expression between control and dystrophic heart. Data on the protein level analysing the effectors of the three Wnt signalling arms (β-catenin, JNK and NFAT) suggested no aberrant expression levels for β-catenin and NFAT. Decreased ratios were observed for the phosphorylated to unphosphorylated ratio of JNK in the dystrophic heart, reaching statistical significance at 24 and 52 weeks of age in the RA, which has also been observed in *mdx* myotubes [549]. This suggests an inactivation of JNK and a possible involvement of the non-canonical PCP pathway in DMD pathology, which may (partially) be regulating the remodelling aspects observed in the dystrophic heart [498].

The mean intensity measured by immunofluorescence indicated a decrease in total sFRP2 protein expression in dystrophic compared to healthy hearts. In conjunction with the mislocalisation of the protein as suggested by Western blot and immunofluorescence, this is suspected to result in a reduction of sFRP2 in the extracellular space, where it exerts its function. One hypothesis on the underlying mechanisms is that sFRP2 is trapped in the perinuclear region (i.e. RER or Golgi apparatus) and fails to become secreted. This process could involve incorrect packaging and/or F-actin. F-actin has been shown to be involved in protein migration through the cell [550] and sFRP2 may utilise this structure for its translocation to the extracellular space. Absence of dystrophin negatively affects F-actin polymerisation, [551], which may decrease migration of the sFRP2 protein. Speculating further, laminin and sFRP2 both contain a netrin domain, which may facilitate binding between these proteins. Studies have observed conformational changes and post-translational modifications in laminin [552,553], and absence of dystrophin may affect these aspects of the laminin protein, and by extension its role in extracellular localisation of sFRP2. An unanswered question remains as to what the influence of a reduction in sFRP2 protein is on the function of the dystrophic heart and will need to be addressed in future experiments.

Functionally, this study illustrated that knockdown of *Sfrp2* transcript reduced myogenic differentiation in dystrophin-deficient myoblasts, suggesting an involvement of *Sfrp2* in differentiation of myogenic cells. It appears these cells are unable to move into late-stage differentiation following

Sfrp2 knockdown. This appears contrary to findings by Descamps *et al.*, who showed that addition of recombinant sFRP2 prevented C2C12 myoblast differentiation [542]. sFRP2 was also observed to be upregulated during myoblast differentiation [190]. Interestingly, Hara *et al.* observed myoblast cell death following knockdown of *Sfrp2* and suggested an importance for this protein in myoblast survival during regeneration. The observed differences may be due to characteristics of sFRP2 protein modulation. This balance has been shown to be important for inhibitory or excitatory functions (see further), with the absence of dystrophin (or its downstream effects) potentially changing attenuation of the role of sFRP2.

Increased *Sfrp2* transcript levels have been observed in TA muscle of *mdx* mice (data not shown), potentially to stimulate satellite cell differentiation, which has been observed previously [534]. However, given that the existence of cardiac stem cells has been questioned [177], to what extent these results can be translated to cardiomyocytes remains to be established. Several studies investigating the role of sFRP2 in the heart have been performed with opposing results. For instance, Mirotsou *et al.* showed that cardiomyocytes treated with sFRP2 exhibited increased expression of β-catenin and anti-apoptotic genes [554]. This could suggest a compensatory mechanism for sFRP2 in the heart, which may be less successful in dystrophic hearts due to the increased perinuclear localisation of sFRP2 protein. Furthermore, exogenous administration of sFRP2 prevented collagen deposition after myocardial infarction in rats, thereby preventing fibrosis and improving cardiac function [555]. In contrast, Kobayashi *et al.* demonstrated a reduction of fibrosis following myocardial infarction in mice negative for sFRP2 [556]. Moreover, Lin *et al.* demonstrated that cardiac fibroblasts proliferate upon activation of the canonical Wnt signalling pathway through sFRP2, which induced the remodelling of the ECM and activation of several MMPs, including MMP9 [533]. Given the detrimental role MMP9 is thought to play in the pathology of DMD (see **Chapter 1.4**), the contrasting results observed in cardiomyocytes and cardiac fibroblasts will need to be addressed further to ascertain sFRP2 function in the dystrophic heart. Additionally, sFRP2 function should not only be reviewed in

the context of the Wnt signalling pathway, but also in relation to its other functions, e.g. apoptosis, BMP signalling and osteoclast formation [531].

Separation of the cardiac anatomical areas does not provide more insight into the functioning of the individual cell types present in the heart (i.e. cardiomyocytes, fibroblasts, epicardium cells, endothelial cells, smooth muscle cells, pacemaker cells and Purkinje fibres [557]) and future studies should address this aspect. Particularly, sFRP2 regulation of the Wnt signalling pathway has been observed to differentially affect the various cell types. For instance, sFRP2 has been shown to induce vascular endothelial cell migration and tube formation *in vitro* through the non-canonical Wnt/Ca^{2+} NFAT pathway [558]. In cardiomyocytes, the canonical β-catenin pathway prevents apoptosis following ischaemic injury [554]. Furthermore, exogenous addition of high (but not low) sFRP2 concentrations (100 nM) prevented type I collagen maturation in primary cardiac fibroblasts by acting on bone morphogenic protein (BMP-1) *in vitro* [555]. In contrast, Lin *et al.* observed that sFRP2 stimulated cardiac fibroblast proliferation through the β-catenin arm, and enhanced MMP-9 activity, among others [533]. Indeed, whether sFRP2 induces activation or inhibition is dependent on its protein levels and the context. Xavier *et al.* demonstrated that low nanomolar levels of the closely-related sFRP1 aided the Wnt3a ligand in activating the canonical Wnt pathway of HEK293 cells. In contrast, high sFRP1 levels reduced β-catenin activity. Furthermore, similarly low levels had an antagonistic effect in fibroblasts [559]. These results suggest that the concentration of sFRP and the target cells influence whether downstream sFRP effects are inhibitory or excitatory and are an important consideration for sFRP2 function.

3.4.4 Study limitations and future directions

An important consideration in this study are the gender differences observed in dystrophic heart pathology. Although females were utilised for transcriptomic studies to better approximate a pre-cardiomyopathic state, this X-linked disease affects the male population (and in rare cases females). While it is expected that gender variabilities solely delay progression of pathology [518], it

may be possible that these also affect different pathways. Therefore, any findings should be confirmed in a representative male model, as realised in the current study by validation of the Wnt signalling effectors and sFRP2 protein localisation in male C57BL/10 and *mdx* mice.

Although this study has shown a downregulation of cytosolic/extracellular sFRP2 protein and a reduction in pJNK/JNK ratio, it remains unclear whether these two are directly linked and if sFRP2 dysregulation affects the non-canonical PCP arm of the Wnt signalling pathway in DMD pathogenesis. Moreover, JNK is involved in a plethora of other processes besides the Wnt cascade which may influence the observed decrease in phosphorylated to unphosphorylated protein ratio [560]. Alternatively, pathways affecting JNK expression may be compensating for altered sFRP2 regulation, or vice versa. To what extent the mislocalisation of sFRP2 influences JNK activation is additionally unclear. To address some of these questions, future experiments could assess the expression of pJNK/JNK ratio in dystrophin-deficient myoblasts, myotubes, cardiomyocytes and/or fibroblasts following *Sfrp2* siRNA knockdown. Following identification of the mechanisms involved in sFRP2 localisation (e.g. potentially F-actin), this could be utilised in dystrophin-positive myoblasts, myotubes, cardiomyocytes and/or fibroblasts to assess whether this impacts the pJNK/JNK ratio.

The total intensity measured by immunofluorescence suggests a decrease in sFRP2 protein in *mdx* hearts, although Western blot data indicates no differences. This may be due to variations affecting the mean intensity in immunofluorescence measurement or the inherent variability of Western blots. Although background and oversaturation were corrected in the former technique, the signal may still be altered due to numerous technical reasons, such as non-specific antibody binding or clustering. The Western blot technique and results should also be further improved and confirmed, respectively. The data showed clear contamination of the nuclear samples (as exemplified by the presence of vinculin) and purity of both fractions could not be correctly assessed due to the absence of a functional nuclear loading control. Nonetheless, the reduction of vinculin in the nuclear samples did suggest at least partial fractionation of the cytoplasm and nucleus. Improved protein

quantification may also require an enhanced Western blotting system such as the ProteinSimple capillary immunoassay (Wes), which has been shown to exhibit less than 20% variability between samples when quantifying dystrophin (compared to 80% for dystrophin in traditional Western blot), though it should be noted that traditional Western blot variability is expected to be reduced with smaller protein sizes [483,561]. Optimisation of both these aspects will allow clarification and confirmation of the currently obtained results. ELISAs could also be utilised to assess whether reduced protein levels may be due to release into the circulation. If increased serum sFRP2 levels are observed, this could be investigated further for (cardiac) biomarker potential. Additional experiments to understand the mechanisms behind altered localisation of sFRP2 could relate to the theory postulated above (failure of sFRP2 secretion, and a requirement of F-actin polymerisation and laminin binding). An approach to address this could involve identifying the localisation of sFRP2 within the RER or Golgi in dystrophic and control hearts, through specific immunofluorescent markers for these structures. Another experiment could inhibit F-actin polymerisation in dystrophin-deficient myotubes and cardiomyocytes and assess the effects on sFRP2 localisation through immunofluorescence, and Western blot of the cytoplasmic and nuclear fractions. Furthermore, immunofluorescence and co-immunoprecipitation could be performed on laminin and sFRP2 to determine co-localisation and binding of these two proteins.

Lastly, while this study aimed to understand the connection between sFRP2 and DMD pathology, the function of sFRP2 in the disease, and whether it is protective or detrimental, remains unclear. Furthermore, solely the role of sFRP2 in the three main arms of the Wnt signalling pathway was partially addressed, but its other functions (e.g. apoptosis and BMP signalling) have not been considered. Future studies will require further investigation into sFRP2 function in the dystrophic heart, particularly in relation to different cell types and disease state. Firstly, it should be identified to which cell types *Sfrp2* and its protein localise, which could be investigated through immunofluorescence. It is expected expression will be predominantly be in cardiomyocytes and/or fibroblasts, based on previous studies identifying functions for sFRP2 in these cells [533,554,558].

Following, these specific cell types could be isolated from healthy and dystrophic hearts to further validate sFRP2 function *in vitro*. As elaborated before, sFRP2 is able to affect cardiomyocyte and fibroblast functioning. As such, cardiomyocyte hypertrophy and/or fibrotic depositions by fibroblasts could be assessed in response to exogenous sFRP2 addition. These studies may aid in further elucidation of sFRP2 cell function in the dystrophic heart. If successful, this pathway could be investigated in mouse models for non-dystrophic cardiomyopathy, to assess the wider influence of this pathway in the diseased heart.

3.4.5 Conclusions

To conclude, progression of cardiomyopathy in the dystrophic heart remains a complex facet of the disease. Early molecular changes are already observed, mainly in the right atrium and ventricle, and most appear to be related to cell migration and cardiac remodelling. The *Sfrp2* gene was consistently upregulated in the various anatomical regions of the heart and associated with many GO terms identified by differential gene expression. Examination of this protein identified an altered expression of the phosphorylated to unphosphorylated ratio of the JNK protein, although it remains unclear to what extent these are related in the dystrophic heart. Furthermore, sFRP2 protein localisation was indicated to be altered in the ventricular regions of the heart, with a reduced expression of sFRP2 in the cytosol/extracellular space and an increase in the nuclear/RER region. While the function of sFRP2 remains to be established, the results indicate early involvement of this protein in the dystrophic heart.

4. Results II

Utilisation of high-resolution proteomics analysis to identify novel differentially expressed proteins associated with disease progression in the skeletal muscle of two DMD mouse models

4.1 Introduction

Understanding the molecular events underlying the absence of dystrophin is important for elucidating the pathological features of DMD. Many transcriptomic studies have been performed which allow for the simultaneous measurement of tens of thousands of genes. However, mRNA expression often does not correlate with protein levels [492,562–564] and therefore independent protein measurements are necessary. Unfortunately, addressing this disparity is impeded by methodological advancements, as equivalent proteomic studies are technically more challenging. Initial studies utilised 2D-electrophoresis, but results were limited by the small number of detected proteins, and even fewer differential expression calls [565,566]. Global proteomic profiling in fibrous tissues such as skeletal muscle is complicated by the presence of very high concentrations of a few structural proteins, such as actins and myosins [567]. Moreover, stage of the disease can differentially influence protein detection of dystrophic muscle, given the varying proteomic content ratios that may vary at certain points in the disease (e.g. changes in myosin presence with age due to loss of myofibres [568,569]). Peptides derived from these proteins mask signals from lower abundant proteins and thereby limit the depth of proteomic coverage that can be achieved. To address these issues, the Wood group, in collaboration with the Lehtiö and EL Andaloussi group, was recently able to simultaneously quantify several thousand proteins in mouse muscle by high-resolution sample pre-fractionation based on narrow-band isoelectric focusing [492]. To date, there have been relatively few high-resolution proteomic studies, and fewer still that have measured global changes in protein

expression in muscle throughout disease progression over time. The ability to detect and quantify a large number of proteins will be required for enhanced understanding of dystrophic pathology.

Several dystrophic mouse strains have been developed to model DMD pathophysiology, and test novel therapeutics *in vivo* [74], of which the most commonly used model is the *mdx* mouse [75,76]. Even though *mdx* mice undergo a brief degeneration-regeneration phase estimated between 2 and 12 weeks of age [570–572], more pronounced muscle pathology and cardiomyopathy only manifest much later in life (as described in **Chapter 1.1.4.1**) [81,573]. Importantly, the exon 23 mutation observed in the *mdx* mouse does not typically occur in DMD patients [574], which has motivated the development of more patient-relevant dystrophic mouse models. To more accurately mimic particular mutations found in patients, Araki *et al.* generated the *mdx52* mouse model in which *Dmd* exon 52 is deleted, leading to the absence of the Dp260 and Dp140 isoforms in addition to Dp427 (**Figure 4.1**; for isoforms see Chapter 1.1.3, Figure 1.1) [575]. Deletions in the 'hot-spot' region (exon 45-55) are some of the most common mutations found in DMD, thereby making this model more patient-relevant than the standard *mdx* mouse [35]. Importantly, the *mdx52* model has the potential to prove useful for development of the exon skipping technique for mutations in this region *in vivo*. In skeletal muscles, the *mdx52* model exhibits a very similar pathology as the *mdx* [575], although differences have been observed in the number of revertant fibres [576]. While these dystrophin-positive cells slowly increase in number with age, they are not sufficient to influence muscle pathology for the better. The *mdx52* mouse exhibits fewer revertant fibres than the *mdx*, which is suggestive of a difference in muscle turnover or alternative endogenous splicing.

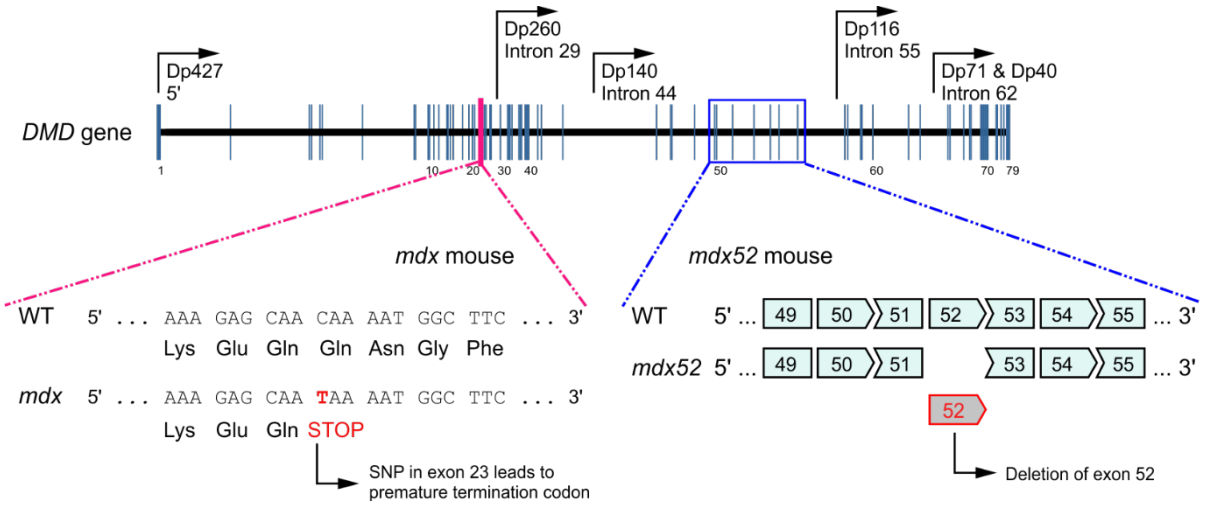

Figure 4.1 Mutation differences between *mdx* and *mdx52* mouse models.
The *mdx* mouse contains a point mutation at exon 23, leading to a premature stop codon. Conversely, the *mdx52* mouse has a deletion of exon 52. Both mutation types lead to a lack of the dystrophin protein (although the various dystrophin isoforms are differentially affected).

Given the need for a deeper characterisation of the dystrophic proteome, this work utilised a high-resolution mass spectrometry-based proteomic profiling to identify the proteome in TA muscle. This high-resolution isoelectric focusing-liquid chromatography-tandem mass spectrometry (HiRIEF-LC-MS/MS) employs strips with a pH gradient of 3.7-4.9 for pre-fractionation to reduce the complexity of the trypsin-digested proteome prior to peptide identification and quantification by LC-MS/MS. This allows for characterisation of a larger number of proteins than traditional 2D-electrophoresis and even other LC-MS/MS approaches. An additional feature concerns isobaric tagging of samples through tandem mass tags (TMT). The utilisation of 10 TMT labels enables the simultaneous measurement of 10 samples during a single LC-MS/MS run, reducing between-run technical variation and the time required on the mass spectrometer.

HiRIEF-LC-MS/MS-based proteomic profiling with TMT was performed in both the *mdx* and *mdx52* mouse models of DMD compared with WT controls at three ages representing different stages of pathology. TA muscle was analysed to enable comparison with the previous proteomic and revertant fibre study from Roberts *et al.* and Echigoya *et al.*, respectively [492,576]. A common dystrophic signature was observed in both *mdx* and *mdx52* muscle. This allowed the merging of the

data for these two groups, and a more robust comparison to the control C57BL/6 group revealed a core set of proteomic changes reflective of the dystrophic phenotype with age. This study provides novel insight into specific proteomic changes characteristic of muscle aging and the relationship of these to dystrophic pathology over time.

4.2 Materials and methods

4.2.1. Animals

Male C57BL/6, *mdx* on a C57BL/6 background (generated as described in [575], and back-crossed 20 times) and *mdx52* mice were housed under 12:12 hour light:dark conditions with food and water *ad libitum* at the National Center of Neurology and Psychiatry, Kodaira, Tokyo, Japan. Mice were kept in individually ventilated cages (IVC), kept specific pathogen free (SPF; testing for a large number of viruses, bacteria and parasites). Tissues and serum were collected at 4, 8, 16, 24, 48 and 80 weeks of age (*n*=3-5 per group).

4.2.2. RNA extraction and RT-qPCR

RNA from tissues and serum was extracted and reverse transcribed as described in **Chapter 2.3**. miRNA primers for RT-qPCR analysis were obtained from ThermoFisher Scientific and are indicated in **Table 4.1**. Primer probe sequences are indicated in **Table 4.2**.

Table 4.1 miRNA assays utilised in RT-qPCR.

miRNA	Assay ID	Sequence 5 ' to 3 '
miR-1a-3p	002222	UGGAAUGUAAAGAAGUAUGUAU
miR-133a-3p	002246	UUUGGUCCCCUUCAACCAGCUG
miR-206-3p	000510	UGGAAUGUAAGGAAGUGUGUGG
miR-223-3p	002295	UGUCAGUUUGUCAAAUACCCCA
cel-miR-39	000200	UGUCAGUUUGUCAAAUACCCCA

Table 4.2 Forward and reverse primer sequences utilised for mRNA detection.

mRNA	Primer	Sequence 5 ’ to 3 ’
Cav3	Forward	CTACTCACTGTGTATCCGCAC
	Reverse	CTCACCTGACCTTTGATCCC
Mvp	Forward	TGACCAGGAGATCCGACTAG
	Reverse	CTTCAAAGTCCAGCAATGCC
Pak1	Forward	ACTCTTGATGTCCCTGTGAATG
	Reverse	CTGTATGGATGAAGGCCAGAT
Rpl10	Forward	TCATGTCCATCCGAACCAAG
	Reverse	GCATTAAACTTGGTGAAGCCC
Tbp	Forward	AAGAAAGGGAGAATCATGGACC
	Reverse	GAGTAAGTCCTGTGCCGTAAG

4.2.3. Proteomic LC-MS/MS

TA muscle was cryosectioned and 50 × 10 µm sections were collected for each sample. Proteomic identification was subsequently performed utilising HiRIEF-LC-MS/MS at the Karolinska Institutet, Stockholm, Sweden. Briefly, samples were digested and labelled with individual TMTs (126, 127N, 127C, 128N, 128C, 129N, 129C, 130N, 130C and 131), allowing for multiplexing of 10 samples per LC-MS/MS run. Each run also included a bridge sample, which was generated by mixing protein lysates from each sample in equal amounts. TMT ratios were then reported relative to the bridge sample. A total of three LC-MS/MS runs was performed, with each run comprising all the samples from 8, 16 or 80 weeks of age. Following mass spectrometry, unique peptide spectrum matches were used to identify individual proteins. Proteins not present in every LC-MS/MS run were filtered out from the final list. For downstream analysis, values were either Log_2 transformed or standardised by scaling expression ratios as such that the mean of the WT 8 weeks was returned to a value of 1.

4.2.4. Protein extraction and Western blotting

Tissue samples were lysed in 75 mM Tris-HCL (pH 6.8), supplemented with 10% SDS, 5% 2-mercapto-ethanol and 3% protease inhibitors (P8340; Sigma-Aldrich), then heated for 3 minutes at 100°C, spun down for 10 minutes at 13,000 x *g* and stored at -80°C. Cells were lysed in RIPA lysis buffer (ThermoFisher Scientific) supplemented with 1% protease inhibitors (P8340; Sigma-Aldrich) and 1% phosphatase inhibitors (P0044; Sigma-Aldrich), and homogenised using a 27.5G syringe. Lysates were then incubated at 4°C for 5 minutes and centrifuged for 10 minutes at 14,000 × *g*. Supernatant was collected and stored at -80°C.

Protein from lysates that were obtained from cells were resolved using SDS-PAGE as described in **Chapter 2.5**, using Lamin B1 as loading control. Protein lysates from tissue were resolved on a 4-20% precast mini-Protean TGF polyacrylamide gels (Bio-Rad, Hercules, USA) and transferred onto 0.45 µM PVDF membranes. Membranes were blocked in TBST, supplemented with 1% non-fat dry milk for 1 hour at room temperature. These were subsequently probed with the primary antibody in 1% milk

overnight at 4°C. After washing, membranes were incubated with the secondary antibody (1:2,500) in 1% milk for 1 hour at room temperature. After washing, membranes were imaged using the ECL Prime Western blotting system (Sigma-Aldrich). Coomassie brilliant blue was utilised to determine protein loading, as a suitable loading control protein could not be identified. Protein separation and immunoblotting was performed by Ms Miyako Seto in the laboratory of Prof Yoshitsugu Aoki. Antibodies and dilutions are indicated in **Table 4.3**.

Table 4.3 Antibodies used for protein detection by Western blot.

Antibody	Dilution Used	Company	Product Code
CAV3	1:500	Abcam	ab2912
MVP	1:500	Abcam	ab152110
PAK1	1:1000	Cell Signalling Technology	2602S
LAMIN B1	1:1000	Abcam	ab16048

4.2.5. *Mvp* knockdown in C2C12 cells

C2C12 cells were seeded in 24-well or 6-well multiplates at 40,000 or 100,000 cells per well respectively. After 2 days in GM a subset of the plate was collected for RNA, protein or immunofluorescence as described in **Chapter 2.2**. (GM; *n*=3). Medium of the remaining wells was changed to DM, whereby a subset was treated with 100 µM of *Mvp* or Ctrl siRNA (ON-TARGET *plus* siRNA, Dharmacon, Cambridge, UK). For 24-well and 6-well plate respectively, 1.5/6 µL RNAiMAX Lipofectamine (ThermoFisher Scientific) was incubated with 5/20 µL of 10 µM siRNA for 5 minutes in 93.5/374 µL low-serum Opti-MEM medium (Life Technologies) to allow the formation of RNAiMAX-siRNA complexes. This was subsequently mixed with 400/1,600 µL DM and added to the cells. Three days after differentiation, siRNA transfection was repeated. Cells were collected three and six days after differentiation (DM3 or DM6; *n*=3 per group) for RNA, protein and immunofluorescence. For *Dmd* transcript measurement following *Mvp* knockdown, cells were collected at GM and two days after the first siMvp treatment (DM2). This latter experiment was performed by Ms Miyako Seto in the laboratory of Prof Yoshitsugu Aoki.

4.2.6. Statistical analysis

TMeV was used to plot heatmaps, perform the initial statistical analysis and calculate *k*-means protein clusters. Student's *t*-tests were performed for comparison of two groups, assuming equal variances with $P<0.01$ based on the *t*-distribution. ANOVA analysis with Bonferroni correction was performed when comparing three or more groups ($P<0.01$). A stringent *P*-value of 0.01 was used to limit the number of significant proteins. Further statistical analysis on individual proteins was performed with GraphPad Prism 7 (GraphPad Software Inc, La Jolla, CA USA), whereby one-way ANOVA comparisons were made at each time point with Tukey *post hoc* correction. PCA analysis was performed utilising the '*prcomp*' function in R i386 3.2.0 (The R Project) with R Studio (Boston, MA, USA). GraphPad Prism 7 was additionally used for visualising PCA, volcano and significance plots, protein rotations, and calculation of Spearman's *r* correlations, following the Shapiro-Wilk normality test.

Canonical pathway analysis and upstream regulator analysis was performed utilising Ingenuity Pathway Analysis (IPA; Qiagen Bioinformatics, Redwood City, CA USA). $P<0.01$ and $Z \geq |2|$ were considered significant. Venn diagrams were based on Venny 2.1.0 [577]. Figures of Merit in TMeV and the elbow method using '*wssplot*' in R were used to determine the optimum number of clusters for *k*-means clustering analysis, which identified seven clusters in both WT and Dystrophic aging. *k*-means plots were visualised in R.

4.3 Results

4.3.1. Experimental design

To investigate differential protein expression associated with dystrophin loss, TA muscles from two dystrophic mouse strains (*mdx* and *mdx52*) were collected. *mdx52* mice were generated on a C57BL/6 background, and *mdx* mice (in which the exon 23 mutation spontaneously occurred in a C57BL/10 colony) were back-crossed with C57BL/6 to obtain consistency in genetic background between models. In parallel, muscles were collected from sex-matched (all mice in this study were male) and age-matched C57BL/6 WT controls.

The observed differences in revertant fibre numbers between the *mdx* and *mdx52* strains may be due to variations in regenerative capacity [576]. The Gait, Morgan, Smith and Wood groups have previously shown that myomiRs are biomarkers of regeneration and muscle turnover, and they are highly enriched in the serum of dystrophic animal models and DMD patients [463,479,480]. Therefore, serum myomiR expression was analysed at different time points throughout DMD pathology.

Serum from animals at 4, 8, 16, 24, 48 and 80 weeks of age was collected, RNA was extracted and the myomiRs miR-1a-3p, miR-133a-3p and miR-206-3p, which have previously been shown to be upregulated in *mdx* mouse serum, were measured (*n*=3-5 per group) [463,478,578]. miR-223-3p was included as a non-myomiR endogenous control as this miRNA was not expected to vary much with mouse strain or age based on previous studies by the Morgan and Wood groups, and others [478,479,579,580]. MyomiR expression was elevated in *mdx* and *mdx52* relative to WT, with fluctuations seen at the earlier time points and consistent abundance levels with age (**Figure 4.2**). Interestingly, serum myomiRs in the *mdx52* mice peak earlier than the *mdx* (8 weeks rather than 16 weeks), consistent with the earlier peak of regeneration observed in this model [575,576]. Based on the association between extracellular myomiR presence and physiological function, in conjunction with previous findings [576], the 8 and 16 week time points were selected for proteomic analysis to

ascertain possible differences in regenerative pathology between the two dystrophic models. The 80 week time point was also selected to provide an additional aging comparison.

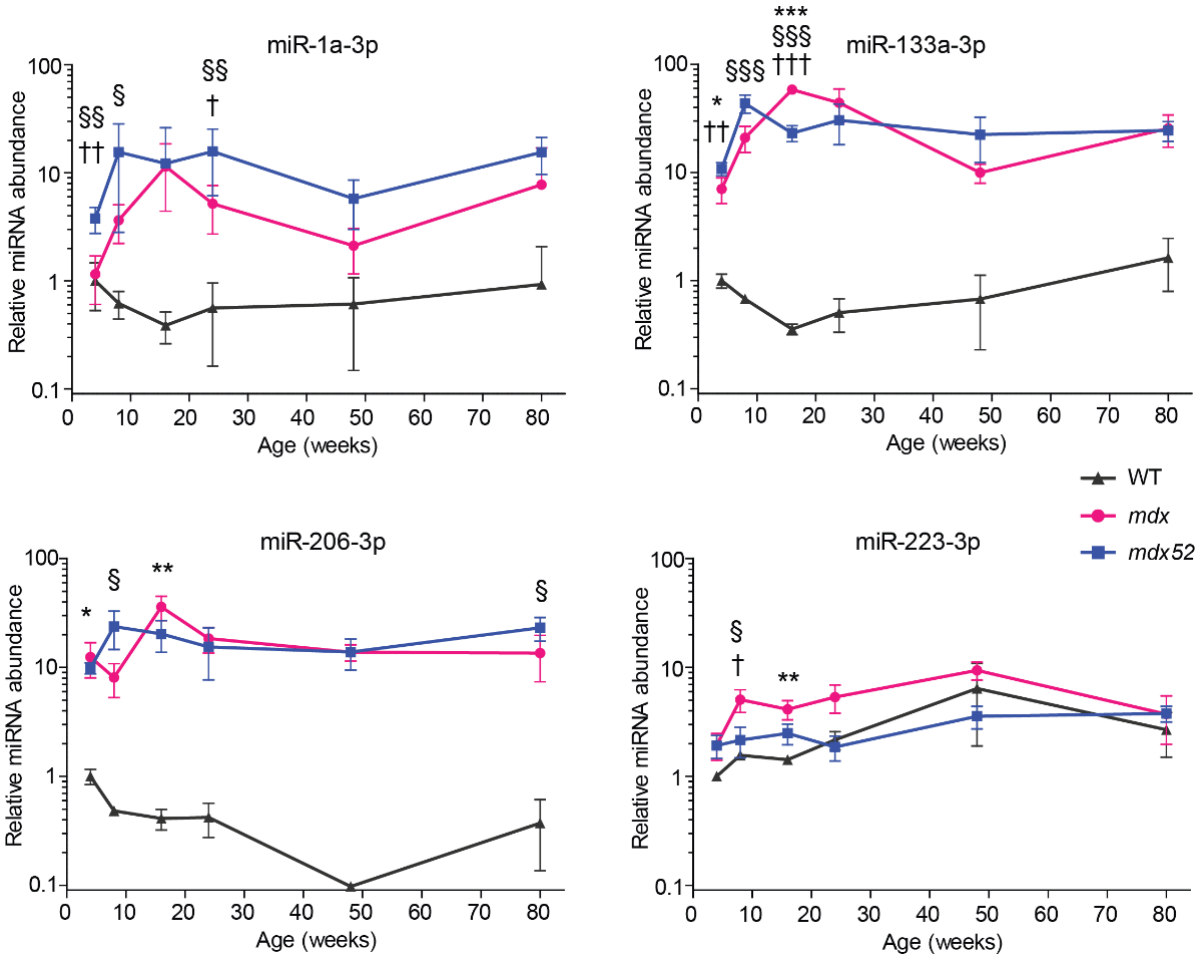

Figure 4.2 Ex-miRNA abundance in WT, *mdx* and *mdx52* serum samples.
Utilising RT-qPCR and cel-miR-39 for normalisation, ex-miRNA abundance was measured in serum samples from WT, *mdx* and *mdx52* mice at 4, 8, 16, 24, 48 and 80 weeks of age (*n*=3-5 per group). Values are mean ± SEM. * *P*<0.05, ** *P*<0.01 and *** *P*<0.001 for comparisons between *mdx* and WT. § *P*<0.05, §§ *P*<0.01 and §§§ *P*<0.001 for comparisons between *mdx52* and WT. † *P*<0.05, †† *P*<0.01 and ††† *P*<0.001 for comparisons between *mdx* and *mdx52*. One-way ANOVA at each time point, with Tukey *post hoc* correction.

TA muscles were harvested from male C57BL/6, *mdx* and *mdx52* mice at 8, 16 and 80 weeks of age (*n*=3 per group) and analysed by HiRIEF-LC-MS/MS [581]. Samples were labelled with isobaric reporter tags using TMT chemistry and a bridge sample was included in each run. TMT ratios were

then reported relative to the bridge sample, thereby allowing for direct comparison of samples between runs and effectively increasing the level of multiplexing to 27-plex.

4.3.2 Proteomic analysis in healthy and dystrophic muscle over time

A total of 7,110 proteins were detected, of which 4,974 (70%) were quantifiable (i.e. detected in all samples measured). This is a substantial improvement on previous data produced by the EL Andaloussi, Lehtiö and Wood groups using similar methodology (iTRAQ labelling with HiRIEF-LC-MS/MS, whereby 3,057 proteins were quantifiable [492]) and is the highest resolution skeletal muscle proteomics dataset reported to date. **Table 4.4** details the characteristics of the HiRIEF-LC-MS/MS run. This illustrates the range of (unique) peptides that were detected for each protein. It further indicates the range of identical proteins identified (proteins) and to what extent the entire protein was covered by these peptides (coverage of protein). The data demonstrated that the average number of unique peptides for protein identification was 7, consistent with high confidence identification of proteins.

Table 4.4 Percentiles, mean, standard deviation and standard error of HiRIEF-LC-MS/MC.
Identification of peptide spectra matches and the number of (unique) peptides associated with a protein group. Also shown are the number of proteins associated with a particular protein group that were identified in the current dataset and the percentage of the protein that is covered by the measured peptides.

	PSMs	Peptides	Unique peptides	Proteins	Coverage of protein
Minimum	3	1	1	1	0.0041
25th Percentile	8	3	3	1	0.0884
Median	16	5	5	2	0.1606
75th Percentile	37	9	8	3	0.2675
Maximum	35017	1951	197	27	0.9309
Mean	102.4318	9.3721	7.2865	2.5420	0.1956
SD	1011.8990	41.6695	9.6780	2.3567	0.1424
SEM	14.3478	0.5908	0.1372	0.0334	0.0020

Analysis of the protein cumulative distribution plot showed that only 25 proteins accounted for 50% of the detected protein mass, whereas the least abundant 1,042 proteins made up only 1% of the detected mass (**Figure 4.3**).

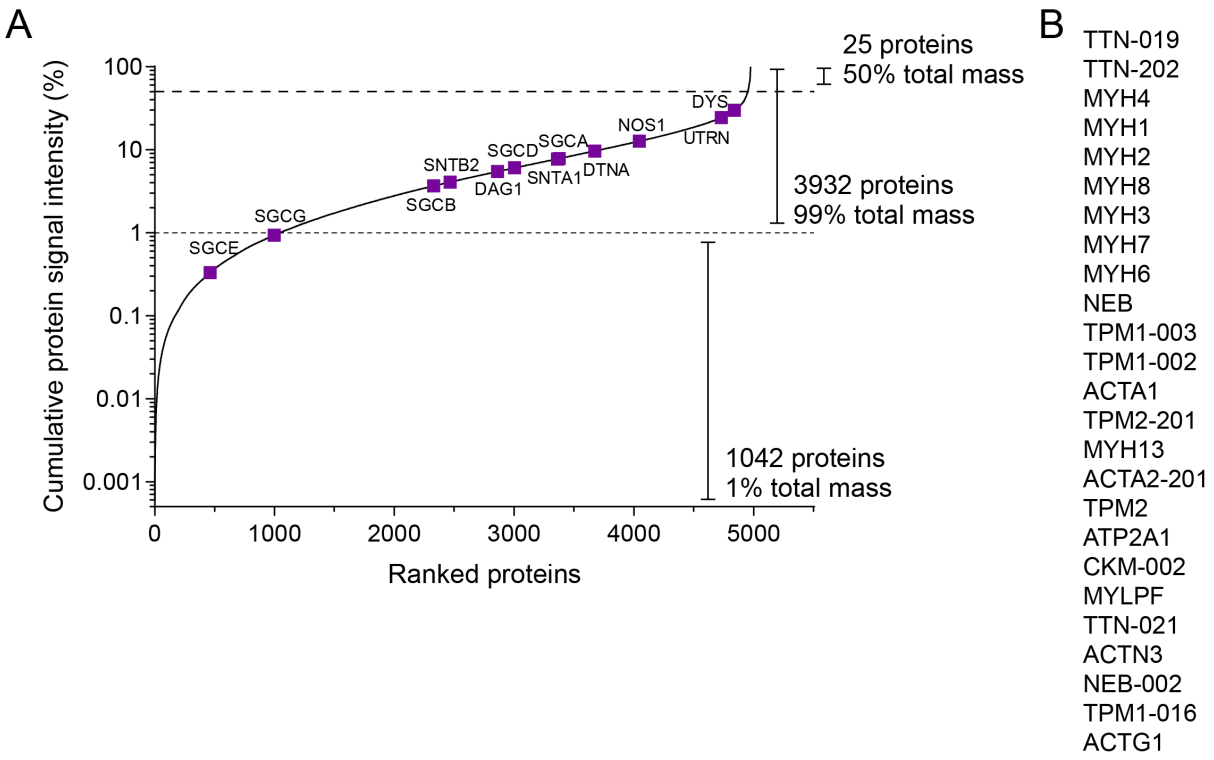

Figure 4.3 Cumulative protein frequency distribution of all proteins identified with HiRIEF-LC-MS/MS.
A Cumulative distribution frequency ranking detected mass of proteins from low to high, identifying key proteins involved in DMD pathology (purple squares). **B** Top 25 proteins accounting for 50% of the detected protein mass.

Differentially expressed proteins were identified by one-way ANOVA analysis across all nine experimental groups, and 2,540 proteins (51.1%) were significantly different in at least one group (P<0.01). Expression of significantly different proteins was visualised by heatmap and PCA (**Figure 4.4**). Both analyses illustrate close replicate groupings, and a clear separation between the WT animals and the two dystrophic strains. However, *mdx* and *mdx52* samples were intermingled, suggestive of a common pattern of proteomic perturbation in these dystrophic models. In addition, a gradual progression of age is apparent in both the WT and dystrophic samples.

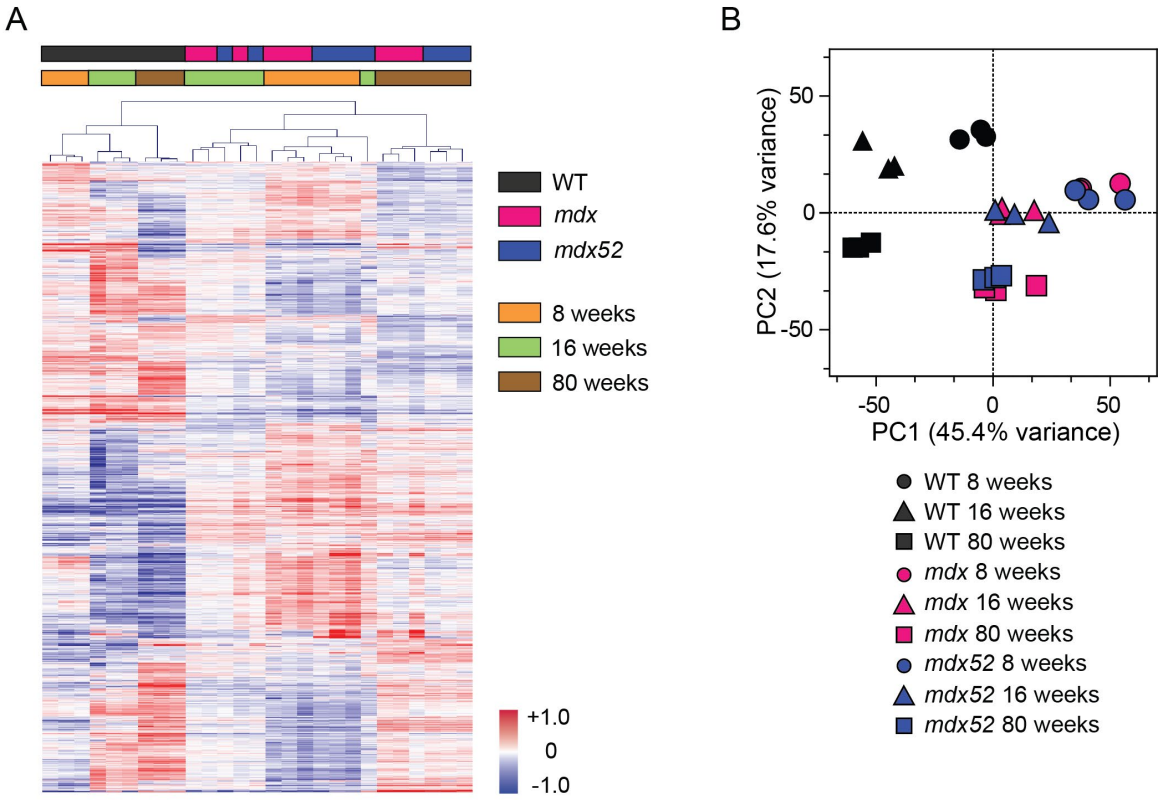

Figure 4.4 Clustering of differentially expressed proteins between WT, *mdx* and *mdx52* samples at 8, 16 and 80 weeks of age.

A Heatmap clustering of samples and proteins identified as differentially expressed by one-way ANOVA (P<0.01) with Bonferroni correction (n=3 per group). Scale bar represents row Z-scores, with red and blue indicating higher and lower than mean abundance respectively. Strain and age are indicated by colour above the heatmap. **B** PCA clustering of samples. One-way ANOVA (P<0.01) with Bonferroni correction (n=3 per group).

4.3.3 Dystrophin-associated protein complex

The expression patterns of dystrophin-associated proteins were examined to assess the performance of the proteomic analysis, which were expected to be differentially expressed in dystrophic muscle. Loss of dystrophin leads to the mislocalisation and subsequent destabilisation of DAPC components. As a result, down-regulation of DAPC proteins is an established feature of dystrophic muscle [492,582]. Protein expression ratios for 10 DAPC proteins are shown in **Figure 4.5**. Relative to controls, the majority of these proteins (DYS, NOS1, SGCA, SGCB, SGCG, DAG1, SNTA1 and DTNA) were significantly down-regulated in both *mdx* and *mdx52* mice at all time points. In contrast, UTRN (utrophin) was significantly upregulated in dystrophic muscle at all ages. The pattern of

differential expression of the different DAPC components was observed in both dystrophic strains across all ages, and therefore demonstrates the robustness of both the proteomic analysis and multiplexing strategy.

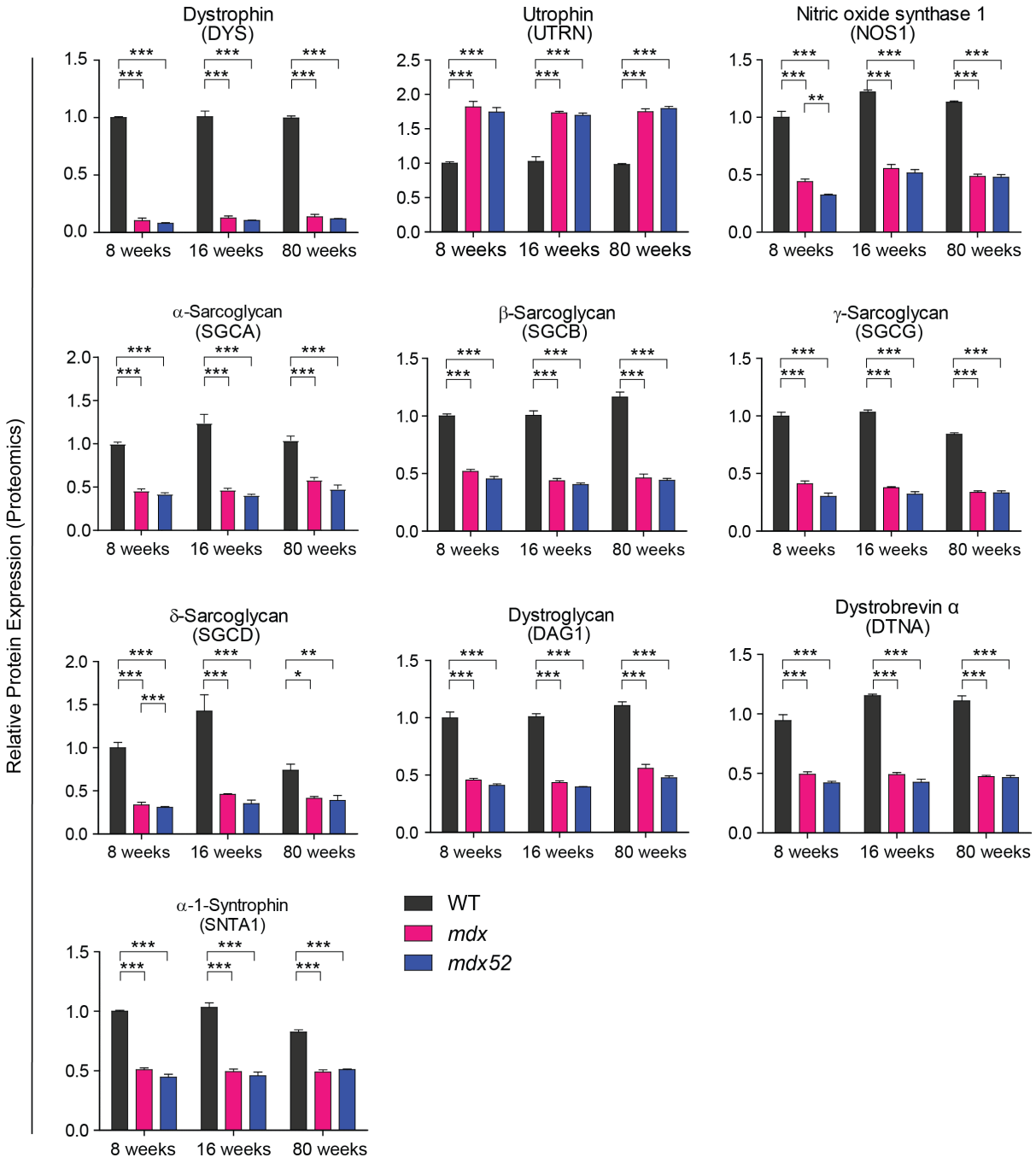

Figure 4.5 Relative protein expression of important proteins involved in the DAPC.
Protein expression levels were identified through HiRIEF-LC-MS/MS of WT, *mdx* and *mdx52* samples at 8, 16 and 80 weeks of age (n=3 per group). Values are mean ± SEM. * P<0.05, ** P<0.01 and *** P<0.001. One-way ANOVA at each time point, with Tukey *post hoc* correction.

4.3.4 Comparison of *mdx* and *mdx52* dystrophic mouse models

To investigate potential differences between the *mdx* and *mdx52* models, a detailed analysis was performed comparing protein expression at each time point using *t*-tests ($P<0.01$). Few differences were observed between the two mouse models (**Figure 4.6A** and **B**). At 8 weeks of age, 126 (2.5% of the quantifiable proteome) proteins were differentially expressed whereby neutrophilic granule protein (NGP) exhibited the highest fold increase (7.4-fold; **Figure 4.6**). Notably, most of these proteins were not significantly different at the other time points. At 16 weeks, only 37 proteins (0.7%) were significantly different between *mdx* and *mdx52*, and the fold changes observed were relatively small (< 1.35-fold). Similarly, at 80 weeks, 79 proteins (1.6%) were differentially expressed with the highest expression ratio being a 2.5-fold decrease (IGHA, immunoglobulin heavy constant alpha). When a multiple comparisons correction was applied (Benjamini-Hochberg, $P<0.05$), no statistical differences were observed between the two dystrophic models.

Subsequently, a comparative analysis using IPA was performed on the uncorrected Student's *t*-tests, whereby the significant proteins from each time point were utilised to identify pathways of interest and results from the different time points were compared to each other. IPA analysis did not identify any canonical pathways that were differentially affected between the *mdx* and *mdx52* model, although upstream regulator analysis (which infers pathway regulation from downstream gene expression) identified an upregulation of HNF1A, IL6, PDGF BB, PRDM1 and RICTOR but only in the *mdx52* mouse at 8 weeks (**Figure 4.6C**). Additionally, this analysis also identified an inhibition of the RICTOR pathway at 80 weeks of age. Together, these observations suggest that there is relatively little difference between *mdx* and *mdx52*, especially at 16 and 80 weeks of age.

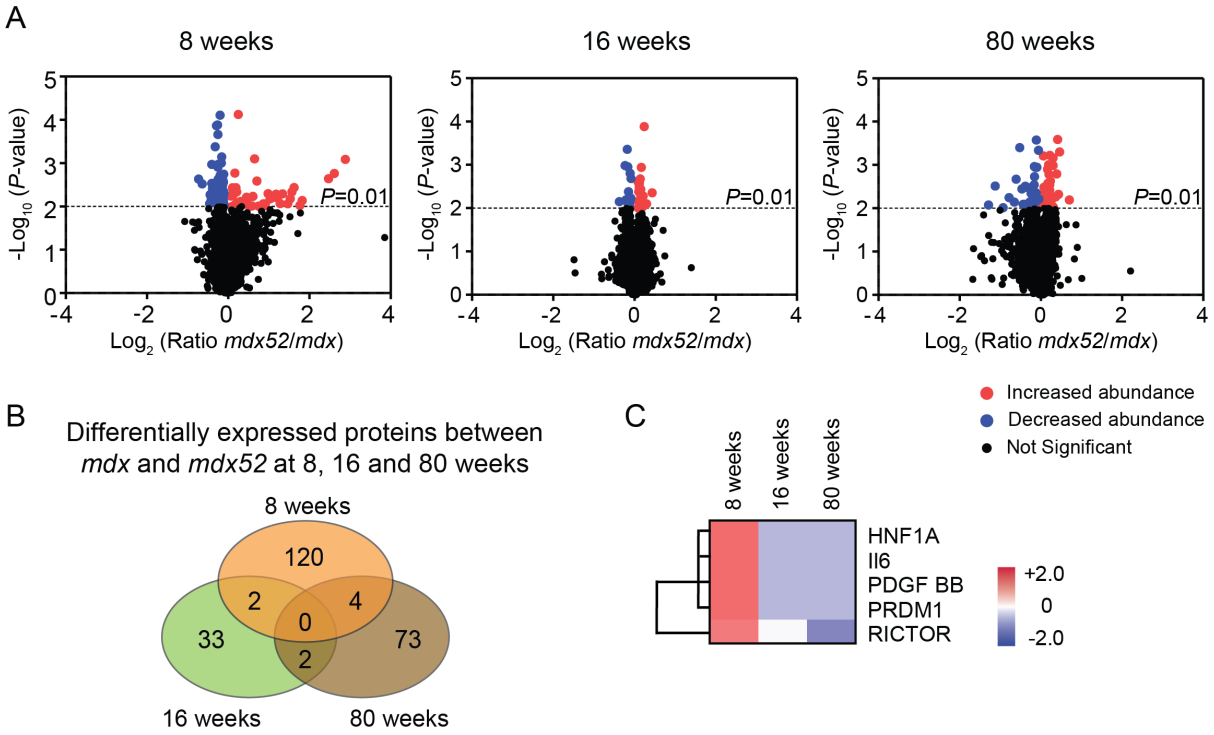

Figure 4.6 Differential protein expression between *mdx* and *mdx52* at 8, 16 and 80 weeks of age
A Volcano plots with $\log_2$ ratios of differentially expressed proteins between *mdx* and *mdx52*. **B** Venn diagram with overlap of differentially expressed proteins between the two strains for each time point. **C** Heatmap of upstream regulators identified through IPA analysis based on the differentially expressed proteins (*P*<0.01). Scale bar represents row Z-scores, with red and blue indicating higher and lower than mean abundance respectively. *n*=3 per group.

4.3.5 Protein expression comparisons between WT versus *mdx* or WT versus *mdx52*.

To further characterise dystrophic pathological features, WT versus *mdx* and WT versus *mdx52* expression ratios were compared at each time point (*P*<0.01). Both comparisons exhibited similar numbers of significant proteins between age. Compared to WT, *mdx* samples displayed differential expression of 1,508 proteins at 8 weeks, 1,305 proteins at 16 weeks and 2,399 proteins at 80 weeks. Similar changes in protein expression were seen for the *mdx52* comparison to WT, with differential expression of 1,622 at 8 weeks, 1,238 at 16 weeks and 2,411 at 80 weeks. Interestingly, differentially expressed proteins were often not similar between the WT versus *mdx* and the WT versus *mdx52* comparison: at 8 weeks only 34% of the significantly different proteins were shared

between the comparisons, whereas this was around 41% at 16 and 80 weeks of age. Given that the previous *mdx* versus *mdx52* analysis identified little differences, it was important to understand whether the currently observed discrepancies were biologically relevant. Therefore, expression ratios from both comparisons at each time point were visualised and correlation analyses were performed on all proteins that were identified as differentially expressed in one or both comparisons (**Figure 4.7A**). The results clearly indicate similar protein directionality (both increased or both decreased in abundance) between comparisons, as further illustrated by the Spearman's *r* correlation efficiency, ranging between 0.9254 and 0.9766, and further confirm minimal proteomic differences between the two dystrophic models. These results suggest that, in many cases, disparities between differential expression calls between the two dystrophic models are likely a consequence of insufficient statistical power (i.e. a protein may be up-regulated in both models but reaches statistical significance in only one model).

Utilising both models allowed for identification of proteins potentially critical to dystrophic pathology at different stages of the disease using a rigorous selection process. As such, only those proteins with a two-fold change at each time point for both *mdx* vs WT and *mdx*52 vs WT comparisons were selected (**Figure 4.7B**). The overlapping proteins at each time point were subsequently compared, whereby 16 proteins were consistently dysregulated at all time points (**Figure 4.7C** and **D**). Expected proteins, such as dystrophin (DMD) and nitric oxide synthase 1 (NOS1) were decreased in abundance in both dystrophic models at all ages compared to WT. Other proteins such as serine protease HTRA1 (HTRA1), prune homolog2 (PRUNE2), calcium-binding mitochondrial carrier protein SCaMC-1 (SLC25A24) and tubulin β class I (TUBB5) showed an increased abundance in both dystrophic models across the ages. Together, these results identify highly up- or downregulated proteins associated with disease pathology in two dystrophic mouse models.

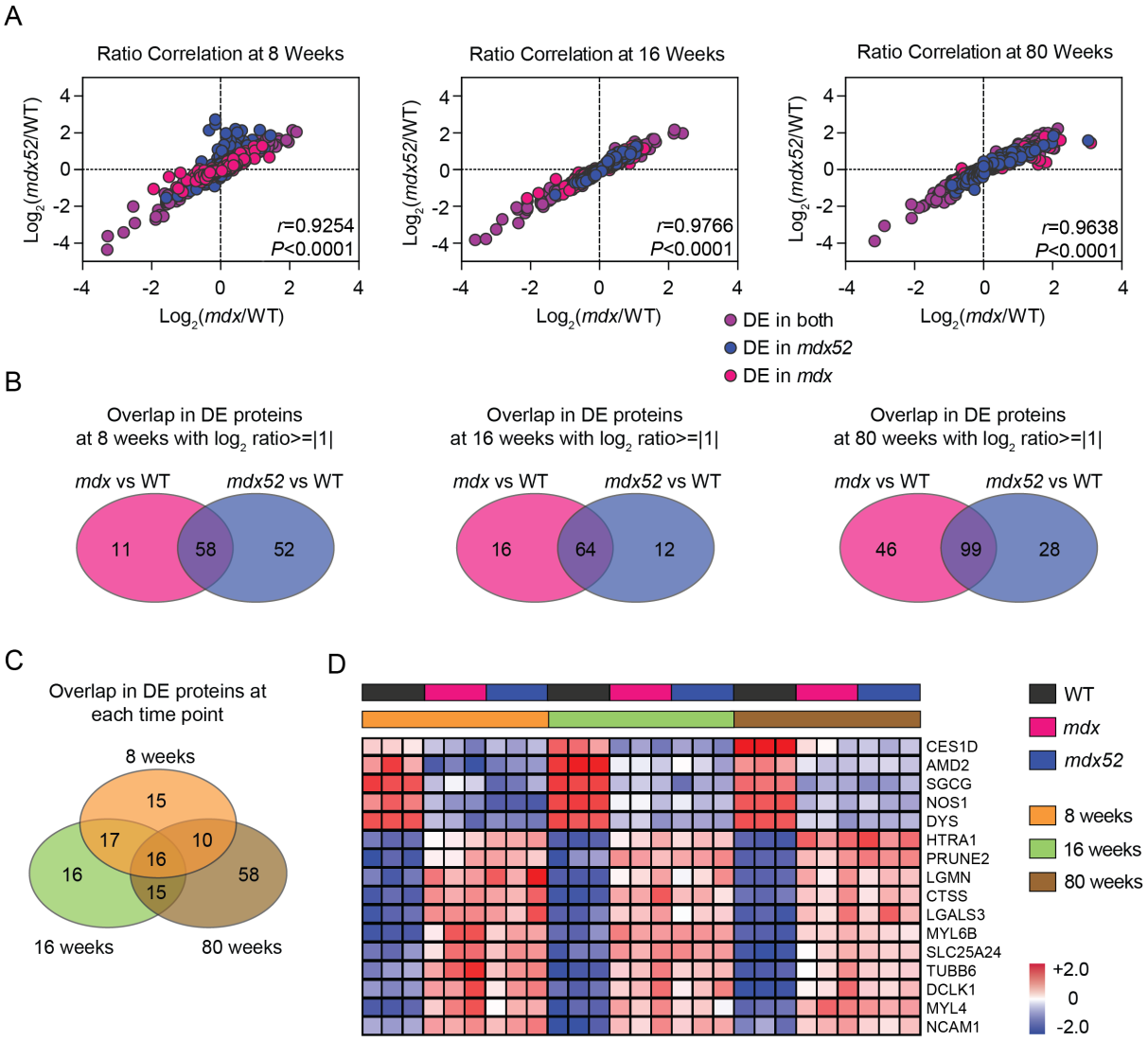

Figure 4.7 Differentially expressed proteins between *mdx* vs WT and *mdx52* vs WT.
A Correlation of protein ratios between *mdx* vs WT and *mdx52* vs WT at 8, 16 and 80 weeks of age. Proteins were identified as significantly different in *mdx* vs WT (pink), *mdx52* vs WT (blue) or in both comparisons (purple). Spearman's *r* correlation coefficients and correlation *P*-values are shown on the plots. **B** Comparison and overlap of differentially expressed proteins with a $\log_2$ ratio |1| identified in *mdx* vs WT and *mdx52* vs WT at each time point. **C** Overlap of commonly expressed proteins identified in **B** comparing each time point. **D** Heatmap of $\log_2$ protein expression ratios for the 16 proteins that are up- or downregulated at each time point for both dystrophic strains, as identified in **C**. Student's *t*-tests, *P*<0.01. Scale bar represents row Z-scores, with red and blue indicating higher and lower than mean abundance respectively. Strain and age are indicated by colour above heatmap. *n*=3 per group.

4.3.6 Mutation-independent dystrophic proteome signature

Given the similarities between *mdx* and *mdx52* samples, TMT ratios were pooled for all dystrophic (*mdx* and *mdx52*, *n*=18; "Dystrophic") and WT (*n*=9) animals and analysed by *t*-test to identify proteins that are differentially expressed in dystrophic muscle irrespective of mutation type or age ($P<0.01$). A benefit of this approach is that the increase in sample sizes offers improved statistical power to detect significant differences and it allows potential identification of proteins involved in most or all stages of the disease. Of the 4,974 proteins, 1,064 were down-regulated (21.4% of the detected proteome) and 1,084 up-regulated (21.8%; **Figure 4.8A**). Key proteins involved in DMD pathology were consistently called as differentially expressed, such as DMD, SGCB, SGCG, NOS1 and UTRN. Canonical pathways were subsequently identified based on differentially expressed proteins between Dystrophic and WT samples and illustrated in **Figure 4.8B** and **C**. This identified several known (e.g. mitochondrial dysfunction, calcium signalling, inflammasome pathway, sonic hedgehog signalling and integrin signalling) and unknown (e.g. NRF2-mediated oxidative stress response and GnRH signalling) DMD pathways. IPA analysis also demonstrated the potential involvement of several upstream regulators, some of which had not been associated with disease pathology in the literature, such as the histone 3 demethylase KDMA5 and RICTOR (**Figure 4.8D**).

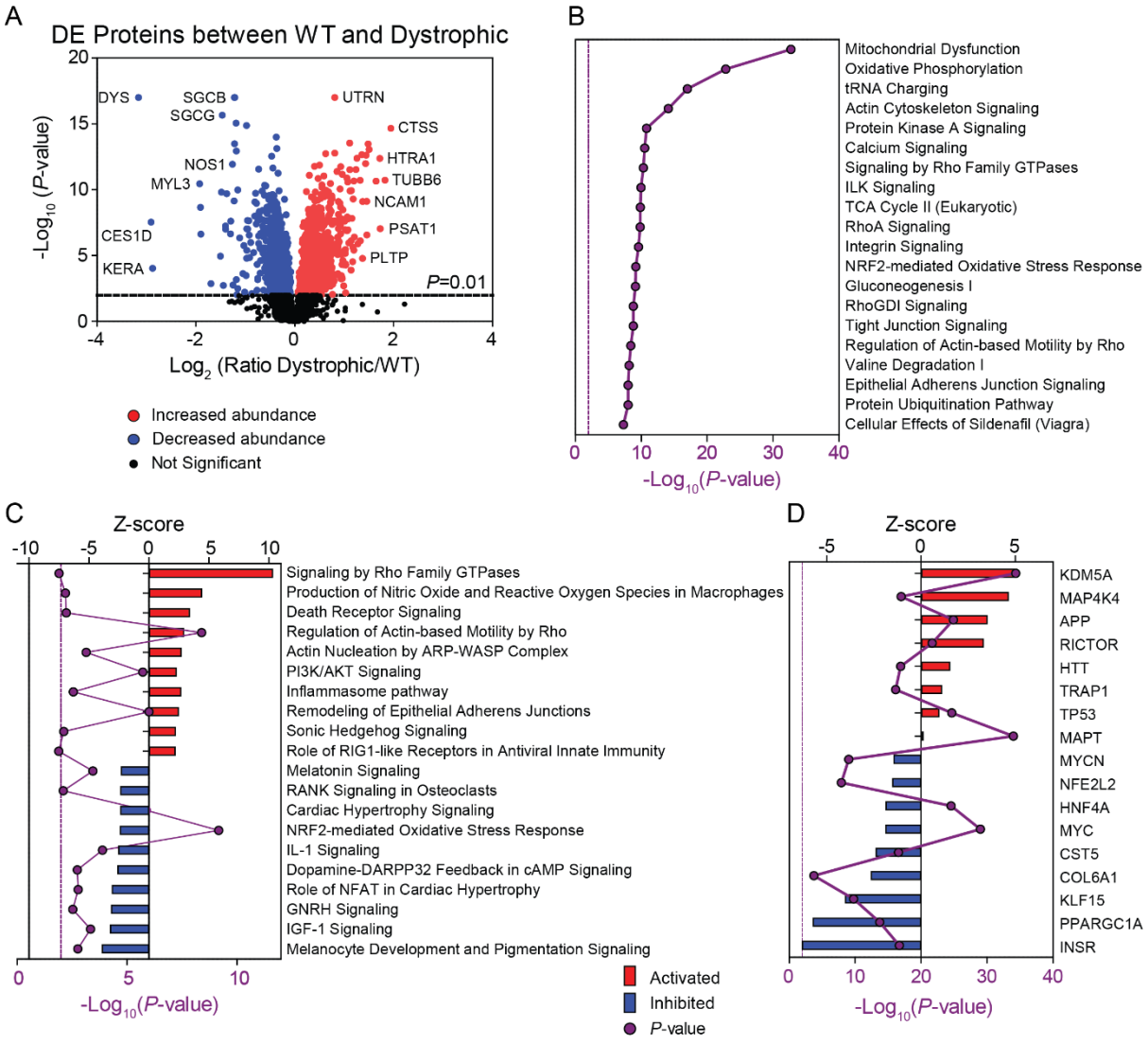

Figure 4.8 Most significant proteins and pathways in DMD pathology, irrespective of age or mutation.

A Expression ratios of differentially expressed proteins, highlighting most significant and/or most up- or downregulated proteins as identified by the ratio Dystrophic/WT. P<0.01, Student's *t*-tests. **B** Top 20 most significant pathways as identified through IPA (*P*<0.01). **C** Top 10 up- and downregulated pathways as identified by IPA through the z-score. Purple line indicates *P*=0.01. **D** Potential upstream regulators involved in up- or downregulation as identified by IPA through the z-score. Purple line indicates *P*=0.01.

4.3.7 Aging protein expression pattern between WT and Dystrophic

Examining those proteins that may be important in aging could illuminate some of the pathological changes seen in the disease over time. To address this, a one-way ANOVA was performed

(P<0.01) to determine protein expression differences between the three time points (8, 16 and 80 weeks, n=9) within WT samples and separately within Dystrophic samples (n=18). The analysis identified 694 and 1,424 proteins in the WT and Dystrophic comparisons, respectively. PCA plots for both groups indicate a clear aging pattern on the X-axis, PC1, which contains 55.1% and 61.1% of the variance for the WT and Dystrophic groups respectively (**Figure 4.9A**). Through the PC1 loading, principal component contribution for each protein was determined (**Figure 4.10A**). Significantly different proteins contributing to aging in the WT group were compared to those proteins identified in the Dystrophic samples, but only 266 proteins were commonly shared (**Figure 4.10C**). Furthermore, when comparing the top 100 proteins contributing to WT aging and Dystrophic aging, only 6 proteins were common between the two aging signatures (GCAT, GSTA4, L2HGDH, PAOX, PRKAR2A and SERPINH1; **Figure 4.10B**). These findings suggest that the process of age-associated changes in protein expression are largely different between the WT and Dystrophic strains.

To further characterise protein expression differences associated with aging, *k*-means clustering analysis was performed on the WT and Dystrophic samples separately. Clusters identified in both analyses were matched between WT and Dystrophic groups based on their expression patterns over time. Those with similar patterns between the two groups were selected for further investigation (4 out of 7; **Figure 4.9B**), whereby proteins identified in the matching WT and Dystrophic clusters were compared (**Figure 4.9C**). Even though the behaviour of expression within matching clusters was similar between WT and Dystrophic, the proteins that comprised these matching clusters were mostly distinct, with little overlap. Proteins common to the matching clusters are illustrated in heatmaps (**Figure 4.9D**). The heatmaps show clear aging progression patterns in both WT and Dystrophic samples, with similar directionality within a cluster. Interestingly, some proteins within the heatmaps, such as major vault protein (MVP) or caveolin-3 (CAV3), exhibit lower or higher expression in the Dystrophic models compared to WT, even though directionality over time is similar. These results underscore that aging manifests differently in WT and Dystrophic models.

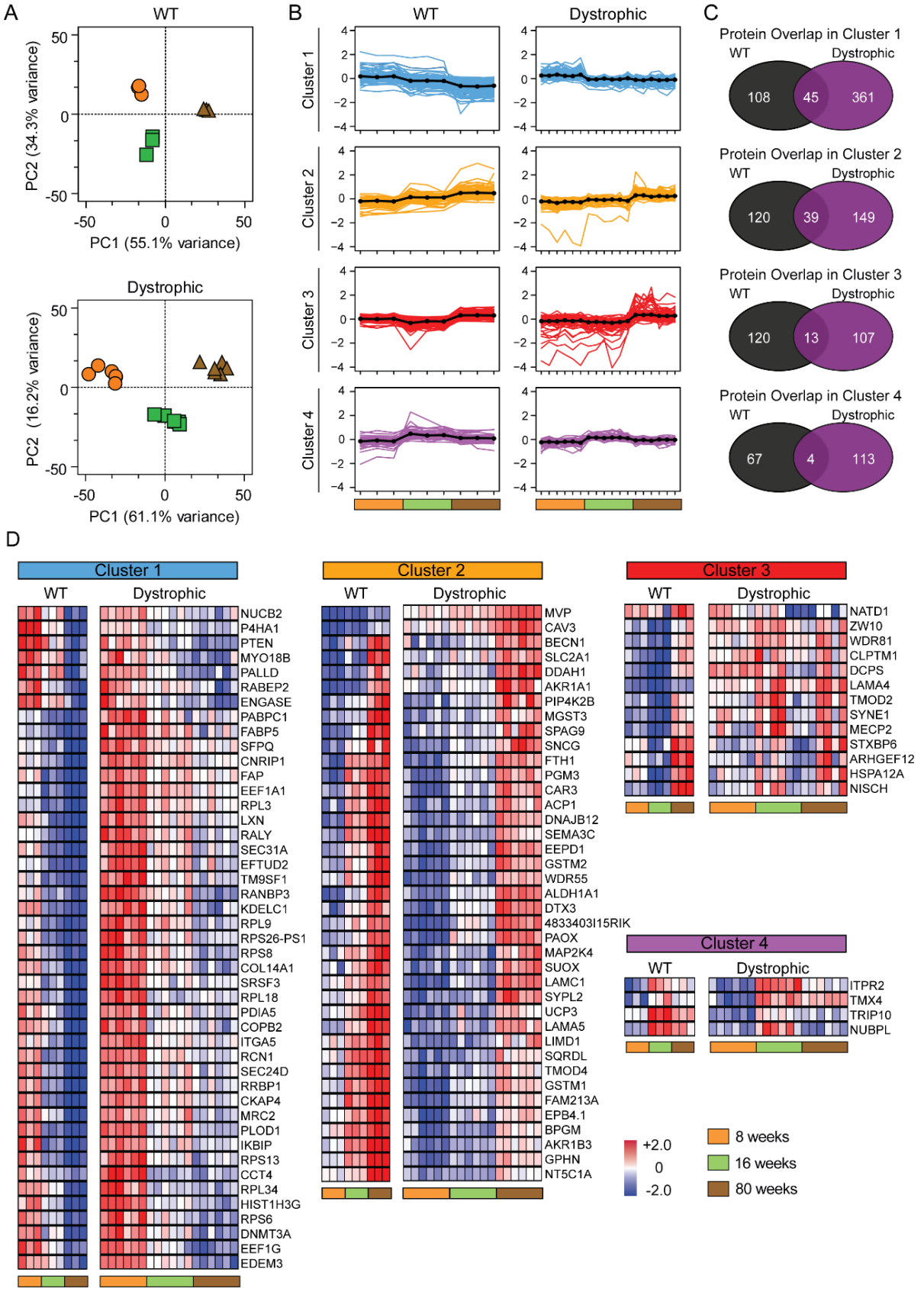
A
WT
PC2 (34.3% variance)
PC1 (55.1% variance)
Dystrophic
PC2 (16.2% variance)
PC1 (61.1% variance)
B
WT
Dystrophic
Cluster 1
Cluster 2
Cluster 3
Cluster 4
C
Protein Overlap in Cluster 1
WT
Dystrophic
108
45
361
Protein Overlap in Cluster 2
120
39
149
Protein Overlap in Cluster 3
120
13
107
Protein Overlap in Cluster 4
67
4
113
D
Cluster 1
Cluster 2
Cluster 3
Cluster 4
NUCB2
P4HA1
PTEN
MYO18B
PALLD
RABEP2
ENGASE
PABPC1
FABP5
SFPQ
CNRIP1
FAP
EEF1A1
RPL3
LXN
RALY
SEC31A
EFTUD2
TM9SF1
RANBP3
KDELC1
RPL9
RPS26-PS1
RPS8
COL14A1
SRSF3
RPL18
PDIA5
COPB2
ITGA5
RCN1
SEC24D
RRBP1
CKAP4
MRC2
PLOD1
IKBIP
RPS13
CCT4
RPL34
HIST1H3G
RPS6
DNMT3A
EEF1G
EDEM3
MVP
CAV3
BECN1
SLC2A1
DDAH1
AKR1A1
PIP4K2B
MGST3
SPAG9
SNCG
FTH1
PGM3
CAR3
ACP1
DNAJB12
SEMA3C
EEPD1
GSTM2
WDR55
ALDH1A1
DTX3
4833403I15RIK
PAOX
MAP2K4
SUOX
LAMC1
SYPL2
UCP3
LAMA5
LIMD1
SQRDL
TMOD4
GSTM1
FAM213A
EPB4.1
BPGM
AKR1B3
GPHN
NT5C1A
NATD1
ZW10
WDR81
CLPTM1
DCPS
LAMA4
TMOD2
SYNE1
MECP2
STXBP6
ARHGEF12
HSPA12A
NISCH
ITPR2
TMX4
TRIP10
NUBPL
+2.0
0
-2.0
8 weeks
16 weeks
80 weeks

Figure 4.9 Proteomic aging signature in WT and Dystrophic samples.
A PCA plot illustrating the clustering of WT (upper panel) and Dystrophic (lower panel) samples. Significantly different proteins were identified through one-way ANOVA, with Bonferroni correction (P<0.01). **B** Visualisation of four clusters identified through *k*-means clustering exhibiting similar expression patterns over time in WT and Dystrophic samples. X-axis represents age as indicated by colour below graphs and Y-axis represents Z-scores. **C** Overlap of proteins between the matched WT and Dystrophic clusters. **D** Heatmap of overlapping proteins between the matching WT and Dystrophic clusters. Scale bar represents row Z-scores, with red and blue indicating higher and lower than mean abundance respectively. Age is indicated by colour below heatmap.

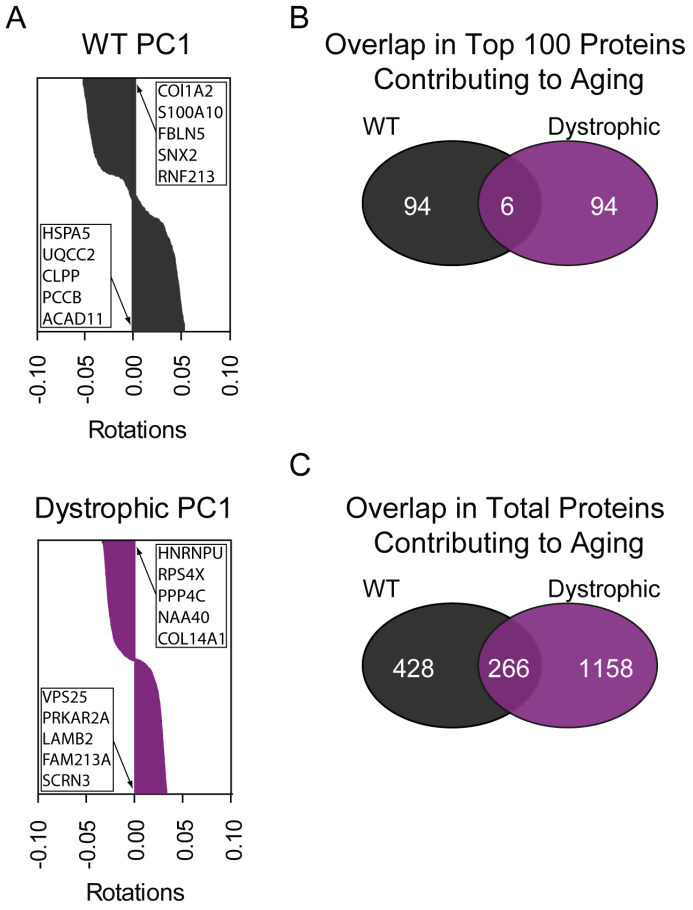

Figure 4.10 Proteins contributing to aging of WT and Dystrophic samples.
A Protein loadings (PC1) from PCA plot identifying proteins in WT (upper panel) and Dystrophic (lower panel) that highly contribute to aging. **B** Overlap in top 100 proteins contributing to WT and Dystrophic aging. **C** Overlap in total number of proteins that are differentially expressed in WT and Dystrophic aging.

4.3.8 Validation of proteomics dataset

Three proteins were selected to validate the proteomics dataset; CAV3, serine/threonine-protein kinase PAK1 (PAK1) and MVP by Western blot and compared with expression levels in the HiRIEF-LC-MS/MS data (**Figure 4.11A** and **B**). These proteins were significantly upregulated in the different proteomic analyses performed and were therefore chosen for validation. Three independent replicates were run on separate Western blots with similar results (n=3 per group). Expression patterns appeared comparable between HiRIEF-LC-MS/MS and Western blot experiments (**Figure 4.11B**), thereby validating the mass spectrometry technique using the gold standard for protein quantification. Expression on the mRNA level was further examined and concordant mRNA and protein directionality was observed for *Mvp* and *Pak1*, indicative of transcriptional up-regulation, although some changes between WT and the dystrophic groups did not reach statistical significance (P<0.05; **Figure 4.11C**). *Cav3* expression was not significantly increased in *mdx* and *mdx52* samples compared to the WT at 8 and 80 weeks of age, in contrast to what was observed in the proteomics dataset. Indeed, transcriptome and proteome directionality often does not match, probably due to post-translational modifications, and as such the results are not surprising. Therefore, even though mRNA and protein do not always consistently correspond with each other, the Western blot protein levels observed validate the mass spectrometry data.

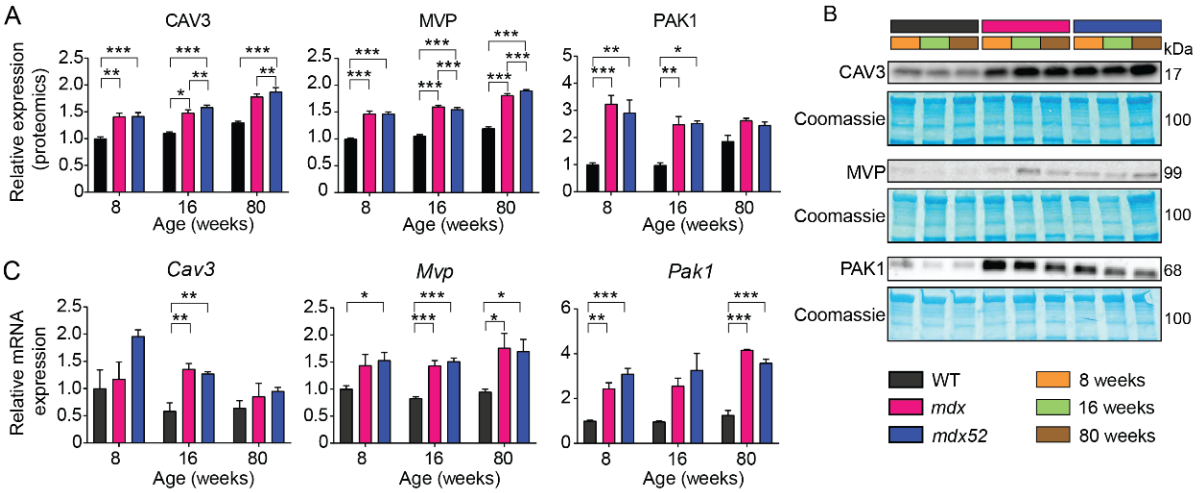

Figure 4.11 Validation of selected protein targets.

A Relative protein expression as identified by HiRIEF-LC-MS/MS for CAV3, MVP and PAK1 (*n*=3 per group). **B** Western blot bands illustrating protein expression of CAV3, MVP and PAK1 (*n*=3 per group). Coomassie was utilised to determine protein loading. Data collected by Ms Miyako Seto. **C** Relative mRNA expression as identified through RT-qPCR for *Cav3*, *Mvp* and *Pak1* (*n*=3 per group). Values were normalised against the geometric average of *Rpl10* and *Tbp*. Values are mean ± SEM. * *P*<0.05, ** *P*<0.01 and *** *P*<0.001. One-way ANOVA per time point, with Tukey *post hoc* correction.

4.3.9 MVP is not required for myogenic differentiation, but may influence *Dmd* expression

The proteomics dataset provided several novel targets of interest and major MVP was selected for further investigation, as this protein has not previously been evaluated in DMD and given its differential expression with age in dystrophic muscle. Ribonucleoparticle vault structures are composed of multiple copies of MVP, but their function is still poorly understood [583]. Recent evidence has shown that vaults can act as scaffold and they are involved in cell survival signaling [584,585]. Moreover, they are observed to regulate growth and survival of respiratory smooth muscle cells [585]. To identify whether MVP plays a role in skeletal muscle cell differentiation, RNA interference was utilised to inhibit protein expression in a commonly used myoblast cell line, C2C12 (*n*=3 per group). Effective knockdown was assessed at the mRNA level, whereby *Mvp* transcript was downregulated by 60% and 83% 3 and 6 days after differentiation, respectively (**Figure 4.12A**). The MVP protein was expressed at only 6% of WT levels at DM3, whereas at DM6 no MVP protein could be detected (**Figure 4.12B**). To investigate a possible role for MVP function in muscle cells, the influence of target siRNA knockdown of *Mvp* on myogenic differentiation was assessed. No observable differences were detected following siMvp (**Figure 4.12*C***).

Interestingly, although transcript levels are present, MVP protein cannot be detected by Western blot in undifferentiated myoblasts, which further suggests that MVP is not required for differentiation and is mainly expressed in myofibres. Therefore, *Dmd* transcript expression was assessed in the dystrophin-deficient myoblasts cell line H2K-*mdx52,* following successful knockdown of *Mvp* with RNA interference (**Figure 4.12D**). While the data are preliminary, a decreasing trend in *Dmd* transcript was observed following *Mvp* knockdown (*n*=2 per group), suggesting that Mvp mRNA or protein may regulate *Dmd* transcription or transcript stability. Further experiments are required to assess whether these data can be reproduced and confirmed.

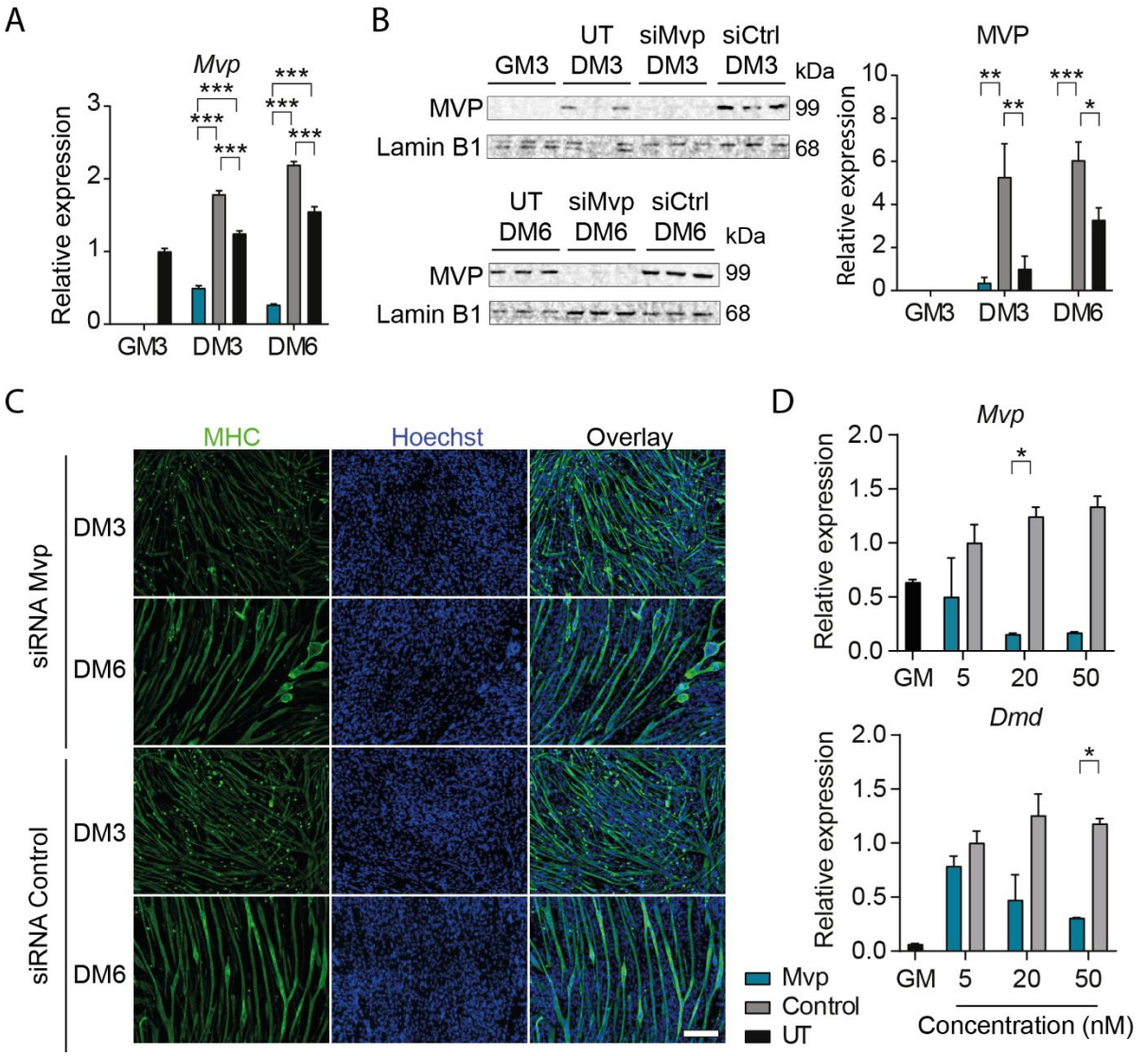

Figure 4.12 *Mvp* siRNA knockdown in C2C12 myoblasts does not affect differentiation, but may influence *Dmd* expression in dystrophin-deficient H2K-*mdx52* myoblasts.

A Relative mRNA expression as identified through RT-qPCR for *Mvp* at GM3, and 3 and 6 days after differentiation (DM3 and DM6) (*n*=3 per group). Values were normalised against the geometric average of *Rpl10* and *Tbp* and are mean ± SEM. * *P*<0.05, ** *P*<0.01 and *** *P*<0.001. One-way ANOVA per time point, with Tukey *post hoc* correction. **B** Western blot bands illustrating protein expression of MVP (*n*=3 per group). Protein was normalised to Lamin B1 protein at GM3, DM3 and DM6. Values are mean ± SEM. * *P*<0.05, ** *P*<0.01. One-way ANOVA with Tukey *post hoc* correction per time point. **C** MHC staining for cells treated with siRNA *Mvp* and Ctrl at DM3 and DM6 (*n*=3 per group). Scale bar indicates 200 µm. **D** Relative mRNA expression as identified through RT-qPCR for *Mvp* and *Dmd a*t GM and 2 days after differentiation, treated with different concentrations of siRNA for *Mvp* and Ctrl (5, 20 and 50 nM) in dystrophin-deficient H2K-*mdx52* cells (*n*=2 per group). Values were normalised against *Abt1*. Values are mean ± SEM. * *P*<0.05, Student's *t*-test per siRNA concentration, comparing cells treated with *Mvp* or Ctrl siRNA. Data in **D** collected by Ms Miyako Seto.

4.4 Discussion

4.4.1 Comparing protein signatures of *mdx* and *mdx52*

This study utilised innovative mass-spectrometry-based profiling to generate the highest resolution profile of dystrophic muscle proteome described to date. Two dystrophic mouse models were utilised, which allowed for the identification of differentially expressed proteins compared to WT, irrespective of the mutation. Previous studies demonstrated differences in revertant fibres between the *mdx* and *mdx52* [576]. The higher number of revertant fibres observed in the *mdx* compared to the *mdx52* mouse is suggestive of (possible) differences in endogenous alternative splicing, mRNA stability and/or regenerative capacity. To further investigate the latter possibility, ex-myomiR abundance was measured, as these have been shown to be indicative of muscle turnover by the Morgan and Wood labs [479]. The results demonstrated differences in peak myomiR abundance between the *mdx* and *mdx52* mice (16 compared to 8 weeks, respectively). This may be especially important in the early necrosis and regeneration phase and the timing corresponds with the observed myomiR peak in *mdx52*. It should be noted that the percentage of RF in either mouse model is considerably low (~1%) and patient data has shown that RF numbers (1-7%) impart no benefit on pathology [586] (although some patients with very low dystrophin levels still exhibit a milder DMD pathology [587].

The mdx and *mdx52* mouse models, and their WT controls, were subsequently compared on a protein level at the degeneration-regeneration phase (8 weeks), during a stable increase of pathology (16 weeks) and in aging pathologic muscle (80 weeks). These ages were chosen based on the myomiR abundance patterns and previous studies. Statistical analyses illustrated that the detected proteome is very similar between the *mdx* and *mdx52* at all analysed ages. Given that studies have demonstrated that dystrophic pathology in the *mdx52* mouse is very similar to the *mdx* in skeletal muscle, these results are not surprising. Even though the *mdx52* mouse exhibits lower numbers of

revertant fibres, this percentage is still small compared to the vast majority of cells that do not express dystrophin. The proteomic signature differences underlying myomiR peak variations between the *mdx* and *mdx52* mice may be of negligible magnitude to be able to detect in a global proteomic analysis. The few upstream regulators identified as differentially expressed between *mdx* and *mdx52* were mostly significant at 8 weeks of age. As this is during the necrosis and regeneration phase, it seems plausible these regulators play a role in these pathological processes. Indeed, platelet-derived growth factor (PDGF) and PRDM proteins are involved in skeletal muscle cell proliferation [588] and vascular smooth muscle cell differentiation [589], respectively. Another consideration is the total number of proteins detected. Although many improvements have been made in the field, including isotope labelling (SILAC) [590] and the technique employed in this study, which has allowed identification of the highest known protein detection to date, many other proteins remained invisible in this proteomic analysis. Therefore, this study may lack the proteomic depth to uncover the reasons for the differences between the two dystrophic models at 8 weeks.

4.4.2 Mutation-independent and/or age-related dystrophic proteome

Further analysis compared *mdx* with WT and *mdx52* with WT. This enabled identification of 16 highly differentially expressed proteins likely to be involved in the dystrophic pathology, irrespective of mutation or age. Two important proteins that are significantly downregulated are dystrophin and nNOS, confirming the validity of the strategy. Among the interesting proteins that are consistently upregulated in both *mdx* and *mdx52* models compared to WT are HTRA1 and SLC25A24. HTRA1 is a serine protease which targets, among others, extracellular matrix proteins such as fibronectin [591] and could be involved in the extracellular matrix remodelling commonly seen in DMD. SLC25A24 is a ATP-Mg/Pi carrier, importing adenine nucleotides and exporting phosphates, and is Ca^{2+} sensitive. This channel is involved the mitochondrial ATP/ADP ratio and its knockdown in a cancel cell line reduces Ca^{2+} buffering capacity, sensitising cells to the mitochondrial permeability transition [592]. To what extent these results can be extrapolated to muscle cells remains to be

established, but an increase of SLC25A24 in *mdx* muscle may be a compensatory mechanism in an effort to increase the Ca^{2+} buffering capacity of the cell and prevent myofibre necrosis.

As the two dystrophic models exhibited similar proteomic patterns, they were further analysed together as a single dystrophic group. IPA analysis identified many pathways differentially expressed between dystrophic and control muscle irrespective of age or mutation, such as those involving the Rho family GTPases. This family hydrolyses GTP to GDP and is involved in many basic cellular processes, such as the actin skeleton and intracellular asymmetric organisation [593]. Indeed, RhoA has already been implicated in ossification, and regulation of utrophin expression and localisation [594,595]. The analysis also demonstrated that gluconeogenesis is significantly dysregulated, and one of the most downregulated predicted regulator is the insulin receptor. Previous studies have identified reduced glucose uptake and an increase in glycogen in *mdx* skeletal muscle [596,597]. Moreover, patients exhibit increased circulating insulin and insulin resistance [598]. These results were irrespective of patient weight, suggesting it is not a cause of fat mass content, but rather dystrophy-related. Dysregulation of the gluconeogenesis may exacerbate the skeletal pathology due to altered energy supply.

Another upstream regulator that is predicted to be involved in the disease is RICTOR, a subunit of mammalian target of rapamycin complex 2 (mTORC2). This protein is involved in important cellular functions, such as cell growth and myoblast differentiation, through its regulation of AKT [599–601]. mTOR is shown to be dysregulated in several studies investigating DMD pathology [602,603] and the mTORC2 pathway specifically is further dysregulated in aged *mdx* mice [604]. Interestingly, not only does dystrophin loss influence mTORC2, loss of RICTOR in non-dystrophic muscle leads to a reduction in dystrophin protein expression [605], suggesting a potentially important dynamic relationship between these two proteins. An additional function of RICTOR is its involvement in skeletal muscle glucose uptake during exercise and loss of mTORC2 leads to insulin resistance and a reduction in the suppression of gluconeogenesis [606,607]. These findings suggest that RICTOR may be an important

pathological mediator for many cellular processes in muscle, including regeneration and glucose metabolism.

This study also sought to investigate how the proteome evolves with pathological progression. Therefore, the pattern of aging in WT and dystrophic models was analysed, which indicated a differential aging behaviour between the two groups. Global analysis specified a difference between the young and old ages in the WT. In contrast, the *mdx* exhibited large disparities between all three ages. Moreover, proteins contributing to the aging pattern were not similar between the WT and dystrophic samples. Many proteins that did correspond in aging signature between WT and dystrophic muscle, were higher or lower expressed in the dystrophic samples relative to their control counterparts, as observed with CAV3 and MVP. This highlights that those proteins contributing to healthy and dystrophic aging are not expressed to similar degrees. CAV3 has previously been demonstrated to be upregulated in muscle from DMD patients [492,608], confirming the results. CAV3 associates with the DAPC through binding to β-dystroglycan [609] and WT mice overexpressing CAV3 exhibit a DMD-like phenotype in skeletal muscle, including associated histological changes and increased CK [610].

4.4.3 Dystrophic involvement of MVP

The proteomic analysis identified many interesting proteins involved in the pathology of DMD, such as MVP. MVP is a constituent of multi-subunit vault micro-organelle structures, the function of which is relatively poorly understood [583]. Recent evidence has shown that vault particles can act a as scaffold for proteins and they are involved in cell survival signalling [584,585]. The unique function and significant data associated with MVP encouraged further investigation into this protein. Although the protein was not required for differentiation of myoblasts, protein expression noticeably increased during this process. The *Dmd* transcript exhibited a trend of reduction following treatment with siRNAs targeting the *Mvp* transcript. These results warrant replication of the current experiment and further investigation into the role of Mvp in dystrophic pathology.

4.4.4 Study limitations and future directions

The current study selected the two early analysed ages (8 and 16 weeks) based on the behaviour of serum miRNAs and previous findings [575,576]. However, given that the molecular mechanism differences between the two dystrophic models were not resolved, it may be possible that endogenous alternative splicing of the *Dmd* transcript is relevant for the *mdx* and *mdx52* comparison. To address this, mRNA stability levels could be investigated. Through addition of actinomycin D, mRNA transcription is inhibited and the decay of the *Dmd* transcript can be measured in myotubes representing the *mdx* and *mdx52* mutations (exon 23 point mutation and exon 52 deletion respectively).

The observed downregulation of the *Dmd* transcript following *Mvp* knockdown is an important new aspect of DMD pathology and necessitates further investigation. As the function of MVP is not clear, initial binding experiments between dystrophin and/or its associated proteins to MVP may provide further information into the mechanisms behind *Mvp*-mediated *Dmd* downregulation. Other experiments could investigate the role of *Mvp* in known aberrant pathways, such as Ca^{2+} signalling, mitochondrial metabolism and fibrosis. Further downstream, *mdx* mice could be crossed with mice negative for MVP ($MVP^{-/-}$, which show no overt phenotype [611]) to examine whether genetic ablation of *Mvp* influences the dystrophic phenotype. These could subsequently be stressed with muscle injury experiments, such as cardiotoxin injections, and the effects on muscle regeneration analysed.

Furthermore, this work analysed protein expression in whole muscle tissue, including the different cell types associated. This may mask any cell-type- and/or myofibre-specific differences between dystrophic and control muscle. Therefore, it is important that future experiments focus on improving the spatial resolution by isolating specific cell types or myofibres that can inform on processes characteristic to those cells.

4.4.5 Conclusions

The investigation of two dystrophic mouse models at three different stages of dystrophic pathology allowed for identification of a dystrophic proteomic signature that is mutation- and age-independent. The data demonstrated no major differences between the *mdx* and *mdx52* mouse in skeletal muscle. However, dystrophic model grouping allowed for a more robust statistical analysis demonstrating an involvement of the Rho GTPase and glucose pathways in the pathology of DMD. The data also highlighted the differential expression of proteins such as SLC25A24, RICTOR, CAV3 and MVP. Moreover, the regulation of the *Dmd* transcript by MVP provides an important new aspect in dystrophin regulation, which warrants further investigation. Overall, this work provides novel insight into specific proteomic changes characteristic of muscle aging and the relationship of these to dystrophic pathology over time.

5. Results III

Uniform dystrophin distribution at the sarcolemma is required to stabilise ex-miRNA release from dystrophic muscle

5.1 Introduction

At present, there is no cure for DMD. Much research effort has been directed towards the development of interventions that can prolong survival and improve quality of life in DMD patients. However, restoration of dystrophin protein in patient muscles remains a significant technical challenge. This is exemplified by the controversy surrounding the approval of eteplirsen by the US FDA [612], given that this compound was shown to achieve restoration of less than 1% of normal dystrophin protein expression. The minimum amount of dystrophin required for therapeutic benefit is therefore a question of key importance. Some patients with BMD are near-asymptomatic as a consequence of ~30% of normal dystrophin expression from birth [613]. Furthermore, Neri *et al.* discovered that 30% dystrophin protein expression was sufficient to prevent muscle weakness in a family with X-linked cardiomyopathy [613]. Similarly, heterozygous *mdx* mice (expressing dystrophin in the heart at the level of ~50%) experience only mild cardiomyopathy [614], and cardiac muscle exhibits minor functional improvements with even as little as ~3% dystrophin expression [615]. Further studies from the Wells group and Wood group suggest that therapeutic re-introduction of ~15% of normal dystrophin in adult *mdx* mice is sufficient to provide protection against contractile damage [616].

Female carriers of DMD-causing mutations typically express ~60% of normal dystrophin protein [617,618] as a consequence of random epigenetic silencing of the 'healthy' chromosome via X-chromosome inactivation (XCI). They generally do not present with muscle pathology on account of the presence of a functional copy of the *DMD* gene on the alternate X-chromosome. Dystrophin

positive myofibres in female carriers experience a selection advantage and become progressively enriched with age, as they are resistant to contraction-induced damage [617]. However, in some rare cases, carriers may present with DMD due to skewed XCI resulting in reduced levels of dystrophin synthesis from the healthy allele [617,619]. These data suggest that high dystrophin levels prevent muscle pathology, although the minimal protein requirement remains unclear.

Aside from the total amount of dystrophin expressed, the length and location of the protein also appear to be important for muscle function and therefore therapeutic improvement. Full-length dystrophin restoration of 20-30% of WT levels in transgenic *mdx* mice completely restored the dystrophic histopathology. In contrast, similar levels of a truncated dystrophin protein ameliorated, but did not completely abolish the disease phenotype [620]. The authors showed that the full length dystrophin was more likely to be associated with the sarcolemma [620]. Furthermore, localisation of the dystrophin protein also impacts muscle function, whereby transgenic *mdx* mice with a mosaic pattern of dystrophin expression (i.e. a mixture of dystrophin-positive and dystrophin-negative myofibres) exhibited less amelioration of pathology than uniform distribution [621].

As detailed in **Chapter 1.6**, many studies have been performed to further understand the miRNAome in the muscle and DMD field, with the myomiRs arguably being the most promising identified miRNAs for biomarker purposes in DMD. The Wood lab and collaborators in the Morgan lab have previously shown that circulating myomiR levels reflect the degree of turnover in dystrophic muscle and that re-expression of dystrophin by PPMO treatment restores ex-miRNA abundance [479] . However, the degree to which ex-miRNA (and other) biomarkers reflect the underlying level of dystrophin protein expression in muscle remains an unresolved question. Therefore, this work aimed to investigate the relationship between dystrophin protein expression and the abundance levels of circulating miRNAs. Utilising XCI, mice exhibiting varying levels of dystrophin were generated, which were further analysed for ex-miRNA abundance. Interestingly, these data demonstrated that a uniform pattern of dystrophin protein expression within myofibres is required for therapeutic

restoration of ex-miRNA levels and, by extension, stabilisation of myofibre turnover in dystrophic muscle.

5.2 Materials and methods

5.2.1 Animals

Experiments regarding the *mdx-Xist*$^{\Delta hs}$ mouse model were performed at the Leiden University Medical Center (Leiden University, the Netherlands) under 12:12 hour light:dark conditions with access to food and water *ad libitum* in individually ventilated cages (IVC), kept specific pathogen free (SPF; testing for a large number of viruses, bacteria and parasites).. Experiments were authorised and approved by the Animal Experimental Commission (DEC) of the LUMC and conform with the Directive 2010/63/EU of the European Parliament. All remaining experiments were performed at the Biomedical Services Building at the University of Oxford, as detailed in Chapter 2.1.

Heterozygote carriers (*n*=4) were generated by crossing male C57BL/10ScSnJ mice with female *mdx* mice. The resulting female progeny was sacrificed at 8 weeks of age by a rising CO_2 concentration and serum and tissues were collected (*n*=4). Serum and tissue from age- and sex-matched C57BL/10 (*n*=4) and homozygous *mdx* (*n*=4) were collected in parallel.

The *Xist*$^{\Delta hs}$ mouse model was utilised to generate female *mdx-Xist*$^{\Delta hs}$ mice. Male *mdx* mice were crossed with female *Xist*$^{\Delta hs}$ mice, which generated a female F1 progeny that expressed varying levels of dystrophin. Serum was collected from *mdx-Xist*$^{\Delta hs}$ mice expressing low (8.4-12.9%; *n*=5; 49 serum collections), medium (18.8-21%; *n*=5; 49 serum collections) and high (32.4-43.5%; *n*=5; 49 serum collections) levels of dystrophin over a 44 week time period (4-48 weeks of age). Serum from age- and sex-matched *mdx* (*n*=5; 46 serum collections), C57BL/10 (*n*=5; 50 serum collections) and *Xist*$^{\Delta hs}$ (*n*=5; 49 serum collections) mice was collected in parallel. Animals were sacrificed through cervical dislocation at 78 weeks of age and tissues were collected. Dystrophin protein expression was determined in the quadriceps femoris muscles by Western blot as described in [622].

Male and female C57BL/10 and *mdx* animals were sacrificed at 10, 24, 52 and 80 weeks of age by an increasing CO_2 concentration, and serum was collected (*n*=4 per group).

5.2.2 Exon skipping utilising PPMO

The cell penetrating peptide Pip9b2 (RXRRBRRFQILYRBRXRB, where X is aminohexanoic acid, and B is β-alanine) was conjugated to a Phosphorodiamidate Morpholino Oligonucleotide, PMO (5'-GGCCAAACCTCGGCTTACCTGAAAT-3'; Gene Tools LLC, Philomath, OR, USA) through an amide linkage between the C-terminus of the peptide and the amine of the morpholine heterocycle on the 3' end of the PMO [303]. Conjugates were subsequently dissolved in sterile H_2O and filtered through a 0.22 µm cellulose acetate membrane. Male *mdx* mice received a single intravenous injection of 12.5 mg/kg Pip9b2-PMO conjugate dissolved in 0.9% saline at 6 weeks of age (*n*=4). Synthesis and injection of the peptide were performed by Dr Andrey Arzumanov and Dr Corinne Betts respectively. Two weeks after administration, Pip9b2-PMO-treated *mdx* mice and their age- and sex-matched controls (C57BL/10, *n*=4, and *mdx*, *n*=3) were sacrificed, and serum and tissues were collected at 8 weeks of age.

5.2.3 FirePlex serum miRNA profiling

Measurement of miRNAs directly in biofluid was performed by Abcam (Cambridge, UK), utilising their FirePlex platform. The assay uses miRNA-specific polyethylene glycol-based hydrogel particles to capture target miRNAs. These target miRNAs were subsequently amplified by PCR, eluted, re-amplified in a second PCR reaction, re-hybridised to the probe-particles, incubated with a fluorescent reporter, and the fluorescence of each particle determined by flow cytometry.

For the FirePlex profiling analyses, miRNAs were measured directly in serum and data were obtained in relative fluorescence units (RFU). All target miRNAs were detected at levels above background. Signal intensities were processed whereby the background was subtracted. Background subtracted values were utilised to assess haemolysis performance. Artificial calibrator bridge samples were included in each FirePlex run to enable performance comparison. These bridge samples consisted of a mixture of serum from *mdx* and C57BL/10 animals. Non-normalised, background

subtracted calibrator values from the two FirePlex measurements were compared for each miRNA and goodness of fit was determined (**Figure 5.1**)

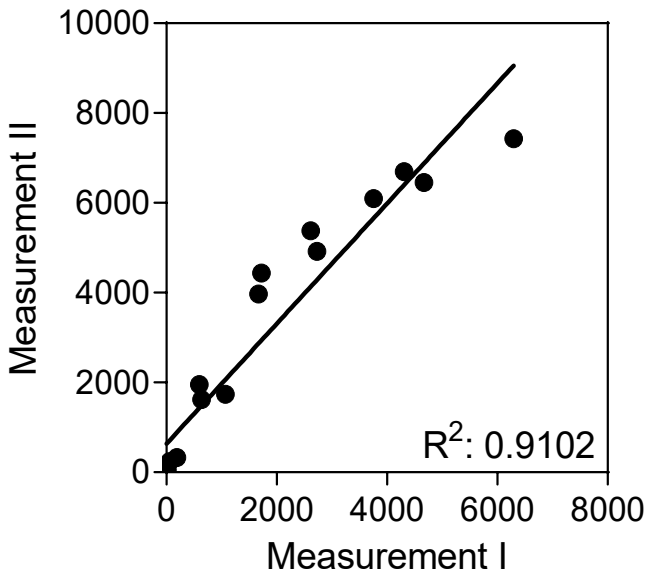

Figure 5.1 Goodness of fit for calibrator values from two FirePlex measurements.
Measurement I indicates the initial FirePlex run measuring 68 miRNAs in C57BL/10 and *mdx* at 12, 24 and 48 weeks of age. Measurement II contains the second profiling of all remaining samples in 12 miRNAs of interest. Goodness of fit contains samples and miRNAs included in both measurement

The regression data indicates close similarity between the two phases and therefore the samples from each phase were grouped together. Each normaliser probe was divided by the geometric average of all normaliser probe values such that values were then 'deflated' (i.e. the average of all deflated normaliser probe values equals one). Probe signal intensities were then divided by the deflated normaliser probe in order to normalise the data while preserving the natural range of fluorescence intensity values.

Log_2 transformed data were used for the heatmap and PCA analysis. All other analyses utilised data whereby abundance ratios were scaled such that the mean of the C57 control was returned to a value of 1.

5.2.4 RNA extraction and RT-qPCR

RNA from serum was extracted and RT-qPCR performed as detailed in **Chapter 2**. miRNA primers were obtained from ThermoFisher Scientific and indicated in **Table 5.1**.

Table 5.1 miRNA primers utilised for RT-qPCR validation.

miRNA	Assay ID	Sequence
miR-1a-3p	002222	UGGAAUGUAAAGAAGUAUGUAU
miR-133a-3p	002246	UUUGGUCCCCUUCAACCAGCUG
miR-16-5p	000391	UAGCAGCACGUAAAUAUUGGCG
miR-193b-3p	002467	AACUGGCCCACAAAGUCCCGCU
miR-206-3p	000510	UGGAAUGUAAGGAAGUGUGUGG
miR-208a-3p	000511	AUAAGACGAGCAAAAAGCUUGU
miR-370-3p	002275	GCCUGCUGGGGUGGAACCUGGU
miR-378-3p	002243	ACUGGACUUGGAGUCAGAAGG
miR-483-3p	002560	UCACUCCUCCCCUCCCGUCUU
miR-486a-5p	001278	UCCUGUACUGAGCUGCCCCGAG
miR-539-5p	001286	GGAGAAAUUAUCCUUGGUGUGU
cel-miR-39	000200	UGUCAGUUUGUCAAAUACCCCA

Serum miRNA RT-qPCR data were normalised to cel-miR-39 and cellular miRNA data to endogenous miR-16 expression, as this miRNA has been utilised previously by us and others and has a stable expression. mRNA extracted from tissue and cells was normalised to the geometric average of the stable housekeeping genes *Rpl10* and *Tbp* (**Table 5.2**).

cDNA for exon skipping analysis was generated from 500 ng of total RNA from TA and diluted 1:5 prior to analysis. Exon skipping of dystrophin was determined through division of the relative abundance of a qPCR assay targeting exon 20-21 by a qPCR assay targeting exon 23-24 (**Table 5.2**). This results in a ratio of un-skipped to total product and was utilised to calculate the percentage of skipped dystrophin mRNA.

Table 5.2 Primers and probes utilised for mRNA detection by qPCR.

Target Gene	Primer/Probe	Sequence 5' to 3'
Rpl10	Forward	TCATGTCCATCCGAACCAAG
	Reverse	GCATTAAACTTGGTGAAGCCC
Tbp	Forward	AAGAAAGGGAGAATCATGGACC
	Reverse	GAGTAAGTCCTGTGCCGTAAG
Dmd exon 20-21	Forward	AGATGACAACTACTGCCGAA
	Reverse	GAAGAGCTGACAATCTGTTGAC
	Probe	AGTCTACCACCCTATCAGAGCCAACA
Dmd exon 23-24	Forward	GAAACTTTCCTCCCAGTTGGT
	Reverse	CAGGCCATTCCTCTTTCAGG
	Probe	TCAACTTCAGCCATCCATTTCTGTAAGGT

5.2.5 Western blotting

Protein was extracted using RIPA lysis and extraction buffer (Pierce, ThermoFisher Scientific), supplemented with 5% SDS, 1% protease inhibitors (Sigma-Aldrich, Dorset, UK) and 1% phosphatase inhibitors (Sigma-Aldrich). Samples were size separate and probed for dystrophin and vinculin as detailed in **Chapter 2.5**.

5.2.6 Cell culture

C2C12 myoblasts were seeded into 24-well or 6-well plates at 40,000 cells or 160,000 cells per well, respectively. Two days after seeding, a subset of the cells was collected for RNA and protein (at GM, *n*=3). Supernatant was also collected, whereby liquid was centrifuged at 4°C for 5 minutes at 2,000 × *g* and passed through a 0.22 µm filter, before storing at -80°C. The remaining wells were treated with RNA interference targeting the *Dmd* gene or a non-targeting siRNA at a concentration of 100 nM per well (ON-TARGET *plus* siRNA; Dharmacon, Cambridge, UK). Cells were transfected twice with siRNA in a reduced serum medium (Opti-MEM; Life Technologies) at a ratio of 1:5 Optimem:DM with two days' rest in between transfections. On the day of the second transfection, supernatant was collected for both conditions (Day 3: D3, *n*=3 per group). 6 days after differentiation, supernatant and cells were collected (D6, *n*=3 per group).

5.2.7 Statistical analysis

FirePlex data were processed and normalised using the Firefly Analysis Workbench v2.0.91 (AbCam). TMeV was used to perform Student's *t*-test and one-way ANOVA analyses, and for heatmap visualisation. PCA was performed in R using the 'prcomp' function. The following additional analyses were performed in GraphPad Prism 7 (GraphPad Software Inc, La Jolla, CA); Student's *t*-test, one-way ANOVA, Pearson/Spearman correlation analysis, receiver operating characteristic (ROC) analysis and cumulative distribution function (CDF) analysis. Typically, one-way ANOVA with Tukey *post hoc* test was used for comparisons between 3 groups or more. For experiments with larger sample sizes (n>10) normality was tested using the Shapiro-Wilk test and the non-parametric Kruskal-Wallis one-way ANOVA with Dunn's post *hoc test* utilised if data were found to not be normally distributed. For correlation analyses, normality was tested using the Shapiro-Wilk test and then Pearson or Spearman correlations performed as appropriate.

5.3 Results

5.3.1 Ex-miRNA abundance is not elevated in heterozygote *mdx* mice

To determine the correlation between skeletal muscle dystrophin protein and ex-myomiR abundance, an appropriate mouse model needed to be established. It has previously been reported that female carriers of DMD mutations exhibit elevated serum levels of the myomiR, miR-206-3p [623], which suggest that female carrier mice may be a suitable model. Therefore, male C57BL/10 were crossed with female *mdx* mice to generate a female heterozygous progeny, that have one functional copy of the *DMD* gene. Serum and tissues were collected from 8 week female heterozygous *mdx* mice and age- and sex-matched C57BL/10 and homozygote *mdx* (n=4 per group). Ex-miRNA abundance was determined by RT-qPCR for miR-1a-3p, miR-133a-3p, miR-206-3p and miR-483-3p. Statistical analysis showed that miR-133a-3p, miR-206-3p and miR-483-3p were significantly upregulated in the *mdx* mouse compared to the WT controls (P<0.05, **Figure 5.2A**). Interestingly, heterozygote ex-miRNA levels are not different from the C57BL/10, and abundance was significantly lower compared to the *mdx*. Given these results, dystrophin protein levels were assessed in the TA muscle of heterozygote *mdx* mice and was determined at 89% of WT (**Figure 5.2B**). TA muscles from C57BL/10, *mdx* heterozygotes and *mdx* homozygotes were then sectioned in both transverse and longitudinal orientations. As expected, the *mdx* homozygote myofibres were almost completely devoid of any dystrophin (**Figure 5.2C**). Interestingly, the *mdx* heterozygote myofibres were almost entirely dystrophin positive, although the intensity of the dystrophin staining was slightly less intense than for the WT C57BL/10 controls (see arrowheads in **Figure 5.2C**). The results illustrate that heterozygote *mdx* mice at this age are not likely to be useful to investigate the relationship between low/intermediate levels of dystrophin and ex-miRNA abundance.

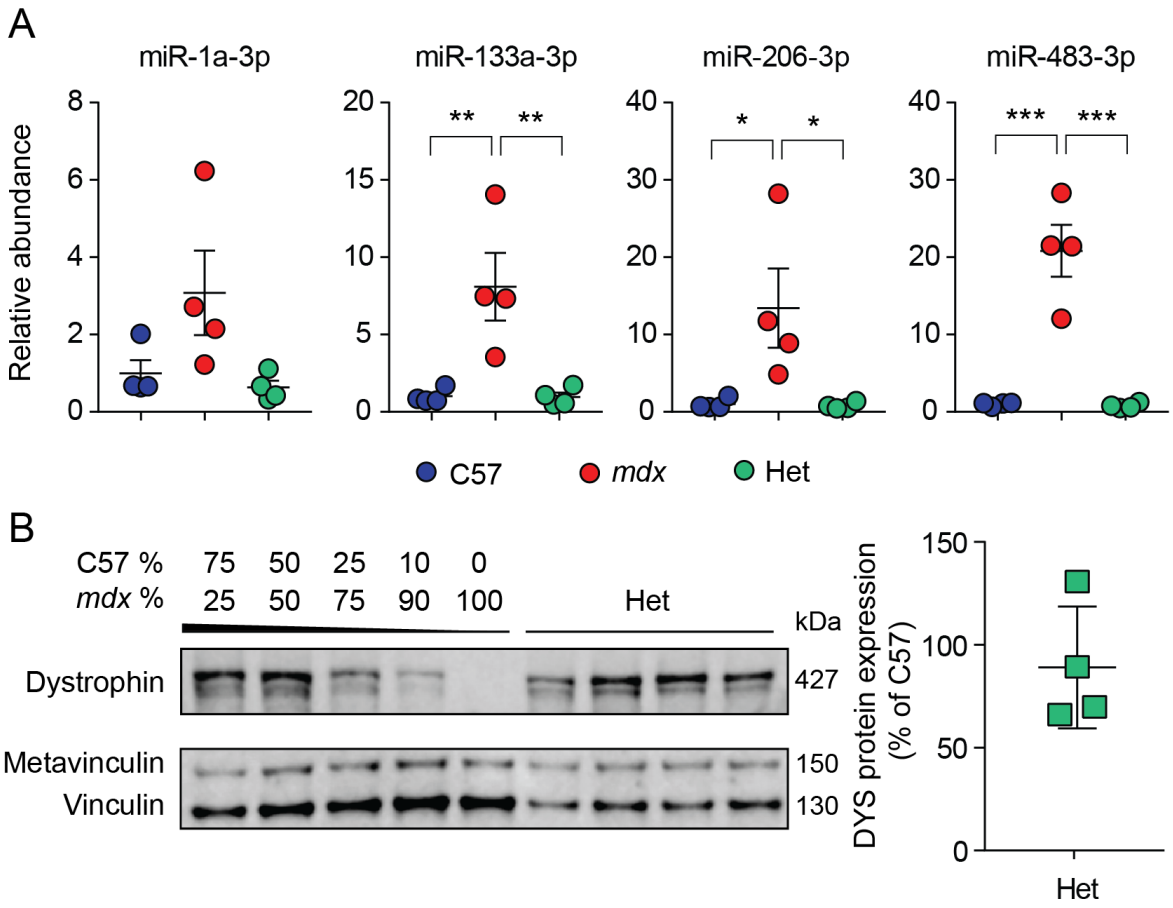
A
miR-1a-3p
miR-133a-3p
miR-206-3p
miR-483-3p
Relative abundance
C57
mdx
Het
B
C57 %
mdx %
75 50 25 10 0
25 50 75 90 100
Het
kDa
Dystrophin
427
Metavinculin
Vinculin
150
130
DYS protein expression (% of C57)
Het
C
Transverse
Longitudinal
Dystrophin
Laminin
C57
mdx
Het

Figure 5.2 Serum miRNA levels and dystrophin expression in *mdx* heterozygote animals.
A Ex-miRNA abundance in serum of C57BL/10, *mdx*, and *mdx* heterozygote (Het) animals (all 8 week old females, *n*=4 per group) was determined by small RNA TaqMan RT-qPCR. qPCR data were normalised to a synthetic spike-in control oligonucleotide (cel-miR-39). **B** Western blot analysis of dystrophin protein expression in TA muscle from C57BL/10, *mdx* and *mdx* heterozygotes. Dystrophin protein was normalised to vinculin expression. A standard curve, consisting of mixtures of C57BL/10 and mdx protein lysates in ratios as indicated, was used to quantify dystrophin protein expression in the *mdx* heterozygotes. **C** Representative immunofluorescence staining of dystrophin protein in transverse and longitudinal TA sections for C57BL/10, *mdx* and *mdx* heterozygote animals. Sections were co-stained with laminin to label myofibres. Arrow heads indicate myofibres with weaker dystrophin staining. All values are mean ± SEM, * $P<0.05$, one-way ANOVA with Tukey *post hoc* test. Scale bars represent 100 µm.

5.3.2 Skewed X-chromosome inactivation induces variable skeletal muscle dystrophin protein levels in *mdx* mice

Given that the heterozygous *mdx* mice expressed high levels of dystrophin protein levels, it was important to explore other genetic models with reduced dystrophin levels that are more likely achieved with currently developing therapeutic interventions (<50% of WT). The *Xist*$^{\Delta hs}$ mouse carries a mutation in the promoter of the *Xist* gene (encoding the long non-coding RNA transcript responsible for the initiation of XCI) which leads to skewed XCI [624,625]. Therefore, female *Xist*$^{\Delta hs}$ mice were crossed with male *mdx* to generate a female *mdx-Xist*$^{\Delta hs}$ progeny. The mutation in the *Xist* gene causes a preferential inactivation of the 'healthy' X-chromosome, leading to less than 50% dystrophin production in these animals [625,626], which express varying levels of dystrophin in a random mosaic pattern across myofibres. This model displays large inter-animal variability (ranging between 3-47% protein), although within each animal skeletal muscles express similar levels of dystrophin [626]. Given the range of dystrophin expression levels, these animals were utilised to investigate the relationship between dystrophin protein expression and ex-miRNA abundance. Serum was collected repeatedly over an eleven month period at 4, 8, 12, 16, 20, 24, 28, 32, 40 and 48 weeks of age by non-terminal tail vain collections (**Figure 5.3**). Serum from age- and sex-matched C57BL/10, *Xist*$^{\Delta hs}$ and *mdx* mice was collected in parallel. At 78 weeks of age mice were sacrificed, after which dystrophin protein expression was determined in the quadriceps femoris muscles by Western blot as described in [622], and each *mdx-Xist*$^{\Delta hs}$ mouse was retrospectively assigned to low (8.4-12.9%), medium (18.8-21%), or high (32.4-43.5%) dystrophin-expressing groups (*n*=5 per group).

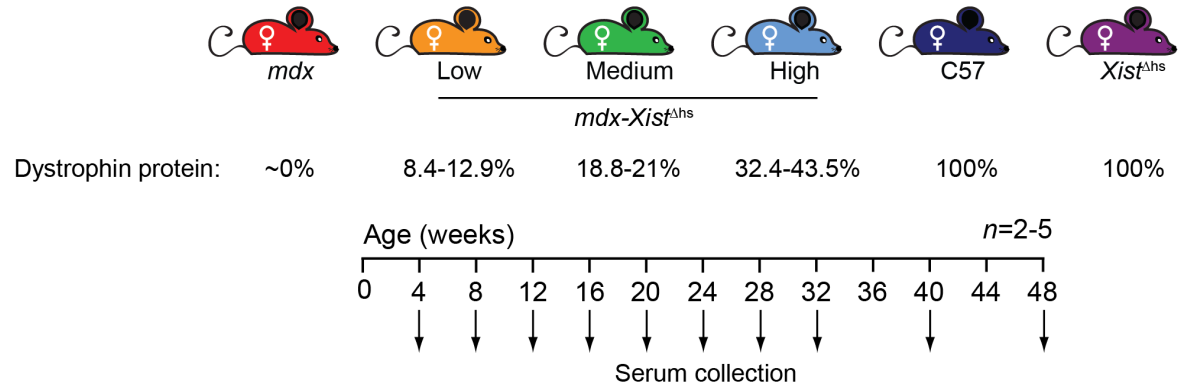

Figure 5.3 Experimental design of longitudinal miRNA profiling study.
Male *mdx* and female *Xist*$^{\Delta hs}$ mice were bred and the female mice from the F1 generation (*mdx-Xist*$^{\Delta hs}$) mice were assigned to low, medium and high dystrophin expression groups based on dystrophin Western blot analysis of quadriceps femoris muscle lysates. Serum for miRNA analysis was collected via the tail vein for all *mdx-Xist*$^{\Delta hs}$ mice at the ages as indicated (4-48 weeks of age). C57BL/10, *Xist*$^{\Delta hs}$ and *mdx* serum samples were collected in parallel. All samples were female, *n*=5 measurements for each group at each age in the majority of cases (range = 2-5).

5.3.3 Identification of novel candidate biomarkers by serum miRNA profiling

To date, several miRNAs have been identified that are upregulated in animal models and/or in patients and the myomiRs specifically have been considered most promising in terms of biomarker potential [485,487]. However, serum abundance levels of these miRNAs decrease over time, which would make it hard to distinguish whether the downregulation is the result of an effective treatment or due to natural pathological progression. Therefore, there is a need to discover novel DMD-related miRNAs. One class of miRNAs with potential are cardiac-related miRNAs (cardiomiRs). Given that cardiomyopathy develops later in the disease, cardiac miRNAs might be expected to exhibit an increase with pathological progression (or at least not decline with age).

For this purpose, serum miRNA profiling was first performed in a selected subset of serum from female C57BL/10 and *mdx* mice (at 12, 24 and 48 weeks, *n*=4 per group). The three ages were selected to represent the progression of dystrophic pathology and cardiomyopathic features observed in the *mdx* mouse, as discussed previously (**Chapter 1.1.4**; i.e. cardiac fibrosis has been reported in the *mdx* mouse at 24 weeks and multiple aberrant cardiac functional parameters by 36 weeks of age

[81,627]). The novel multiplexing FirePlex miRNA assay system was utilised to detect miRNA abundance. This technique uses hydrogel-based particles to measure the abundance of multiple miRNAs directly in serum, without the need for RNA extraction. A custom-designed FirePlex panel of 68 miRNA probes included (I) miRNAs that the Wood lab and others have previously identified as elevated in dystrophic serum [463,478,479,487,578,628] (II) cardiac process-associated miRNAs and (III) putative normalisation/quality controls. A list of all miRNAs measured can be found in **Appendix 8.2**.

Differentially abundant miRNAs (P<0.05) were identified by Student's *t*-test and visualised by heatmaps (**Figure 5.4A**) and volcano plots (**Figure 5.4B**) for each age group. Of those miRNAs that were differentially abundant, the majority were found to be increased in *mdx* serum relative to C57BL/10 controls. Additionally, the highest number of differentially abundant miRNAs were identified at 12 weeks of age, but not all 12 of these miRNAs were differentially increased at all time points. Seven miRNAs were consistently upregulated in *mdx* serum at all three time points (miR-1a-3p, miR-193b-3p, miR-22-3p, miR-30a-5p, miR-370-3p, miR-378a-3p, miR-483-3p; **Figure 5.4C**). Notably, except for miR-1a-3p, the myomiRs (miR-133a/b-3p, miR-206-3p) were only significantly upregulated (P<0.05) at the earlier two time points and did not reach statistical significance at 48 weeks of age, likely as a consequence of the high variability between replicates at these time points. 14 miRNAs were differentially abundant at two or more time points, of which 12 were selected for further analysis in all longitudinal samples (**Appendix 8.3**).

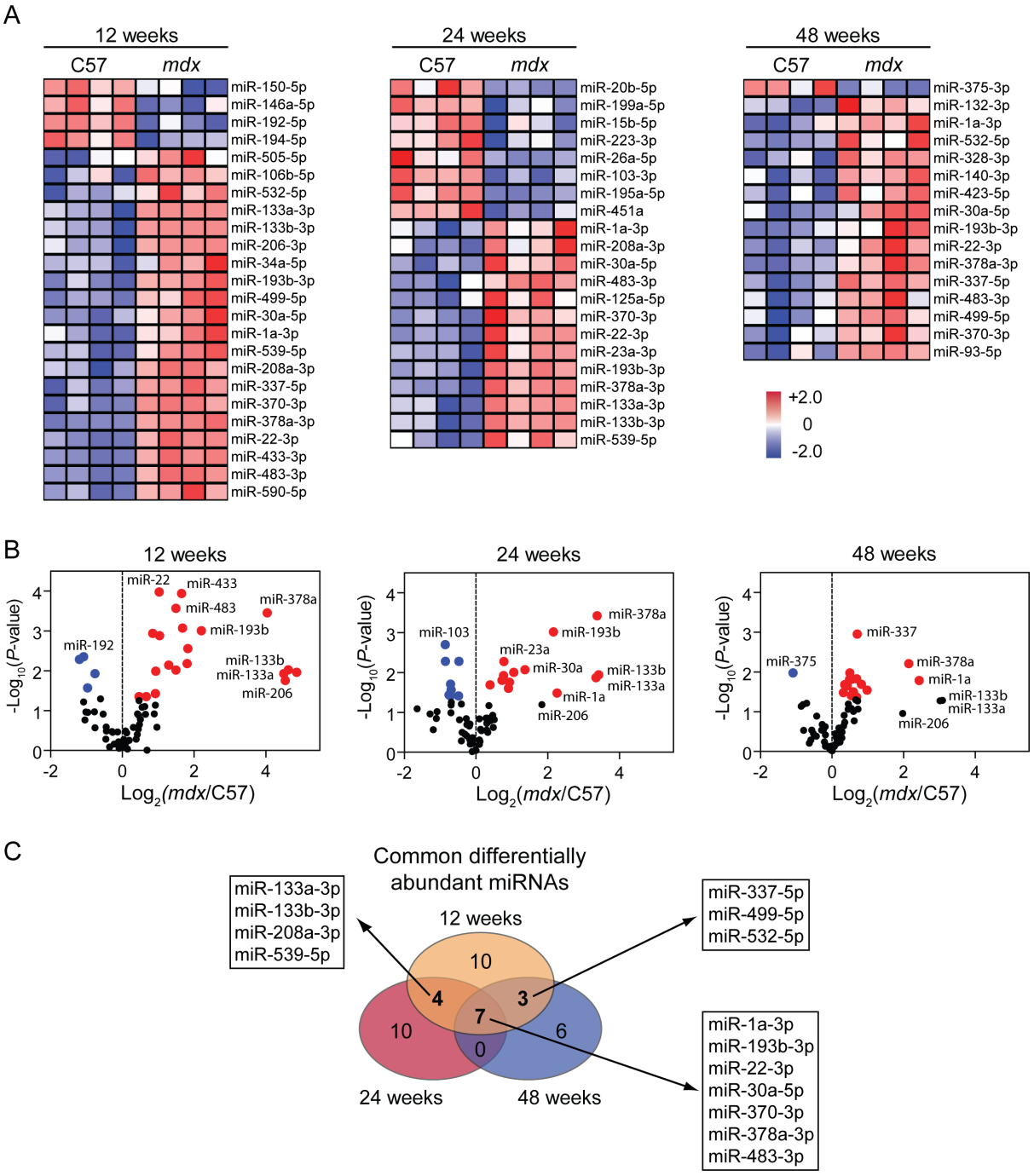

Figure 5.4 Screen for differentially abundant ex-miRNAs in dystrophic serum.
The serum of female C57BL/10 and *mdx* mice was analysed with a custom miRNA panel (68 miRNAs) using the FirePlex methodology at three ages (12, 24 and 48 weeks, *n*=4 per group). FirePlex miRNA data were normalised to the geometric average of miR-16-5p, miR-17-5p and miR-92a-3p. Differentially abundant miRNAs ($P<0.05$, Student's *t*-test) were visualised by **A** heatmap and **B** volcano plot. The scale bar for the heatmap represents row Z-scores with red and blue indicating higher and lower than mean abundance respectively. Statistically significant *mdx* vs C57BL/10 changes are highlighted in red and blue (for elevated and lowered miRNAs respectively) on the volcano plots. **C** Venn diagram illustrating the common differentially abundant miRNAs between the different ages.

5.3.4 Longitudinal analysis of serum miRNAs in *mdx* mice expressing varying levels of dystrophin protein

A second FirePlex profiling analysis was performed in all remaining samples (*i.e.* female Low, Medium and High dystrophin-expressing *mdx-Xist*$^{\Delta hs}$ mice, *mdx*, C57BL/10 and Xist$^{\Delta hs}$ at ages 4-48 weeks, *N*=291) using the more focused miRNA panel described in **Appendix 8.3**. The data collected was combined with the data obtained from the initial screening to generate a complete dataset for all 17 miRNAs at each age. Variation in non-normalised reference miRNA abundance was minimal between experimental groups (**Figure 5.5A** and **B**). Correlation analysis of non-normalised, background subtracted signal intensities illustrated that the reference miRNAs (normalisers) were positively correlated with one another (Spearman *r* range: 0.64 to 0.8, *P*=0), but not with the myomiRs (Spearman *r* range: -0.1 to 0.06, not significant) (**Figure 5.5D**), consistent with a robust normalisation strategy.

miRNA RFU values were subsequently normalised to the geometric average of miR-16-5p, miR-17-5p and miR-92a-3p. As haemolysis has the potential to confound ex-miRNA biomarker analysis, the ratio between the erythrocyte-enriched miRNA miR-451a and the normalisers was analysed, whereby a ratio of <5 is indicative of low haemolysis [629]. The analysed samples exhibited low ratio levels (ratio: 0.29-2.39), which were consistent between samples (**Figure 5.5C**) and were correlated with abundance of the normaliser control miRNAs (Spearman *r* range: 0.49 to 0.8, *P*=0, **Figure 5.5D**). This suggests that their levels reflect global miRNA abundance in these samples and thus confirming that none of the samples were compromised by haemolysis.

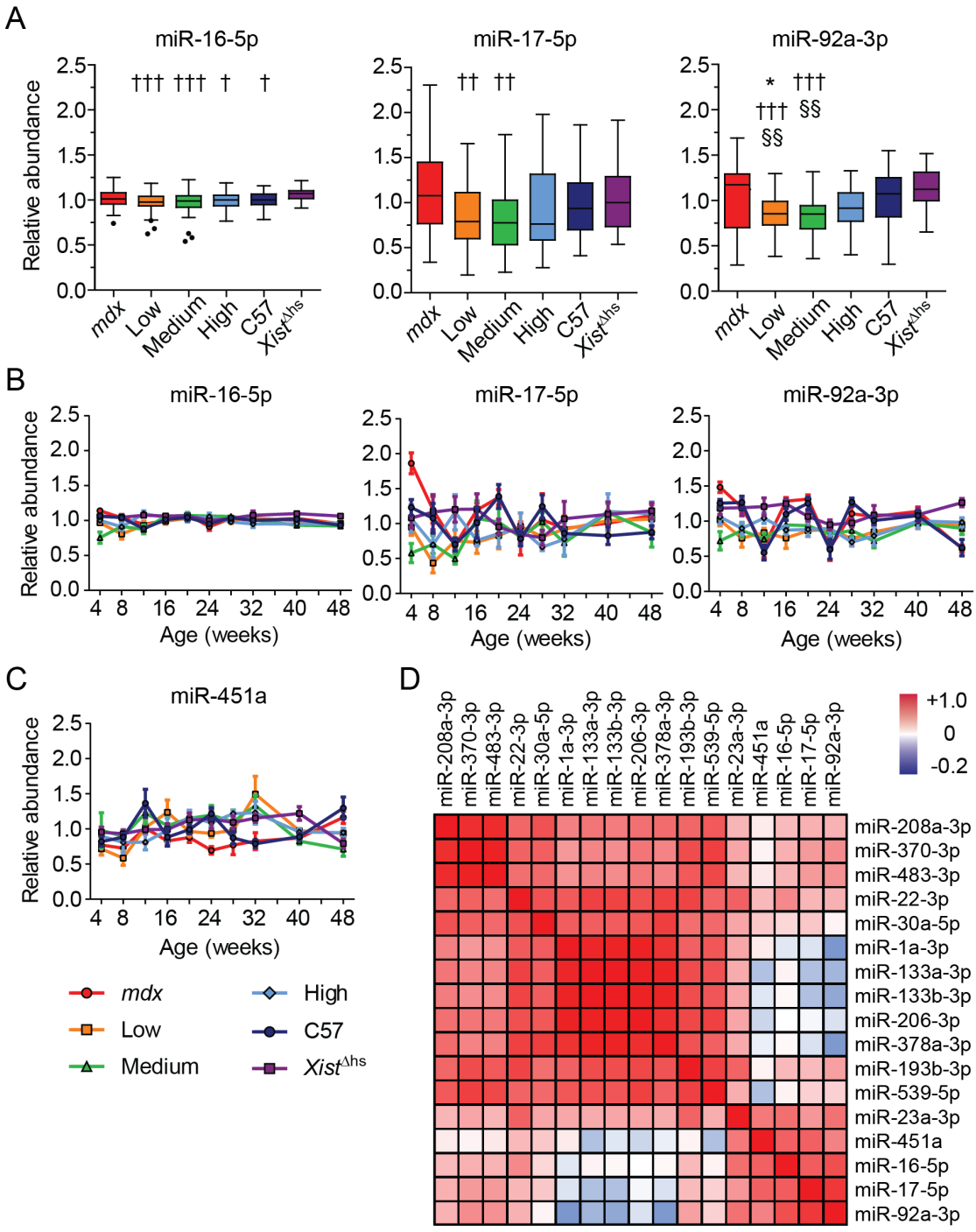

Figure 5.5 Serum miRNA screening quality control analyses.
The miRNAs miR-16-5p, miR-17-5p and miR-92a-3p were selected as normalisers for the FirePlex data based on their stable abundance (determined using geNorm method). Non-normalised, background-subtracted serum levels are shown by **A** Tukey box plots of all measurements pooled for each mouse strain ($n \geq 46$ measurements, range = 46-50), and **B** longitudinal time course plots of the mean for every group at each age. * $P<0.05$ for comparisons to the C57 group. † $P<0.05$, †† $P<0.01$, ††† $P<0.001$ for comparisons to the *Xist*$^{\Delta hs}$ group. §§ $P<0.01$ for comparison to the *mdx* group. *P*-values are for one-way ANOVA with Tukey *post hoc* test. **C** Normalised longitudinal serum abundance of miR-451a, an erythrocyte-enriched miRNA used as haemolysis marker. **D** Heatmap of correlation matrix comparing the non-normalised abundance patterns for all 17 miRNAs. Scale bar represents Spearman's *r* correlation coefficients. Values in **B** and **C** are mean ± SEM, n=5 in most cases.

Samples were subsequently visualised in a heatmap, where a clear difference was observed between the non-dystrophic controls and the dystrophin-deficient strains (**Figure 5.6A**). Hierarchical clustering revealed several clusters of miRNAs: (I) the classical myomiRs (miR-1a-3p, miR-133a/b-3p and miR-206-3p) and miR-378a-3p, which were significantly increased in all the *mdx* strains; (II) the novel myomiR miR-483-3p, miR-193b-3p and the putative cardiomiRs (miR370-3p, miR-208a-3p and miR-539-5p); (III) other putative miRNA biomarkers (miR-22-3p and miR-30a-5p) which were elevated in the *mdx* strains, but exhibited a less clearly defined expression pattern; (IV) normalisation and haemolysis-associated miRNAs. PCA primarily exhibited that samples clustered according to WT (C57BL/10 and *Xist*$^{\Delta hs}$) or dystrophin-deficient (*mdx* and *mdx-Xist*$^{\Delta hs}$) groups (**Figure 5.6B**). In addition, the C57 and *Xist*$^{\Delta hs}$ controls clustered together and samples from *mdx* and *mdx-Xist*$^{\Delta hs}$ mice were mostly intermingled. Conversely, there was no obvious age-associated sample separation apparent from the PCA plot (**Figure 5.6C**).

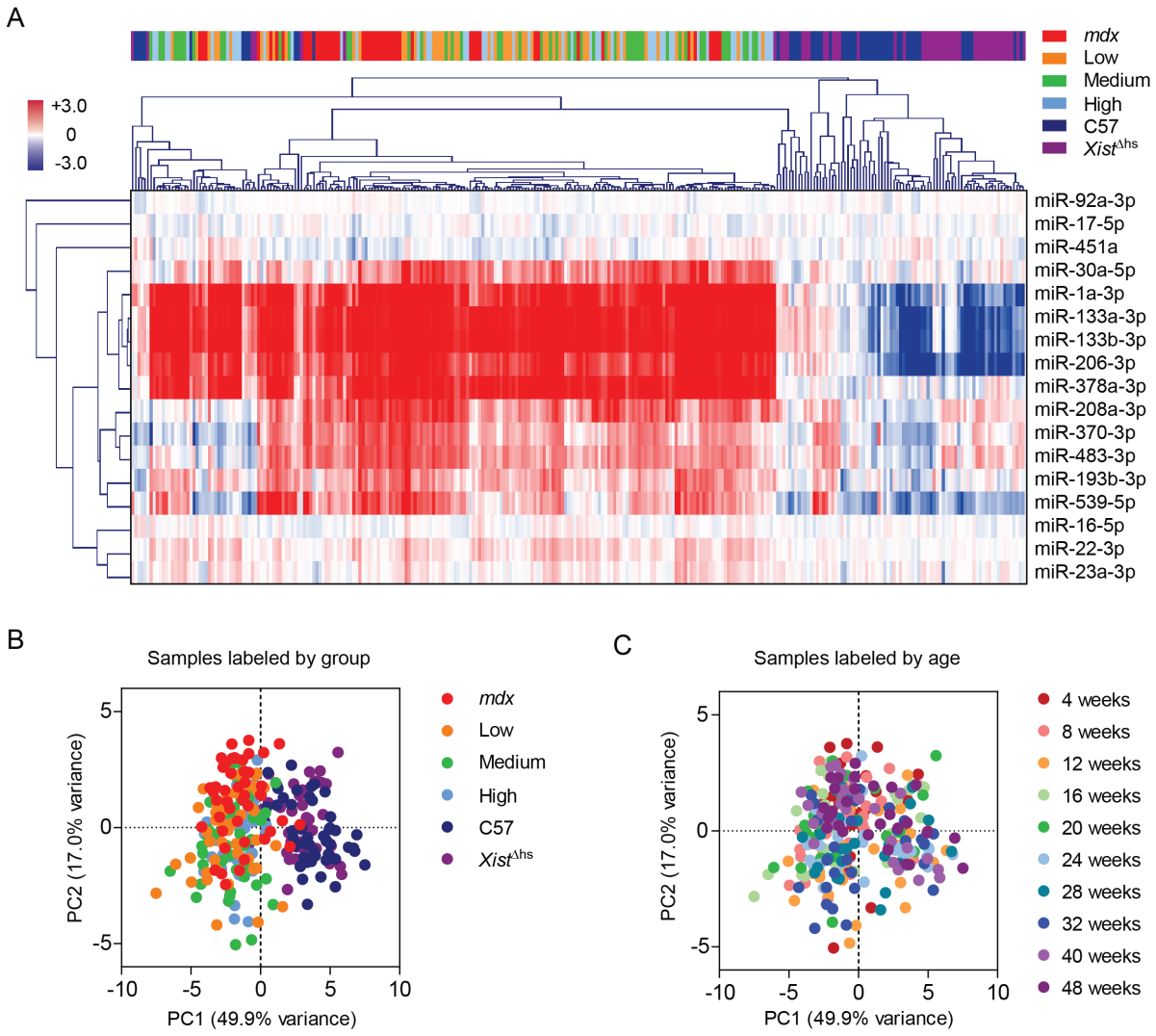

Figure 5.6 Longitudinal analysis of serum miRNA levels in mice expressing various levels of dystrophin protein.

A Heatmap showing hierarchical clustering of serum miRNA abundance data in all samples. The scale bar represents row Z-scores with red and blue indicating higher and lower than mean abundance respectively. PCA of serum miRNA abundance data was performed and samples clustered accordingly. The resulting PCA plot was labelled according to either **B** strain, or **C** age.

Data for each individual miRNA were then considered separately and visualised by **A** box plots of miRNA abundance ratios aggregated over all ages, **B** CDF plots, **C** ROC plots to assess the potential of each putative miRNA biomarker to discriminate test groups from the C57 control, and **D** a longitudinal time course plot of miRNA abundance ratios separated by mouse strain. All miRNAs measured are differentially expressed in the *mdx* mouse relative to the WT controls.

The myomiRs (miR-1a-3p, miR-133a-3p, and miR-206-3p) (**Figure 5.7**) are the most commonly reported, and arguably the most promising, DMD miRNA biomarkers [477]. The FirePlex data showed a significant increase in serum abundance of the myomiRs in all dystrophin-deficient strains, which exhibited a tendency to decline towards WT levels at the later ages (**Figure 5.7A**, and **D**). Interestingly, the box plots and CDFs illustrated a clear difference between the WT control strains and the dystrophin-deficient strains, but there was no distinction between *mdx* mice and the three *mdx-Xist*$^{\Delta hs}$ groups expressing varying levels of dystrophin (**Figure 5.7A**, and **B**). These results were surprising given previous reports from the Bozzoni group, and the Wood and Smith labs of serum miRNA normalisation following partial dystrophin restoration [463,478], and the observation that BMD patients have been reported to exhibit intermediate serum myomiR levels between those of DMD patients and healthy controls [478,481,485]. ROC curve analysis for the myomiRs showed near perfect discrimination between dystrophic and WT animals (**Figure 5.7C**). Area Under the Curve (AUC) values for all ROC curve analyses are provided in **Figure 5.8**.

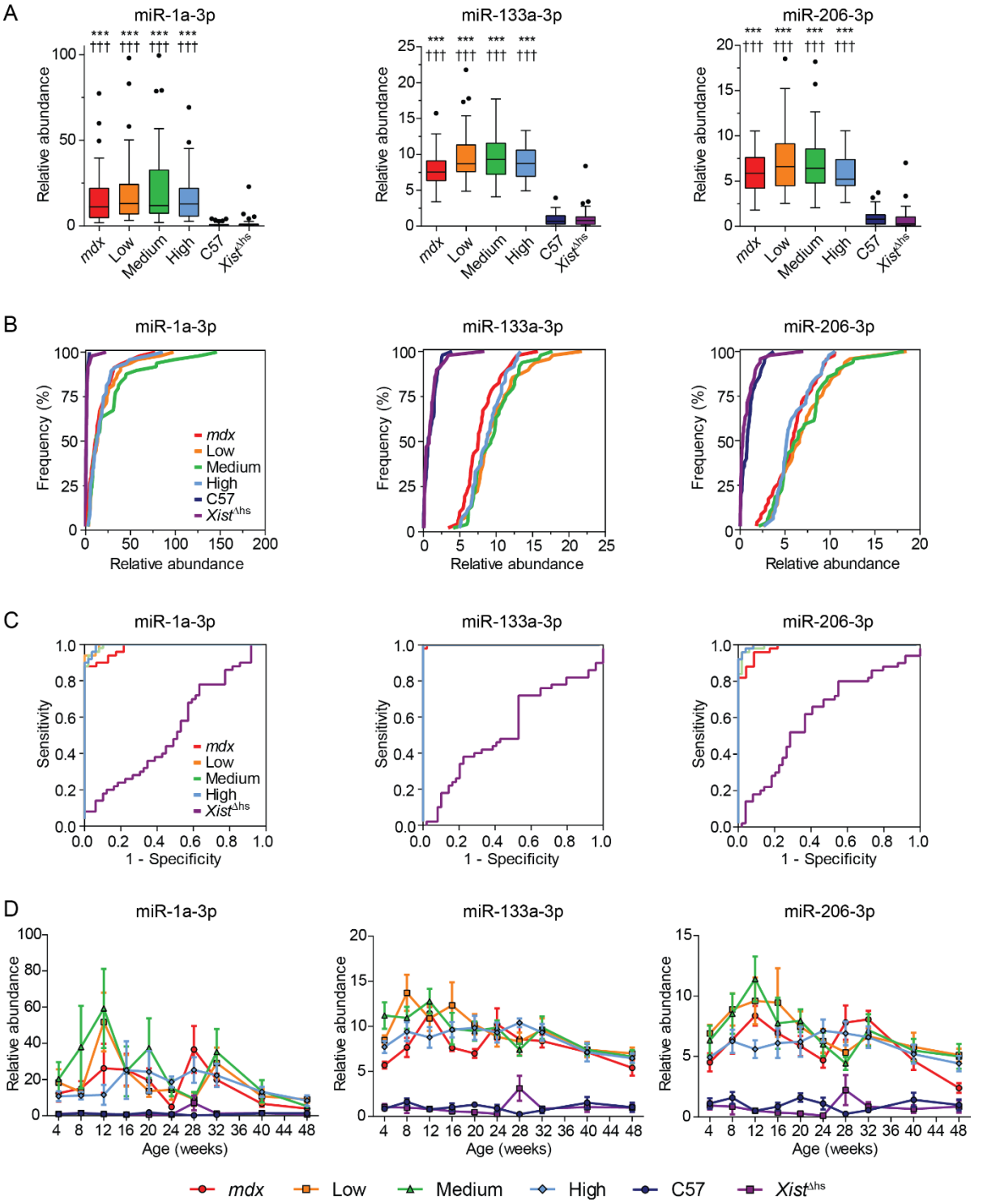
A
miR-1a-3p
miR-133a-3p
miR-206-3p
Relative abundance
mdx
Low
Medium
High
C57
Xist^Δhs
B
Frequency (%)
Relative abundance
C
Sensitivity
1 - Specificity
D
Age (weeks)

Figure 5.7 Serum myomiRs are elevated irrespective of dystrophin protein levels in *mdx-Xist*$^{\Delta hs}$ mice.

Serum miRNA abundance data for selected individual miRNAs (miR-1a-3p, miR-133a-3p and miR-206-3p) measured using the FirePlex methodology. Data are shown as **A** Tukey box plots of all measurements pooled for each mouse strain ($n \geq 46$ measurements, range = 46-50), **B** CDF comparing experimental groups, **C** ROC curves to assess the potential of each miRNA to distinguish experimental groups from the C57BL/10 controls, and **D** time course plots of the mean for every group at each age over the full 4-48 week time period (n=2-5 per group). FirePlex miRNA data were normalised to the geometric average of miR-16-5p, miR-17-5p and miR-92a-3p. Values in **A** and **D** are mean ± SEM. *** P<0.001 for comparison to C57BL/10 group. ††† P<0.001 for comparison to the *Xist*$^{\Delta hs}$ group. P-values are for Kruskal-Wallis one-way ANOVA with Dunn's *post hoc* test.

	AUC				
	mdx	Low	Medium	High	*Xist*$^{\Delta hs}$
miR-1a-3p	0.97	0.99	0.98	0.98	0.55
miR-133a-3p	1.00	1.00	1.00	1.00	0.51
miR-133b-3p	1.00	1.00	1.00	1.00	0.50
miR-206a-3p	0.97	0.99	0.98	0.98	0.60
miR-193b-3p	0.82	0.81	0.80	0.77	0.59
miR-22-3p	0.84	0.85	0.82	0.85	0.61
miR-30a-5p	0.90	0.89	0.85	0.89	0.68
miR-378a-3p	1.00	1.00	1.00	1.00	0.57
miR-483-3p	0.89	0.86	0.80	0.82	0.71
miR-208a-3p	0.91	0.90	0.82	0.88	0.77
miR-370-3p	0.84	0.79	0.71	0.75	0.63
miR-539-5p	0.89	0.83	0.82	0.83	0.58

Figure 5.8 Area under the curve (AUC) values from the ROC curve analysis.

ROC analysis was performed, which assesses the potential of each putative miRNA biomarker to discriminate test groups from the C57BL/10 control. AUC values indicate the extent of similarities with higher values representing a higher ability to discriminate between groups.

In contrast to the myomiRs, serum abundance of miR-193b-3p, miR-370-3p and miR-483-3p was found to be inversely related to the level of muscle dystrophin expression in the *mdx-Xist*$^{\Delta hs}$ mice (**Figure 5.9A**, and **B**). These three miRNAs are significantly elevated in dystrophin-deficient strains compared to WT controls, although the magnitude of the difference observed was less than for the myomiRs (**Figure 5.9A**, and **D**). ROC curve analysis showed that these miRNAs exhibited reduced power to discriminate between healthy and affected mice relative to the myomiR group, described above (**Figures 5.9C** and **5.8C**).

The miRNAs miR-208a-3p, miR-378a-3p and miR-539-5p were also differentially elevated in dystrophic samples compared to WTs, but were highly variable over time (**Figure 5.10A**, and **D**). Generally, these miRNAs did not exhibit the same gradation effect with dystrophin expression as observed in **Figure 5.9,** with the exception of miR-539-5p. ROC curve analysis showed that miR-378a-3p exhibits near perfect discrimination between dystrophic and WT samples, but, as with the myomiRs, no correlation with dystrophin expression was observed in the *mdx-Xist*$^{\Delta hs}$. In contrast, the cardiomiR, miR-208a-3p, exhibited a lower capacity for distinguishing between healthy and affected mice, and minor but significant differences can be observed between the C57LB/10 and *Xist*$^{\Delta hs}$ control strains. These two characteristics make this miRNA less attractive for potential biomarker purposes, despite its cardiac specificity.

The remaining miRNAs measured were miR-133b-3p, miR-22-3p and miR-30a-5p (**Figure 5.11**). miR-133a and miR-133b are highly similar in sequence and only differ by one base pair on the 3' end (miR-133a-3p: 5'-UUUGGUCCCCUUCAACCAGCUG-3'; and miR-133b-3p: 5'-UUUGGUCCCCUUCAACCAGCUA-3') [630]. miR-22-3p shows low relative abundance differences between the *mdx* groups and controls. miR-30a-5p is differentially expressed between the WT controls and the dystrophin-deficient groups, but the CDF and ROC plots are not as pronounced as for the myomiRs and this miRNA also shows no gradation. These characteristics make these miRNAs less interesting for further analysis.

Generally, no miRNAs were observed to be positively correlated with disease progression. Instead there appeared to be a global decrease in ex-miRNA abundance with age. This is potentially due to the relatively mild pathology in the *mdx* model and/or the accumulation of fibrotic tissue in dystrophic muscle which may exert global inhibitory effects on the miRNA secretome. Unexpectedly, the results have also shown that the myomiRs are not inversely related with dystrophin protein levels in the *mdx-Xist*$^{\Delta hs}$ mouse, whereas other miRNAs are. This suggests that the relationship between

dystrophin protein expression and serum miRNA abundance is miRNA specific and highlights the complexity of the miRNA secretome in dystrophin-deficient animals.

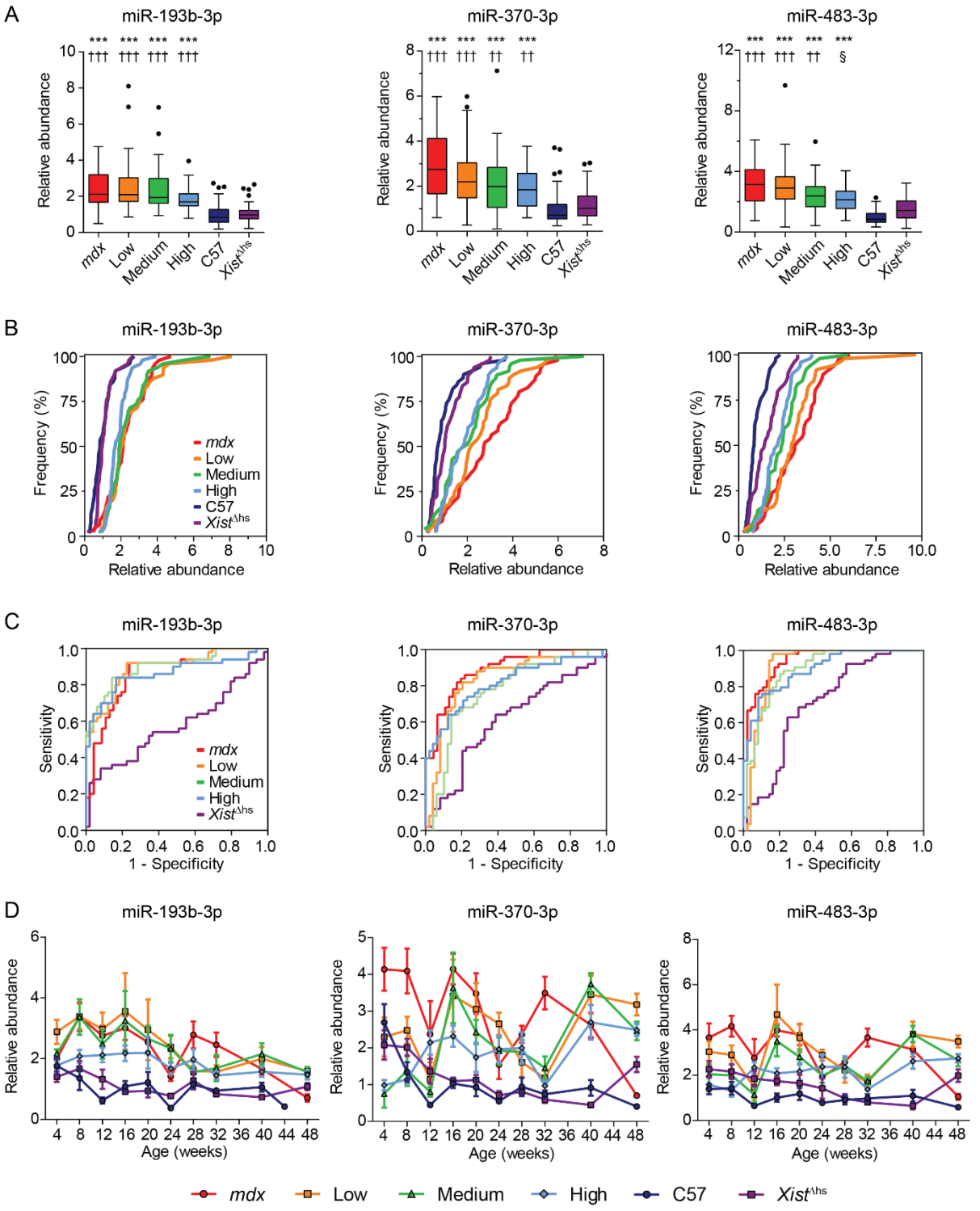

Figure 5.9 Dystrophin-dependent reductions in serum levels of miR-193b-3p, miR-370-3p, and miR-483-3p in *mdx-Xist*$^{\Delta hs}$ mice.

Serum miRNA abundance data for selected individual miRNAs (miR-193b-3p, miR-370-3p and miR-483-3p) measured using the FirePlex methodology. Data are shown as **A** Tukey box plots of all measurements pooled for each mouse strain ($n \geq 46$ measurements, range = 46-50), **B** CDF comparing experimental groups, **C** ROC curves to assess the potential of each miRNA to distinguish experimental groups from the C57BL/10 controls, and **D** time course plots of the mean for every group at each age over the full 4-48 week time period (n=2-5 per group). FirePlex miRNA data were normalised to the geometric average of miR-16-5p, miR-17-5p and miR-92a-3p. Values in **A** and **D** are mean ± SEM. *** $P<0.001$ for comparisons to the C57BL/10 group. †† $P<0.01$, ††† $P<0.001$ for comparisons to the *Xist*$^{\Delta hs}$ group. § $P<0.05$ for comparison to the *mdx* group. P-values are for Kruskal-Wallis one-way ANOVA with Dunn's *post hoc* test.

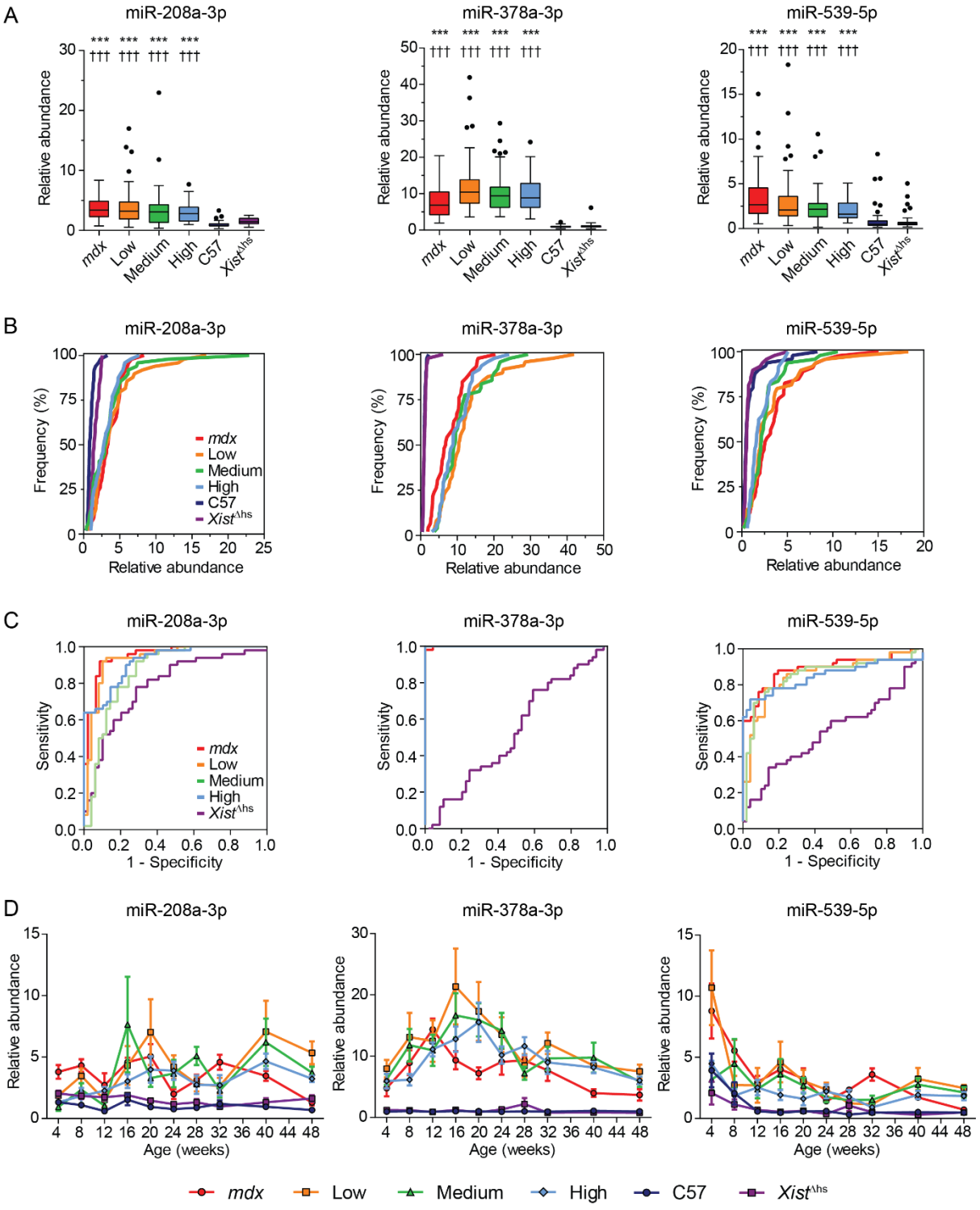
A
miR-208a-3p
miR-378a-3p
miR-539-5p
Relative abundance
mdx
Low
Medium
High
C57
Xist^Δhs
B
Frequency (%)
Relative abundance
C
Sensitivity
1 - Specificity
D
Age (weeks)

Figure 5.10 Analysis of individual serum miRNAs – miR-208-3p, miR-378a-3p and miR-539-5p in *mdx-Xist*$^{\Delta hs}$ mice.

Serum miRNA abundance data for selected individual miRNAs (miR-208a-3p, miR-378-3p and miR-539-5p) measured using the FirePlex methodology. Data are shown as **A** Tukey box plots of all measurements pooled for each mouse strain ($n \geq 46$ measurements, range = 46-50), **B** CDF comparing experimental groups, **C** ROC curves to assess the potential of each miRNA to distinguish experimental groups from the C57BL/10 controls, and **D** time course plots of the mean for every group at each age over the full 4-48 week time period (n=2-5 per group). FirePlex miRNA data were normalised to the geometric average of miR-16-5p, miR-17-5p and miR-92a-3p. Values in **A** and **D** are mean ± SEM. *** $P<0.001$ for comparisons to the C57BL/10 group. ††† $P<0.001$ for comparisons to the *Xist*$^{\Delta hs}$ group. P-values are for Kruskal-Wallis one-way ANOVA with Dunn's *post hoc* test.

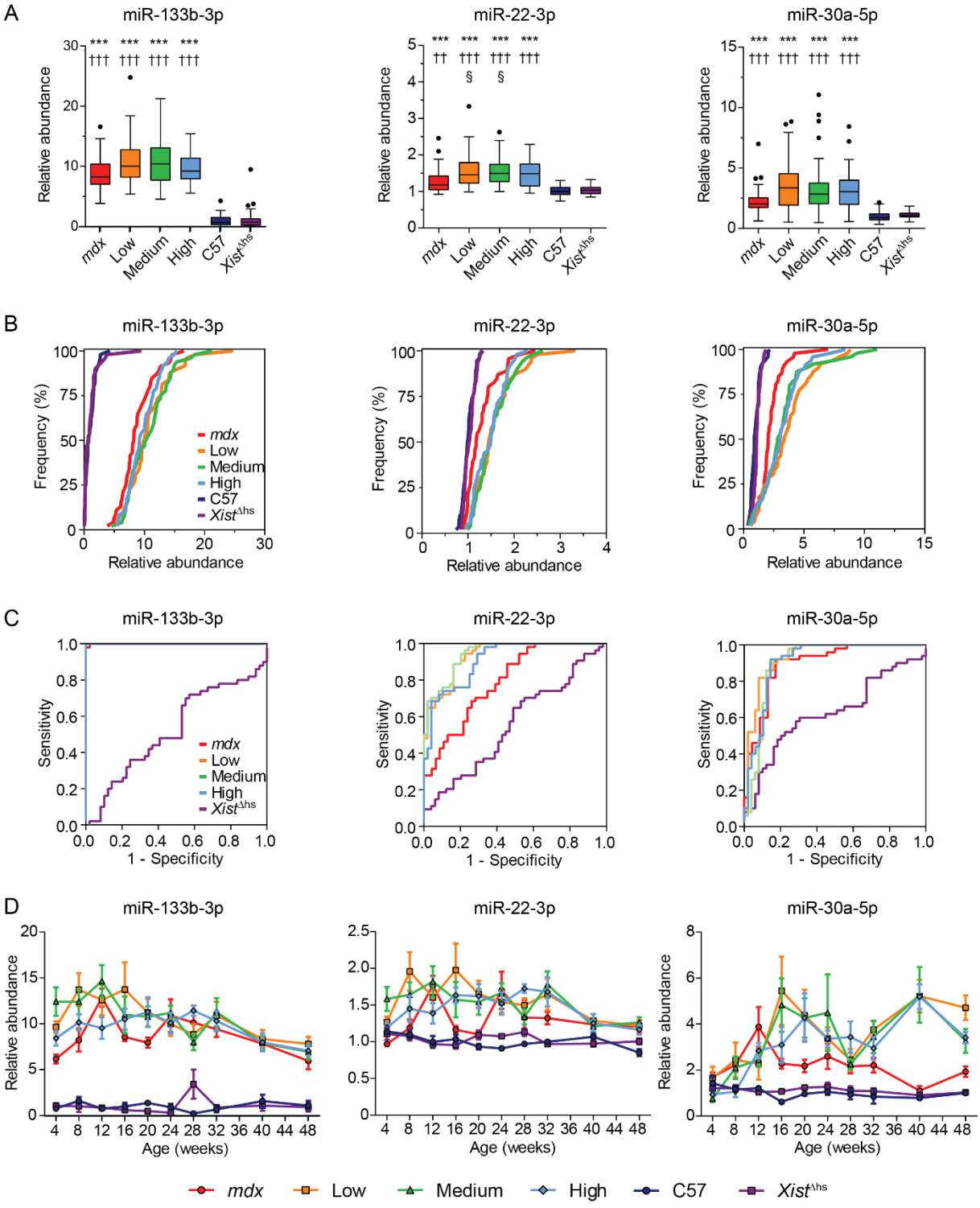
A
miR-133b-3p
miR-22-3p
miR-30a-5p
Relative abundance
mdx
Low
Medium
High
C57
Xist^Δhs
B
Frequency (%)
Relative abundance
C
Sensitivity
1 - Specificity
D
Age (weeks)

Figure 5.11 Analysis of individual serum miRNAs - miR-133b-3p, miR-22-3p and miR-30a-5p in *mdx-Xist*$^{\Delta hs}$ mice.
Serum miRNA abundance data for selected individual miRNAs (miR-1a-3p, miR-133a-3p and miR-206-3p) measured using the FirePlex methodology. Data are shown as **A** Tukey box plots of all measurements pooled for each mouse strain ($n \geq 46$ measurements, range = 46-50), **B** CDF comparing experimental groups, **C** ROC curves to assess the potential of each miRNA to distinguish experimental groups from the C57 controls, and **D** time course plots of the mean for every group at each age over the full 4-48 week time period (n=2-5 per group). FirePlex miRNA data were normalised to the geometric average of miR-16-5p, miR-17-5p and miR-92a-3p. Values in **A** and **D** are mean ± SEM. *** P<0.001 for comparisons to the C57BL/10 group. ††† P<0.001 for comparisons to the *Xist*$^{\Delta hs}$ group. § P<0.05 for comparison to the *mdx* group. P-values are for Kruskal-Wallis one-way ANOVA with Dunn's *post hoc* test.

5.3.4 Orthogonal methodology RT-qPCR exhibits similar miRNA patterns as FirePlex

Key findings from the FirePlex study were validated using an orthogonal methodology. While the totality of the FirePlex data (i.e. aggregated measurements from all time points) clearly showed that there was no dystrophin-dependent effect on the ex-myomiR levels, analysis for some individual time points showed that a dystrophin-dependent relationship was apparent at some time points. These differences may be explained by technical variability inherent in serum miRNA measurement, or by biological variability as serum miRNA abundance is a product of release from the entire musculature (with various muscles contributing to ex-miRNA abundance to different extents, depending on their relative mass and the degree of degenerative and regenerative pathology occurring at a given time) [463]. Therefore, to assess whether these variations were technical or biological, two time points were selected as representatives of dystrophin-dependent (16 weeks) and dystrophin-independent (24 weeks) relationships, and miRNA abundance was measured by RT-qPCR (n=3-5 per group). Small variations between the FirePlex and RT-qPCR method were observed in all miRNAs (**Figures 5.12** and **5.13**). However, these are to be expected, especially given the different data normalisation strategies used for each methodology (i.e. geometric average of stable endogenous miRNAs vs external spike-in control). Upon closer inspection, individual samples were significantly

correlated between the FirePlex and RT-qPCR method for all miRNAs (Spearman *r* range: 0.43 to 0.96, *P*<0.0447). For the *mdx* and *mdx-Xist*$^{\Delta hs}$ groups detection of miR-133a-3p abundance potentially reaches its maximum threshold in the FirePlex analysis, although this seems unlikely given the normal distribution of samples within some of these groups (Medium and High; Shapiro-Wilk normality test not significant). Together, these RT-qPCR data confirm the FirePlex results, and suggest that the observed variation in the dystrophin-dependent alterations in ex-myomiR levels over time is a true reflection of biological differences.

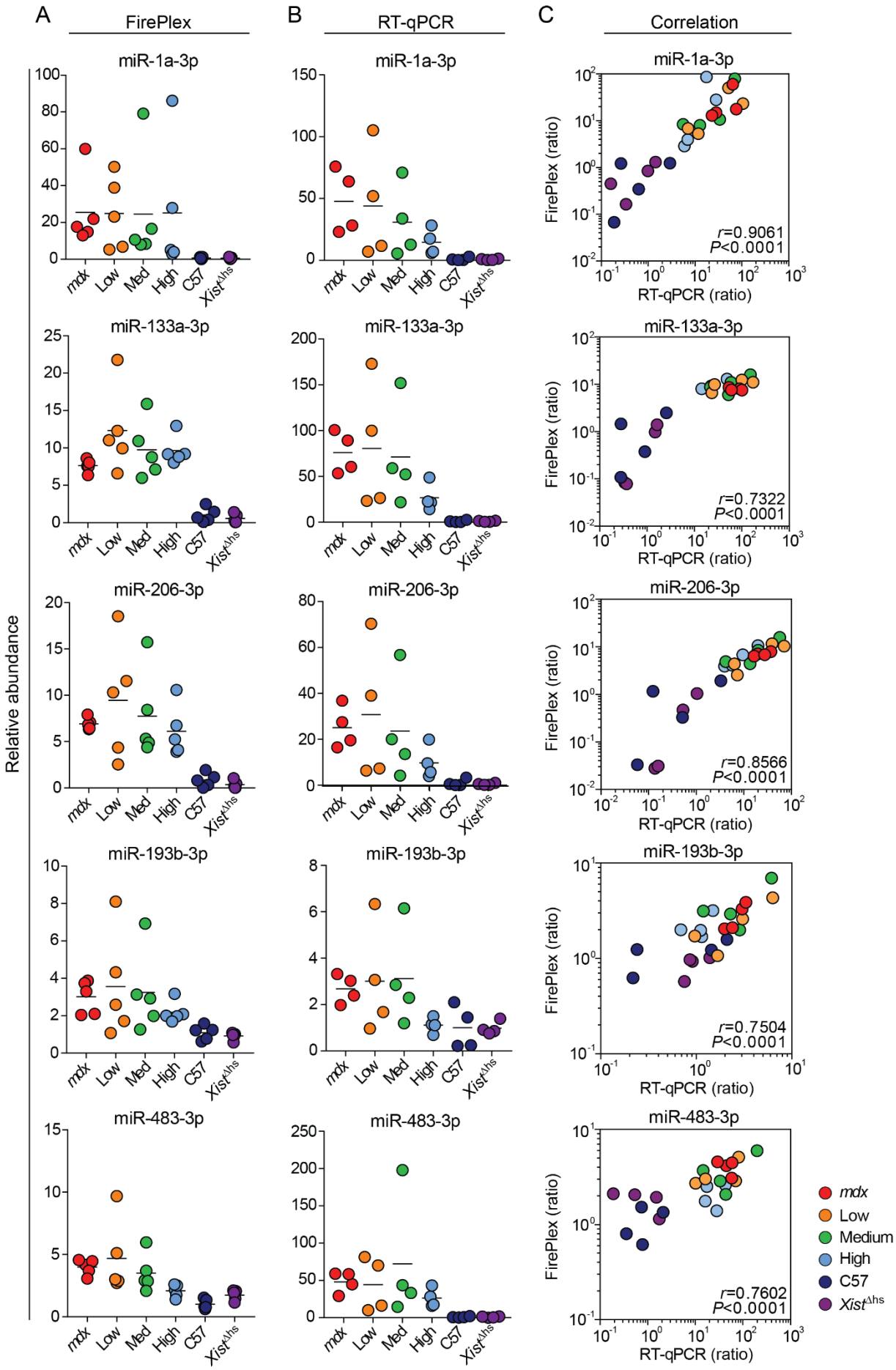
A
FirePlex
B
RT-qPCR
C
Correlation
Relative abundance
miR-1a-3p
miR-133a-3p
miR-206-3p
miR-193b-3p
miR-483-3p
mdx
Low
Med
High
C57
Xist^Δhs
FirePlex (ratio)
RT-qPCR (ratio)
r=0.9061
P<0.0001
r=0.7322
P<0.0001
r=0.8566
P<0.0001
r=0.7504
P<0.0001
r=0.7602
P<0.0001
mdx
Low
Medium
High
C57
Xist^Δhs

Figure 5.12 RT-qPCR validation of serum miRNA abundance at 16 weeks of age.
The 16 week serum samples were reanalysed in order to validate the FirePlex experiment (*n*=4-5 per group). Relative abundance of selected serum miRNAs was visualised for **A** FirePlex data, and **B** orthogonal validation using small RNA TaqMan RT-qPCR. FirePlex data were normalised to the geometric average of miR-16-5p, miR-17-5p and miR-92a-3p. RT-qPCR data were normalised to a synthetic spike-in control oligonucleotide (cel-miR-39). Mean ratios are indicated per group. **C** Data from the two methodologies were plotted against each other. Pearson or Spearman's *r* correlation coefficients and correlation *P*-values are shown on the plots.

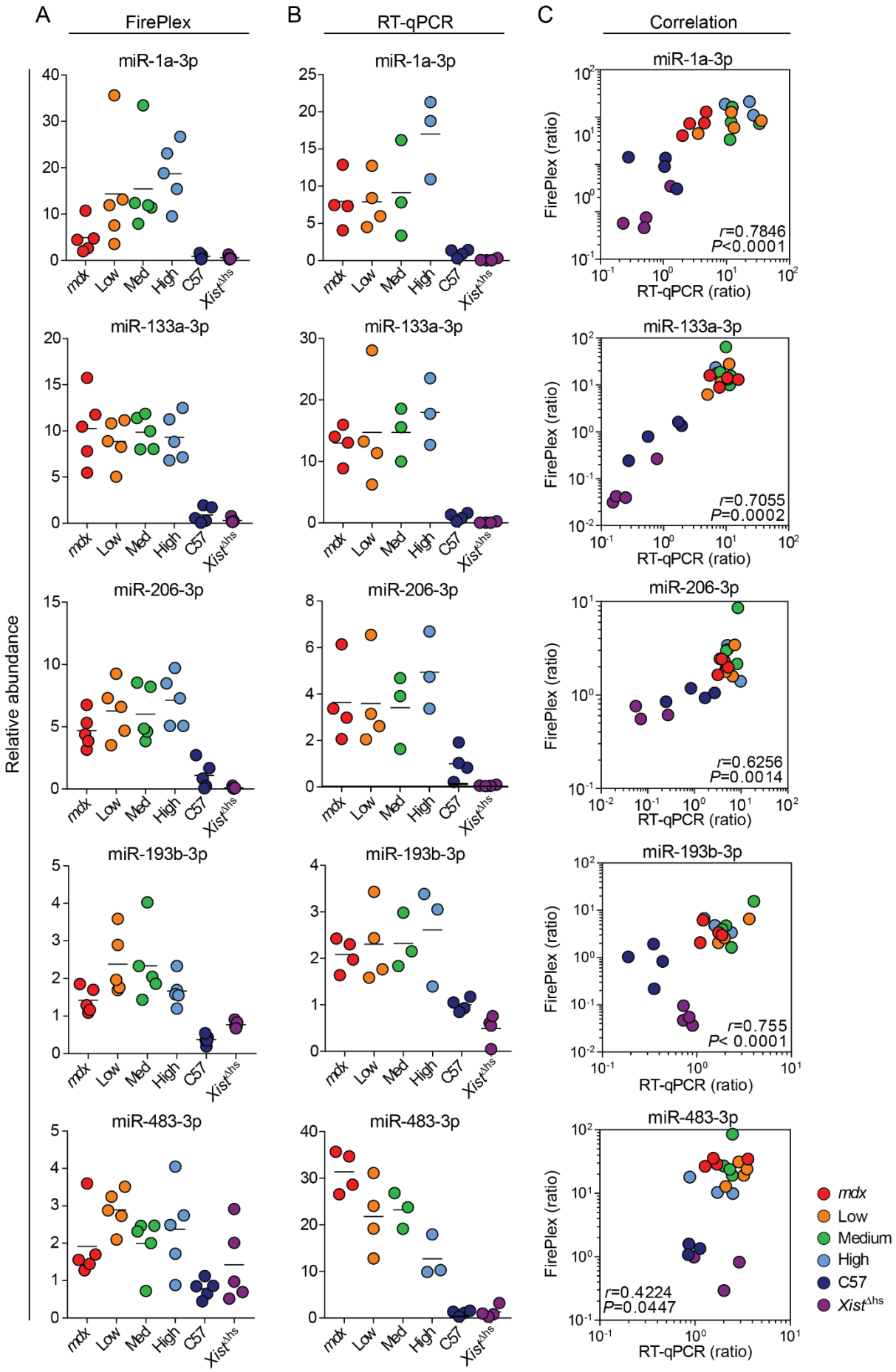
A
FirePlex
B
RT-qPCR
C
Correlation
Relative abundance
miR-1a-3p
miR-133a-3p
miR-206-3p
miR-193b-3p
miR-483-3p
mdx
Low
Med
High
C57
Xist^Δhs
FirePlex (ratio)
RT-qPCR (ratio)
r=0.7846
P<0.0001
r=0.7055
P=0.0002
r=0.6256
P=0.0014
r=0.755
P< 0.0001
r=0.4224
P=0.0447
mdx
Low
Medium
High
C57
Xist^Δhs

Figure 5.13 RT-qPCR validation of serum miRNA abundance at 24 weeks of age.
The 24 week serum samples were reanalysed in order to validate the FirePlex experiment (*n*=3-5 per group). Relative abundance of selected serum miRNAs was visualised for **A** FirePlex data, and **B** orthogonal validation using small RNA TaqMan RT-qPCR. FirePlex data were normalised to the geometric average of miR-16-5p, miR-17-5p and miR-92a-3p. RT-qPCR data were normalised to a synthetic spike-in control oligonucleotide (cel-miR-39). Mean ratios are indicated per group. **C** Data from the two methodologies were plotted against each other. Pearson or Spearman's *r* correlation coefficients and correlation *P*-values are shown on the plots.

5.3.5 Uniform dystrophin expression is associated with serum miRNA restoration

The observation that serum miRNA levels were not affected by differences in muscle dystrophin expression was somewhat surprising, given that (I) the Wood lab and others have previously shown that the level of dystrophin rescue by exon skipping is commensurate with the level of serum myomiR restoration, and (II) the levels of dystrophin expressed in the muscles of *mdx-Xist*$^{\Delta hs}$ mice is similar to exon skipping-treated *mdx* muscles. One possible explanation for this apparent paradox is the uniform vs non-uniform patterns of dystrophin protein distribution in the exon skipping-treated *mdx* relative to *mdx-Xist*$^{\Delta hs}$ muscles [626]. To test this possibility, exon skipping-treated *mdx* mice were directly compared with *mdx-Xist*$^{\Delta hs}$ mice at the same age. For treatment, male *mdx* mice were injected with a single 12.5 mg/kg dose of a PPMO conjugate via the tail vein at 6 weeks of age and sacrificed 2 weeks later (*n*=4). Exon skipping efficiency was determined to be 53.5% by RT-qPCR as measured by the level of Δexon23 *Dmd* transcripts (range: 52.5-54.9%, **Figure 5.14A**). Restoration of dystrophin protein was quantified by Western blot and determined to be 41.8% of WT levels (**Figure 5.14B**). In parallel, dystrophin expression was quantified in a new set of 8 week old female *mdx-Xist*$^{\Delta hs}$ mice (*n*=4) whereby two mice exhibited low levels (~2%) and the other two exhibited high levels (~47%) of dystrophin protein expression, representative of the high and low groups categorised earlier. The high group expressed similar levels of dystrophin protein compared to the PPMO-treated *mdx* mice. Ex-miRNA levels were determined in the serum of PPMO-treated animals (*n*=4) and compared with untreated *mdx* (*n*=3) and C57 WT controls (*n*=4). Circulating miRNA

levels were restored towards WT levels in the treated animals (**Figure 5.14C**) consistent with previous reports [463,479,631].

The restoration of ex-myomiR abundance that was observed following PPMO treatment was not recapitulated in the high *mdx-Xist*$^{\Delta hs}$ group (**Figure 5.7**), even though both groups express similar levels of dystrophin. Given these results, TA muscle from PPMO-treated animals and *mdx-Xist*$^{\Delta hs}$ mice at 8 weeks was sectioned in both transverse and longitudinal direction and subsequently stained for dystrophin, utilising laminin for identification of the muscle fibre. A uniform distribution of dystrophin was observed in the PPMO-treated animals, although dystrophin staining was often less intense compared to controls (**Figure 5.14D**). Conversely, TA from the *mdx-Xist*$^{\Delta hs}$ mice exhibited a patchy, non-homogenous distribution of dystrophin in both transverse and longitudinal sections, whereby incomplete staining of the periphery of each myofibre was observed for both the low and high dystrophin-expressing groups. These chimeric fibres are therefore likely to still be susceptible to contractile damage [4] resulting in the release of ex-miRNAs into the circulation.

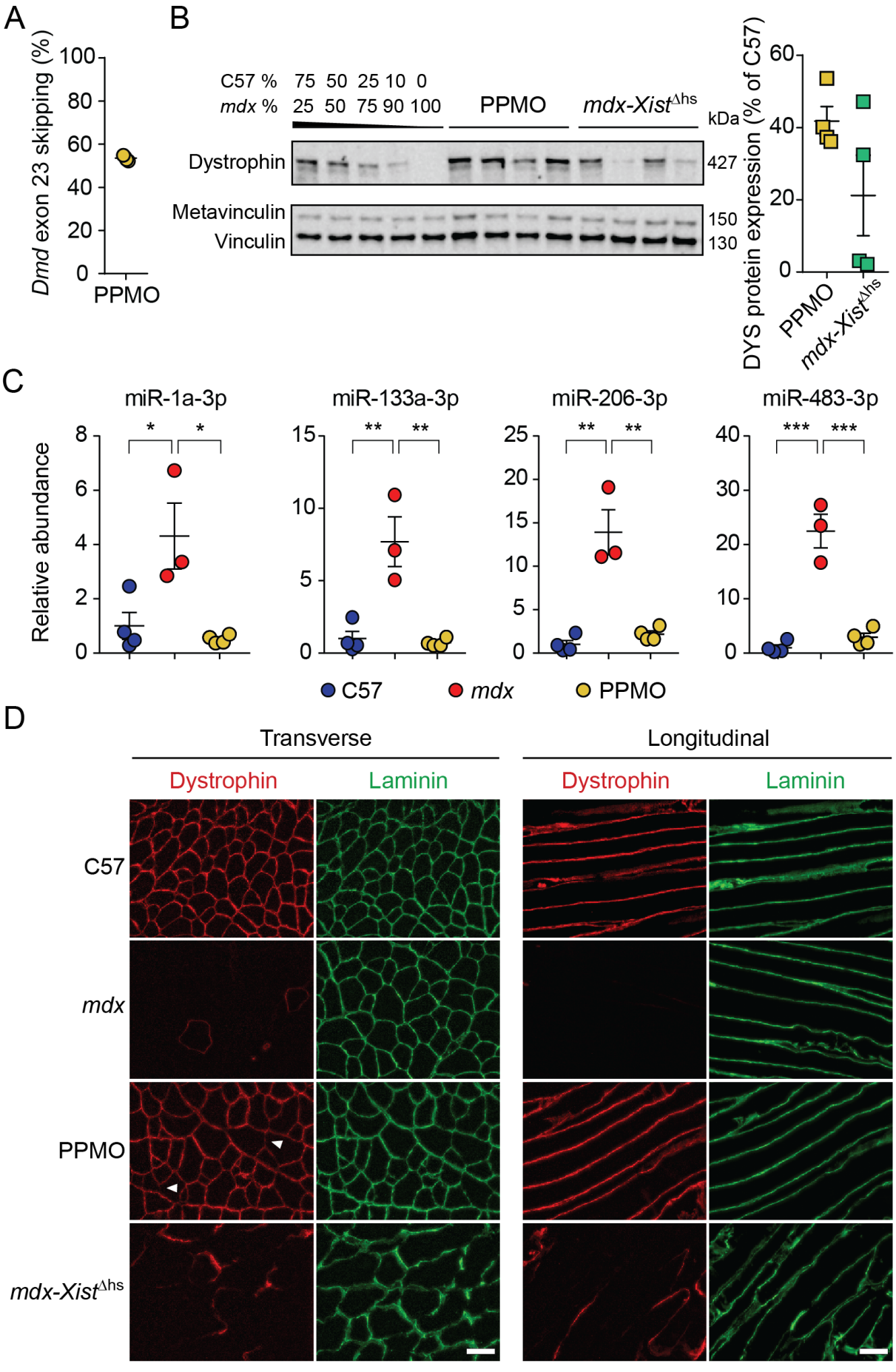
A
Dmd exon 23 skipping (%)
100
80
60
40
20
0
PPMO
B
C57 % 75 50 25 10 0
mdx % 25 50 75 90 100
PPMO
mdx-Xist^Δhs
kDa
Dystrophin
427
Metavinculin
Vinculin
150
130
DYS protein expression (% of C57)
60
40
20
0
PPMO
mdx-Xist^Δhs
C
miR-1a-3p
miR-133a-3p
miR-206-3p
miR-483-3p
Relative abundance
C57
mdx
PPMO
D
Transverse
Longitudinal
Dystrophin
Laminin
C57
mdx
PPMO
mdx-Xist^Δhs

Figure 5.14 Uniform dystrophin protein expression is required for restoration of ex-miRNA levels. **A** Exon skipping efficiency in TA of PPMO-treated *mdx* mice (*n*=4). **B** Western blot analysis of dystrophin protein expression in TA muscle from C57BL/10, *mdx*, PPMO-treated *mdx*, and *mdx-Xist*$^{\Delta hs}$ mice. Dystrophin protein was normalised to vinculin. A standard curve, consisting of mixtures of C57BL/10 and *mdx* protein lysates in ratios as indicated, was used to quantify dystrophin protein expression in the PPMO-treated *mdx* and *mdx-Xist*$^{\Delta hs}$ samples. **C** Ex-miRNA abundance in serum of C57BL/10 (*n*=4), *mdx* (*n*=3) and PPMO-treated *mdx* (*n*=4) mice. qPCR data were normalised to a synthetic spike-in control oligonucleotide (cel-miR-39). Abundance ratios were such that the mean of the C57BL/10 controls was returned to a value of 1. **D** Representative immunofluorescence staining of dystrophin protein in transverse and longitudinal TA sections for C57BL/10, *mdx*, PPMO-treated *mdx* and *mdx-Xist*$^{\Delta hs}$ mice. Sections were co-stained with laminin to label myofibres. All values are mean ± SEM. * *P*<0.05, ** *P*<0.01, *** *P*<0.001, for one-way ANOVA with Tukey *post hoc* test. Scale bars represent 100 µm.

5.3.6 Ex-miRNA abundance levels are influenced by gender

Given that all the mice used for the FirePlex study were necessarily female (due to the requirement for skewed XCI), a serum miRNA time course was performed comparing ex-miRNA abundance in males and females, to assess if findings in female mice can be confirmed in the more disease-relevant male model. As such, end-point serum miRNA measurements were performed at 4 ages (10, 24, 52 and 80 weeks, *n*=3-4 per group) and mice from both genders were analysed (the 80 week age time point was included to extend measurements beyond the range of the samples analysed by FirePlex, above). Both male and female *mdx* mice exhibited higher ex-miRNA abundance compared to their corresponding WT controls (**Figure 5.15**). These findings serve as further validation of the FirePlex time course, and exhibit the progressive decline in ex-miRNA abundance levels that has been reported in previous studies [480,481,631]. Interestingly, abundance was significantly higher in male compared to female *mdx* mice at 24 weeks of age for all measured miRNAs (*P*<0.0186). Previous studies have shown that male *mdx* mice exhibit increased sarcolemma permeability at 6 weeks and decreased muscle function at 6 months of age compared to females, highlighting the importance of sex steroid levels on the severity of DMD pathology [632,633], and potentially in the regulation of ex-miRNA release.

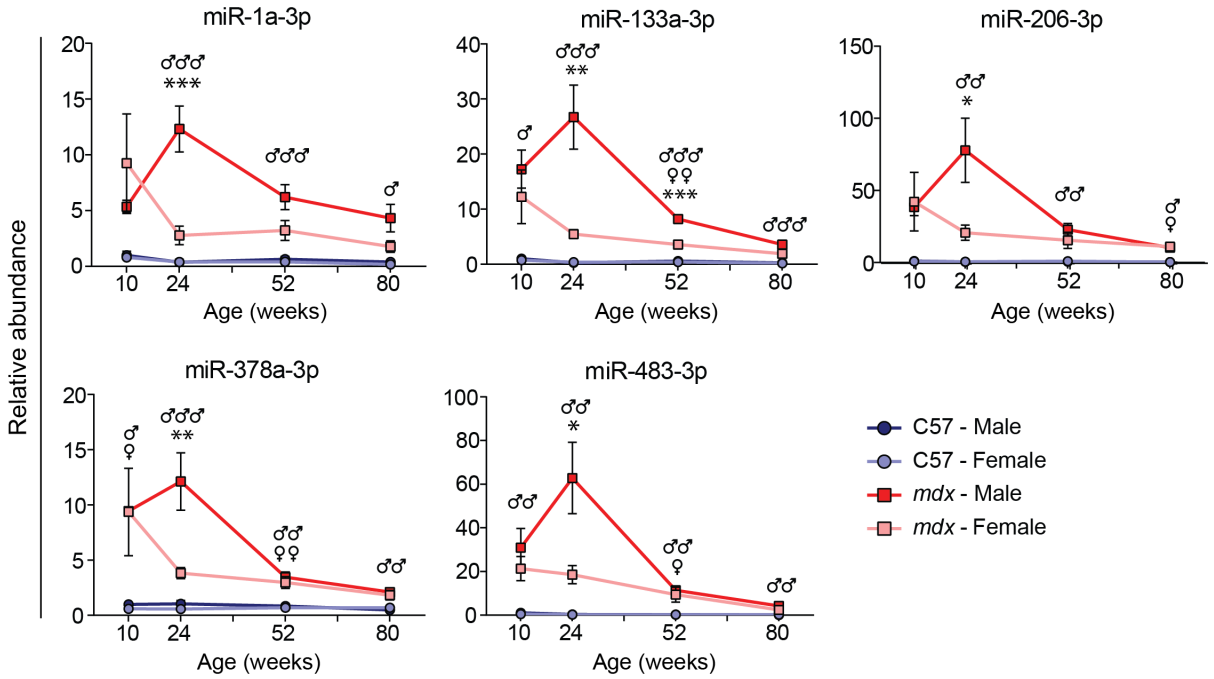

Figure 5.15 Comparison of differential miRNA abundance in serum from male and female mice. Ex-miRNA levels were assessed by small RNA TaqMan RT-qPCR in serum from male and female *mdx* mice at four different ages (10, 24, 52 and 80 weeks old, all *n*=4 except for C57BL/10 female 80 weeks, which is *n*=3). Age-matched male and female C57BL/10 mice were used as controls. qPCR data were normalised to a synthetic spike-in control oligonucleotide (cel-miR-39). All values are mean ± SEM. ♂ *P*<0.05, ♂♂ *P*<0.01, ♂♂♂ *P*<0.001 comparing male C57BL/10 with male *mdx*. ♀ *P*<0.05, ♀♀ *P*<0.01 comparing female C57BL/10 with female *mdx*. * *P*<0.05, ** *P*<0.01, *** *P*<0.001 comparing male *mdx* with female *mdx*. One-way ANOVA at each time point with Tukey *post hoc* test.

5.3.7 RT-qPCR fails to measure several low abundant miRNAs detected by FirePlex

While the majority of findings from the FirePlex study were independently validated, there were several inconsistencies between measurements made with the two methodologies (i.e. FirePlex and RT-qPCR). This study failed to validate miR-208a-3p, miR-370-3p and miR-539-5p in the majority of the time course samples by RT-qPCR (**Figure 5.16A**). Inspection of raw FirePlex signal intensities revealed that these miRNAs were very lowly abundant, which likely contributed to the inconsistency in their measurement (**Figure 5.16B**). miR-370-3p abundance was further analysed in *mdx*, *mdx-Xist*$^{\Delta hs}$ and control samples at 16 weeks. Correlation between miR-370-3p measurements was poor

(Spearman *r*=0.1635, **Figure 5.16C)** although failure to detect ex-miRNAs by RT-qPCR in the majority of samples limits the usefulness of this comparison. These differences are most likely attributed to the method of detection, whereby FirePlex measures miRNAs directly from biofluids. In contrast, RT-qPCR requires RNA extraction, certain methods of which are known to exhibit sequence-dependent differences in miRNA extraction efficiency [634,635]. As such, the FirePlex method may exhibit greater sensitivity with respect to the detection of some miRNAs, though the biological/clinical usefulness of measuring ex-miRNAs with such low abundance levels is debatable.

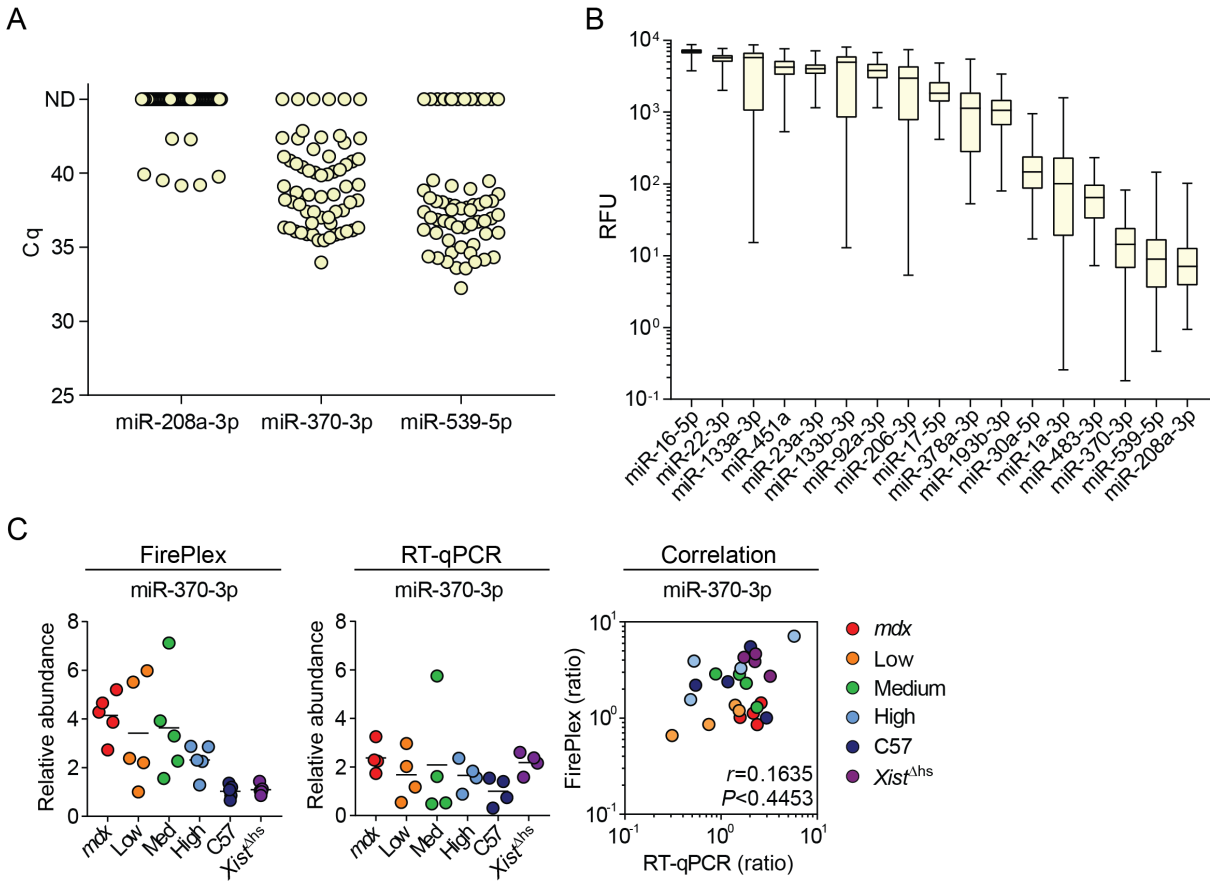

Figure 5.16 miRNAs exhibiting low abundance in FirePlex fail to validate with RT-qPCR.
A Cq values for lowly abundant miRNAs as measured by RT-qPCR. ND indicates not detected. **B** Total raw fluorescence units for every miRNA analysed in the second profiling measured by FirePlex. Min to max box plots on $\log_{10}$ scale. **C** Relative, normalised, abundance of 16-week serum samples for miR-370-3p as measured by FirePlex and RT-qPCR (*n*=4-5 per group). Abundance ratios were scaled such that the mean of the C57BL/10 control was returned to a value of 1. The mean values are indicated for each group. Data from the two methodologies were plotted against one another and analysed with Spearman's *r* correlation coefficient. The correlation coefficient and *P*-value are shown on the plot.

5.3.8 Measured miRNAs decrease abundance with age

Considering the progressive nature of the disease, and the age-associated decline in serum abundance levels observed for all ex-miRNA biomarkers investigated thus far, it is important to identify new biomarkers that are either stably expressed over time or increase with disease progression. For this purpose, the initial FirePlex screen was utilised to analyse the 68 miRNAs of interest in male C57 and *mdx* at 80 weeks of age (**Appendix 8.2**). Of the 19 upregulated miRNAs in the *mdx* mice (Student's *t*-test, $P<0.05$, $n=3$ per group, **Figure 5.17A** and **B**), miR-486a-5p was selected for further investigation because its differential expression only became significant at 80 weeks of age, making it a potential marker for late-stage disease progression. A normal range of Cq values (mean= 25.8) was observed, indicating that this miRNA is relatively abundant in serum, although neither male nor female *mdx* samples were significantly different from their respective controls in validation experiments ($n=4$ per group, **Figure 5.17C** and **D**). Furthermore, these results showed a progressive decrease in miR-486a-5p abundance over time, suggesting that this miRNA offers no advantage over existing (and more promising) biomarker candidates. While ex-miRNAs could have use for monitoring disease progression and/or response to therapy in younger patients, it may prove difficult to identify a serum miRNA biomarker that increases over time with disease progression, possibly due to a general impairment in miRNA release from aged dystrophic muscle.

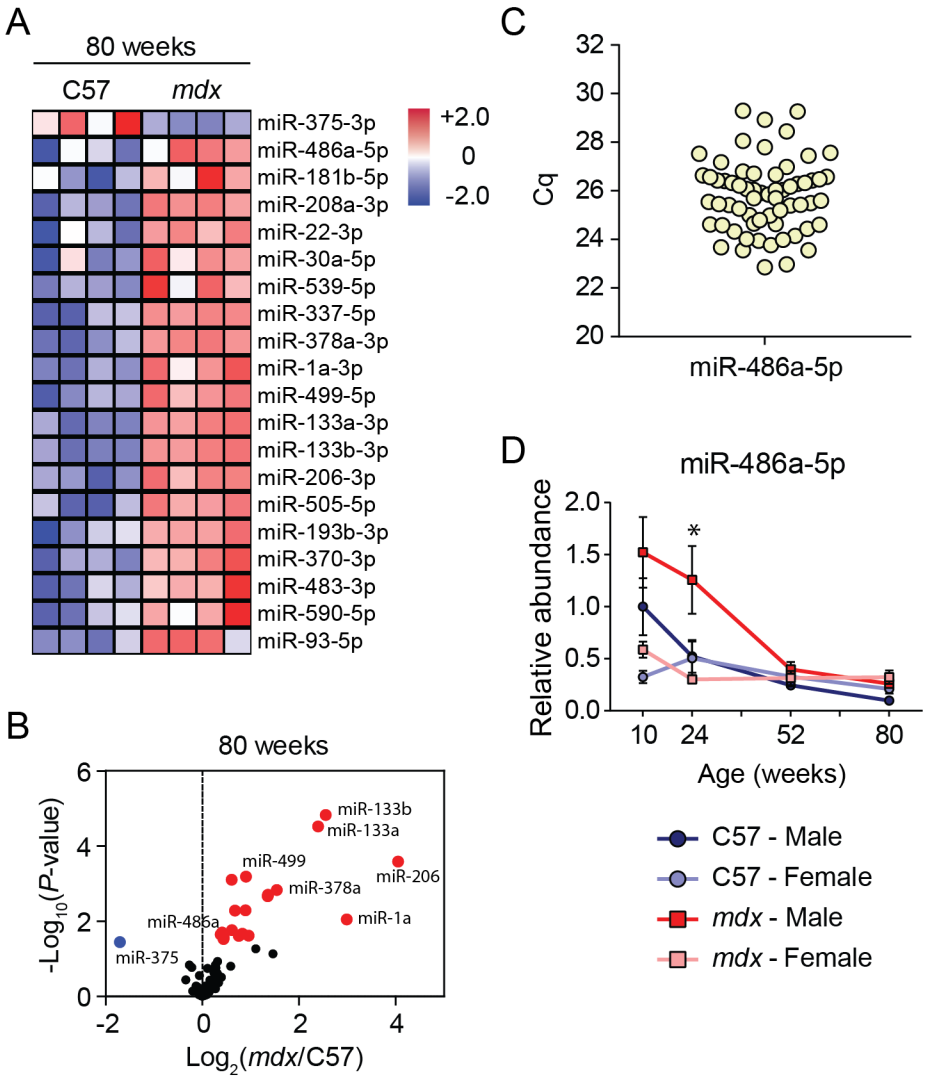

Figure 5.17 Differentially expressed miRNAs at 80 weeks of age.

The serum of C57 and *mdx* mice was analysed with a custom miRNA panel (68 miRNAs) using the FirePlex methodology at 80 weeks of age. FirePlex miRNA data were normalised to the geometric average of miR-16-5p, miR-17-5p and miR-92a-3p. Differentially abundant miRNAs (P<0.05) were visualised by **A** heatmap and **B** volcano plot. The scale bar for the heatmap represents row Z-scores with red and blue indicating higher and lower than mean abundance respectively. Statistically significant changes in the *mdx* compared to C57BL/10 are highlighted in red and blue (for elevated and lowered miRNAs respectively) on the volcano plots. $P < 0.05$, Student's t-test, n=4 per group. **C** Cq for miR-486a-5p as measured by RT-qPCR. **D** Ex-miRNA levels were assessed by small RNA TaqMan RT-qPCR in serum from male and female *mdx* mice at four different ages (10, 24, 52 and 80 weeks old, all n=4, except C57 female 80 weeks, which is n=3). Age-matched male and female C57BL/10 WT mice were used as controls. qPCR data were normalised to a synthetic spike-in control oligonucleotide (cel-miR-39). All values are mean ± SEM. * P<0.05 comparing male *mdx* with female *mdx*. One-way ANOVA at each time point with Tukey *post hoc* correction.

5.3.9 myomiRs, miR-193b-3p and miR-483-3p are released from myoblasts upon differentiation

The results so far have indicated the importance of uniform dystrophin distribution, which is thought to stabilise the myofibre. The within-fibre dystrophin mosaicism observed in the *mdx-Xist*$^{\Delta hs}$ mouse is unable to restore ex-myomiR abundance, which are indicative of muscle turnover and differentiation. To investigate whether differentiation influences miRNA release, intracellular and extracellular abundance of miR-1a-3p, miR-133a-3p, miR-206-3p, miR-193b-3p and miR-483-3p was analysed in differentiating C2C12 myoblasts (a cellular model for *in vivo* muscle regeneration). Differentiation was induced two days after cell seeding by replacing GM with DM to allow formation of multinucleated myocytes after 6 days. Cells and supernatant were collected during GM, and 3 and 6 days after differentiation (*n*=3 per group). Successful differentiation was confirmed by the visualisation of MHC-positive myotubes (**Figure 5.18A**). Cellular expression and extracellular abundance of miR-1a-3p, miR-133a-3p, miR-206-3p, miR-193b-3p and miR-483-3p were subsequently measured in C2C12 cells and supernatant (**Figure 5.18B** and **C**). Interestingly, when differentiation is induced, intra- and extracellular levels increase significantly for miR-1a-3p, miR-133a-3p, miR-206-3p and miR-483-3p. The results illustrate that the expression/abundance levels of these miRNAs are related to myoblast differentiation. Moreover, it was observed that ex-miRNA abundance is not proportionally related to intracellular expression. This is especially true for miR-193b-3p. This miRNA exhibits low intracellular levels in myoblasts and myotubes, but extracellular abundance is increased following differentiation. This study confirmed previous findings by the Wood lab and others (illustrating increased extracellular miR-1a-3p, miR-133a-3p and miR-206-3p) and identified two new miRNAs that are released upon myogenic differentiation.

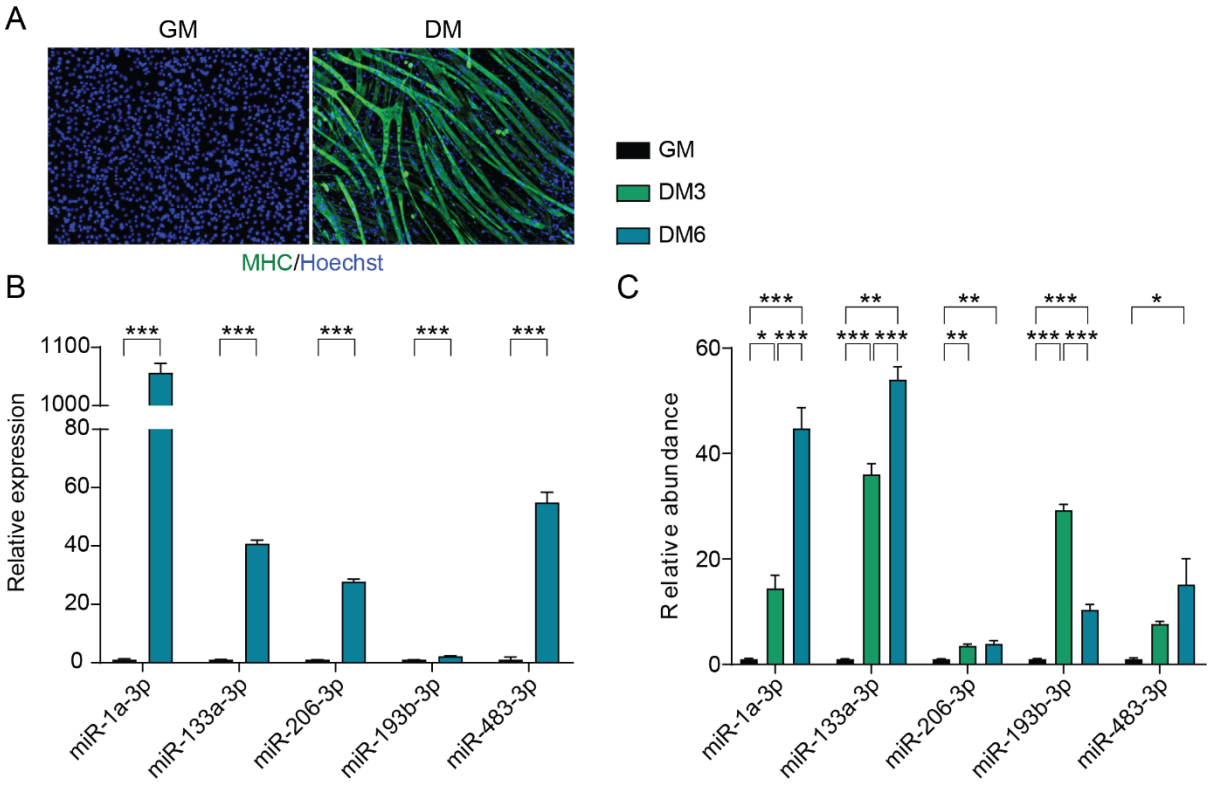

Figure 5.18 C2C12 myoblast differentiation induces release of miRNAs of interest.
A MHC antibody stain in C2C12 cells collected at GM or 6 days after differentiation (DM), to identify differentiated myotubes (green). **B** Relative miRNA expression in C2C12 cells collected at GM or 6 days after differentiation (n=3 per group). Values are mean ± SEM. * P<0.05, ** P<0.01 and *** P<0.001, for Student's t-test. **C** Relative miRNA abundance in supernatant from C2C12 cells collected at GM or 3 (DM3) and 6 (DM6) days after differentiation (n=3 per group). Values are mean ± SEM. * P<0.05, ** P<0.01, and *** P<0.001, for one-way ANOVA with Tukey *post hoc* correction.

5.4 Discussion

5.4.1 The relationship between skeletal muscle dystrophin expression and ex-miRNA abundance

With the advancement of therapies for DMD, it remains vital that there is a continued improvement in the understanding of dystrophin function and restoration. Therefore, this study sought to investigate the relationship between skeletal muscle dystrophin protein levels and the abundance of ex-miRNAs, with respect to their potential as pharmacodynamic biomarkers. Initially, *mdx* heterozygotes were investigated to assess whether this model could be utilised assessing serum miRNA levels in response to dystrophin. However, these mice exhibited similar levels of ex-miRNA abundance to the WT controls and analysis of protein expression by Western blot and immunofluorescence demonstrated near-normal dystrophin levels and distribution. As discussed in **Chapter 1.3.1**, dystrophin-negative satellite cells most likely differentiate less efficiently, allowing a positive selection advantage of the dystrophin-positive satellite cells over time, leading to a gradual accumulation of myofibres containing dystrophin [191,636–638]. Together the data suggested limited usefulness for this model.

Therefore, a cross between the *mdx* and *Xist*$^{\Delta hs}$ mouse models was utilised. In the resulting *mdx-Xist*$^{\Delta hs}$ mouse, a mutation in the *Xist* gene results in skewed XCI, resulting in F1 progeny expressing various levels of dystrophin protein that are similar to the levels achieved by exon skipping (~2-44% of WT). The Aartsma-Rus lab has previously shown that increased dystrophin protein leads to improved muscle function, life span and CK levels in these mice [626,639,640]. A secondary aim was to identify novel (cardiac pathology-related) miRNAs with biomarker potential to inform on processes occurring in- and outside of myofibres, such as fibrosis, adipose deposition, and inflammation, which contribute to DMD pathological progression. In addition, minimally-invasive indicators of dilated cardiomyopathy would offer considerable advantages over existing biomarker approaches, as these could potentially predict the onset of lethal cardiac failure. While the skeletal muscle-enriched

myomiRs, miR-1a-3p and miR-133-3p, are also expressed in cardiac muscle (and have also been reported to be elevated in human plasma after myocardial infarction [641]) other miRNAs have more heart-restricted patterns of expression (i.e. cardiomiRs, such as miR-208a-3p and miR-449).

Ideally, ex-miRNAs would serve as pharmacodynamic biomarkers that inform on either (a) the level of dystrophin protein re-expression, or (b) improvement in pathophysiology in dystrophic muscle. To facilitate biomarker potential, the miRNA would exhibit a progressive increase in abundance over time.

Thus, an initial FirePlex assay panel of 68 miRNAs was measured in serum from C57BL/10 and *mdx.* Utilising this methodology presented several advantages: (I) the number of miRNAs measured per sample could be multiplexed up to 68-plex; and (II) measurement could be performed directly from biofluids thereby eliminating possible technical variation associated with RNA extraction. These data showed that the majority of miRNAs were elevated compared to the WT controls. These results were somewhat expected, and are consistent with previous observations [478,631]. This screen provided a useful tool to select only the most promising miRNAs for measurement in the dystrophin-variable *mdx-Xist*$^{\Delta hs}$ mouse and controls (*mdx*, C57 and *Xist*$^{\Delta hs}$), and the selection was based on differential abundance at multiple time points and/or previously reported evidence.

Surprisingly, profiling analysis suggested little differences in ex-miRNAs between the different *mdx-Xist*$^{\Delta hs}$ groups and *mdx* (although generally elevated compared to controls) and it was unexpectedly observed in the individual miRNA analysis that the three myomiRs, miR-1a-3p, miR-133a-3p and miR-206-3p, were consistently elevated in all *mdx-Xist*$^{\Delta hs}$ groups and not significantly different from *mdx*, irrespective of the level of dystrophin expressed in skeletal muscle. This is in direct contrast with what has been observed in PPMO-treated mice, whereby similar levels of dystrophin re-expression by exon skipping treatment resulted in complete restoration of extracellular myomiR abundance to WT levels [479,631].

Interestingly, other miRNAs such as miR-193b-3p, miR-370-3p and miR-483-3p did exhibit a decrease in ex-miRNA abundance with increasing skeletal muscle dystrophin protein levels. This

gradation is particularly noticeable in the CDF plots. However, in contrast to the myomiRs, their potential to discriminate between healthy and dystrophic mice was diminished. Similar results were observed for miR-208a-3p, miR-378a-3p and miR-539-5p, although ex-miRNA abundance differences between the *mdx-Xist*$^{\Delta hs}$ groups were less striking, and these results could not be independently validated by RT-qPCR. The divergence in ex-miRNA response to skeletal muscle dystrophin protein suggests that their levels are most likely related to the function of the miRNA and points to the existence of multiple mechanisms responsible for ex-miRNA release into the circulation. Indeed, this theory is consistent with previous hypotheses advanced by the EL Andaloussi, Morgan, Smith and Wood labs suggesting purposeful miRNA release into the serum [463,477,479,480].

This study was unsuccessful in the attempt to find cardiac-specific biomarkers, potentially due to the relatively mild (cardiac) pathology in the *mdx* model. It was also unable to observe any miRNAs that were positively correlated with disease progression, instead there appeared to be a global decrease in ex-miRNA abundance with age. Perhaps this is due to accumulation of fibrosis in dystrophic muscle which may affect the secretome as a whole.

Given their involvement in regeneration, the serum abundance of ex-myomiRs may be affected by the distribution of the dystrophin protein, which contributes to muscle fibre stability and turnover. To test this hypothesis, the distribution of dystrophin protein expression in *mdx-Xist*$^{\Delta hs}$ and PPMO-treated *mdx* mice was compared, which highlighted that the PPMO-treated animals exhibited a uniform dystrophin expression, whereas the *mdx-Xist*$^{\Delta hs}$ mice showed a patchy, non-homogenous distribution within fibres, where discontinuous regions of dystrophin expression were observed at the sarcolemma. These data suggest that ex-myomiR abundance is a function of both the total dystrophin expression and its pattern of distribution at the sarcolemma. Moreover, the results have shown that response to dystrophin protein expression can markedly differ between ex-miRNAs and highlight the complexity of the miRNA secretome in dystrophin-deficient animals.

5.4.2 Gender-specific miRNA abundance

Due to the genetics of the model system used (XCI-driven dystrophin variability), *mdx-Xist*$^{\Delta hs}$ mice utilised in this study were necessarily female. However, given that the disease is X-linked and so in general only affects males, findings for several key miRNAs of interested were further characterised in a gender time course experiment, which analysed serum from C57BL/10 and *mdx* males and females at 10, 24, 52 and 80 weeks of age. Both male and female *mdx* mice exhibited significantly elevated serum abundance levels of miR-1a-3p, miR-133a-3p, miR-206-3p, miR-378a-3p and miR-483-3p compared to their respective controls, but abundance of all miRNAs was significantly higher in the male compared to the female *mdx* at 24 weeks. This may be due to divergences in regeneration. Sex steroid expression may also contribute to the observed results, as previous studies have observed that males exhibit increased sarcolemma permeability at 6 weeks of age and decreased muscle function at 6 months compared to females [632,633]. Moreover, exercised female *mdx* mice exhibit reduced numbers of regenerating fibres and an increase in oestrogen receptors expression in the diaphragm compared to exercised *mdx* males and non-exercised *mdx* females, respectively [642]. Overexpression of the oestrogen-related receptor γ improved metabolic gene expression and exercise tolerance in *mdx* skeletal muscle [643]. More directly, testosterone was found to positively regulate miR-133a/b expression in skeletal muscle from human and mice males [644]. These studies highlight a potential role for sex hormones in serum miRNA expression, although to what extent these differences affect ex-miRNA abundance remains to be established.

5.4.3 Therapeutic implications

The patchy sarcolemmal staining observed in *mdx-Xist*$^{\Delta hs}$ mice is consistent with the myonuclear domain hypothesis [645], whereby each myonucleus serves its proximal myofibre territorial domain. Accordingly, these data suggest that diffusion of dystrophin mRNA and protein is subject to some degree of spatial restriction, as has been suggested in other contexts [646]. The resulting segmented pattern of dystrophin expression is unlikely to be fully sufficient to protect a

myofibre from degeneration, as contractile damage will still occur at non-protected, dystrophin-negative regions of the sarcolemma. Similar effects have been reported in terms of between-myofibre mosaicism. Low levels of dystrophin expressed in the majority of myofibres were found to result in an improvement in dystrophic pathology, whereas mice expressing high levels of dystrophin in a smaller number of fibres exhibited typical dystrophic features [621]. A further consideration is the length of the restored dystrophin protein. Here, the effect of varied expression of levels of full length dystrophin (*mdx-Xist*$^{\Delta hs}$) was examined which contained a small internal deletion after removal of *Dmd* exon 23 by exon skipping. However, other therapies such as microdystrophin gene therapy generate a much shorter dystrophin protein with a concomitant reduction in functional correction [647–649].

Another important consideration concerns recent developments in therapeutic strategies which potentially result in suboptimal dystrophin protein re-expression, as predicted with CRISPR and cell-based therapeutics [347,348]. While the former approach has yielded impressive results *in vivo* [349,350], it will most likely be less efficacious in humans due to the requirement for enormous viral titres, possible immune responses to Cas9 protein [650] or pre-existing immunity to adeno-associated virus [651], and difficulties associated with repeated administration [652]. Suboptimal CRISPR treatment would likely lead to an analogous within-fibre mosaicism as observed in the *mdx-Xist*$^{\Delta hs}$ mouse, with parts of the myofibre positive and other parts negative for dystrophin, due to incomplete editing of all myonuclei. Similarly, current strategies for cell-based therapies involve transplantation of dystrophin-expressing cells with myogenic potential which subsequently fuse with existing dystrophin-negative myofibres in the host muscle, thereby generating chimeric fibres [330]. The expected outcomes of these two therapeutic strategies are therefore approximated by the XCI-driven non-homogenous dystrophin expression pattern in the *mdx-Xist*$^{\Delta hs}$ mouse. The results highlight an important new aspect when targeting dystrophin restoration, as sub-optimal, non-homogenous dystrophin re-expression may result in similar effects seen in the *mdx-Xist*$^{\Delta hs}$ model. Interestingly, a subset of BMD patients exhibits non-homogenous staining at the sarcolemma, which is correlated with a worse clinical pathology [653]. The results observed in the *mdx-Xist*$^{\Delta hs}$ mouse are therefore

directly relevant to this clinical phenotype and provide new insights into the relationship between dystrophin and disease presentation.

5.4.4 Study limitations and future directions

Even though the FirePlex exhibited greater sensitivity than RT-qPCR with respect to the detection of some miRNAs, the biological/clinical usefulness of measuring ex-miRNAs with such low abundance levels is debatable as they may not be measured in patients or by the gold standard methodology, RT-qPCR.

It will be important to investigate other outcome measures of dystrophin restoration such as histopathology and/or muscle function. Even though the Morgan and Wood labs have previously shown that myomiRs are indicative of muscle fibre stability [479], these solely are an indirect measurement of the underlying muscle pathology. Therefore, future studies are required to address this. For instance, embryonic myosin heavy chain (eMHC) has been shown to be a marker for regeneration [654] and analysing its expression in *mdx-Xist*$^{\Delta hs}$ and PPMO-treated *mdx* mice will provide invaluable insight into the current regenerative processes in the muscle of these animals. It is hypothesised that the uniform dystrophin distribution induced by PPMO treatment will stabilise the muscle, thereby preventing muscle turnover. This may be reflected in a reduction of eMHC in these treated animals. In contrast, the non-homogenous dystrophin distribution observed in the *mdx-Xist*$^{\Delta hs}$ mouse is hypothesised not to prevent these pathological processes and therefore eMHC would be present. Conversely, the number of centrally nucleated fibres may likely be similar, or perhaps reduced, in *mdx* treated animals compared to *mdx-Xist*$^{\Delta hs}$, as central nucleation is an indicator of both current and historic muscle regeneration.

Other experiments of importance include confirmation of muscle membrane stability. Through injection of Evan's blue dye in *mdx-Xist*$^{\Delta hs}$ and PPMO-treated *mdx* mice, infiltration into the muscle can be observed, indicating the degree of sarcolemma permeability. It is hypothesised that the

mdx-Xist$^{\Delta hs}$ mice will exhibit higher levels of EBD incorporation than PPMO-treated mice, consistent with increased membrane fragility in the former.

5.4.5 Conclusions

In summary, the relationship between skeletal muscle dystrophin and serum miRNA abundance is complex. While some miRNAs (miR-193b-3p, miR-370-3p and miR-483-3p) exhibited decreased serum abundance in response to higher levels of skeletal muscle dystrophin, others, such as the myomiRs, did not. This may be related to differences in the functional roles of these miRNAs, and is suggestive of distinct release mechanisms, rather than a passive miRNA release model. Indeed, treatment with PPMO is thought to stabilise the muscle membrane and result in restoration of ex-myomiRs, which are indicative of muscle turnover. More importantly, muscle stabilisation appears to be related to the distribution of dystrophin at the level of the sarcolemma, with a requirement of uniform dystrophin expression throughout the periphery of the myofibre. These results are directly relevant to the development of therapeutic strategies for dystrophin re-expression.

6. Discussion and conclusion

6.1 Summary of results

This thesis has focused on how the absence of the dystrophin protein affects the transcriptome, proteome and miRNA secretome in murine models of DMD. In **Chapter 3**, this study utilised microarrays to investigate the effects of dystrophin absence on the transcriptome during different stages of the early dystrophic cardiomyopathy, with the aim of identifying novel pathways associated with the initial cardiomyopathic development. Given the differential pathology advancement between the chambers [81], the heart was further dissected into separate anatomical regions. This allowed for a more detailed analysis of aberrant molecular pathways and how the chambers may be differentially affected. The results showed earlier molecular changes in the right atrium and ventricle compared to the left, which corresponds to physiological studies performed [81]. The heart appears to undergo many remodelling and migration processes, which may be related to changes in morphology (hypertrophy) and fibrotic degeneration. Among the many differentially expressed genes identified, a major regulator of the Wnt signalling pathway, *Sfrp2*, was observed to be consistently upregulated (FC >2.5) in all chambers except the RA at 10 weeks. Downstream protein analysis of three arms of the Wnt signalling pathway demonstrated expression changes in the ratio of phosphorylated to unphosphorylated JNK, suggesting a decrease in pJNK, the effector inducing downstream transcription. Given that many other cascades can influence pJNK expression, further research is required to investigate the relationship between *Sfrp2* and JNK expression.

Protein extraction of all cellular fractions indicated no differences in sFRP2 protein expression between healthy and dystrophic hearts. To elucidate the opposing results observed between *Sfrp2* gene and sFRP2 protein expression, levels of this protein were further quantified in the nuclear and cytoplasmic fractions. Furthermore, immunofluorescence was utilised to assess total sFRP2 protein and expression around the nucleus. Although preliminary, these results together indicated that sFRP2

is reduced in the cytoplasm/extracellular space and increased in the nuclear/RER regions. Utilisation of improved methodology is required to confirm these results and understand the underlying mechanisms, but the data suggest a mislocalisation of the sFRP2 protein in the absence of dystrophin.

Chapter 4 focused on identifying differentially expressed proteins and pathological pathways resulting from dystrophin absence in the skeletal muscle TA at different stages of dystrophic pathology. A high resolution proteomic comparison was performed between two dystrophic models, the *mdx* exhibiting a point mutation in exon 23 and the *mdx52* containing an exon 52 deletion. Although previous studies and results obtained from serum myomiR levels in **Chapter 4.3.1** demonstrated potential differences in regenerative capacity between the *mdx* and *mdx52*, the proteomic analysis identified no substantial variations between the two dystrophic models. Instead, these samples were combined to increase statistical power and therefore the number of differential expression calls between dystrophic and control samples. As such, this allowed for the identification of several pathways (Rho GTPase and gluconeogenesis) and proteins (SLC25A24, RICTOR and CAV3) of interest. Specifically, MVP, a constituent of multi subunit vault micro-organelle structures, was observed to increase in dystrophic muscle over time. To uncover aspects of its role in DMD muscle pathology, the effect of *Mvp* knockdown was assessed on C2C12 myoblast differentiation, which did not affect myogenic differentiation, although MVP protein levels were observed to increase with myotube formation. Interestingly, while *Mvp* was not required for differentiation, *Mvp* knockdown resulted in a trend in reduction of the *Dmd* transcript in the C2C12 cells. These results suggested a potential novel role for MVP in the regulation of *Dmd* gene expression.

The relationship between dystrophin and the miRNA secretome was assessed in **Chapter 5**. Data from a 68-plex panel of putative miRNA biomarkers demonstrated that ex-myomiR abundance did not decrease in response to increasing skeletal muscle dystrophin levels. This was unexpected given that previous studies demonstrated restoration of ex-myomiR levels in response to effective dystrophin re-expression. These results indicated that ex-myomiR release might be affected by the

localisation of dystrophin expression of the sarcolemma, as patchy, non-homogenous dystrophin expression was observed at the sarcolemma in the *mdx-Xist*$^{\Delta hs}$ mouse. Sub-optimal dystrophin expression as a result of CRISPR-Cas9 and cell-based therapies are likely approximated by the XCI-driven within-fibre mosaicism observed in the *mdx-Xist*$^{\Delta hs}$ mouse. In contrast to the myomiRs, other miRNAs (miR-193b-3p, miR-370-3p and miR-483-3p) did exhibit a decrease in abundance following increasing dystrophin levels. These results indicate there are multiple mechanisms of miRNA release and highlight the complexity of the miRNA secretome in dystrophic muscle. These findings have direct therapeutic implications and should be considered in future dystrophin restoration strategies.

6.2 High-throughput methodologies in DMD

Characterising the molecular mechanisms underlying diseases such as DMD remains important for understanding pathology, developing novel therapies for patients, and for identifying potential biomarkers. With the emergence of techniques such as RNA-sequencing and microarrays that encompass a large proportion of the known protein-coding transcripts, analysis of the transcriptome has greatly contributed to the current understanding of gene expression. Indeed, several studies have addressed identification of differentially expressed genes in dystrophic compared to healthy muscle [491,492]. The vast number of transcripts identified by RNA-sequencing in these studies has greatly contributed to the understanding of changes in gene expression in dystrophic muscle. Similarly, microarrays, qPCR arrays and RNA-sequencing have facilitated the identification of miRNAs in tissue and serum, and utilisation of these methods have resulted in establishment of novel putative biomarkers in muscle and serum for DMD. The current study utilised the novel FirePlex technology, which allows direct measurement in biological fluid, without the need for RNA extraction. Although this reduces technical variation in one aspect, it introduces new biases associated with quantification from serum. Nevertheless, these studies have demonstrated the utility of RNA analysis in contributing to the understanding of dystrophic pathology.

In contrast, full resolution of the proteome has remained challenging due to technical limitations, the masking of peptides by more highly abundant ones and the discarding of many proteins due to selection of a narrow pH range. Resolving these difficulties is important not only to widen the view of the proteome but also to potentially allow for a greater grasp on the discrepancies between mRNA and protein directionality and thereby better understand the intricacies of molecular cell signalling. The Lehtiö and Wood labs have previously made significant efforts to bridge the transcriptome and proteome field and, among others, demonstrated a weak correlation between concordant gene and protein directionality proteins (i.e. both up- or downregulated), as previously observed [492,655]. Further understanding of this discrepancy would benefit from identification of a

larger number of proteins. The work presented in this thesis has made significant progress in characterisation of the dystrophic proteome, with identification of over 7,000 proteins (just under 5,000 detected in all samples) in TA, the best performance in skeletal muscle to date. While this is an impressive feat given the tissue analysed (i.e. prone to peptide masking by myosin and actin), numbers could still be considered low in contrast to the genes analysed by transcriptomic arrays. As proteins execute many of the functional aspects of the cell, one could argue that protein data may provide more valuable information than mRNA, especially given their poor correlation in expression directionality. An improved proteomic resolution will allow for better integration with the transcriptome. Furthermore, cell type-specific differences should be considered in future investigations. Ultimately, addressing these different aspects will significantly advance the understanding of the molecular underpinnings of dystrophic pathology.

6.3 Mouse models for DMD research

One of the limiting factors in DMD research is the current availability of appropriate mouse models. While the *mdx* carries a mutation in the dystrophin gene resulting in the loss of the dystrophin gene, many of the dystrophic features are not as severe as those observed in patients and the life span of these mice is near normal [84]. This impedes a detailed understanding of the underlying pathology, especially in the less-affected heart. Cardiomyopathy could be exacerbated by involuntary exercise [304], although this labour-intensive method may be less preferred to genetic models. As such, it is of importance that novel models are established and, indeed, many studies have aimed to discover a more severe mouse model. Although the dko better approximates the severity of DMD [73,85], the absence of the utrophin protein does not mimic the natural state of patients, who instead express increased levels of this protein [364]. Other models like the Cmah$^{-/-}$*mdx* have aimed to 'humanise' the *mdx* mouse by inducing a mutation in the *Cmah* gene, which alters the expression of sialic acids found on glycans and is not active in humans [86]. While the cardiomyopathy does indeed appear worse, the Tyler, Wells and Wood groups were unable to corroborate a severe skeletal muscle pathology [87], thereby challenging the appropriateness (and usefulness) of this model. Perhaps the most promising model may be the *mdx* mouse generated on a DBA/2 background, whereby several studies have observed a worsened skeletal pathology relative to the *mdx* [88–90]. However, this model has only recently been generated (2010) and further studies will be required to corroborate if this model is superior to the *mdx* on the C57BL/10 background. Ultimately, current research has yet to establish a severe mouse model recapitulating DMD pathology, which will be required for better disease approximation.

6.4 Circulating biomarkers in DMD

There is an unmet clinical need for non-invasive biomarkers to effectively measure disease progression and response to therapy in DMD patients. This absence has been particularly noticeable in the drisapersen and eteplirsen clinical trials with the problems associated with current outcome measures (i.e. 6MWT and biopsies). Many ex-miRNAs have been considered as putative non-invasive biomarkers to assess the stage of DMD disease, with the myomiRs arguably exhibiting the most promise. Ideally, ex-miRNAs would serve as pharmacodynamic biomarkers that inform on either (a) the level of dystrophin protein re-expression, or (b) improvement in pathophysiology in dystrophic muscle. To facilitate biomarker potential, the miRNA would exhibit a progressive increase in abundance over time. However, the serum abundance of currently established DMD-related miRNAs decreases with age, which may limit the usefulness of these miRNAs as biomarkers. Therefore, this study aimed to identify novel putative biomarkers in relation to cardiac pathology. Given that the heart displays overt pathological signs later than skeletal muscle in patients and mice, it was hypothesised that cardiomiRs would exhibit a consistent or increasing abundance pattern with pathological status. However, the results did not establish any putative cardiomiR that was significantly elevated in dystrophic serum over time. CardiomiR identification may be limited by the severity of the model utilised. Though dilated cardiomyopathy is evident in *mdx* mice at 42 weeks of age [519], severe fibrotic pathology is only apparent from 15 months of age [627]. Therefore, putative cardiomiRs are best analysed in more severe cardiac models and patient serum at different stages of the disease to assess abundance consistency. Nevertheless, it should be noted that the ex-myomiR abundance was restored to WT levels following PPMO dystrophin re-expression and these may prove useful as a non-invasive measures of effective dystrophin restoration, perhaps making them more appropriate biomarkers than CK.

In addition to miRNAs, circulating proteins have also been considered for their biomarker potential in DMD. Hathout *et al.* utilised mass spectrometry to identify 305 proteins that were

differentially expressed in dystrophic serum compared to controls, including myoglobin and somatic cytochrome c [656]. Interestingly, several proteins were consistently upregulated at different ages (3 weeks and 2, 4 and 7 months), which were related to glycolysis and myofibrils. One of the proteins, PGAM2, was further examined in patient serum and exhibited a decrease over time [656], highlighting the importance for biomarker confirmation in patients. The Wood lab, in collaboration with the Gait and Lochmüller groups, has utilised a novel aptamer-based approach to analyse differential expression of proteins in control and dystrophic serum. Among the 96 candidates, the enzyme ADAMTS5 was consistently upregulated in *mdx* and patient serum [657], although elevation was not observed in another study investigating circulating ADAMTS5 abundance in patients [658]. These opposing results highlight the technical and/or biological variability between patient samples and require careful consideration. Together these studies demonstrate the importance of further progress in the field of circulating biomarkers, which require significant and rapid advancement to keep up with clinical trial development.

6.5 Concluding remarks

Since the discovery of the dystrophin gene in 1986 [30] and the protein in 1987 [659], much progress has been made in understanding the underlying molecular pathology of DMD. Despite several decades of advancements, an effective treatment strategy is not yet available for patients. This work has shown that the efficacy of dystrophin restoration therapy is not only dependent on the percentage of dystrophin, but also on its distribution around the periphery of the sarcolemma, which will be of importance for future protein correction strategies. Although the genetic basis of the disease is relatively straightforward, the different aberrant processes involved in the progression of the disease as a result of absence of the dystrophin protein are more complex. Evidence from re-expression of cardiac dystrophin in animal models in this thesis and other studies suggests that disease pathology is not simply 'cured' by reinstating the dystrophin protein. Instead, it is becoming increasingly apparent that it is necessary to address other aberrant pathways, especially in patients with a more advanced disease state. The work presented in this thesis has aimed to address these important aspects of DMD research and demonstrated differences in early dystrophic pathology between the various cardiac anatomical regions. In addition, *Sfrp2* was significantly elevated in *mdx* hearts, with a potential perinuclear mislocalisation of the sFRP2 protein. Furthermore, this work discovered novel protein expression signatures and patterns that change with aging in dystrophic skeletal muscle, and highlighted a potential role for MVP in DMD. For these purposes, it remains vital that research into the underlying dystrophic mechanisms continues, as these may one day prove useful for combinatorial therapeutic strategies. The results provide new insights into the molecular pathology of DMD with implications for therapy.

7. References

1. Mah, J.K.; Korngut, L.; Dykeman, J.; Day, L.; Pringsheim, T.; Jette, N. A systematic review and meta-analysis on the epidemiology of Duchenne and Becker muscular dystrophy. *Neuromuscul. Disord.* **2014**, *24*, 482–491.
2. Ervasti, J.M.; Campbell, K.P. Membrane organization of the dystrophin-glycoprotein complex. *Cell* **1991**, *66*, 1121–1131.
3. Ervasti, J.M.; Campbell, K.P. A role for the dystrophin-glycoprotein complex as a transmembrane linker between laminin and actin. *J. Cell Biol.* **1993**, *122*, 809–823.
4. Petrof, B.J.; Shrager, J.B.; Stedman, H.H.; Kelly, a M.; Sweeney, H.L. Dystrophin protects the sarcolemma from stresses developed during muscle contraction. *Proc. Natl. Acad. Sci. U. S. A.* **1993**, *90*, 3710–3714.
5. Cyrulnik, S.E.; Fee, R.J.; De Vivo, D.C.; Goldstein, E.; Hinton, V.J. Delayed developmental language milestones in children with Duchenne's muscular dystrophy. *J. Pediatr.* **2007**, *150*, 474–8.
6. Connolly, A.M.; Florence, J.M.; Cradock, M.M.; Malkus, E.C.; Schierbecker, J.R.; Siener, C.A.; Wulf, C.O.; Anand, P.; Golumbek, P.T.; Zaidman, C.M.; Philip Miller, J.; Lowes, L.P.; Alfano, L.N.; Viollet-Callendret, L.; Flanigan, K.M.; Mendell, J.R.; McDonald, C.M.; Goude, E.; Johnson, L.; Nicorici, A.; Karachunski, P.I.; Day, J.W.; Dalton, J.C.; Farber, J.M.; Buser, K.K.; Darras, B.T.; Kang, P.B.; Riley, S.O.; Shriber, E.; Parad, R.; Bushby, K.; Eagle, M. Motor and cognitive assessment of infants and young boys with Duchenne muscular dystrophy: Results from the muscular dystrophy association DMD clinical research network. *Neuromuscul. Disord.* **2013**, *23*, 529–39.
7. Mazzone, E.; Martinelli, D.; Berardinelli, A.; Messina, S.; D'Amico, A.; Vasco, G.; Main, M.; Doglio, L.; Politano, L.; Cavallaro, F.; Frosini, S.; Bello, L.; Carlesi, A.; Bonetti, A.M.; Zucchini, E.; Sanctis, R. De; Scutifero, M.; Bianco, F.; Rossi, F.; Motta, M.C.; Sacco, A.; Donati, M.A.; Mongini, T.; Pini, A.; Battini, R.; Pegoraro, E.; Pane, M.; Pasquini, E.; Bruno, C.; Vita, G.; Waure, C. de; Bertini, E.; Mercuri, E. North Star Ambulatory Assessment, 6-minute walk test and timed items in ambulant boys with Duchenne muscular dystrophy. *Neuromuscul. Disord.* **2010**, *20*, 712–6.
8. Nardes, F.; Araújo, A.P.Q.C.; Ribeiro, M.G. Mental retardation in Duchenne muscular dystrophy. *J. Pediatr. (Rio. J).* **2012**, *88*, 6–16.
9. Brooke, M.H.; Fenichel, G.M.; Griggs, R.C.; Mendell, J.R.; Moxley, R.; Florence, J.; King, W.M.; Pandya, S.; Robison, J.; Schierbecker, J.; Signore, L.; Miller, J.P.; Gilder, B.F.; Kaiser, K.K.; Mandel, S.; Arfken, C. Duchenne muscular dystrophy: Patterns of clinical progression and effects of supportive therapy. *Neurology* **1989**, *39*, 475–81.
10. Chang, R.F.; Mubarak, S.J. Pathomechanics of gowers' sign: A video analysis of a spectrum of gowers' maneuvers. *Clin. Orthop. Relat. Res.* **2012**, *470*, 1987–71.
11. Birnkrant, D.J.; Bushby, K.; Bann, C.M.; Apkon, S.D.; Blackwell, A.; Brumbaugh, D.; Case, L.E.; Clemens, P.R.; Hadjiyannakis, S.; Pandya, S.; Street, N.; Tomezsko, J.; Wagner, K.R.; Ward, L.M.; Weber, D.R. Diagnosis and management of Duchenne muscular dystrophy, part 1: diagnosis, and neuromuscular, rehabilitation, endocrine, and gastrointestinal and nutritional management. *Lancet Neurol.* **2018**, *17*, 251–67.
12. Bushby, K.; Hill, A.; Steele, J. Failure of early diagnosis in symptomatic Duchenne muscular dystrophy. *Lancet* **1999**, *353*, 557–8.
13. Wong, S.H.; McClaren, B.J.; Archibald, A.D.; Weeks, A.; Langmaid, T.; Ryan, M.M.; Kornberg, A.; Metcalfe, S.A. A mixed methods study of age at diagnosis and diagnostic odyssey for Duchenne muscular dystrophy. *Eur. J. Hum. Genet.* **2015**, *23*, 1294–300.

14. Koeks, Z.; Bladen, C.L.; Salgado, D.; Van Zwet, E.; Pogoryelova, O.; McMacken, G.; Monges, S.; Foncuberta, M.E.; Kekou, K.; Kosma, K.; Dawkins, H.; Lamont, L.; Bellgard, M.I.; Roy, A.J.; Chamova, T.; Guergueltcheva, V.; Chan, S.; Korngut, L.; Campbell, C.; Dai, Y.; Wang, J.; Barišić, N.; Brabec, P.; Lähdetie, J.; Walter, M.C.; Schreiber-Katz, O.; Karcagi, V.; Garami, M.; Herczegfalvi, A.; Viswanathan, V.; Bayat, F.; Buccella, F.; Ferlini, A.; Kimura, E.; Van Den Bergen, J.C.; Rodrigues, M.; Roxburgh, R.; Lusakowska, A.; Kostera-Pruszczyk, A.; Santos, R.; Neagu, E.; Artemieva, S.; Rasic, V.M.; Vojinovic, D.; Posada, M.; Bloetzer, C.; Klein, A.; Díaz-Manera, J.; Gallardo, E.; Karaduman, A.A.; Oznur, T.; Topalolu, H.; El Sherif, R.; Stringer, A.; Shatillo, A. V.; Martin, A.S.; Peay, H.L.; Kirschner, J.; Flanigan, K.M.; Straub, V.; Bushby, K.; Béroud, C.; Verschuuren, J.J.; Lochmüller, H. Clinical Outcomes in Duchenne Muscular Dystrophy: A Study of 5345 Patients from the TREAT-NMD DMD Global Database. *J. Neuromuscul. Dis.* **2017**, *4*, 293–306.

15. Moizard, M.P.; Toutain, A.; Fournier, D.; Berret, F.; Raynaud, M.; Billard, C.; Andres, C.; Moraine, C. Severe cognitive impairment in DMD: obvious clinical indication for Dp71 isoform point mutation screening. *Eur. J. Hum. Genet.* **2000**, *8*, 552–6.

16. Daoud, F.; Angeard, N.; Demerre, B.; Martie, I.; Benyaou, R.; Leturcq, F.; Cossée, M.; Deburgrave, N.; Saillour, Y.; Tuffery, S.; Urtizberea, A.; Toutain, A.; Echenne, B.; Frischman, M.; Mayer, M.; Desguerre, I.; Estournet, B.; Réveillère, C.; Penisson-Besnier; Cuisset, J.M.; Kaplan, J.C.; Héron, D.; Rivier, F.; Chelly, J. Analysis of Dp71 contribution in the severity of mental retardation through comparison of Duchenne and Becker patients differing by mutation consequences on Dp71 expression. *Hum. Mol. Genet.* **2009**, *18*, 3779–94.

17. Battini, R.; Chieffo, D.; Bulgheroni, S.; Piccini, G.; Pecini, C.; Lucibello, S.; Lenzi, S.; Moriconi, F.; Pane, M.; Astrea, G.; Baranello, G.; Alfieri, P.; Vicari, S.; Riva, D.; Cioni, G.; Mercuri, E. Cognitive profile in Duchenne muscular dystrophy boys without intellectual disability: The role of executive functions. *Neuromuscul. Disord.* **2018**, *28*, 122–8.

18. Passamano, L.; Taglia, A.; Palladino, A.; Viggiano, E.; D'Ambrosio, P.; Scutifero, M.; Cecio, M.R.; Torre, V.; De Luca, F.; Picillo, E.; Paciello, O.; Piluso, G.; Nigro, G.; Politano, L. Improvement of survival in Duchenne Muscular Dystrophy: Retrospective analysis of 835 patients. *Acta Myol.* **2012**, *31*, 121–5.

19. Henricson, E.K.; Abresch, R.T.; Cnaan, A.; Hu, F.; Duong, T.; Arrieta, A.; Han, J.; Escolar, D.M.; Florence, J.M.; Clemens, P.R.; Hoffman, E.P.; McDonald, C.M.; Vishwanathan, V.; Chidambaranathan, S.; Biggar, W.D.; Mah, J.K.; Tulinius, M.; Leshner, R.; Tesi-Rocha, C.; Kornberg, A.; Ryan, M.; Nevo, Y.; Dubrovsky, A.; Kuntz, N.; Driscoll, S.; Connolly, A.; Pestronk, A.; Teasley, J.; Bertorini, T.; North, K.; Kolski, H.; Carlo, J.; Gorni, K.; Lotze, T.; Day, J.; Benditt, J.; Boitano, L.; Birnkrant, D.; Connuck, D.; Finder, J.; Hinton, V.; Mathews, K.; Moxley, R.; Sparks, S.; Gordon, E.; Cregan, M.; Goude, E.; Glick, M.; Johnson, L.; Joyce, N.; Lipa, B.; Nicorici, A.; Skalsky, A.; Witt, A.; Kumar, S.; Eliasoph, L.; Hosaki, E.; Gonzales, A.; Harris, V.; Chiu, A.; Goia, E.; Thannhauser, J.; Walker, L.; Wright, C.; Yousefi, M.; Alhander, A.C.; Berglund, L.; Ekstrom, A.B.; Kroksmark, A.K.; Sterky, U.; Birkmeier, M.; Kaminski, S.; Carroll, K.; DeValle, K.; Kennedy, R.; Villano, D.; Leve, A.B.; Shurr, I.; Wisband, E.; Yaffe, D.; Andreone, L.; Corderi, J.; Mesa, L.; Levi, L.; Coleman-Wood, K.; Hoffman, A.; Korn-Petersen, W.; Selcen, D.; Abdel-Hamid, H.; Bise, C.; Craig, A.; Hughes, S.; Nguyen, C.; Weimer, J.; Golumbak, P.; Lopate, G.; Malane, J.; Malkus, B.; Nozaki, K.; Renna, R.; Schierbacker, J.; Seiner, C.; Wulf, C.; Blair, S.; Grillo, B.; Jones, K.; Monasterio, E.; Clift, J.; Feliciano, C.; Igarashi, M.; Young, R.; Rose, K.; Webster, R.; Wicks, S.; Chen, L.; Kennedy, C.; Deliz, B.; Espada, S.; Fuste, P.; Luciano, C.; Capone, L.; Beneggi, M.; Morettini, V.; Gupta, A.; McNeil, R.; Erickson, A.; Margolis, M.; Naughton, C.; Parry, G.; Walk, D.; Bartley, N.; Canelos, P.; Casper, R.; Hache, L.; Ahmed, M.; Zimmerman, A. The cooperative international neuromuscular research group Duchenne natural history study: Glucocorticoid treatment preserves clinically meaningful functional milestones and reduces rate of disease progression as measured by manual muscle testing and othe. *Muscle and Nerve* **2013**, *48*, 55–

67.

20. Power, L.C.; O'Grady, G.L.; Hornung, T.S.; Jefferies, C.; Gusso, S.; Hofman, P.L. Imaging the heart to detect cardiomyopathy in Duchenne muscular dystrophy: A review. *Neuromuscul. Disord.* **2018**, *28*, 717–30.

21. Sanyal, S.K.; Johnson, W.W.; Thapar, M.K.; Pitner, S.E. An ultrastructural basis for electrocardiographic alterations associated with Duchenne's progressive muscular dystrophy. *Circulation* **1978**, *57*, 1122–9.

22. Sanyal, S.K.; Johnson, W.W. Cardiac conduction abnormalities in children with Duchenne's progressive muscular dystrophy: electrocardiographic features and morphologic correlates. *Circulation* **1982**, *66*, 853–63.

23. Perloff, J.K.; Roberts, W.C.; de Leon, A.C., J.; O'Doherty, D. The distinctive electrocardiogram of Duchenne's progressive muscular dystrophy. An electrocardiographic-pathologic correlative study. *Am. J. Med.* **1967**, *42*, 179–88.

24. Mehmood, M.; Hor, K.N.; Al-Khalidi, H.R.; Benson, D.W.; Jefferies, J.L.; Taylor, M.D.; Egnaczyk, G.F.; Raman, S. V.; Basu, S.K.; Cripe, L.H.; Germann, J.; Mazur, W. Comparison of right and left ventricular function and size in Duchenne muscular dystrophy. *Eur. J. Radiol.* **2015**, *84*, 1938–42.

25. Frankel, K.A.; Rosser, R.J. The pathology of the heart in progressive muscular dystrophy: Epimyocardial fibrosis. *Hum. Pathol.* **1976**, *7*, 375–86.

26. Hor, K.N.; Taylor, M.D.; Al-Khalidi, H.R.; Cripe, L.H.; Raman, S. V; Jefferies, J.L.; O'Donnell, R.; Benson, D.W.; Mazur, W. Prevalence and distribution of late gadolinium enhancement in a large population of patients with Duchenne muscular dystrophy: effect of age and left ventricular systolic function. *J. Cardiovasc. Magn. Reson.* **2013**, *15*, 107.

27. Nigro, G.; Comi, L.I.; Politano, L.; Bain, R.J.I. The incidence and evolution of cardiomyopathy in Duchenne muscular dystrophy. *Int. J. Cardiol.* **1990**, *26*, 271–7.

28. Wang, M.; Birnkrant, D.J.; Super, D.M.; Jacobs, I.B.; Bahler, R.C. Progressive left ventricular dysfunction and long-term outcomes in patients with Duchenne muscular dystrophy receiving cardiopulmonary therapies. *Open Hear.* **2018**, *5*, 1–8.

29. da Silva, T.D.; Massetti, T.; Crocetta, T.B.; de Mello Monteiro, C.B.; Carll, A.; Vanderlei, L.C.M.; Arbaugh, C.; Oliveira, F.R.; de Abreu, L.C.; Ferreira Filho, C.; Godleski, J.; Ferreira, C. Heart Rate Variability and Cardiopulmonary Dysfunction in Patients with Duchenne Muscular Dystrophy: A Systematic Review. *Pediatr. Cardiol.* **2018**, *39*, 869–83.

30. Monaco, A.P.; Neve, R.L.; Colletti-Feener, C.; Bertelson, C.J.; Kurnit, D.M.; Kunkel, L.M. Isolation of candidate cDNAs for portions of the Duchenne muscular dystrophy gene. *Nature* **1986**, *323*, 646–50.

31. Taglia, A.; Petillo, R.; D'Ambrosio, P.; Picillo, E.; Torella, A.; Orsini, C.; Ergoli, M.; Scutifero, M.; Passamano, L.; Palladino, A.; Nigro, G.; Politano, L. Clinical features of patients with dystrophinopathy sharing the 45-55 exon deletion of DMD gene. *Acta Myol.* **2015**, *34*, 9–13.

32. Mori-Yoshimura, M.; Mitsuhashi, S.; Nakamura, H.; Komaki, H.; Goto, K.; Yonemoto, N.; Takeuchi, F.; Hayashi, Y.K.; Murata, M.; Takahashi, Y.; Nishino, I.; Takeda, S.; Kimura, E. Characteristics of Japanese patients with becker muscular dystrophy and intermediate muscular dystrophy in a Japanese national registry of muscular dystrophy (Remudy): Heterogeneity and clinical variation. *J. Neuromuscul. Dis.* **2018**, *5*, 193–203.

33. Aartsma-Rus, A.; Van Deutekom, J.C.T.; Fokkema, I.F.; Van Ommen, G.J.B.; Den Dunnen, J.T. Entries in the Leiden Duchenne muscular dystrophy mutation database: An overview of mutation types and paradoxical cases that confirm the reading-frame rule. *Muscle and Nerve*

2006, *34*, 135–44.

34. Monaco, A.P.; Bertelson, C.J.; Liechti-Gallati, S.; Moser, H.; Kunkel, L.M. An explanation for the phenotypic differences between patients bearing partial deletions of the DMD locus. *Genomics* **1988**, *2*, 90–5.

35. Bladen, C.L.; Salgado, D.; Monges, S.; Foncuberta, M.E.; Kekou, K.; Kosma, K.; Dawkins, H.; Lamont, L.; Roy, A.J.; Chamova, T.; Guergueltcheva, V.; Chan, S.; Korngut, L.; Campbell, C.; Dai, Y.; Wang, J.; Barisic, N.; Brabec, P.; Lahdetie, J.; Walter, M.C.; Schreiber-Katz, O.; Karcagi, V.; Garami, M.; Viswanathan, V.; Bayat, F.; Buccella, F.; Kimura, E.; Koeks, Z.; van den Bergen, J.C.; Rodrigues, M.; Roxburgh, R.; Lusakowska, A.; Kostera-Pruszczyk, A.; Zimowski, J.; Santos, R.; Neagu, E.; Artemieva, S.; Rasic, V.M.; Vojinovic, D.; Posada, M.; Bloetzer, C.; Jeannet, P.Y.; Joncourt, F.; Díaz-Manera, J.; Gallardo, E.; Karaduman, A.A.; Topaloglu, H.; El Sherif, R.; Stringer, A.; Shatillo, A. V.; Martin, A.S.; Peay, H.L.; Bellgard, M.I.; Kirschner, J.; Flanigan, K.M.; Straub, V.; Bushby, K.; Verschuuren, J.; Aartsma-Rus, A.; Béroud, C.; Lochmüller, H. The TREAT-NMD DMD global database: Analysis of more than 7,000 duchenne muscular dystrophy mutations. *Hum. Mutat.* **2015**, *36*, 395–402.

36. Van Den Bergen, J.C.; Wokke, B.H.; Janson, A.A.; Van Duinen, S.G.; Hulsker, M.A.; Ginjaar, H.B.; Van Deutekom, J.C.; Aartsma-Rus, A.; Kan, H.E.; Verschuuren, J.J.G.M. Dystrophin levels and clinical severity in Becker muscular dystrophy patients. *J. Neurol. Neurosurg. Psychiatry* **2014**, *85*, 747–53.

37. Carsana, A.; Frisso, G.; Tremolaterra, M.R.; Lanzillo, R.; Vitale, D.F.; Santoro, L.; Salvatore, F. Analysis of dystrophin gene deletions indicates that the hinge III region of the protein correlates with disease severity. *Ann. Hum. Genet.* **2005**, *69*, 253–9.

38. Ricotti, V.; Mandy, W.P.L.; Scoto, M.; Pane, M.; Deconinck, N.; Messina, S.; Mercuri, E.; Skuse, D.H.; Muntoni, F. Neurodevelopmental, emotional, and behavioural problems in Duchenne muscular dystrophy in relation to underlying dystrophin gene mutations. *Dev. Med. Child Neurol.* **2016**, *58*, 77–84.

39. Nudel, U.; Zuk, D.; Einat, P.; Zeelon, E.; Levy, Z.; Neuman, S.; Yaffe, D. Duchenne muscular dystrophy gene product is not identical in muscle and brain. *Nature* **1989**, *337*, 76–8.

40. Muntoni, F.; Melis, M.A.; Ganau, A.; Dubowitz, V. Transcription of the dystrophin gene in normal tissues and in skeletal muscle of a family with X-linked dilated cardiomyopathy. *Am J Hum Genet* **1995**, *56*, 151–7.

41. Bies, R.D.; Friedman, D.; Roberts, R.; Perryman, M.B.; Caskey, C.T. Expression and localization of dystrophin in human cardiac Purkinje fibers. *Circulation* **1992**, *86*, 147–53.

42. D'souza, V.N.; Man, N.T.; Morris, G.E.; Karges, W.; Pillers, D.A.M.; Ray, P.N. A novel dystrophin isoform is required for normal retinal electrophysiology. *Hum. Mol. Genet.* **1995**, *4*, 837–42.

43. Muntoni, F.; Torelli, S.; Ferlini, A. Dystrophin and mutations: One gene, several proteins, multiple phenotypes. *Lancet Neurol.* **2003**, *2*, 731–40.

44. Lidov, H.G.W.; Selig, S.; Kunkel, L.M. Dp140: A novel 140 kDa CNS transcript from the dystrophin locus. *Hum. Mol. Genet.* **1995**, *4*, 329–35.

45. Byers, T.J.; Lidov, H.G.W.; Kunkel, L.M. An alternative dystrophin transcript specific to peripheral nerve. *Nat. Genet.* **1993**, *4*, 77–81.

46. Hugnot, J.P.; Gilgenkrantz, H.; Vincent, N.; Chafey, P.; Morris, G.E.; Monaco, A.P.; Berwald-Netter, Y.; Koulakoff, A.; Kaplan, J.C.; Kahn, A. Distal transcript of the dystrophin gene initiated from an alternative first exon and encoding a 75-kDa protein widely distributed in nonmuscle tissues. *Proc. Natl. Acad. Sci. U. S. A.* **1992**, *89*, 7506–10.

47. Tadayoni, R.; Rendon, A.; Soria-Jasso, L.E.; Cisneros, B. Dystrophin Dp71: The smallest but

multifunctional product of the duchenne muscular dystrophy gene. *Mol. Neurobiol.* **2012**, *45*, 43–60.

48. Tozawa, T.; Itoh, K.; Yaoi, T.; Tando, S.; Umekage, M.; Dai, H.; Hosoi, H.; Fushiki, S. The shortest isoform of dystrophin (Dp40) interacts with a group of presynaptic proteins to form a presumptive novel complex in the mouse brain. *Mol. Neurobiol.* **2012**, *45*, 287–97.

49. Martínez-Herrera, A.; Aragón, J.; Bermúdez-Cruz, R.M.; Bazán, M.L.; Soid-Raggi, G.; Ceja, V.; Santos Coy-Arechavaleta, A.; Alemán, V.; Depardón, F.; Montañez, C. In silico analyses of dystrophin Dp40 cellular distribution, nuclear export signals and structure modeling. *Data Br.* **2015**, *4*, 349–52.

50. Way, M.; Pope, B.; Cross, R.A.; Kendrick-Jones, J.; Weeds, A.G. Expression of the N-terminal domain of dystrophin in E. coli and demonstration of binding to F-actin. *FEBS Lett.* **1992**, *301*, 243–5.

51. Stone, M.R.; O'Neill, A.; Catino, D.; Bloch, R.J. Specific Interaction of the Actin-binding Domain of Dystrophin with Intermediate Filaments Containing Keratin 19. *Mol. Biol. Cell* **2005**, *16*, 4280–93.

52. Rybakova, I.N.; Humston, J.L.; Sonnemann, K.J.; Ervasti, J.M. Dystrophin and utrophin bind actin through distinct modes of contact. *J. Biol. Chem.* **2006**, *281*, 9996–10001.

53. Gao, Q.Q.; McNally, E.M. The dystrophin complex: Structure, function, and implications for therapy. *Compr. Physiol.* **2015**, *5*, 1223–39.

54. Jung, D.; Yang, B.; Meyer, J.; Chamberlain, J.S.; Campbell, K.P. Identification and characterization of the dystrophin anchoring site on β-dystroglycan. *J. Biol. Chem.* **1995**, *270*, 27305–10.

55. Sadoulet-Puccio, H.M.; Rajala, M.; Kunkel, L.M. Dystrobrevin and dystrophin: an interaction through coiled-coil motifs. *Proc. Natl. Acad. Sci. U. S. A.* **1997**, *94*, 12413–8.

56. Adams, M.E.; Odom, G.L.; Kim, M.J.; Chamberlain, J.S.; Froehner, S.C. Syntrophin binds directly to multiple spectrin-like repeats in dystrophin and mediates binding of nNOS to repeats 16-17. *Hum. Mol. Genet.* **2018**, *27*, 2978–85.

57. Blake, D.J.; Weir, A.; Newey, S.E.; Davies, K.E. Function and genetics of dystrophin and dystrophin-related proteins in muscle. *Physiol. Rev.* **2002**, *82*, 291–329.

58. Davies, K.E.; Nowak, K.J. Molecular mechanisms of muscular dystrophies: old and new players. *Nat Rev Mol Cell Biol* **2006**, *7*, 762–73.

59. Koenig, M.; Monaco, A.P.; Kunkel, L.M. The complete sequence of dystrophin predicts a rod-shaped cytoskeletal protein. *Cell* **1988**, *53*, 219–28.

60. Kahana, E.; Marsh, P.J.; Henry, A.J.; Way, M.; Gratzer, W.B. Conformation and phasing of dystrophin structural repeats. *J. Mol. Biol.* **1994**, *235*, 1271–7.

61. Delalande, O.; Molza, A.E.; Dos Santos Morais, R.; Chéron, A.; Pollet, É.; Raguenes-Nicol, C.; Tascon, C.; Giudice, E.; Guilbaud, M.; Nicolas, A.; Bondon, A.; Leturcq, F.; Férey, N.; Baaden, M.; Perez, J.; Roblin, P.; Piétri-Rouxel, F.; Hubert, J.F.; Czjzek, M.; Le Rumeur, E. Dystrophin's central domain forms a complex filament that becomes disorganized by in-frame deletions. *J. Biol. Chem.* **2018**, *293*, 6637–46.

62. Belanto, J.J.; Mader, T.L.; Eckhoff, M.D.; Strandjord, D.M.; Banks, G.B.; Gardner, M.K.; Lowe, D.A.; Ervasti, J.M. Microtubule binding distinguishes dystrophin from utrophin. *Proc. Natl. Acad. Sci. U. S. A.* **2014**, *111*, 5723–5728.

63. Le Rumeur, E.; Fichou, Y.; Pottier, S.; Gaboriau, F.; Rondeau-Mouro, C.; Vincent, M.; Gallay, J.; Bondon, A. Interaction of dystrophin rod domain with membrane phospholipids: Evidence of a close proximity between tryptophan residues and lipids. *J. Biol. Chem.* **2003**, *278*, 5993–6001.

64. Hnia, K.; Zouiten, D.; Cantel, S.; Chazalette, D.; Hugon, G.; Fehrentz, J.-A.; Masmoudi, A.; Diment, A.; Bramham, J.; Mornet, D.; Winder, S.J. ZZ domain of dystrophin and utrophin: topology and mapping of a β-dystroglycan interaction site. *Biochem. J.* **2007**, *401*, 667–77.

65. Amenta, A.R.; Yilmaz, A.; Bogdanovich, S.; McKechnie, B.A.; Abedi, M.; Khurana, T.S.; Fallon, J.R. Biglycan recruits utrophin to the sarcolemma and counters dystrophic pathology in mdx mice. *Proc. Natl. Acad. Sci. U. S. A.* **2011**, *108*, 762–7.

66. Haddix, S.G.; Lee, Y. Il; Kornegay, J.N.; Thompson, W.J. Cycles of myofiber degeneration and regeneration lead to remodeling of the neuromuscular junction in two mammalian models of Duchenne muscular dystrophy. *PLoS One* **2018**, *13*, e0205926.

67. van der Pijl, E.M.; van Putten, M.; Niks, E.H.; Verschuuren, J.J.G.M.; Aartsma-Rus, A.; Plomp, J.J. Low dystrophin levels are insufficient to normalize the neuromuscular synaptic abnormalities of mdx mice. *Neuromuscul. Disord.* **2018**, *28*, 427–42.

68. Clerk, A.; Morris, G.E.; Dubowitz, V.; Davies, K.E.; Sewry, C.A. Dystrophin-related protein, utrophin, in normal and dystrophic human fetal skeletal muscle. *Histochem. J.* **1993**, *25*, 554–61.

69. Helliwell, T.R.; Nguyen thi, M.; Morris, G.E.; Davies, K.E. The dystrophin-related protein, utrophin, is expressed on the sarcolemma of regenerating human skeletal muscle fibres in dystrophies and inflammatory myopathies. *Neuromuscul. Disord.* **1992**, *2*, 177–84.

70. Law, D.J.; Allen, D.L.; Tidball, J.G. Talin, vinculin and DRP (utrophin) concentrations are increased at mdx myotendinous junctions following onset of necrosis. *J. Cell Sci.* **1994**, *107*, 1477–83.

71. Blake, D.J.; Tinsley, J.M.; Davies, K.E. Utrophin: A structural and functional comparison to dystrophin. *Brain Pathol.* **1996**, *6*, 37–47.

72. Winder, S.J.; Hemmings, L.; Maciver, S.K.; Bolton, S.J.; Tinsley, J.M.; Davies, K.E.; Critchley, D.R.; Kendrick-Jones, J. Utrophin actin binding domain: analysis of actin binding and cellular targeting. *J. Cell Sci.* **1995**, *108*, 63–71.

73. Deconinck, a E.; Rafael, J. a; Skinner, J. a; Brown, S.C.; Potter, a C.; Metzinger, L.; Watt, D.J.; Dickson, J.G.; Tinsley, J.M.; Davies, K.E. Utrophin-dystrophin-deficient mice as a model for Duchenne muscular dystrophy. *Cell* **1997**, *90*, 717–27.

74. McGreevy, J.W.; Hakim, C.H.; McIntosh, M.A.; Duan, D. Animal models of Duchenne muscular dystrophy: from basic mechanisms to gene therapy. *Dis Model Mech* **2015**, *8*, 195–213.

75. Bulfield, G.; Siller, W.G.; Wight, P.A.; Moore, K.J. X chromosome-linked muscular dystrophy (mdx) in the mouse. *Proc. Natl. Acad. Sci. U. S. A.* **1984**, *81*, 1189–92.

76. Sicinski, P.; Geng, Y.; Ryder-Cook, A.S.; Barnard, E.A.; Darlison, M.G.; Barnard, P.J. The molecular basis of muscular dystrophy in the mdx mouse: a point mutation. *Science* **1989**, *244*, 1578–80.

77. Pastoret, C.; Sebille, A. mdx mice show progressive weakness and muscle deterioration with age. *J. Neurol. Sci.* **1995**, *129*, 97–105.

78. Lynch, G.S.; Hinkle, R.T.; Chamberlain, J.S.; Brooks, S. V.; Faulkner, J.A. Force and power output of fast and slow skeletal muscles from mdx mice 6-28 months old. *J. Physiol.* **2001**, *535*, 591–600.

79. Dupont-Versteegden, E.E.; McCarter, R.J. Differential expression of muscular dystrophy in diaphragm versus hindlimb muscles of mdx mice. *Muscle Nerve* **1992**, *15*, 1105–10.

80. Louboutin, J.P.; Fichter-Gagnepain, V.; Thaon, E.; Fardeau, M. Morphometric analysis of mdx diaphragm muscle fibres. Comparison with hindlimb muscles. *Neuromuscul. Disord.* **1993**, *3*, 463–9.

81. Stuckey, D.J.; Carr, C.A.; Camelliti, P.; Tyler, D.J.; Davies, K.E.; Clarke, K. In vivo MRI characterization of progressive cardiac dysfunction in the mdx mouse model of muscular dystrophy. *PLoS One* **2012**, *7*, e28569.

82. Chu, V.; Otero, J.M.; Lopez, O.; Sullivan, M.F.; Morgan, J.P.; Amende, I.; Hampton, T.G. Electrocardiographic findings in mdx mice: A cardiac phenotype of Duchenne muscular dystrophy. *Muscle and Nerve* **2002**, *26*, 513–9.

83. Wehling-Henricks, M.; Jordan, M.C.; Roos, K.P.; Deng, B.; Tidball, J.G. Cardiomyopathy in dystrophin-deficient hearts is prevented by expression of a neuronal nitric oxide synthase transgene in the myocardium. *Hum. Mol. Genet.* **2005**, *14*, 1921–33.

84. Chamberlain, J.S.; Metzger, J.; Reyes, M.; Townsend, D.; Faulkner, J. a Dystrophin-deficient mdx mice display a reduced life span and are susceptible to spontaneous rhabdomyosarcoma. *FASEB J.* **2007**, *21*, 2195–2204.

85. Verhaart, I.E.C.; van Duijn, R.J.M.; den Adel, B.; Roest, A. a. W.; Verschuuren, J.J.G.M.; Aartsma-Rus, A.; van der Weerd, L. Assessment of cardiac function in three mouse dystrophinopathies by magnetic resonance imaging. *Neuromuscul. Disord.* **2012**, *22*, 418–26.

86. Chandrasekharan, K.; Yoon, J.H.; Xu, Y.; DeVries, S.; Camboni, M.; Janssen, P.M.L.; Varki, A.; Martin, P.T. A human-specific deletion in mouse Cmah increases disease severity in the mdx model of Duchenne muscular dystrophy. *Sci. Transl. Med.* **2010**, *2*, 42ra54.

87. Betts, C.A.; McClorey, G.; Healicon, R.; Hammond, S.M.; Manzano, R.; Muses, S.; Ball, V.; Godfrey, C.; Merritt, T.M.; Westering, T.; O'Donovan, L.; Wells, K.E.; Gait, M.J.; Wells, D.J.; Tyler, D.; Wood, M.J. Cmah-dystrophin deficient mdx mice display an accelerated cardiac phenotype that is improved following peptide-PMO exon skipping treatment. *Hum. Mol. Genet.* **2018**, *28*, 396–406.

88. Fukada, S.I.; Morikawa, D.; Yamamoto, Y.; Yoshida, T.; Sumie, N.; Yamaguchi, M.; Ito, T.; Miyagoe-Suzuki, Y.; Takeda, S.; Tsujikawa, K.; Yamamoto, H. Genetic background affects properties of satellite cells and mdx phenotypes. *Am. J. Pathol.* **2010**, *176*, 2414–24.

89. Rodrigues, M.; Echigoya, Y.; Maruyama, R.; Lim, K.R.Q.; Fukada, S.I.; Yokota, T. Impaired regenerative capacity and lower revertant fibre expansion in dystrophin-deficient mdx muscles on DBA/2 background. *Sci. Rep.* **2016**, *6*, p38371.

90. Gordish-Dressman, H.; Willmann, R.; Pazze, L.D.; Kreibich, A.; van Putten, M.; Heydemann, A.; Bogdanik, L.; Lutz, C.; Davies, K.; Demonbruen, A.R.; Duan, D.; Elsey, D.; Fukada, S.-I.; Girgenrath, M.; Gonzalez, J.P.; Grounds, M.D.; Nichols, A.; Partridge, T.; Passini, M.; Sanarica, F.; Schnell, F.J.; Wells, D.J.; Yokota, T.; Young, C.S.; Zhong, Z.; Spurney, C.; Spencer, M.; De Luca, A.; Nagaraju, K.; Aartsma-Rus, A. "Of Mice and Measures": A Project to Improve How We Advance Duchenne Muscular Dystrophy Therapies to the Clinic. *J. Neuromuscul. Dis.* **2018**, *5*, 407–17.

91. Coley, W.D.; Bogdanik, L.; Vila, M.C.; Yu, Q.; Van Der Meulen, J.H.; Rayavarapu, S.; Novak, J.S.; Nearing, M.; Quinn, J.L.; Saunders, A.; Dolan, C.; Andrews, W.; Lammert, C.; Austin, A.; Partridge, T.A.; Cox, G.A.; Lutz, C.; Nagaraju, K. Effect of genetic background on the dystrophic phenotype in mdx mice. *Hum. Mol. Genet.* **2016**, *25*, 130–45.

92. Zhao, W.; Zhao, T.; Chen, Y.; Zhao, F.; Gu, Q.; Williams, R.W.; Bhattacharya, S.K.; Lu, L.; Sun, Y. A murine hypertrophic cardiomyopathy model: The DBA/2J strain. *PLoS One* **2015**, *10*, e0133132.

93. Cooper, B.J.; Winand, N.J.; Stedman, H.; Valentine, B.A.; Hoffman, E.P.; Kunkel, L.M.; Scott, M.O.; Fischbeck, K.H.; Kornegay, J.N.; Avery, R.J.; Williams, J.R.; Schmickel, R.D.; Sylvester, J.E. The homologue of the Duchenne locus is defective in X-linked muscular dystrophy of dogs. *Nature* **1988**, *334*, 154–6.

94. Duan, D. Duchenne muscular dystrophy gene therapy in the canine model. *Hum. Gene Ther. Clin. Dev.* **2015**, *26*, 57–69.

95. Shimatsu, Y.; Katagiri, K.; Furuta, T.; Nakura, M.; Tanioka, Y.; Yuasa, K.; Tomohiro, M.; Kornegay, J.N.; Nonaka, I.; Takeda, S. Canine X-linked muscular dystrophy in Japan (CXMDJ). *Exp. Anim.* **2003**, *52*, 93–7.

96. Yugeta, N.; Urasawa, N.; Fujii, Y.; Yoshimura, M.; Yuasa, K.; Wada, M.R.; Nakura, M.; Shimatsu, Y.; Tomohiro, M.; Takahashi, A.; Machida, N.; Wakao, Y.; Nakamura, A.; Takeda, S. Cardiac involvement in Beagle-based canine X-linked muscular dystrophy in Japan (CXMDJ): Electrocardiographic, echocardiographic, and morphologic studies. *BMC Cardiovasc. Disord.* **2006**, *6*.

97. Yu, X.; Bao, B.; Echigoya, Y.; Yokota, T. Dystrophin-deficient large animal models: Translational research and exon skipping. *Am. J. Transl. Res.* **2015**, *7*, 1314–31.

98. Passerini, L.; Bernasconi, P.; Baggi, F.; Confalonieri, P.; Cozzi, F.; Cornelio, F.; Mantegazza, R. Fibrogenic cytokines and extent of fibrosis in muscle of dogs with X-linked golden retriever muscular dystrophy. *Neuromuscul. Disord.* **2002**, *12*, 828–35.

99. Shimatsu, Y.; Yoshimura, M.; Yuasa, K.; Urasawa, N.; Tomohiro, M.; Nakura, M.; Tanigawa, M.; Nakamura, A.; Takeda, S. Major clinical and histopathological characteristics of canine X-linked muscular dystrophy in Japan, CXMDJ. *Acta Myol.* **2005**, *24*, 145–54.

100. Barthélémy, I.; Pinto-Mariz, F.; Yada, E.; Desquilbet, L.; Savino, W.; Silva-Barbosa, S.D.; Faussat, A.-M.; Mouly, V.; Voit, T.; Blot, S.; Butler-Browne, G. Predictive markers of clinical outcome in the GRMD dog model of Duchenne muscular dystrophy. *Dis. Model. Mech.* **2014**, *7*, 1253–61.

101. Moise, N.S.; Valentine, B.A.; Brown, C.A.; Erb, H.N.; Beck, K.A.; Cooper, B.J.; Gilmour, R.F. Duchenne's cardiomyopathy in a canine model: Electrocardiographic and echocardiographic studies. *J. Am. Coll. Cardiol.* **1991**, *17*, 812–20.

102. Kornegay, J.N. The golden retriever model of Duchenne muscular dystrophy. *Skelet. Muscle* **2017**, *7*, 9.

103. Allen, D.G.; Whitehead, N.P. Duchenne muscular dystrophy--what causes the increased membrane permeability in skeletal muscle? *Int. J. Biochem. Cell Biol.* **2011**, *43*, 290–4.

104. Wehrens, X.H.T.; Lehnart, S.E.; Reiken, S.R.; Marks, A.R. Ca2+/calmodulin-dependent protein kinase II phosphorylation regulates the cardiac ryanodine receptor. *Circ. Res.* **2004**, *94*, e61-70.

105. Shan, J.; Betzenhauser, M.J.; Kushnir, A.; Reiken, S.; Meli, A.C.; Wronska, A.; Dura, M.; Chen, B.X.; Marks, A.R. Role of chronic ryanodine receptor phosphorylation in heart failure and beta-adrenergic receptor blockade in mice. *J. Clin. Invest.* **2010**, *120*, 4375–87.

106. Shirokova, N.; Niggli, E. Cardiac phenotype of Duchenne Muscular Dystrophy: Insights from cellular studies. *J. Mol. Cell. Cardiol.* **2013**, *58*, 217–24.

107. Reiken, S.; Lacampagne, A.; Zhou, H.; Kherani, A.; Lehnart, S.E.; Ward, C.; Huang, F.; Gaburjakova, M.; Gaburjakova, J.; Rosemblit, N.; Warren, M.S.; He, K. lun; Yi, G. hua; Wang, J.; Burkhoff, D.; Vassort, G.; Marks, A.R. PKA phosphorylation activates the calcium release channel (ryanodine receptor)-in skeletal muscle: Defective regulation in heart failure. *J. Cell Biol.* **2003**, *160*, 919–28.

108. Altamirano, F.; López, J.R.; Henríquez, C.; Molinski, T.; Allen, P.D.; Jaimovich, E. Increased resting intracellular calcium modulates NF-κB-dependent inducible nitric-oxide synthase gene expression in dystrophic mdx skeletal myotubes. *J. Biol. Chem.* **2012**, *287*, 20876–87.

109. Shin, J.; Tajrishi, M.M.; Ogura, Y.; Kumar, A. Wasting mechanisms in muscular dystrophy. *Int. J. Biochem. Cell Biol.* **2013**, *45*, 2266–79.

110. Yeung, E.W.; Whitehead, N.P.; Suchyna, T.M.; Gottlieb, P. a; Sachs, F.; Allen, D.G. Effects of

stretch-activated channel blockers on [Ca2+]i and muscle damage in the mdx mouse. *J. Physiol.* **2005**, *562*, 367–80.

111. Yasuda, S.; Townsend, D.; Michele, D.E.; Favre, E.G.; Day, S.M.; Metzger, J.M. Dystrophic heart failure blocked by membrane sealant poloxamer. *Nature* **2005**, *436*, 1025–9.

112. Fanchaouy, M.; Polakova, E.; Jung, C.; Ogrodnik, J.; Shirokova, N.; Niggli, E. Pathways of abnormal stress-induced Ca2+ influx into dystrophic mdx cardiomyocytes. *Cell Calcium* **2009**, *46*, 114–21.

113. Quinlan, J.G.; Wong, B.L.; Niemeier, R.T.; McCullough, A.S.; Levin, L.; Emanuele, M. Poloxamer 188 failed to prevent exercise-induced membrane breakdown in mdx skeletal muscle fibers. *Neuromuscul. Disord.* **2006**, *16*, 855–64.

114. Terry, R.L.; Kaneb, H.M.; Wells, D.J. Poloxomer 188 has a deleterious effect on dystrophic skeletal muscle function. *PLoS One* **2015**, *10*, e0119252.

115. McNeil, P.L.; Khakee, R. Disruptions of muscle fiber plasma membranes. Role in exercise-induced damage. *Am J Pathol* **1992**, *140*, 1097–109.

116. Ward, M.L.; Williams, I. a.; Chu, Y.; Cooper, P.J.; Ju, Y.K.; Allen, D.G. Stretch-activated channels in the heart: Contributions to length-dependence and to cardiomyopathy. *Prog. Biophys. Mol. Biol.* **2008**, *97*, 232–49.

117. Harisseh, R.; Chatelier, A.; Magaud, C.; Déliot, N.; Constantin, B. Involvement of TRPV2 and SOCE in calcium influx disorder in DMD primary human myotubes with a specific contribution of α1-syntrophin and PLC/PKC in SOCE regulation. *Am. J. Physiol. Cell Physiol.* **2013**, *304*, C881-94.

118. Blaustein, M.P.; Lederer, W.J. Sodium/calcium exchange: its physiological implications. *Physiol. Rev.* **1999**, *79*, 763–854.

119. Gavillet, B.; Rougier, J.S.; Domenighetti, A. a.; Behar, R.; Boixel, C.; Ruchat, P.; Lehr, H.A.; Pedrazzini, T.; Abriel, H. Cardiac sodium channel Nav1.5 is regulated by a multiprotein complex composed of syntrophins and dystrophin. *Circ. Res.* **2006**, *99*, 407–14.

120. Burr, A.R.; Millay, D.P.; Goonasekera, S. a; Park, K.H.; Sargent, M. a; Collins, J.; Altamirano, F.; Philipson, K.D.; Allen, P.D.; Ma, J.; López, J.R.; Molkentin, J.D. Na+ dysregulation coupled with Ca2+ entry through NCX1 promotes muscular dystrophy in mice. *Mol. Cell. Biol.* **2014**, *34*, 1991–2002.

121. Gervásio, O.L.; Whitehead, N.P.; Yeung, E.W.; Phillips, W.D.; Allen, D.G. TRPC1 binds to caveolin-3 and is regulated by Src kinase - role in Duchenne muscular dystrophy. *J. Cell Sci.* **2008**, *121*, 2246–55.

122. Vandebrouck, A.; Sabourin, J.; Rivet, J.; Balghi, H.; Sebille, S.; Kitzis, A.; Raymond, G.; Cognard, C.; Bourmeyster, N.; Constantin, B. Regulation of capacitative calcium entries by 1-syntrophin: association of TRPC1 with dystrophin complex and the PDZ domain of 1-syntrophin. *FASEB J.* **2007**, *21*, 608–17.

123. Millay, D.P.; Goonasekera, S.A.; Sargent, M.A.; Maillet, M.; Aronow, B.J.; Molkentin, J.D. Calcium influx is sufficient to induce muscular dystrophy through a TRPC-dependent mechanism. *Proc. Natl. Acad. Sci.* **2009**, *106*, 19023–8.

124. Vandebrouck, C.; Martin, D.; Schoor, M.C. Van; Debaix, H.; Gailly, P. Involvement of TRPC in the abnormal calcium influx observed in dystrophic (mdx) mouse skeletal muscle fibers. *J. Cell Biol.* **2002**, *16*, 1089–96.

125. Seo, K.; Rainer, P.P.; Lee, D.I.; Hao, S.; Bedja, D.; Birnbaumer, L.; Cingolani, O.H.; Kass, D. a. Hyperactive adverse mechanical stress responses in dystrophic heart are coupled to transient receptor potential canonical 6 and blocked by cgmp-protein kinase g modulation. *Circ. Res.*

2014, *114*, 823–32.

126. Chung, H.S.; Kim, G.E.; Holewinski, R.J.; Venkatraman, V.; Zhu, G.; Bedja, D.; Kass, D.A.; Van Eyk, J.E. Transient receptor potential channel 6 regulates abnormal cardiac S-nitrosylation in Duchenne muscular dystrophy. *Proc. Natl. Acad. Sci.* **2017**, *114*, E10763-71.

127. Zanou, N.; Iwata, Y.; Schakman, O.; Lebacq, J.; Wakabayashi, S.; Gailly, P. Essential role of TRPV2 ion channel in the sensitivity of dystrophic muscle to eccentric contractions. *FEBS Lett.* **2009**, *583*, 3600–4.

128. Lorin, C.; Vögeli, I.; Niggli, E.; Vogeli, I.; Niggli, E. Dystrophic cardiomyopathy: role of TRPV2 channels in stretch-induced cell damage. *Cardiovasc. Res.* **2015**, *106*, 153–62.

129. Hohaus, A.; Person, V.; Behlke, J.; Schaper, J.; Morano, I.; Haase, H. The carboxyl-terminal region of ahnak provides a link between cardiac L-type Ca2+ channels and the actin-based cytoskeleton. *FASEB J.* **2002**, *16*, 1205–16.

130. Sadeghi, A.; Doyle, A.D.; Johnson, B.D. Regulation of the cardiac L-type Ca2+ channel by the actin-binding proteins alpha-actinin and dystrophin. *Am. J. Physiol. Cell Physiol.* **2002**, *282*, C1502-11.

131. Tanabe, T.; Beam, K.G.; Adams, B. a; Niidome, T.; Numa, S. Regions of the skeletal muscle dihydropyridine receptor critical for excitation-contraction coupling. *Nature* **1990**, *346*, 567–9.

132. Koenig, X.; Rubi, L.; Obermair, G.J.; Cervenka, R.; Dang, X.B.; Lukacs, P.; Kummer, S.; Bittner, R.E.; Kubista, H.; Todt, H.; Hilber, K. Enhanced currents through L-type calcium channels in cardiomyocytes disturb the electrophysiology of the dystrophic heart. *Am. J. Physiol. Heart Circ. Physiol.* **2013**, *306*, H564-73.

133. Viola, H.M.; Arthur, P.G.; Hool, L.C. Evidence for regulation of mitochondrial function by the L-type Ca2+ channel in ventricular myocytes. *J. Mol. Cell. Cardiol.* **2009**, *46*, 1016–26.

134. Viola, H.M.; Adams, A.M.; Davies, S.M.K.; Fletcher, S.; Filipovska, A.; Hool, L.C. Impaired functional communication between the L-type calcium channel and mitochondria contributes to metabolic inhibition in the mdx heart. *Proc. Natl. Acad. Sci. U. S. A.* **2014**, *111*, E2905-14.

135. Rubi, L.; Todt, H.; Kubista, H.; Koenig, X.; Hilber, K. Calcium current properties in dystrophin-deficient ventricular cardiomyocytes from aged mdx mice. *Physiol. Rep.* **2018**, *6*, 1–8.

136. Divet, A.; Lompré, A.M.; Huchet-Cadiou, C. Effect of cyclopiazonic acid, an inhibitor of the sarcoplasmic reticulum Ca-ATPase, on skeletal muscles from normal and mdx mice. *Acta Physiol. Scand.* **2005**, *184*, 173–86.

137. Li, Y.; Zhang, S.; Zhang, X.; Li, J.; Ai, X.; Zhang, L.; Yu, D.; Ge, S.; Peng, Y.; Chen, X. Blunted cardiac beta-adrenergic response as an early indication of cardiac dysfunction in Duchenne muscular dystrophy. *Cardiovasc. Res.* **2014**, *103*, 60–71.

138. Rohman, M.S.; Emoto, N.; Takeshima, Y.; Yokoyama, M.; Matsuo, M. Decreased mAKAP, ryanodine receptor, and SERCA2a gene expression in mdx hearts. *Biochem. Biophys. Res. Commun.* **2003**, *310*, 228–35.

139. Tanihata, J.; Nagata, T.; Ito, N.; Saito, T.; Nakamura, A.; Minamisawa, S.; Aoki, Y.; Ruegg, U.T.; Takeda, S. Truncated dystrophin ameliorates the dystrophic phenotype of mdx mice by reducing sarcolipin-mediated SERCA inhibition. *Biochem. Biophys. Res. Commun.* **2018**, *505*, 51–9.

140. Voit, A.; Patel, V.; Pachon, R.; Shah, V.; Bakhutma, M.; Kohlbrenner, E.; McArdle, J.J.; Dell'Italia, L.J.; Mendell, J.R.; Xie, L.H.; Hajjar, R.J.; Duan, D.; Fraidenraich, D.; Babu, G.J. Reducing sarcolipin expression mitigates Duchenne muscular dystrophy and associated cardiomyopathy in mice. *Nat. Commun.* **2017**, *8*, 1–14.

141. Alberts, B.; Johnson, A.; Lewis, J.; Raff, M.; Roberts, K.; Walter, P.; Wilson, J.; Hunt, T. *Molecular*

Biology of the Cell; 5th ed.; 2008; ISBN 0815332181.

142. Niggli, E.; Ullrich, N.D.; Gutierrez, D.; Kyrychenko, S.; Poláková, E.; Shirokova, N. Posttranslational modifications of cardiac ryanodine receptors: Ca2+ signaling and EC-coupling. *Biochim. Biophys. Acta - Mol. Cell Res.* **2013**, *1833*, 866–75.

143. Respress, J.L.; van Oort, R.J.; Li, N.; Rolim, N.; Dixit, S.; DeAlmeida, A.; Voigt, N.; Lawrence, W.S.; Skapura, D.G.; Skardal, K.; Wisloff, U.; Wieland, T.; Ai, X.; Pogwizd, S.M.; Dobrev, D.; Wehrens, X.H.T. Role of RyR2 Phosphorylation at S2814 during Heart Failure Progression. *Circ. Res.* **2012**, *110*, 1474–83.

144. Marx, S.O.; Reiken, S.; Hisamatsu, Y.; Jayaraman, T.; Burkhoff, D.; Rosemblit, N.; Marks, a R. PKA phosphorylation dissociates FKBP12.6 from the calcium release channel (ryanodine receptor): defective regulation in failing hearts. *Cell* **2000**, *101*, 365–76.

145. Capogrosso, R.F.; Mantuano, P.; Uaesoontrachoon, K.; Cozzoli, A.; Giustino, A.; Dow, T.; Srinivassane, S.; Filipovic, M.; Bell, C.; Vandermeulen, J.; Massari, A.M.; De Bellis, M.; Conte, E.; Pierno, S.; Camerino, G.M.; Liantonio, A.; Nagaraju, K.; De Luca, A. Ryanodine channel complex stabilizer compound S48168/ARM210 as a disease modifier in dystrophin-deficient mdx mice: Proof-of-concept study and independent validation of efficacy. *FASEB J.* **2018**, *32*, 1025–43.

146. Liberona, J.L.; Powell, J.A.; Shenoi, S.; Petherbridge, L.; Caviedes, R.; Jaimovich, E. Differences in both inositol 1,4,5-triphosphate mass and inositol 1,4,5- triphosphate receptors between normal and dystrophic between normal and dystrophic skeletal muscle cell lines. *Muscle and Nerve* **1998**, *21*, 902–9.

147. Valladares, D.; Utreras-Mendoza, Y.; Campos, C.; Morales, C.; Diaz-Vegas, A.; Contreras-Ferrat, A.; Westermeier, F.; Jaimovich, E.; Marchi, S.; Pinton, P.; Lavandero, S. IP3 receptor blockade restores autophagy and mitochondrial function in skeletal muscle fibers of dystrophic mice. *Biochim. Biophys. Acta - Mol. Basis Dis.* **2018**, *1864*, 3685–95.

148. Mijares, A.; Altamirano, F.; Kolster, J.; Adams, J.A.; López, J.R. Biochemical and Biophysical Research Communications Age-dependent changes in diastolic Ca 2 + and Na + concentrations in dystrophic cardiomyopathy : Role of Ca 2 + entry and IP 3. *Biochem. Biophys. Res. Commun.* **2014**, *452*, 1054–9.

149. Pal, R.; Palmieri, M.; Loehr, J.A.; Li, S.; Abo-Zahrah, R.; Monroe, T.O.; Thakur, P.B.; Sardiello, M.; Rodney, G.G. Src-dependent impairment of autophagy by oxidative stress in a mouse model of Duchenne muscular dystrophy. *Nat. Commun.* **2014**, *5*, 4425.

150. Henríquez-Olguín, C.; Altamirano, F.; Valladares, D.; López, J.R.; Allen, P.D.; Jaimovich, E. Altered ROS production, NF-κB activation and interleukin-6 gene expression induced by electrical stimulation in dystrophic mdx skeletal muscle cells. *Biochim. Biophys. Acta - Mol. Basis Dis.* **2015**, *1852*, 1410–9.

151. Stern, L.Z.; Ringel, S.P.; Ziter, F.A.; Menander Huber, K.B.; Ionasescu, V.; Pellegrino, R.J.; Snyder, R.D. Drug trial of superoxide dismutase in Duchenne's muscular dystrophy. *Arch. Neurol.* **1982**, *39*, 342–6.

152. Bäckman, E.; Nylander, E.; Johansson, I.; Henriksson, K.G.; Tagesson, C. Selenium and vitamin E treatment of Duchenne muscular dystrophy: no effect on muscle function. *Acta Neurol. Scand.* **1988**, *78*, 429–35.

153. Haycock, J.W.; MacNeil, S.; Jones, P.; Harris, J.B.; Mantle, D. Oxidative damage to muscle protein in Duchenne muscular dystrophy. *Neuroreport* **1996**, *8*, 357–61.

154. Selsby, J.T. Increased catalase expression improves muscle function in mdx mice. *Exp. Physiol.* **2011**, *96*, 194–202.

155. Whitehead, N.P.; Pham, C.; Gervasio, O.L.; Allen, D.G. N-Acetylcysteine ameliorates skeletal

muscle pathophysiology in mdx mice. *J. Physiol.* **2008**, *586*, 2003–14.

156. Whitehead, N.P.; Yeung, E.W.; Froehner, S.C.; Allen, D.G. Skeletal muscle NADPH oxidase is increased and triggers stretch-induced damage in the mdx mouse. *PLoS One* **2010**, *5*, e15354.

157. Alonso, M.T.; Villalobos, C.; Chamero, P.; Alvarez, J.; García-Sancho, J. Calcium microdomains in mitochondria and nucleus. *Cell Calcium* **2006**, *40*, 513–25.

158. Ichas, F.; Jouaville, L.S.; Mazat, J.P. Mitochondria are excitable organelles capable of generating and conveying electrical and calcium signals. *Cell* **1997**, *89*, 1145–53.

159. Zorov, D.B.; Juhaszova, M.; Sollott, S.J. Mitochondrial Reactive Oxygen Species (ROS) and ROS-Induced ROS Release. *Physiol. Rev.* **2014**, *94*, 909–50.

160. Percival, J.M.; Siegel, M.P.; Knowels, G.; Marcinek, D.J. Defects in mitochondrial localization and ATP synthesis in the mdx mouse model of duchenne muscular dystrophy are not alleviated by PDE5 inhibition. *Hum. Mol. Genet.* **2013**, *22*, 153–67.

161. Bernardi, P.; di Lisa, F. The mitochondrial permeability transition pore: Molecular nature and role as a target in cardioprotection. *J. Mol. Cell. Cardiol.* **2015**, *78*, 100–6.

162. Pan, X.; Liu, J.; Nguyen, T.; Liu, C.; Sun, J.; Teng, Y.; Fergusson, M.M.; Rovira, I.I.; Allen, M.; Springer, D. a; Aponte, A.M.; Gucek, M.; Balaban, R.S.; Murphy, E.; Finkel, T. The physiological role of mitochondrial calcium revealed by mice lacking the mitochondrial calcium uniporter. *Nat. Cell Biol.* **2013**, *15*, 1464–72.

163. Millay, D.P.; Sargent, M. a; Osinska, H.; Baines, C.P.; Barton, E.R.; Vuagniaux, G.; Sweeney, H.L.; Robbins, J.; Molkentin, J.D. Genetic and pharmacologic inhibition of mitochondrial-dependent necrosis attenuates muscular dystrophy. *Nat. Med.* **2008**, *14*, 442–7.

164. De Palma, C.; Clementi, E. Nitric oxide in myogenesis and therapeutic muscle repair. *Mol. Neurobiol.* **2012**, *46*, 682–92.

165. Simon, J.N.; Duglan, D.; Casadei, B.; Carnicer, R. Nitric oxide synthase regulation of cardiac excitation-contraction coupling in health and disease. *J. Mol. Cell. Cardiol.* **2014**, *73*, 80–91.

166. Zhang, Y.H.; Casadei, B. Sub-cellular targeting of constitutive NOS in health and disease. *J. Mol. Cell. Cardiol.* **2012**, *52*, 341–50.

167. Mosqueira, M.; Zeiger, U.; Förderer, M.; Brinkmeier, H.; Fink, R.H. Cardiac and respiratory dysfunction in duchenne muscular dystrophy and the role of second messengers. *Med. Res. Rev.* **2013**, *33*, 1174–213.

168. Chang, W.J.; Iannaccone, S.T.; Lau, K.S.; Masters, B.S.; McCabe, T.J.; McMillan, K.; Padre, R.C.; Spencer, M.J.; Tidball, J.G.; Stull, J.T. Neuronal nitric oxide synthase and dystrophin-deficient muscular dystrophy. *Proc. Natl. Acad. Sci. U. S. A.* **1996**, *93*, 9142–7.

169. Lau, K.S.; Grange, R.W.; Chang, W.J.; Kamm, K.E.; Sarelius, I.; Stull, J.T. Skeletal muscle contractions stimulate cGMP formation and attenuate vascular smooth muscle myosin phosphorylation via nitric oxide. *FEBS Lett.* **1998**, *431*, 71–4.

170. Froehner, S.C.; Reed, S.M.; Anderson, K.N.; Huang, P.L.; Percival, J.M. Loss of nNOS inhibits compensatory muscle hypertrophy and exacerbates inflammation and eccentric contraction-induced damage in mdx mice. *Hum. Mol. Genet.* **2014**, *24*, 492–505.

171. Wehling, M.; Spencer, M.J.; Tidball, J.G. A nitric oxide synthase transgene ameliorates muscular dystrophy in mdx mice. *J. Cell Biol.* **2001**, *155*, 123–31.

172. Lai, Y.; Zhao, J.; Yue, Y.; Wasala, N.B.; Duan, D. Partial restoration of cardiac function with ΔPDZ nNOS in aged mdx model of Duchenne cardiomyopathy. *Hum. Mol. Genet.* **2014**, *23*, 3189–99.

173. Song, K.S.; Scherer, P.E.; Tang, Z.; Okamoto, T.; Li, S.; Chafel, M.; Chu, C.; Kohtz, D.S.; Lisanti, M.P. Expression of caveolin-3 in skeletal, cardiac, and smooth muscle cells: Caveolin-3 is a

component of the sarcolemma and co-fractionates with dystrophin and dystrophin-associated glycoproteins. *J. Biol. Chem.* **1996**, *271*, 15160–5.

174. Crosbie, R.H.; Yamada, H.; Venzke, D.P.; Lisanti, M.P.; Campbell, K.P. Caveolin-3 is not an integral component of the dystrophin glycoprotein complex. *FEBS Lett.* **1998**, *427*, 279–82.

175. Khairallah, R.J.; Khairallah, M.; Gélinas, R.; Bouchard, B.; Young, M.E.; Allen, B.G.; Lopaschuk, G.D.; Deschepper, C.F.; Des Rosiers, C. Cyclic GMP signaling in cardiomyocytes modulates fatty acid trafficking and prevents triglyceride accumulation. *J. Mol. Cell. Cardiol.* **2008**, *45*, 230–9.

176. Khairallah, M.; Khairallah, R.; Young, M.E.; Dyck, J.R.B.; Petrof, B.J.; Des Rosiers, C. Metabolic and signaling alterations in dystrophin-deficient hearts precede overt cardiomyopathy. *J. Mol. Cell. Cardiol.* **2007**, *43*, 119–29.

177. Li, Y.; He, L.; Huang, X.; Issa Bhaloo, S.; Zhao, H.; Zhang, S.; Pu, W.; Tian, X.; Li, Y.; Liu, Q.; Yu, W.; Zhang, L.; Liu, X.; Liu, K.; Tang, J.; Zhang, H.; Cai, D.; Adams, R.H.; Xu, Q.; Lui, K.O.; Zhou, B. Genetic lineage tracing of non-myocyte population by dual recombinases. *Circulation* **2018**, *138*, 793–805.

178. Fukada, S.; Uezumi, A.; Ikemoto, M.; Masuda, S.; Segawa, M.; Tanimura, N.; Yamamoto, H.; Miyagoe-Suzuki, Y.; Takeda, S. Molecular signature of quiescent satellite cells in adult skeletal muscle. *Stem Cells* **2007**, *25*, 2448–59.

179. Seale, P.; Sabourin, L.A.; Girgis-Gabardo, A.; Mansouri, A.; Gruss, P.; Rudnicki, M.A. Pax7 is required for the specification of myogenic satellite cells. *Cell* **2000**, *102*, 777–86.

180. Schultz, E. Satellite cell proliferative compartments in growing skeletal muscles. *Dev. Biol.* **1996**, *175*, 84–94.

181. Megeney, L.A.; Kablar, B.; Garrett, K.; Anderson, J.E.; Rudnicki, M.A. MyoD is required for myogenic stem cell function in adult skeletal muscle. *Genes Dev.* **1996**, *10*, 1173–83.

182. Yablonka-Reuveni, Z.; Rudnicki, M.A.; Rivera, A.J.; Primig, M.; Anderson, J.E.; Natanson, P. The transition from proliferation to differentiation is delayed in satellite cells from mice lacking MyoD. *Dev. Biol.* **1999**, *210*, 440–55.

183. Cooper, R.N.; Tajbakhsh, S.; Mouly, V.; Cossu, G.; Buckingham, M.; Butler-Browne, G.S. In vivo satellite cell activation via Myf5 and MyoD in regenerating mouse skeletal muscle. *J. Cell Sci.* **1999**, *112*, 2895–901.

184. Ustanina, S.; Carvajal, J.; Rigby, P.; Braun, T. The myogenic factor Myf5 supports efficient skeletal muscle regeneration by enabling transient myoblast amplification. *Stem Cells* **2007**, *25*, 2006–16.

185. Almada, A.E.; Wagers, A.J. Molecular circuitry of stem cell fate in skeletal muscle regeneration, ageing and disease. *Nat. Rev. Mol. Cell Biol.* **2016**, *17*, 267–79.

186. Troy, A.; Cadwallader, A.B.; Fedorov, Y.; Tyner, K.; Tanaka, K.K.; Olwin, B.B. Coordination of satellite cell activation and self-renewal by par-complex-dependent asymmetric activation of p38α/β MAPK. *Cell Stem Cell* **2012**, *11*, 541–53.

187. Deato, M.D.E.; Marr, M.T.; Sottero, T.; Inouye, C.; Hu, P.; Tjian, R. MyoD targets TAF3/TRF3 to activate myogenin transcription. *Mol. Cell* **2008**, *32*, 96–105.

188. Kuang, S.; Kuroda, K.; Le Grand, F.; Rudnicki, M.A. Asymmetric self-renewal and commitment of satellite stem cells in muscle. *Cell* **2007**, *129*, 999–1010.

189. Le Grand, F.; Jones, A.E.; Seale, V.; Scimè, A.; Rudnicki, M.A. Wnt7a activates the planar cell polarity pathway to drive the symmetric expansion of satellite stem cells. *Cell Stem Cell* **2009**, *4*, 535–47.

190. Tanaka, S.; Terada, K.; Nohno, T. Canonical Wnt signaling is involved in switching from cell

proliferation to myogenic differentiation of mouse myoblast cells. *J. Mol. Signal.* **2011**, *6*, 1–16.

191. Dumont, N.A.; Wang, Y.X.; von Maltzahn, J.; Pasut, A.; Bentzinger, C.F.; Brun, C.E.; Rudnicki, M.A. Dystrophin expression in muscle stem cells regulates their polarity and asymmetric division. *Nat. Med.* **2015**, *21*, 1455–63.

192. Jiang, C.; Wen, Y.; Kuroda, K.; Hannon, K.; Rudnicki, M.A.; Kuang, S. Notch signaling deficiency underlies age-dependent depletion of satellite cells in muscular dystrophy. *Anal. Quant. Cytol. Histol.* **2014**, *7*, 997–1004.

193. Kottlors, M.; Kirschner, J. Elevated satellite cell number in Duchenne muscular dystrophy. *Cell Tissue Res.* **2010**, *340*, 541–8.

194. Bankolé, L.C.; Feasson, L.; Ponsot, E.; Kadi, F. Fibre type-specific satellite cell content in two models of muscle disease. *Histopathology* **2013**, *63*, 826–32.

195. Kollu, S.; Abou-Khalil, R.; Shen, C.; Brack, A.S. The spindle assembly checkpoint safeguards genomic integrity of skeletal muscle satellite cells. *Stem Cell Reports* **2015**, *4*, 1061–74.

196. Chang, N.C.; Chevalier, F.P.; Rudnicki, M.A. Satellite cells in muscular dystrophy - lost in polarity. *Trends Mol. Med.* **2016**, *22*, 479–96.

197. Boldrin, L.; Zammit, P.S.; Morgan, J.E. Satellite cells from dystrophic muscle retain regenerative capacity. *Stem Cell Res.* **2015**, *14*, 20–9.

198. Meng, J.; Counsell, J.R.; Reza, M.; Laval, S.H.; Danos, O.; Thrasher, A.; Lochmüller, H.; Muntoni, F.; Morgan, J.E. Autologous skeletal muscle derived cells expressing a novel functional dystrophin provide a potential therapy for Duchenne Muscular Dystrophy. *Sci. Rep.* **2016**, *6*, 1–12.

199. Meng, J.; Muntoni, F.; Morgan, J. CD133+ cells derived from skeletal muscles of Duchenne muscular dystrophy patients have a compromised myogenic and muscle regenerative capability. *Stem Cell Res.* **2018**, *30*, 43–52.

200. Brack, A.S.; Conboy, M.J.; Roy, S.; Lee, M.; Kuo, C.J.; Keller, C.; Rando, T.A. Increased Wnt signaling during aging alters muscle stem cell fate and increases fibrosis. *Science (80-.).* **2007**, *317*, 807–10.

201. Biressi, S.; Miyabara, E.H.; Gopinath, S.D.; Carlig, P.M.M.; Rando, T.A. A Wnt-TGF2 axis induces a fibrogenic program in muscle stem cells from dystrophic mice. *Sci. Transl. Med.* **2014**, *6*, 1–13.

202. Joe, A.W.B.; Yi, L.; Natarajan, A.; Le Grand, F.; So, L.; Wang, J.; Rudnicki, M.A.; Rossi, F.M.V. Muscle injury activates resident fibro/adipogenic progenitors that facilitate myogenesis. *Nat. Cell Biol.* **2010**, *12*, 153–63.

203. Uezumi, A.; Fukada, S.; Yamamoto, N.; Takeda, S.; Tsuchida, K. Mesenchymal progenitors distinct from satellite cells contribute to ectopic fat cell formation in skeletal muscle. *Nat Cell Biol* **2010**, *12*, 143–52.

204. Natarajan, A.; Lemos, D.R.; Rossi, F.M.V. Fibro/adipogenic progenitors: A double-edged sword in skeletal muscle regeneration. *Cell Cycle* **2010**, *9*, 2045–6.

205. Lombardi, R.; Chen, S.N.; Ruggiero, A.; Gurha, P.; Czernuszewicz, G.Z.; Willerson, J.T.; Marian, A.J. Cardiac fibro-adipocyte progenitors express desmosome proteins and preferentially differentiate to adipocytes upon deletion of the desmoplakin gene. *Circ. Res.* **2016**, *119*, 41–54.

206. Pawlikowski, B.; Vogler, T.O.; Gadek, K.; Olwin, B.B. Regulation of skeletal muscle stem cells by fibroblast growth factors. *Dev. Dyn.* **2017**, *246*, 359–67.

207. Contreras, O.; Rebolledo, D.L.; Oyarzún, J.E.; Olguín, H.C.; Brandan, E. Connective tissue cells

expressing fibro/adipogenic progenitor markers increase under chronic damage: relevance in fibroblast-myofibroblast differentiation and skeletal muscle fibrosis. *Cell Tissue Res.* **2016**, *364*, 647–60.

208. Cordani, N.; Pisa, V.; Pozzi, L.; Sciorati, C.; Clementi, E. Nitric oxide controls fat deposition in dystrophic skeletal muscle by regulating fibro-adipogenic precursor differentiation. *Stem Cells* **2014**, *32*, 874–85.

209. Mozzetta, C.; Consalvi, S.; Saccone, V.; Tierney, M.; Diamantini, A.; Mitchell, K.J.; Marazzi, G.; Borsellino, G.; Battistini, L.; Sassoon, D.; Sacco, A.; Puri, P.L. Fibroadipogenic progenitors mediate the ability of HDAC inhibitors to promote regeneration in dystrophic muscles of young, but not old Mdx mice. *EMBO Mol. Med.* **2013**, *5*, 626–39.

210. Saccone, V.; Consalvi, S.; Giordani, L.; Mozzetta, C.; Barozzi, I.; Sandoná, M.; Ryan, T.; Rojas-Muñoz, A.; Madaro, L.; Fasanaro, P.; Borsellino, G.; De Bardi, M.; Frigè, G.; Termanini, A.; Sun, X.; Rossant, J.; Bruneau, B.G.; Mercola, M.; Minucci, S.; Puri, P.L. HDAC-regulated myomiRs control BAF60 variant exchange and direct the functional phenotype of fibro-adipogenic progenitors in dystrophic muscles. *Genes Dev.* **2014**, *28*, 841–57.

211. Murphy, M.M.; Lawson, J.A.; Mathew, S.J.; Hutcheson, D.A.; Kardon, G. Satellite cells, connective tissue fibroblasts and their interactions are crucial for muscle regeneration. *Development* **2011**, *138*, 3625–37.

212. Bittner, R.E.; Schöfer, C.; Weipoltshammer, K.; Ivanova, S.; Streubel, B.; Hauser, E.; Freilinger, M.; Höger, H.; Elbe-Bürger, A.; Wachtler, F. Recruitment of bone-marrow-derived cells by skeletal and cardiac muscle in adult dystrophic mdx mice. *Anat. Embryol. (Berl).* **1999**, *199*, 391–6.

213. Asakura, A.; Komaki, M.; Rudnicki, M.A. Muscle satellite cells are multipotential stem cells that exhibit myogenic, osteogenic, and adipogenic differentiation. *Differentiation* **2001**, *68*, 245–53.

214. Wada, M.R.; Inagawa-Ogashiwa, M.; Shimizu, S.; Yasumoto, S.; Hashimoto, N. Generation of different fates from multipotent muscle stem cells. *Development* **2002**, *129*, 2987–95.

215. Cao, B.; Zheng, B.; Jankowski, R.J.; Kimura, S.; Ikezawa, M.; Deasy, B.; Cummins, J.; Epperly, M.; Qu-Petersen, Z.; Huard, J. Muscle stem cells differentiate into haematopoietic lineages but retain myogenic potential. *Nat. Cell Biol.* **2003**, *5*, 640–6.

216. Asakura, A.; Seale, P.; Girgis-Gabardo, A.; Rudnicki, M.A. Myogenic specification of side population cells in skeletal muscle. *J. Cell Biol.* **2002**, *159*, 123–34.

217. De Angelis, L.; Berghella, L.; Coletta, M.; Lattanzi, L.; Zanchi, M.; Cusella-De Angelis, M.G.; Ponzetto, C.; Cossu, G. Skeletal myogenic progenitors originating from embryonic dorsal aorta coexpress endothelial and myogenic markers and contribute to postnatal muscle growth and regeneration. *J. Cell Biol.* **1999**, *147*, 869–78.

218. Dellavalle, A.; Sampaolesi, M.; Tonlorenzi, R.; Tagliafico, E.; Sacchetti, B.; Perani, L.; Innocenzi, A.; Galvez, B.G.; Messina, G.; Morosetti, R.; Li, S.; Belicchi, M.; Peretti, G.; Chamberlain, J.S.; Wright, W.E.; Torrente, Y.; Ferrari, S.; Bianco, P.; Cossu, G. Pericytes of human skeletal muscle are myogenic precursors distinct from satellite cells. *Nat. Cell Biol.* **2007**, *9*, 255–67.

219. Dellavalle, A.; Maroli, G.; Covarello, D.; Azzoni, E.; Innocenzi, A.; Perani, L.; Antonini, S.; Sambasivan, R.; Brunelli, S.; Tajbakhsh, S.; Cossu, Ǵ Pericytes resident in postnatal skeletal muscle differentiate into muscle fibres and generate satellite cells. *Nat. Commun.* **2011**, *2*, 499.

220. Mitchell, K.J.; Pannérec, A.; Cadot, B.; Parlakian, A.; Besson, V.; Gomes, E.R.; Marazzi, G.; Sassoon, D.A. Identification and characterization of a non-satellite cell muscle resident progenitor during postnatal development. *Nat. Cell Biol.* **2010**, *12*, 257–66.

221. Liu, N.; Garry, G.A.; Li, S.; Bezprozvannaya, S.; Sanchez-Ortiz, E.; Chen, B.; Shelton, J.M.;

Jaichander, P.; Bassel-Duby, R.; Olson, E.N. A Twist2-dependent progenitor cell contributes to adult skeletal muscle. *Nat. Cell Biol.* **2017**, *19*, 202–13.

222. Lepper, C.; Partridge, T.A.; Fan, C.M. An absolute requirement for Pax7-positive satellite cells in acute injury-induced skeletal muscle regeneration. *Development* **2011**, *138*, 3639–46.

223. Sambasivan, R.; Yao, R.; Kissenpfennig, A.; Van Wittenberghe, L.; Paldi, A.; Gayraud-Morel, B.; Guenou, H.; Malissen, B.; Tajbakhsh, S.; Galy, A. Pax7-expressing satellite cells are indispensable for adult skeletal muscle regeneration. *Development* **2011**, *138*, 3647–56.

224. Bachrach, E.; Li, S.; Perez, A.L.; Schienda, J.; Liadaki, K.; Volinski, J.; Flint, A.; Chamberlain, J.; Kunkel, L.M. Systemic delivery of human microdystrophin to regenerating mouse dystrophic muscle by muscle progenitor cells. *Proc. Natl. Acad. Sci.* **2004**, *101*, 3581–6.

225. Rouger, K.; Larcher, T.; Dubreil, L.; Deschamps, J.-Y.; Le Guiner, C.; Jouvion, G.; Delorme, B.; Lieubeau, B.; Carlus, M.; Fornasari, B.; Theret, M.; Orlando, P.; Ledevin, M.; Zuber, C.; Leroux, I.; Deleau, S.; Guigand, L.; Testault, I.; Le Rumeur, E.; Fiszman, M.; Chérel, Y. Systemic delivery of allogenic muscle stem cells induces long-term muscle repair and clinical efficacy in Duchenne muscular dystrophy dogs. *Am. J. Pathol.* **2011**, *179*, 2501–18.

226. Gillies, A.R.; Lieber, R.L. Structure and function of the skeletal muscle extracellular matrix. *Muscle nerve* **2012**, *44*, 318–31.

227. Kharraz, Y.; Guerra, J.; Pessina, P.; Serrano, A.L.; Muñoz-Cánoves, P. Understanding the process of fibrosis in duchenne muscular dystrophy. *Biomed Res. Int.* **2014**, *2014*, 1–11.

228. Foidart, M.; Foidart, J.M.; Engel, W.K. Collagen localization in normal and fibrotic human skeletal muscle. *Arch. Neurol.* **1981**, *38*, 152–7.

229. Marden, F.A.; Connolly, A.M.; Siegel, M.J.; Rubin, D.A. Compositional analysis of muscle in boys with Duchenne muscular dystrophy using MR imaging. *Skeletal Radiol.* **2005**, *34*, 140–8.

230. Sabatelli, P.; Gualandi, F.; Gara, S.K.; Grumati, P.; Zamparelli, A.; Martoni, E.; Pellegrini, C.; Merlini, L.; Ferlini, A.; Bonaldo, P.; Maraldi, N.M.; Paulsson, M.; Squarzoni, S.; Wagener, R. Expression of collagen VI α5 and α6 chains in human muscle and in Duchenne muscular dystrophy-related muscle fibrosis. *Matrix Biol.* **2012**, *31*, 187–96.

231. Li, M.O.; Wan, Y.Y.; Sanjabi, S.; Robertson, A.-K.L.; Flavell, R.A. Transforming growth factor-beta regulation of immune responses. *Annu. Rev. Immunol.* **2006**, *24*, 99–146.

232. Dong, Y.; Lakhia, R.; Thomas, S.S.; Dong, Y.; Wang, X.H.; Silva, K.A.S.; Zhang, L. Interactions between p-Akt and Smad3 in injured muscles initiate myogenesis or fibrogenesis. *AJP Endocrinol. Metab.* **2013**, *305*, E367-75.

233. Parada, C.; Li, J.; Iwata, J.; Suzuki, A.; Chai, Y. CTGF mediates smad-dependent transforming growth factor β signaling to regulate mesenchymal cell proliferation during palate development. *Mol. Cell. Biol.* **2013**, *33*, 3482–93.

234. Morales, M.G.; Gutierrez, J.; Cabello-Verrugio, C.; Cabrera, D.; Lipson, K.E.; Goldschmeding, R.; Brandan, E. Reducing CTGF/CCN2 slows down mdx muscle dystrophy and improves cell therapy. *Hum. Mol. Genet.* **2013**, *22*, 4938–51.

235. Vial, C.; Zúñiga, L.M.; Cabello-Verrugio, C.; Cañón, P.; Fadic, R.; Brandan, E. Skeletal muscle cells express the profibrotic cytokine connective tissue growth factor (CTGF/CCN2), which induces their dedifferentiation. *J. Cell. Physiol.* **2008**, *215*, 410–21.

236. Song, Y.; Yao, S.; Liu, Y.; Long, L.; Yang, H.; Li, Q.; Liang, J.; Li, X.; Lu, Y.; Zhu, H.; Zhang, N. Expression levels of TGF-β1 and CTGF are associated with the severity of duchenne muscular dystrophy. *Exp. Ther. Med.* **2017**, *13*, 1209–14.

237. Au, C.G.; Butler, T.L.; Sherwood, M.C.; Egan, J.R.; North, K.N.; Winlaw, D.S. Increased connective tissue growth factor associated with cardiac fibrosis in the mdx mouse model of

dystrophic cardiomyopathy. *Int. J. Exp. Pathol.* **2011**, *92*, 57–65.

238. Sun, G.; Haginoya, K.; Dai, H.; Chiba, Y.; Uematsu, M.; Hino-Fukuyo, N.; Onuma, A.; Iinuma, K.; Tsuchiya, S. Intramuscular renin-angiotensin system is activated in human muscular dystrophy. *J. Neurol. Sci.* **2009**, *280*, 40–8.

239. Morales, M.G.; Cabrera, D.; Céspedes, C.; Vio, C.P.; Vazquez, Y.; Brandan, E.; Cabello-Verrugio, C. Inhibition of the angiotensin-converting enzyme decreases skeletal muscle fibrosis in dystrophic mice by a diminution in the expression and activity of connective tissue growth factor (CTGF/CCN-2). *Cell Tissue Res.* **2013**, *353*, 173–87.

240. von Moers, A.; Zwirner, A.; Reinhold, A.; Brückmann, O.; van Landeghem, F.; Stoltenburg-Didinger, G.; Schuppan, D.; Herbst, H.; Schuelke, M. Increased mRNA expression of tissue inhibitors of metalloproteinase-1 and -2 in Duchenne muscular dystrophy. *Acta Neuropathol.* **2005**, *109*, 285–93.

241. Miyazaki, D.; Nakamura, A.; Fukushima, K.; Yoshida, K.; Takeda, S.; Ikeda, S.I. Matrix metalloproteinase-2 ablation in dystrophin-deficient mdx muscles reduces angiogenesis resulting in impaired growth of regenerated muscle fibers. *Hum. Mol. Genet.* **2011**, *20*, 1787–99.

242. Bobadilla, M.; Sáinz, N.; Rodriguez, J.; Abizanda, G.; Orbe, J.; De Martino, A.; Verdugo, J.G.; Páramo, J.A.; Prósper, F.; Pérez-Ruiz, A. MMP-10 is required for efficient muscle regeneration in mouse models of injury and muscular dystrophy. *Stem Cells* **2014**, *32*, 447–61.

243. Ogura, Y.; Tajrishi, M.M.; Sato, S.; Hindi, S.M.; Kumar, A. Therapeutic potential of matrix metalloproteinases in Duchenne muscular dystrophy. *Front. Cell Dev. Biol.* **2014**, *2*, 1–11.

244. Lourbakos, A.; Yau, N.; De Bruijn, P.; Hiller, M.; Kozaczynska, K.; Jean-Baptiste, R.; Reza, M.; Wolterbeek, R.; Koeks, Z.; Ayoglu, B.; De Klerk, D.; Campion, G.; Zaharieva, I.; Nadarajah, V.D.; Nilsson, P.; Al-Khalili Szigyarto, C.; Muntoni, F.; Lochmüller, H.; Verschuuren, J.J.; Goemans, N.; Tulinius, M.; Niks, E.H.; De Kimpe, S.; Aartsma-Rus, A.; T'Hoen, P.A.C.; Spitali, P. Evaluation of serum MMP-9 as predictive biomarker for antisense therapy in Duchenne. *Sci. Rep.* **2017**, *7*, 1–10.

245. Yu, Q.; Stamenkovic, I. Cell surface-localized matrix mealloproteinase-9 proteolytically activates TGF-beta and promotes tumor invasion and angiogenesis. *Genes Dev.* **2000**, *14*, 163–76.

246. Boroujerdi, A.; Welser-Alves, J. V.; Milner, R. Matrix metalloproteinase-9 mediates post-hypoxic vascular pruning of cerebral blood vessels by degrading laminin and claudin-5. *Angiogenesis* **2015**, *18*, 255–64.

247. Zhong, D.; Saito, F.; Saito, Y.; Nakamura, A.; Shimizu, T.; Matsumura, K. Characterization of the protease activity that cleaves the extracellular domain of β-dystroglycan. *Biochem. Biophys. Res. Commun.* **2006**, *345*, 867–71.

248. Dahiya, S.; Bhatnagar, S.; Hindi, S.M.; Jiang, C.; Paul, P.K.; Kuang, S.; Kumar, A. Elevated levels of active matrix metalloproteinase-9 cause hypertrophy in skeletal muscle of normal and dystrophin-deficient mdx mice. *Hum. Mol. Genet.* **2011**, *20*, 4345–59.

249. Li, H.; Mittal, A.; Makonchuk, D.Y.; Bhatnagar, S.; Kumar, A. Matrix metalloproteinase-9 inhibition ameliorates pathogenesis and improves skeletal muscle regeneration in muscular dystrophy. *Hum. Mol. Genet.* **2009**, *18*, 2584–98.

250. Dahiya, S.; Givvimani, S.; Bhatnagar, S.; Qipshidze, N.; Tyagi, S.C.; Kumar, A. Osteopontin-Stimulated Expression of Matrix Metalloproteinase-9 Causes Cardiomyopathy in the mdx Model of Duchenne Muscular Dystrophy. *J. Immunol.* **2011**, *187*, 2723–31.

251. Hindi, S.M.; Shin, J.; Ogura, Y.; Li, H.; Kumar, A. Matrix metalloproteinase-9 inhibition improves

proliferation and engraftment of myogenic cells in dystrophic muscle of mdx mice. *PLoS One* **2013**, *8*, e72121.

252. Ardite, E.; Perdiguero, E.; Vidal, B.; Gutarra, S.; Serrano, A.L.; Muñoz-Cánoves, P. PAI-1-regulated miR-21 defines a novel age-associated fibrogenic pathway in muscular dystrophy. *J. Cell Biol.* **2012**, *196*, 163–75.

253. Bowen, T.; Jenkins, R.H.; Fraser, D.J. MicroRNAs, transforming growth factor beta-1, and tissue fibrosis. *J. Pathol.* **2013**, *229*, 274–85.

254. Winbanks, C.E.; Wang, B.; Beyer, C.; Koh, P.; White, L.; Kantharidis, P.; Gregorevic, P. TGF-β regulates miR-206 and miR-29 to control myogenic differentiation through regulation of HDAC4. *J. Biol. Chem.* **2011**, *286*, 13805–14.

255. Griggs, R.C.; Moxley, R.T.; Mendell, J.R.; Fenichel, G.M.; Brooke, M.H.; Pestronk, A.; Miller, J.P. Prednisone in Duchenne dystrophy. A randomized, controlled trial defining the time course and dose response. Clinical Investigation of Duchenne Dystrophy Group. *Arch. Neurol.* **1991**, *48*, 383–8.

256. Biggar, W.D.; Harris, V.A.; Eliasoph, L.; Alman, B. Long-term benefits of deflazacort treatment for boys with Duchenne muscular dystrophy in their second decade. *Neuromuscul. Disord.* **2006**, *16*, 249–55.

257. McDonald, C.M.; Henricson, E.K.; Abresch, R.T.; Duong, T.; Joyce, N.C.; Hu, F.; Clemens, P.R.; Hoffman, E.P.; Cnaan, A.; Gordish-Dressman, H. Long-term effects of glucocorticoids on function, quality of life, and survival in patients with Duchenne muscular dystrophy: A prospective cohort study. *Lancet* **2018**, *391*, 451–61.

258. Barber, B.J.; Andrews, J.G.; Lu, Z.; West, N.A.; Meaney, F.J.; Price, E.T.; Gray, A.; Sheehan, D.W.; Pandya, S.; Yang, M.; Cunniff, C. Oral corticosteroids and onset of cardiomyopathy in Duchenne muscular dystrophy. *J. Pediatr.* **2013**, *163*, 1080–4.

259. Wagner, K.R.; Lechtzin, N.; Judge, D.P. Current treatment of adult Duchenne muscular dystrophy. *Biochim. Biophys. Acta* **2007**, *1772*, 229–37.

260. Bushby, K.; Finkel, R.; Birnkrant, D.J.; Case, L.E.; Clemens, P.R.; Cripe, L.; Kaul, A.; Kinnett, K.; McDonald, C.; Pandya, S.; Poysky, J.; Shapiro, F.; Tomezsko, J.; Constantin, C. Diagnosis and management of Duchenne muscular dystrophy, part 1: diagnosis, and pharmacological and psychosocial management. *Lancet Neurol.* **2010**, *9*, 77–93.

261. Wong, B.L.; Rybalsky, I.; Shellenbarger, K.C.; Tian, C.; McMahon, M.A.; Rutter, M.M.; Sawnani, H.; Jefferies, J.L. Long-term outcome of interdisciplinary management of patients with Duchenne muscular dystrophy receiving daily glucocorticoid treatment. *J. Pediatr.* **2017**, *182*, 296–303.

262. Melacini, P.; Vianello, A.; Villanova, C.; Fanin, M.; Miorin, M.; Angelini, C.; Dalla Volta, S. Cardiac and respiratory involvement in advanced stage Duchenne muscular dystrophy. *Neuromuscul. Disord.* **1996**, *6*, 367–76.

263. Finsterer, J. Cardiopulmonary support in Duchenne muscular dystrophy. *Lung* **2006**, *184*, 205–15.

264. Toussaint, M.; Chatwin, M.; Soudon, P. Mechanical ventilation in Duchenne patients with chronic respiratory insufficiency: clinical implications of 20 years published experience. *Chron. Respir. Dis.* **2007**, *4*, 167–77.

265. Bushby, K.; Finkel, R.; Birnkrant, D.J.; Case, L.E.; Clemens, P.R.; Cripe, L.; Kaul, A.; Kinnett, K.; McDonald, C.; Pandya, S.; Poysky, J.; Shapiro, F.; Tomezsko, J.; Constantin, C. Diagnosis and management of Duchenne muscular dystrophy, part 2: implementation of multidisciplinary care. *Lancet Neurol.* **2010**, *9*, 177–89.

266. Goemans, N.; Buyse, G. Current treatment and management of dystrophinopathies. *Curr. Treat. Options Neurol.* **2014**, *16*, 287.

267. Raman, S. V.; Hor, K.N.; Mazur, W.; Halnon, N.J.; Kissel, J.T.; He, X.; Tran, T.; Smart, S.; McCarthy, B.; Taylor, M.D.; Jefferies, J.L.; Rafael-Fortney, J.A.; Lowe, J.; Roble, S.L.; Cripe, L.H. Eplerenone for early cardiomyopathy in Duchenne muscular dystrophy: A randomised, double-blind, placebo-controlled trial. *Lancet Neurol.* **2015**, *14*, 153–61.

268. Russo, V.; Papa, A.A.; Williams, E.A.; Rago, A.; Palladino, A.; Politano, L.; Nigro, G. ACE inhibition to slow progression of myocardial fibrosis in muscular dystrophies. *Trends Cardiovasc. Med.* **2018**, *28*, 330–7.

269. Birnkrant, D.J.; Bushby, K.; Bann, C.M.; Alman, B.A.; Apkon, S.D.; Blackwell, A.; Case, L.E.; Cripe, L.; Hadjiyannakis, S.; Olson, A.K.; Sheehan, D.W.; Bolen, J.; Weber, D.R.; Ward, L.M. Diagnosis and management of Duchenne muscular dystrophy, part 2: respiratory, cardiac, bone health, and orthopaedic management. *Lancet Neurol.* **2018**, *17*, 347–61.

270. Viollet, L.; Thrush, P.T.; Flanigan, K.M.; Mendell, J.R.; Allen, H.D. Effects of angiotensin-converting enzyme inhibitors and/or beta blockers on the cardiomyopathy in duchenne muscular dystrophy. *Am. J. Cardiol.* **2012**, *110*, 98–102.

271. Ogata, H.; Ishikawa, Y.; Minami, R. Beneficial effects of beta-blockers and angiotensin-converting enzyme inhibitors in Duchenne muscular dystrophy. *J. Cardiol.* **2009**, *53*, 72–8.

272. Blain, A.; Greally, E.; Laval, S.; Blamire, A.; Straub, V.; MacGowan, G.A. Beta-blockers, left and right ventricular function, and in-vivo calcium influx in muscular dystrophy cardiomyopathy. *PLoS One* **2013**, *8*, e57260.

273. Fayssoil, A.; Nardi, O.; Annane, D.; Orlikowski, D. Successful cardiac resynchronisation therapy in Duchenne muscular dystrophy: a 5-year follow-up. *Press. médicale* **2014**, *43*, 330–1.

274. Ryan, T.D.; Jefferies, J.L.; Sawnani, H.; Wong, B.L.; Gardner, A.; Del Corral, M.; Lorts, A.; Morales, D.L.S. Implantation of the HeartMate II and HeartWare left ventricular assist devices in patients with Duchenne muscular dystrophy: Lessons learned from the first applications. *ASAIO J.* **2014**, *60*, 246–8.

275. Stoller, D.; Araj, F.; Amin, A.; Fitzsimmons, C.; Morlend, R.; Thibodeau, J.T.; Ramaciotti, C.; Drazner, M.H.; Meyer, D.M.; Mammen, P.P.A. Implantation of a left ventricular assist device to provide long-term support for end-stage Duchenne muscular dystrophy-associated cardiomyopathy. *ESC Hear. Fail.* **2017**, *4*, 379–83.

276. Wilton, S.D.; Lloyd, F.; Carville, K.; Fletcher, S.; Honeyman, K.; Agrawal, S.; Kole, R. Specific removal of the nonsense mutation from the mdx dystrophin mRNA using antisense oligonucleotides. *Neuromuscul. Disord.* **1999**, *9*, 330–8.

277. Cartegni, L.; Chew, S.L.; Krainer, A.R. Listening to silence and understanding nonsense: exonic mutations that affect splicing. *Nat. Rev. Genet.* **2002**, *3*, 285–98.

278. Aartsma-Rus, A.; Fokkema, I.; Verschuuren, J.; Ginjaar, I.; Van Deutekom, J.; Van Ommen, G.J.; den Dunnen, J.T. Theoretic applicability of antisense-mediated exon skipping for Duchenne muscular dystrophy mutations. *Hum. Mutat.* **2009**, *30*, 293–9.

279. Aoki, Y.; Yokota, T.; Nagata, T.; Nakamura, A.; Tanihata, J.; Saito, T.; Duguez, S.M.R.; Nagaraju, K.; Hoffman, E.P.; Partridge, T.; Takeda, S. Bodywide skipping of exons 45-55 in dystrophic mdx52 mice by systemic antisense delivery. *Proc. Natl. Acad. Sci.* **2012**, *109*, 13763–8.

280. Miskew Nichols, B.; Aoki, Y.; Kuraoka, M.; Lee, J.J.A.; Takeda, S.; Yokota, T. Multi-exon skipping using cocktail antisense oligonucleotides in the canine X-linked muscular dystrophy. *J. Vis. Exp.* **2016**, *111*, e53776.

281. Lim, K.R.Q.; Echigoya, Y.; Nagata, T.; Kuraoka, M.; Kobayashi, M.; Aoki, Y.; Partridge, T.;

Maruyama, R.; Takeda, S.; Yokota, T. Efficacy of multi-exon skipping treatment in Duchenne muscular dystrophy dog model neonates. *Mol. Ther.* **2018**, *27*, 76–86.

282. Alter, J.; Lou, F.; Rabinowitz, A.; Yin, H.; Rosenfeld, J.; Wilton, S.D.; Partridge, T.A.; Lu, Q.L. Systemic delivery of morpholino oligonucleotide restores dystrophin expression bodywide and improves dystrophic pathology. *Nat. Med.* **2006**, *12*, 175–7.

283. Lu, Q.L.; Rabinowitz, A.; Chen, Y.C.; Yokota, T.; Yin, H.; Alter, J.; Jadoon, A.; Bou-Gharios, G.; Partridge, T. Systemic delivery of antisense oligoribonucleotide restores dystrophin expression in body-wide skeletal muscles. *Proc. Natl. Acad. Sci. U. S. A.* **2005**, *102*, 198–203.

284. Mendell, J.R.; Rodino-Klapac, L.R.; Sahenk, Z.; Roush, K.; Bird, L.; Lowes, L.P.; Alfano, L.; Gomez, A.M.; Lewis, S.; Kota, J.; Malik, V.; Shontz, K.; Walker, C.M.; Flanigan, K.M.; Corridore, M.; Kean, J.R.; Allen, H.D.; Shilling, C.; Melia, K.R.; Sazani, P.; Saoud, J.B.; Kaye, E.M.; R Mendell, J.; Rodino-Klapac, L.R.; Sahenk, Z.; Roush, K.; Bird, L.; Lowes, L.P.; Alfano, L.; Gomez, A.M.; Lewis, S.; Kota, J.; Malik, V.; Shontz, K.; Walker, C.M.; Flanigan, K.M.; Corridore, M.; Kean, J.R.; Allen, H.D.; Shilling, C.; Melia, K.R.; Sazani, P.; Saoud, J.B.; Kaye, E.M. Eteplirsen for the treatment of Duchenne muscular dystrophy. *Ann. Neurol.* **2013**, *74*, 637–47.

285. Voit, T.; Topaloglu, H.; Straub, V.; Muntoni, F.; Deconinck, N.; Campion, G.; De Kimpe, S.J.; Eagle, M.; Guglieri, M.; Hood, S.; Liefaard, L.; Lourbakos, A.; Morgan, A.; Nakielny, J.; Quarcoo, N.; Ricotti, V.; Rolfe, K.; Servais, L.; Wardell, C.; Wilson, R.; Wright, P.; Kraus, J.E. Safety and efficacy of drisapersen for the treatment of Duchenne muscular dystrophy (DEMAND II): an exploratory, randomised, placebo-controlled phase 2 study. *Lancet Neurol.* **2014**, *13*, 987–96.

286. Rinaldi, C.; Wood, M.J.A. Antisense oligonucleotides: The next frontier for treatment of neurological disorders. *Nat. Rev. Neurol.* **2018**, *14*, 9–21.

287. Goemans, N.M.N.; Tulinius, M.; van den Akker, J.T.; Burm, B.E.; Ph, D.; Ekhart, P.F.; Sc, M.; Heuvelmans, N.; Holling, T.; Janson, A.A.; Platenburg, G.J.; Sipkens, J.A.; Sitsen, J.M.A.; Aartsma-Rus, A.; Ommen, G.B. Van; Kimpe, S.J. De; Deutekom, J.C. Van; van Ommen, G.-J.B.; Buyse, G.; Darin, N.; Verschuuren, J.J.; Campion, G. V; de Kimpe, S.J.; van Deutekom, J.C.; Ph, D.; Ekhart, P.F.; Sc, M.; Heuvelmans, N.; Holling, T.; Janson, A.A.; Platenburg, G.J.; Sipkens, J.A.; Sitsen, J.M.A.; Aartsma-Rus, A.; Ommen, G.B. Van; Kimpe, S.J. De; Deutekom, J.C. Van Systemic Administration of PRO051 in Duchenne's Muscular Dystrophy. *N. Engl. J. Med.* **2011**, *364*, 1513–22.

288. Goemans, N.; Mercuri, E.; Belousova, E.; Komaki, H.; Dubrovsky, A.; McDonald, C.M.; Kraus, J.E.; Lourbakos, A.; Lin, Z.; Campion, G.; Wang, S.X.; Campbell, C. A randomized placebo-controlled phase 3 trial of an antisense oligonucleotide, drisapersen, in Duchenne muscular dystrophy. *Neuromuscul. Disord.* **2017**, *28*, 4–15.

289. Flanigan, K.M.; Voit, T.; Rosales, X.Q.; Servais, L.; Kraus, J.E.; Wardell, C.; Morgan, A.; Dorricott, S.; Nakielny, J.; Quarcoo, N.; Liefaard, L.; Drury, T.; Campion, G.; Wright, P. Pharmacokinetics and safety of single doses of drisapersen in non-ambulant subjects with Duchenne muscular dystrophy: Results of a double-blind randomized clinical trial. *Neuromuscul. Disord.* **2014**, *24*, 16–24.

290. Mendell, J.R.; Sahenk, Z.; Rodino-Klapac, L.R. Clinical trials of exon skipping in Duchenne muscular dystrophy. *Expert Opin. Orphan Drugs* **2017**, *5*, 683–90.

291. Cirak, S.; Arechavala-Gomeza, V.; Guglieri, M.; Feng, L.; Torelli, S.; Anthony, K.; Abbs, S.; Garralda, M.E.; Bourke, J.; Wells, D.J.; Dickson, G.; Wood, M.J.; Wilton, S.D.; Straub, V.; Kole, R.; Shrewsbury, S.B.; Sewry, C.; Morgan, J.E.; Bushby, K.; Muntoni, F. Exon skipping and dystrophin restoration in patients with Duchenne muscular dystrophy after systemic phosphorodiamidate morpholino oligomer treatment: An open-label, phase 2, dose-escalation study. *Lancet* **2011**, *378*, 595–605.

292. Mendell, J.R.; Goemans, N.; Lowes, L.P.; Alfano, L.N.; Berry, K.; Shao, J.; Kaye, E.M.; Mercuri, E. Longitudinal effect of eteplirsen versus historical control on ambulation in Duchenne muscular dystrophy. *Ann. Neurol.* **2016**, *79*, 257–71.

293. Aartsma-Rus, A.; Krieg, A.M. FDA approves Eteplirsen for Duchenne muscular dystrophy: The next chapter in the Eteplirsen saga. *Nucleic Acid Ther.* **2017**, *27*, 1–3.

294. Charleston, J.S.; Schnell, F.J.; Dworzak, J.; Donoghue, C.; Lewis, S.; Chen, L.; David Young, G.; Milici, A.J.; Voss, J.; Dealwis, U.; Wentworth, B.; Rodino-Klapac, L.R.; Sahenk, Z.; Frank, D.; Mendell, J.R. Eteplirsen treatment for Duchenne muscular dystrophy: Exon skipping and dystrophin production. *Neurology* **2018**, *90*, e2146-54.

295. Komaki, H.; Nagata, T.; Saito, T.; Masuda, S.; Takeshita, E.; Sasaki, M.; Tachimori, H.; Nakamura, H.; Aoki, Y.; Takeda, S. Systemic administration of the antisense oligonucleotide NS-065/NCNP-01 for skipping of exon 53 in patients with Duchenne muscular dystrophy. *Sci. Transl. Med.* **2018**, *10*, 1–11.

296. Malerba, A.; Thorogood, F.C.; Dickson, G.; Graham, I.R. Dosing regimen has a significant impact on the efficiency of morpholino oligomer-induced exon skipping in mdx mice. *Hum. Gene Ther.* **2009**, *20*, 955–65.

297. Malerba, A.; Sharp, P.S.; Graham, I.R.; Arechavala-Gomeza, V.; Foster, K.; Muntoni, F.; Wells, D.J.; Dickson, G. Chronic systemic therapy with low-dose morpholino oligomers ameliorates the pathology and normalizes locomotor behavior in mdx mice. *Mol. Ther.* **2011**, *19*, 345–54.

298. Goyenvalle, A.; Griffith, G.; Babbs, A.; Andaloussi, S. El; Ezzat, K.; Avril, A.; Dugovic, B.; Chaussenot, R.; Ferry, A.; Voit, T.; Amthor, H.; Bühr, C.; Schürch, S.; Wood, M.J. a; Davies, K.E.; Vaillend, C.; Leumann, C.; Garcia, L. Functional correction in mouse models of muscular dystrophy using exon-skipping tricyclo-DNA oligomers. *Nat. Med.* **2015**, *21*, 270–5.

299. Ivanova, G.D.; Fabani, M.M.; Arzumanov, A.A.; Abes, R.; Yin, H.; Lebleu, B.; Wood, M.; Gait, M.J. PNA-peptide conjugates as intracellular gene control agents. In *Nucleic Acids Symp.Ser.(Oxf)*; 2008; pp. 31–2.

300. Ivanova, G.D.; Arzumanov, A.; Abes, R.; Yin, H.; Wood, M.J.A.A.; Lebleu, B.; Gait, M.J. Improved cell-penetrating peptide-PNA conjugates for splicing redirection in HeLa cells and exon skipping in mdx mouse muscle. *Nucleic Acids Res.* **2008**, *36*, 6418–28.

301. Yin, H.; Saleh, A.F.; Betts, C.; Camelliti, P.; Seow, Y.; Ashraf, S.; Arzumanov, A.; Hammond, S.; Merritt, T.; Gait, M.J.; Wood, M.J.A.J. Pip5 transduction peptides direct high efficiency oligonucleotide-mediated dystrophin exon skipping in heart and phenotypic correction in mdx mice. *Mol. Ther.* **2011**, *19*, 1295–1303.

302. Yin, H.; Moulton, H.M.; Seow, Y.; Boyd, C.; Boutilier, J.; Iverson, P.; Wood, M.J.A. Cell-penetrating peptide-conjugated antisense oligonucleotides restore systemic muscle and cardiac dystrophin expression and function. *Hum. Mol. Genet.* **2008**, *17*, 3909–18.

303. Betts, C.; Saleh, A.F.; Arzumanov, A.A.; Hammond, S.M.; Godfrey, C.; Coursindel, T.; Gait, M.J.; Wood, M.J. Pip6-PMO, a new generation of peptide-oligonucleotide conjugates with improved cardiac exon skipping activity for DMD treatment. *Mol. Ther. — Nucleic Acids* **2012**, *1*, e38.

304. Betts, C. a.; Saleh, A.F.; Carr, C. a.; Hammond, S.M.; Coenen-Stass, A.M.L.; Godfrey, C.; McClorey, G.; Varela, M. a.; Roberts, T.C.; Clarke, K.; Gait, M.J.; Wood, M.J. a. Prevention of exercised induced cardiomyopathy following Pip-PMO treatment in dystrophic mdx mice. *Sci. Rep.* **2015**, *5*, 1–9.

305. Gait, M.J.; Arzumanov, A.A.; McClorey, G.; Godfrey, C.; Betts, C.; Hammond, S.; Wood, M.J.A. Cell-penetrating peptide conjugates of steric blocking oligonucleotides as therapeutics for neuromuscular diseases from a historical perspective to current prospects of treatment. *Nucleic Acid Ther.* **2019**, *29*, 1–12.

306. Finkel, R.S. Read-through strategies for suppression of nonsense mutations in Duchenne/ Becker muscular dystrophy: aminoglycosides and ataluren (PTC124). *J. Child Neurol.* **2010**, *25*, 1158–64.

307. Konieczny, P.; Swiderski, K.; Chamberlain, J.S. Gene and cell-mediated therapies for muscular dystrophy. *Muscle and Nerve* **2013**, *47*, 649–3.

308. Muntoni, F.; Wood, M.J.A. Targeting RNA to treat neuromuscular disease. *Nat. Rev. Drug Discov.* **2011**, *10*, 621–37.

309. Welch, E.M.; Barton, E.R.; Zhuo, J.; Tomizawa, Y.; Friesen, W.J.; Trifillis, P.; Paushkin, S.; Patel, M.; Trotta, C.R.; Hwang, S.; Wilde, R.G.; Karp, G.; Takasugi, J.; Chen, G.; Jones, S.; Ren, H.; Moon, Y.-C.; Corson, D.; Turpoff, A. a; Campbell, J. a; Conn, M.M.; Khan, A.; Almstead, N.G.; Hedrick, J.; Mollin, A.; Risher, N.; Weetall, M.; Yeh, S.; Branstrom, A. a; Colacino, J.M.; Babiak, J.; Ju, W.D.; Hirawat, S.; Northcutt, V.J.; Miller, L.L.; Spatrick, P.; He, F.; Kawana, M.; Feng, H.; Jacobson, A.; Peltz, S.W.; Sweeney, H.L. PTC124 targets genetic disorders caused by nonsense mutations. *Nature* **2007**, *447*, 87–91.

310. McDonald, C.M.; Campbell, C.; Torricelli, R.E.; Finkel, R.S.; Flanigan, K.M.; Goemans, N.; Heydemann, P.; Kaminska, A.; Kirschner, J.; Muntoni, F.; Osorio, A.N.; Schara, U.; Sejersen, T.; Shieh, P.B.; Sweeney, H.L.; Topaloglu, H.; Tulinius, M.; Vilchez, J.J.; Voit, T.; Wong, B.; Elfring, G.; Kroger, H.; Luo, X.; McIntosh, J.; Ong, T.; Riebling, P.; Souza, M.; Spiegel, R.J.; Peltz, S.W.; Mercuri, E.; Alfano, L.N.; Eagle, M.; James, M.K.; Lowes, L.; Mayhew, A.; Mazzone, E.S.; Nelson, L.; Rose, K.J.; Abdel-Hamid, H.Z.; Apkon, S.D.; Barohn, R.J.; Bertini, E.; Bloetzer, C.; de Vaud, L.C.; Butterfield, R.J.; Chabrol, B.; Chae, J.H.; Jongno-gu, D. ro; Comi, G. Pietro; Darras, B.T.; Dastgir, J.; Desguerre, I.; Escobar, R.G.; Finanger, E.; Guglieri, M.; Hughes, I.; Iannaccone, S.T.; Jones, K.J.; Karachunski, P.; Kudr, M.; Lotze, T.; Mah, J.K.; Mathews, K.; Nevo, Y.; Parsons, J.; Péréon, Y.; de Queiroz Campos Araujo, A.P.; Renfroe, J. Ben; de Resende, M.B.D.; Ryan, M.; Selby, K.; Tennekoon, G.; Vita, G. Ataluren in patients with nonsense mutation Duchenne muscular dystrophy (ACT DMD): a multicentre, randomised, double-blind, placebo-controlled, phase 3 trial. *Lancet* **2017**, *390*, 1489–98.

311. EMA Translarna Available online: https://www.ema.europa.eu/medicines/human/EPAR/translarna.

312. McElroy, S.P.; Nomura, T.; Torrie, L.S.; Warbrick, E.; Gartner, U.; Wood, G.; McLean, W.H.I. A lack of premature termination codon read-through efficacy of PTC124 (Ataluren) in a diverse array of reporter assays. *PLoS Biol.* **2013**, *11*, e1001593.

313. Kayali, R.; Ku, J.M.; Khitrov, G.; Jung, M.E.; Prikhodko, O.; Bertoni, C. Read-through compound 13 restores dystrophin expression and improves muscle function in the MDX mouse model for duchenne muscular dystrophy. *Hum. Mol. Genet.* **2012**, *21*, 4007–20.

314. UCLA Technology Development Group Read-Through Compound Prodrugs Suppressing Premature Nonsense Mutations Available online: https://techtransfer.universityofcalifornia.edu/NCD/24094.html.

315. Skuk, D.; Goulet, M.; Roy, B.; Tremblay, J.P. Efficacy of myoblast transplantation in nonhuman primates following simple intramuscular cell injections: toward defining strategies applicable to humans. *Exp. Neurol.* **2002**, *175*, 112–26.

316. Partridge, T.A.; Morgan, J.E.; Coulton, G.R.; Hoffman, E.P.; Kunkel, L.M. Conversion of mdx myofibres from dystrophin-negative to -positive by injection of normal myoblasts. *Nature* **1989**, *337*, 176–9.

317. Mendell, J.R.; Kissel, J.T.; Amato, a a; King, W.; Signore, L.; Prior, T.W.; Sahenk, Z.; Benson, S.; McAndrew, P.E.; Rice, R. Myoblast transfer in the treatment of Duchenne's muscular dystrophy. *N. Engl. J. Med.* **1995**, *333*, 832–8.

318. Huard, C.; Moisset, P. a; Dicaire, A.; Merly, F.; Tardif, F.; Asselin, I.; Tremblay, J.P. Transplantation of dermal fibroblasts expressing MyoD1 in mouse muscles. *Biochem. Biophys. Res. Commun.* **1998**, *248*, 648–54.

319. Muir, L.A.; Nguyen, Q.G.; Hauschka, S.D.; Chamberlain, J.S. Engraftment potential of dermal fibroblasts following in vivo myogenic conversion in immunocompetent dystrophic skeletal muscle. *Mol. Ther. - Methods Clin. Dev.* **2014**, *1*, 1–10.

320. Goodell, M.A.; Brose, K.; Paradis, G.; Conner, A.S.; Mulligan, R.C. Isolation and functional properties of murine hematopoietic stem cells that are replicating in vivo. *J. Exp. Med.* **1996**, *183*, 1797–806.

321. Gussoni, E.; Soneoka, Y.; Strickland, C.D.; Buzney, E. a; Khan, M.K.; Flint, a F.; Kunkel, L.M.; Mulligan, R.C. Dystrophin expression in the mdx mouse restored by stem cell transplantation. *Nature* **1999**, *401*, 390–4.

322. Dell'Agnola, C.; Wang, Z.; Storb, R.; Tapscott, S.J.; Kuhr, C.S.; Hauschka, S.D.; Lee, R.S.; Sale, G.E.; Zellmer, E.; Gisburne, S.; Bogan, J.; Kornegay, J.N.; Cooper, B.J.; Gooley, T. a.; Little, M.T. Hematopoietic stem cell transplantation does not restore dystrophin expression in Duchenne muscular dystrophy dogs. *Blood* **2004**, *104*, 4311–8.

323. Benchaouir, R.; Meregalli, M.; Farini, A.; D'Antona, G.; Belicchi, M.; Goyenvalle, A.; Battistelli, M.; Bresolin, N.; Bottinelli, R.; Garcia, L.; Torrente, Y. Restoration of human dystrophin following transplantation of exon-skipping-engineered DMD patient stem cells into dystrophic mice. *Cell Stem Cell* **2007**, *1*, 646–57.

324. Torrente, Y.; Belicchi, M.; Marchesi, C.; D'Antona, G.; Cogiamanian, F.; Pisati, F.; Gavina, M.; Giordano, R.; Tonlorenzi, R.; Fagiolari, G.; Lamperti, C.; Porretti, L.; Lopa, R.; Sampaolesi, M.; Vicentini, L.; Grimoldi, N.; Tiberio, F.; Songa, V.; Baratta, P.; Prelle, A.; Forzenigo, L.; Guglieri, M.; Pansarasa, O.; Rinaldi, C.; Mouly, V.; Butler-Browne, G.S.; Comi, G.P.; Biondetti, P.; Moggio, M.; Gaini, S.M.; Stocchetti, N.; Priori, A.; D'Angelo, M.G.; Turconi, A.; Bottinelli, R.; Cossu, G.; Rebulla, P.; Bresolin, N. Autologous transplantation of muscle-derived CD133+ stem cells in Duchenne muscle patients. *Cell Transplant.* **2007**, *16*, 563–77.

325. Sampaolesi, M.; Blot, S.; D'Antona, G.; Granger, N.; Tonlorenzi, R.; Innocenzi, A.; Mognol, P.; Thibaud, J.-L.; Galvez, B.G.; Barthélémy, I.; Perani, L.; Mantero, S.; Guttinger, M.; Pansarasa, O.; Rinaldi, C.; Cusella De Angelis, M.G.; Torrente, Y.; Bordignon, C.; Bottinelli, R.; Cossu, G. Mesoangioblast stem cells ameliorate muscle function in dystrophic dogs. *Nature* **2006**, *444*, 574–9.

326. Muir, L.A.; Murry, C.E.; Chamberlain, J.S. Prosurvival factors improve functional engraftment of myogenically converted dermal cells into dystrophic skeletal muscle. *Stem Cells Dev.* **2016**, *25*, 1559–69.

327. Rousseau, J.; Chapdelaine, P.; Boisvert, S.; Almeida, L.P.; Corbeil, J.; Montpetit, A.; Tremblay, J.P. Endonucleases: tools to correct the dystrophin gene. *J. Gene Med.* **2011**, *13*, 522–37.

328. Li, H.L.; Fujimoto, N.; Sasakawa, N.; Shirai, S.; Ohkame, T.; Sakuma, T.; Tanaka, M.; Amano, N.; Watanabe, A.; Sakurai, H.; Yamamoto, T.; Yamanaka, S.; Hotta, A. Precise correction of the dystrophin gene in Duchenne muscular dystrophy patient induced pluripotent stem cells by TALEN and CRISPR-Cas9. *Stem Cell Reports* **2015**, *4*, 143–54.

329. Popplewell, L.; Koo, T.; Leclerc, X.; Duclert, A.; Mamchaoui, K.; Gouble, A.; Mouly, V.; Voit, T.; Pâques, F.; Cédrone, F.; Isman, O.; Yáñez-Muñoz, R.J.; Dickson, G. Gene correction of a duchenne muscular dystrophy mutation by meganuclease-enhanced exon knock-in. *Hum. Gene Ther.* **2013**, *24*, 692–701.

330. Siemionow, M.; Cwykiel, J.; Heydemann, A.; Garcia-Martinez, J.; Siemionow, K.; Szilagyi, E. Creation of dystrophin expressing chimeric cells of myoblast origin as a novel stem cell based

therapy for Duchenne muscular dystrophy. *Stem Cell Rev. Reports* **2018**, *14*, 189–99.

331. Scott, J.M.; Li, S.; Harper, S.Q.; Welikson, R.; Bourque, D.; DelloRusso, C.; Hauschka, S.D.; Chamberlain, J.S. Viral vectors for gene transfer of micro-, mini-, or full-length dystrophin. *Neuromuscul. Disord.* **2002**, *12*, 23–9.

332. Asokan, A.; Schaffer, D. V; Jude Samulski, R. The AAV Vector Toolkit: Poised at the Clinical Crossroads. *Mol. Ther.* **2012**, *20*, 699–708.

333. Zincarelli, C.; Soltys, S.; Rengo, G.; Rabinowitz, J.E. Analysis of AAV serotypes 1-9 mediated gene expression and tropism in mice after systemic injection. *Mol. Ther.* **2008**, *16*, 1073–80.

334. Srivastava, A. In vivo tissue-tropism of adeno-associated viral vectors. *Curr. Opin. Virol.* **2016**, *21*, 75–80.

335. Gregorevic, P.; Allen, J.M.; Minami, E.; Blankinship, M.J.; Haraguchi, M.; Meuse, L.; Finn, E.; Adams, M.E.; Froehner, S.C.; Murry, C.E.; Chamberlain, J.S. rAAV6-microdystrophin preserves muscle function and extends lifespan in severely dystrophic mice. *Nat. Med.* **2006**, *12*, 787–9.

336. Gregorevic, P.; Blankinship, M.J.; Allen, J.M.; Chamberlain, J.S. Systemic microdystrophin gene delivery improves skeletal muscle structure and function in old dystrophic mdx mice. *Mol. Ther.* **2008**, *16*, 657–64.

337. Bostick, B.; Yue, Y.; Lai, Y.; Long, C.; Li, D.; Duan, D. Adeno-associated virus serotype-9 microdystrophin gene therapy ameliorates electrocardiographic abnormalities in mdx mice. *Hum. Gene Ther.* **2008**, *19*, 851–6.

338. Kornegay, J.N.; Li, J.; Bogan, J.R.; Bogan, D.J.; Chen, C.; Zheng, H.; Wang, B.; Qiao, C.; Howard, J.F.; Xiao, X. Widespread muscle expression of an AAV9 human mini-dystrophin vector after intravenous injection in neonatal dystrophin-deficient dogs. *Mol. Ther.* **2010**, *18*, 1501–8.

339. Wasala, N.B.; Shin, J.-H.; Lai, Y.; Yue, Y.; Montanaro, F.; Duan, D. Cardiac-specificeExpression of ΔH2-R15 mini-dystrophin normalized all electrocardiogram abnormalities and the end-diastolic volume in a 23-month-old mouse model of Duchenne dilated cardiomyopathy. *Hum. Gene Ther.* **2018**, *29*, 737–48.

340. Schinkel, S.; Bauer, R.; Bekeredjian, R.; Stucka, R.; Rutschow, D.; Lochmüller, H.; Kleinschmidt, J. a.; Katus, H. a.; Müller, O.J. Long-term preservation of cardiac structure and function after adeno-associated virus serotype 9-mediated microdystrophin gene transfer in mdx mice. *Hum. Gene Ther.* **2012**, *23*, 566–75.

341. Bowles, D.E.; McPhee, S.W.; Li, C.; Gray, S.J.; Samulski, J.J.; Camp, A.S.; Li, J.; Wang, B.; Monahan, P.E.; Rabinowitz, J.E.; Grieger, J.C.; Govindasamy, L.; Agbandje-McKenna, M.; Xiao, X.; Samulski, R.J. Phase 1 gene therapy for Duchenne muscular dystrophy using a translational optimized AAV vector. *Mol. Ther.* **2012**, *20*, 443–55.

342. Mendell, J.R.; Campbell, K.; Rodino-Klapac, L.; Sahenk, Z.; Shilling, C.; Lewis, S.; Bowles, D.; Gray, S.; Li, C.; Galloway, G.; Malik, V.; Coley, B.; Clark, K.R.; Li, J.; Xiao, X.; Samulski, J.; McPhee, S.W.; Samulski, R.J.; Walker, C.M. Dystrophin immunity in Duchenne's muscular dystrophy. *N. Engl. J. Med.* **2010**, *363*, 1429–37.

343. Fairclough, R.J.; Wood, M.J.; Davies, K.E. Therapy for Duchenne muscular dystrophy: renewed optimism from genetic approaches. *Nat. Rev. Genet.* **2013**, *14*, 373–8.

344. Mendell, J.R.; Rodino-Klapac, L.; Sahenk, Z.; Malik, V.; Kaspar, B.K.; Walker, C.M.; Clark, K.R. Gene therapy for muscular dystrophy: Lessons learned and path forward. *Neurosci. Lett.* **2012**, *527*, 90–9.

345. Foster, H.; Sharp, P.S.; Athanasopoulos, T.; Trollet, C.; Graham, I.R.; Foster, K.; Wells, D.J.; Dickson, G. Codon and mRNA sequence optimization of microdystrophin transgenes improves expression and physiological outcome in dystrophic mdx mice following AAV2/8 gene transfer.

Mol. Ther. **2008**, *16*, 1825–32.

346. Foster, H.; Popplewell, L.; Dickson, G. Genetic therapeutic approaches for Duchenne muscular dystrophy. *Hum. Gene Ther.* **2012**, *23*, 676–87.

347. Nelson, C.E.; Hakim, C.H.; Ousterout, D.G.; Thakore, P.I.; Moreb, E.A.; Castellanos Rivera, R.M.; Madhavan, S.; Pan, X.; Ran, F.A.; Yan, W.X.; Asokan, A.; Zhang, F.; Duan, D.; Gersbach, C.A. In vivo genome editing improves muscle function in a mouse model of Duchenne muscular dystrophy. *Science (80-.).* **2016**, *351*, 403–7.

348. Tabebordbar, M.; Zhu, K.; Cheng, J.K.W.W.; Chew, W.L.; Widrick, J.J.; Yan, W.X.; Maesner, C.; Wu, E.Y.; Xiao, R.; Ran, F.A.; Cong, L.; Zhang, F.; Vandenberghe, L.H.; Church, G.M.; Wagers, A.J. In vivo gene editing in dystrophic mouse muscle and muscle stem cells. *Science (80-.).* **2016**, *351*, 407–11.

349. Bengtsson, N.E.; Hall, J.K.; Odom, G.L.; Phelps, M.P.; Andrus, C.R.; Hawkins, R.D.; Hauschka, S.D.; Chamberlain, J.R.; Chamberlain, J.S. Muscle-specific CRISPR/Cas9 dystrophin gene editing ameliorates pathophysiology in a mouse model for Duchenne muscular dystrophy. *Nat. Commun.* **2017**, *8*, 1–10.

350. Amoasii, L.; Hildyard, J.C.W.; Li, H.; Sanchez-Ortiz, E.; Mireault, A.; Caballero, D.; Harron, R.; Stathopoulou, T.-R.; Massey, C.; Shelton, J.M.; Bassel-Duby, R.; Piercy, R.J.; Olson, E.N. Gene editing restores dystrophin expression in a canine model of Duchenne muscular dystrophy. *Science (80-.).* **2018**, *362*, 86–91.

351. Deconinck, N.; Rafael, J. a.; Beckers-Bleukx, G.; Kahn, D.; Deconinck, a. E.; Davies, K.E.; Gillis, J.M. Consequences of the combined deficiency in dystrophin and utrophin on the mechanical properties and myosin composition of some limb and respiratory muscles of the mouse. *Neuromuscul. Disord.* **1998**, *8*, 362–70.

352. Chun, J.L.; O'Brien, R.; Berry, S.E. Cardiac dysfunction and pathology in the dystrophin and utrophin-deficient mouse during development of dilated cardiomyopathy. *Neuromuscul. Disord.* **2012**, *22*, 368–79.

353. Tinsley, J.; Deconinck, N.; Fisher, R.; Kahn, D.; Phelps, S.; Gillis, J.M.; Davies, K. Expression of full-length utrophin prevents muscular dystrophy in mdx mice. *Nat. Med.* **1998**, *4*, 1441–4.

354. Perkins, K.J.; Davies, K.E. Alternative utrophin mRNAs contribute to phenotypic differences between dystrophin-deficient mice and Duchenne muscular dystrophy. *FEBS Lett.* **2018**, *592*, 1856–69.

355. Tinsley, J.M.; Potter, a C.; Phelps, S.R.; Fisher, R.; Trickett, J.I.; Davies, K.E. Amelioration of the dystrophic phenotype of mdx mice using a truncated utrophin transgene. *Nature* **1996**, *384*, 349–53.

356. Gilbert, R.; Nalbanoglu, J.; Tinsley, J.M.; Massie, B.; Davies, K.E.; Karpati, G. Efficient utrophin expression following adenovirus gene transfer in dystrophic muscle. *Biochem. Biophys. Res. Commun.* **1998**, *242*, 244–7.

357. Corbi, N.; Libri, V.; Fanciulli, M.; Tinsley, J.M.; Davies, K.E.; Passananti, C. The artificial zinc finger coding gene "Jazz" binds the utrophin promoter and activates transcription. *Gene Ther.* **2000**, *7*, 1076–83.

358. Lu, Y.; Tian, C.; Danialou, G.; Gilbert, R.; Petrof, B.J.; Karpati, G.; Nalbantoglu, J. Targeting artificial transcription factors to the utrophin A promoter: Effects on dystrophic pathology and muscle function. *J. Biol. Chem.* **2008**, *283*, 34720–7.

359. Onori, A.; Pisani, C.; Strimpakos, G.; Monaco, L.; Mattei, E.; Passananti, C.; Corbi, N. UtroUp is a novel six zinc finger artificial transcription factor that recognises 18 base pairs of the utrophin promoter and efficiently drives utrophin upregulation. *BMC Mol. Biol.* **2013**, *14*, 3.

360. Kennedy, T.L.; Guiraud, S.; Edwards, B.; Squire, S.; Moir, L.; Babbs, A.; Odom, G.; Golebiowski, D.; Schneider, J.; Chamberlain, J.S.; Davies, K.E. Micro-utrophin improves cardiac and skeletal muscle function of severely affected D2/mdx mice. *Mol. Ther. - Methods Clin. Dev.* **2018**, *11*, 92–105.

361. Tinsley, J.M.; Fairclough, R.J.; Storer, R.; Wilkes, F.J.; Potter, A.C.; Squire, S.E.; Powell, D.S.; Cozzoli, A.; Capogrosso, R.F.; Lambert, A.; Wilson, F.X.; Wren, S.P.; de Luca, A.; Davies, K.E. Daily treatment with SMTC1100, a novel small molecule utrophin upregulator, dramatically reduces the dystrophic symptoms in the mdx mouse. *PLoS One* **2011**, *6*, e19189.

362. Tinsley, J.; Robinson, N.; Davies, K.E. Safety, tolerability, and pharmacokinetics of SMT C1100, a 2-arylbenzoxazole utrophin modulator, following single- and multiple-dose administration to healthy male adult volunteers. *J. Clin. Pharmacol.* **2015**, *55*, 698–707.

363. Fallon, J.R.; McNally, E.M. Non-Glycanated Biglycan and LTBP4: Leveraging the extracellular matrix for Duchenne Muscular Dystrophy therapeutics. *Matrix Biol.* **2018**, *68–69*, 616–27.

364. Kleopa, K.A.; Drousiotou, A.; Mavrikiou, E.; Ormiston, A.; Kyriakides, T. Naturally occurring utrophin correlates with disease severity in Duchenne muscular dystrophy. *Hum. Mol. Genet.* **2006**, *15*, 1623–8.

365. van Westering, T.L.E.; Betts, C.A.; Wood, M.J.A. Current understanding of molecular pathology and treatment of cardiomyopathy in duchenne muscular dystrophy. *Molecules* **2015**, *20*, 8823–55.

366. Lu, Q.L.; Mann, C.J.; Lou, F.; Bou-Gharios, G.; Morris, G.E.; Xue, S.; Fletcher, S.; Partridge, T.A.; Wilton, S.D. Functional amounts of dystrophin produced by skipping the mutated exon in the mdx dystrophic mouse. *Nat. Med.* **2003**, *9*, 1009–14.

367. Jearawiriyapaisarn, N.; Moulton, H.M.; Buckley, B.; Roberts, J.; Sazani, P.; Fucharoen, S.; Iversen, P.L.; Kole, R. Sustained dystrophin expression induced by peptide-conjugated morpholino oligomers in the muscles of mdx mice. *Mol. Ther.* **2008**, *16*, 1624–9.

368. Wu, B.; Moulton, H.M.; Iversen, P.L.; Jiang, J.; Li, J.; Li, J.; Spurney, C.F.; Sali, A.; Guerron, A.D.; Nagaraju, K.; Doran, T.; Lu, P.; Xiao, X.; Lu, Q.L. Effective rescue of dystrophin improves cardiac function in dystrophin-deficient mice by a modified morpholino oligomer. *Proc. Natl. Acad. Sci. U. S. A.* **2008**, *105*, 14814–9.

369. Moulton, H.M.; Fletcher, S.; Neuman, B.W.; McClorey, G.; Stein, D.A.; Abes, S.; Wilton, S.D.; Buchmeier, M.J.; Lebleu, B.; Iversen, P.L. Cell-penetrating peptide-morpholino conjugates alter pre-mRNA splicing of DMD (Duchenne muscular dystrophy) and inhibit murine coronavirus replication in vivo. *Biochem. Soc. Trans.* **2007**, *35*, 826–8.

370. Fletcher, S.; Honeyman, K.; Fall, A.M.; Harding, P.L.; Johnsen, R.D.; Steinhaus, J.P.; Moulton, H.M.; Iversen, P.L.; Wilton, S.D. Morpholino oligomer-mediated exon skipping averts the onset of dystrophic pathology in the mdx mouse. *Mol. Ther.* **2007**, *15*, 1587–92.

371. Goyenvalle, A.; Babbs, A.; Powell, D.; Kole, R.; Fletcher, S.; Wilton, S.D.; Davies, K.E. Prevention of dystrophic pathology in severely affected dystrophin/utrophin-deficient mice by morpholino-oligomer-mediated exon-skipping. *Mol. Ther.* **2010**, *18*, 198–205.

372. Wu, R.P.; Youngblood, D.S.; Hassinger, J.N.; Lovejoy, C.E.; Nelson, M.H.; Iversen, P.L.; Moulton, H.M. Cell-penetrating peptides as transporters for morpholino oligomers: Effects of amino acid composition on intracellular delivery and cytotoxicity. *Nucleic Acids Res.* **2007**, *35*, 5182–91.

373. Echigoya, Y.; Nakamura, A.; Nagata, T.; Urasawa, N.; Lim, K.R.Q.; Trieu, N.; Panesar, D.; Kuraoka, M.; Moulton, H.M.; Saito, T.; Aoki, Y.; Iversen, P.; Sazani, P.; Kole, R.; Maruyama, R.; Partridge, T.; Takeda, S.; Yokota, T. Effects of systemic multiexon skipping with peptide-conjugated morpholinos in the heart of a dog model of Duchenne muscular dystrophy. *Proc. Natl. Acad. Sci.* **2017**, *114*, 4213–8.

374. Samoylova, T.I.; Smith, B.F. Elucidation of muscle-binding peptides by phage display screening. *Muscle and Nerve* **1999**, *22*, 460–6.

375. Yin, H.; Lu, Q.; Wood, M. Effective exon skipping and restoration of dystrophin expression by peptide nucleic acid antisense oligonucleotides in mdx mice. *Mol. Ther.* **2008**, *16*, 38–45.

376. Yin, H.; Moulton, H.M.; Betts, C.; Seow, Y.; Boutilier, J.; Iverson, P.L.; Wood, M.J.A. A fusion peptide directs enhanced systemic dystrophin exon skipping and functional restoration in dystrophin-deficient mdx mice. *Hum. Mol. Genet.* **2009**, *18*, 4405–14.

377. Seow, Y.; Yin, H.; Wood, M.J.A. Identification of a novel muscle targeting peptide in mdx mice. *Peptides* **2010**, *31*, 1873–7.

378. Jirka, S.M.G.; Heemskerk, H.; Tanganyika-de Winter, C.L.; Muilwijk, D.; Pang, K.H.; de Visser, P.C.; Janson, A.; Karnaoukh, T.G.; Vermue, R.; 't Hoen, P. a C.; van Deutekom, J.C.T.; Aguilera, B.; Aartsma-Rus, A. Peptide conjugation of 2'-O-methyl phosphorothioate antisense oligonucleotides enhances cardiac uptake and exon skipping in mdx mice. *Nucleic Acid Ther.* **2014**, *24*, 25–36.

379. Jirka, S.M.G.; 't Hoen, P.A.C.; Diaz Parillas, V.; Tanganyika-de Winter, C.L.; Verheul, R.C.; Aguilera, B.; de Visser, P.C.; Aartsma-Rus, A.M. Cyclic peptides to improve delivery and exon skipping of antisense oligonucleotides in a mouse model for Duchenne muscular dystrophy. *Mol. Ther.* **2018**, *26*, 132–47.

380. Watanabe, N.; Nagata, T.; Satou, Y.; Masuda, S.; Saito, T.; Kitagawa, H.; Komaki, H.; Takagaki, K.; Takeda, S. NS-065/NCNP-01: An antisense oligonucleotide for potential treatment of exon 53 skipping in Duchenne muscular dystrophy. *Mol. Ther. - Nucleic Acids* **2018**, *13*, 442–9.

381. Wu, B.; Li, Y.; Morcos, P.A.; Doran, T.J.; Lu, P.; Lu, Q.L. Octa-guanidine morpholino restores dystrophin expression in cardiac and skeletal muscles and ameliorates pathology in dystrophic mdx mice. *Mol. Ther.* **2009**, *17*, 864–71.

382. Yokota, T.; Nakamura, A.; Nagata, T.; Saito, T.; Kobayashi, M.; Aoki, Y.; Echigoya, Y.; Partridge, T.; Hoffman, E.P.; Takeda, S. Extensive and prolonged restoration of dystrophin expression with vivo-morpholino-mediated multiple exon skipping in dystrophic dogs. *Nucleic Acid Ther.* **2012**, *22*, 306–15.

383. Echigoya, Y.; Aoki, Y.; Miskew, B.; Panesar, D.; Touznik, A.; Nagata, T.; Tanihata, J.; Nakamura, A.; Nagaraju, K.; Yokota, T. Long-term efficacy of systemic multiexon skipping targeting Dystrophin exons 45-55 with a cocktail of vivo-morpholinos in Mdx52 mice. *Mol. Ther. - Nucleic Acids* **2015**, *4*, e225.

384. Wu, B.; Xiao, B.; Cloer, C.; Shaban, M.; Sali, A.; Lu, P.; Li, J.; Nagaraju, K.; Xiao, X.; Lu, Q.L. One-year treatment of morpholino antisense oligomer improves skeletal and cardiac muscle functions in dystrophic mdx mice. *Mol. Ther.* **2011**, *19*, 576–83.

385. Kinali, M.; Arechavala-Gomeza, V.; Feng, L.; Cirak, S.; Hunt, D.; Adkin, C.; Guglieri, M.; Ashton, E.; Abbs, S.; Nihoyannopoulos, P.; Garralda, M.E.; Rutherford, M.; Mcculley, C.; Popplewell, L.; Graham, I.R.; Dickson, G.; Wood, M.J.; Wells, D.J.; Wilton, S.D.; Kole, R.; Straub, V.; Bushby, K.; Sewry, C.; Morgan, J.E.; Muntoni, F. Local restoration of dystrophin expression with the morpholino oligomer AVI-4658 in Duchenne muscular dystrophy: a single-blind, placebo-controlled, dose-escalation, proof-of-concept study. *Lancet Neurol.* **2009**, *8*, 918–28.

386. Relizani, K.; Griffith, G.; Echevarría, L.; Zarrouki, F.; Facchinetti, P.; Vaillend, C.; Leumann, C.; Garcia, L.; Goyenvalle, A. Efficacy and safety profile of tricyclo-DNA antisense oligonucleotides in Duchenne muscular dystrophy mouse model. *Mol. Ther. - Nucleic Acids* **2017**, *8*, 144–57.

387. Barton-Davis, E.R.; Cordier, L.; Shoturma, D.I.; Leland, S.E.; Sweeney, H.L. Aminoglycoside antibiotics restore dystrophin function to skeletal muscles of mdx mice. *J. Clin. Invest.* **1999**, *104*, 375–81.

388. Malik, V.; Rodino-Klapac, L.R.; Viollet, L.; Wall, C.; King, W.; Al-Dahhak, R.; Lewis, S.; Shilling, C.J.; Kota, J.; Serrano-Munuera, C.; Hayes, J.; Mahan, J.D.; Campbell, K.J.; Banwell, B.; Dasouki, M.; Watts, V.; Sivakumar, K.; Bien-Willner, R.; Flanigan, K.M.; Sahenk, Z.; Barohn, R.J.; Walker, C.M.; Mendell, J.R. Gentamicin-induced readthrough of stop codons in Duchenne muscular dystrophy. *Ann. Neurol.* **2010**, *67*, 771–80.

389. Lee, H.N.; Sawnani, H.; Wong, B.L. Gentamicin treatment of nonsense-mediated Duchenne Muscular Dystrophy: A case report. *Neuromuscul. Disord.* **2012**, *22*, 850–1, doi:10.1016/j.nmd.2012.06.160.

390. Baradaran-Heravi, A.; Niesser, J.; Balgi, A.D.; Choi, K.; Zimmerman, C.; South, A.P.; Anderson, H.J.; Strynadka, N.C.; Bally, M.B.; Roberge, M. Gentamicin B1 is a minor gentamicin component with major nonsense mutation suppression activity. *Proc. Natl. Acad. Sci.* **2017**, *114*, 3479–84.

391. Arakawa, M.; Shiozuka, M.; Nakayama, Y.; Hara, T.; Hamada, M.; Kondo, S.; Ikeda, D.; Takahashi, Y.; Sawa, R.; Nonomura, Y.; Sheykholeslami, K.; Kondo, K.; Kaga, K.; Kitamura, T.; Suzuki-Miyagoe, Y.; Takeda, S.; Matsuda, R. Negamycin Restores Dystrophin Expression in Skeletal and Cardiac Muscles of mdx Mice. *J. Biochem.* **2003**, *134*, 751–8.

392. Hirawat, S.; Welch, E.M.; Elfring, G.L.; Northcutt, V.J.; Paushkin, S.; Hwang, S.; Leonard, E.M.; Almstead, N.G.; Ju, W.; Peltz, S.W.; Miller, L.L. Safety, tolerability, and pharmacokinetics of PTC124, a nonaminoglycoside nonsense mutation suppressor, following single- and multiple-dose administration to healthy male and female adult volunteers. *J. Clin. Pharmacol.* **2007**, *47*, 430–44.

393. Finkel, R.S.; Flanigan, K.M.; Wong, B.; Bönnemann, C.; Sampson, J.; Sweeney, H.L.; Reha, A.; Northcutt, V.J.; Elfring, G.; Barth, J.; Peltz, S.W. Phase 2a study of ataluren-mediated dystrophin production in patients with nonsense mutation Duchenne muscular dystrophy. *PLoS One* **2013**, *8*, e81302.

394. Bushby, K.; Finkel, R.; Wong, B.; Barohn, R.; Campbell, C.; Comi, G.P.; Connolly, M.; Day, J.W.; Flanigan, K.M. Ataluren treatment of patients with nonsense mutation dystrophinopathy. *Muscle Nerve* **2014**, *50*, 477–87.

395. Goudenege, S.; Lamarre, Y.; Dumont, N.; Rousseau, J.; Frenette, J.; Skuk, D.; Tremblay, J.P. Laminin-111: a potential therapeutic agent for Duchenne muscular dystrophy. *Mol. Ther.* **2010**, *18*, 2155–63.

396. Goudenege, S.; Lebel, C.; Huot, N.B.; Dufour, C.; Fujii, I.; Gekas, J.; Rousseau, J.; Tremblay, J.P. Myoblasts derived from normal hESCs and dystrophic hiPSCs efficiently fuse with existing muscle fibers following transplantation. *Mol. Ther.* **2012**, *20*, 2153–67.

397. Darabi, R.; Arpke, R.W.; Irion, S.; Dimos, J.T.; Grskovic, M.; Kyba, M.; Perlingeiro, R.C.R. Human ES- and iPS-derived myogenic progenitors restore dystrophin and improve contractility upon transplantation in dystrophic mice. *Cell Stem Cell* **2012**, *10*, 610–9.

398. Feng Cai, W.; Huang, W.; Wang, L.; Wang, J.P.; Zhang, L.; Ashraf, M.; Wu, S.; Wang, Y. Induced pluripotent stem cells derived muscle progenitors effectively mitigate muscular dystrophy through restoring the dystrophin distribution. *J. Stem Cell Res. Ther.* **2016**, *6*.

399. Iyer, P.S.; Mavoungou, L.O.; Ronzoni, F.; Zemla, J.; Schmid-Siegert, E.; Antonini, S.; Neff, L.A.; Dorchies, O.M.; Jaconi, M.; Lekka, M.; Messina, G.; Mermod, N. Autologous cell therapy approach for Duchenne muscular dystrophy using piggybac transposons and mesoangioblasts. *Mol. Ther.* **2018**, *26*, 1093–1108.

400. Cossu, G.; Previtali, S.C.; Napolitano, S.; Cicalese, M.P.; Tedesco, F.S.; Nicastro, F.; Noviello, M.; Roostalu, U.; Natali Sora, M.G.; Scarlato, M.; De Pellegrin, M.; Godi, C.; Giuliani, S.; Ciotti, F.; Tonlorenzi, R.; Lorenzetti, I.; Rivellini, C.; Benedetti, S.; Gatti, R.; Marktel, S.; Mazzi, B.; Tettamanti, A.; Ragazzi, M.; Imro, M.A.; Marano, G.; Ambrosi, A.; Fiori, R.; Sormani, M.P.;

Bonini, C.; Venturini, M.; Politi, L.S.; Torrente, Y.; Ciceri, F. Intra-arterial transplantation of HLA-matched donor mesoangioblasts in Duchenne muscular dystrophy. *EMBO Mol. Med.* **2016**, *8*, 1470–1.

401. DelloRusso, C.; Scott, J.M.; Hartigan-O'Connor, D.; Salvatori, G.; Barjot, C.; Robinson, A.S.; Crawford, R.W.; Brooks, S. V; Chamberlain, J.S. Functional correction of adult mdx mouse muscle using gutted adenoviral vectors expressing full-length dystrophin. *Proc. Natl. Acad. Sci. U. S. A.* **2002**, *99*, 12979–84.

402. Yue, Y.; Pan, X.; Hakim, C.H.; Kodippili, K.; Zhang, K.; Shin, J.H.; Yang, H.T.; McDonald, T.; Duan, D. Safe and bodywide muscle transduction in young adult Duchenne muscular dystrophy dogs with adeno-associated virus. *Hum. Mol. Genet.* **2015**, *24*, 5880–90.

403. Hakim, C.H.; Wasala, N.B.; Pan, X.; Kodippili, K.; Yue, Y.; Zhang, K.; Yao, G.; Haffner, B.; Duan, S.X.; Ramos, J.; Schneider, J.S.; Yang, N.N.; Chamberlain, J.S.; Duan, D. A five-repeat micro-dystrophin gene ameliorated dystrophic phenotype in the severe DBA/2J-mdx model of Duchenne muscular dystrophy. *Mol. Ther. - Methods Clin. Dev.* **2017**, *6*, 216–30.

404. Li, S.; Kimura, E.; Fall, B.M.; Reyes, M.; Angello, J.C.; Welikson, R.; Hauschka, S.D.; Chamberlain, J.S. Stable transduction of myogenic cells with lentiviral vectors expressing a minidystrophin. *Gene Ther.* **2005**, *12*, 1099–1108.

405. Wang, X.; Ha, T.; Liu, L.; Zou, J.; Zhang, X.; Kalbfleisch, J.; Gao, X.; Williams, D.; Li, C. Increased expression of microRNA-146a decreases myocardial ischaemia/reperfusion injury. *Cardiovasc. Res.* **2013**, *97*, 432–42.

406. Kimura, E.; Li, S.; Gregorevic, P.; Fall, B.M.; Chamberlain, J.S. Dystrophin delivery to muscles of mdx mice using lentiviral vectors leads to myogenic progenitor targeting and stable gene expression. *Mol. Ther.* **2010**, *18*, 206–13.

407. Counsell, J.R.; Asgarian, Z.; Meng, J.; Ferrer, V.; Vink, C.A.; Howe, S.J.; Waddington, S.N.; Thrasher, A.J.; Muntoni, F.; Morgan, J.E.; Danos, O. Lentiviral vectors can be used for full-length dystrophin gene therapy. *Sci. Rep.* **2017**, *7*.

408. Pisani, C.; Strimpakos, G.; Gabanella, F.; Di Certo, M.G.; Onori, A.; Severini, C.; Luvisetto, S.; Farioli-Vecchioli, S.; Carrozzo, I.; Esposito, A.; Canu, T.; Mattei, E.; Corbi, N.; Passananti, C. Utrophin up-regulation by artificial transcription factors induces muscle rescue and impacts the neuromuscular junction in mdx mice. *Biochim. Biophys. Acta - Mol. Basis Dis.* **2018**, *1864*, 1172–82.

409. Ito, M.; Ehara, Y.; Li, J.; Inada, K.; Ohno, K. Protein-Anchoring Therapy of Biglycan for Mdx Mouse Model of Duchenne Muscular Dystrophy. *Hum. Gene Ther.* **2017**, *28*, 428–36.

410. Mishra, M.K.; Loro, E.; Sengupta, K.; Wilton, S.D.; Khurana, T.S. Functional improvement of dystrophic muscle by repression of utrophin: Let-7c interaction. *PLoS One* **2017**, *12*, e0182676.

411. Amirouche, A.; Tadesse, H.; Lunde, J.A.; Bélanger, G.; Côté, J.; Jasmin, B.J. Activation of p38 signaling increases utrophin A expression in skeletal muscle via the RNA-binding protein KSRP and inhibition of AU-rich element-mediated mRNA decay: Implications for novel DMD therapeutics. *Hum. Mol. Genet.* **2013**, *22*, 3093–111.

412. Péladeau, C.; Adam, N.J.; Jasmin, B.J. Celecoxib treatment improves muscle function in mdx mice and increases utrophin A expression. *FASEB J.* **2018**, *32*, 5090–103.

413. Ricotti, V.; Spinty, S.; Roper, H.; Hughes, I.; Tejura, B.; Robinson, N.; Layton, G.; Davies, K.; Muntoni, F.; Tinsley, J. Safety, tolerability, and pharmacokinetics of SMT c1100, a 2-arylbenzoxazole utrophin modulator, following single-and multiple-dose administration to pediatric patients with duchenne muscular dystrophy. *PLoS One* **2016**, *11*, e0152840.

414. Guiraud, S.; Squire, S.E.; Edwards, B.; Chen, H.; Burns, D.T.; Shah, N.; Babbs, A.; Davies, S.G.;

Wynne, G.M.; Russell, A.J.; Elsey, D.; Wilson, F.X.; Tinsley, J.M.; Davies, K.E. Second-generation compound for the modulation of utrophin in the therapy of DMD. *Hum. Mol. Genet.* **2015**, *24*, 4212–24.

415. Lee, R.C.; Feinbaum, R.L.; Ambros, V. The C. elegans heterochronic gene lin-4 encodes small RNAs with antisense complementarity to lin-14. *Cell* **1993**, *75*, 843–54.

416. Lagos-Quintana, M.; Rauhut, R.; Lendeckel, W.; Tuschl, T. Identification of novel genes coding for small expressed RNAs. *Science (80-.).* **2001**, *294*, 853–8.

417. Mendell, J.T. MicroRNAs: Critical regulators of development, cellular physiology and malignancy. *Cell Cycle* **2005**, *4*, 1179–84.

418. Treiber, T.; Treiber, N.; Meister, G. Regulation of microRNA biogenesis and its crosstalk with other cellular pathways. *Nat. Rev. Mol. Cell Biol.* **2019**, *20*, 5–20.

419. De Rie, D.; Abugessaisa, I.; Alam, T.; Arner, E.; Arner, P.; Ashoor, H.; Åström, G.; Babina, M.; Bertin, N.; Burroughs, A.M.; Carlisle, A.J.; Daub, C.O.; Detmar, M.; Deviatiiarov, R.; Fort, A.; Gebhard, C.; Goldowitz, D.; Guhl, S.; Ha, T.J.; Harshbarger, J.; Hasegawa, A.; Hashimoto, K.; Herlyn, M.; Heutink, P.; Hitchens, K.J.; Hon, C.C.; Huang, E.; Ishizu, Y.; Kai, C.; Kasukawa, T.; Klinken, P.; Lassmann, T.; Lecellier, C.H.; Lee, W.; Lizio, M.; Makeev, V.; Mathelier, A.; Medvedeva, Y.A.; Mejhert, N.; Mungall, C.J.; Noma, S.; Ohshima, M.; Okada-Hatakeyama, M.; Persson, H.; Rizzu, P.; Roudnicky, F.; Sætrom, P.; Sato, H.; Severin, J.; Shin, J.W.; Swoboda, R.K.; Tarui, H.; Toyoda, H.; Vitting-Seerup, K.; Winteringham, L.; Yamaguchi, Y.; Yasuzawa, K.; Yoneda, M.; Yumoto, N.; Zabierowski, S.; Zhang, P.G.; Wells, C.A.; Summers, K.M.; Kawaji, H.; Sandelin, A.; Rehli, M.; Hayashizaki, Y.; Carninci, P.; Forrest, A.R.R.; De Hoon, M.J.L. An integrated expression atlas of miRNAs and their promoters in human and mouse. *Nat. Biotechnol.* **2017**, *35*, 872–8.

420. Carthew, R.W.; Sontheimer, E.J. Origins and mechanisms of miRNAs and siRNAs. *Cell* **2009**, *136*, 642–55.

421. Lee, Y.; Kim, M.; Han, J.; Yeom, K.H.; Lee, S.; Baek, S.H.; Kim, V.N. MicroRNA genes are transcribed by RNA polymerase II. *EMBO J.* **2004**, *23*, 4051–60.

422. Lee, Y.; Ahn, C.; Han, J.; Choi, H.; Kim, J.; Yim, J.; Lee, J.; Provost, P.; Rådmark, O.; Kim, S.; Kim, V.N. The nuclear RNase III Drosha initiates microRNA processing. *Nature* **2003**, *425*, 415–9.

423. Denli, A.M.; Tops, B.B.J.; Plasterk, R.H.A.; Ketting, R.F.; Hannon, G.J. Processing of primary microRNAs by the Microprocessor complex. *Nature* **2004**, *432*, 231–5.

424. Alarcón, C.R.; Lee, H.; Goodarzi, H.; Halberg, N.; Tavazoie, S.F. N6-methyladenosine marks primary microRNAs for processing. *Nature* **2015**, *519*, 482–5.

425. Han, J.; Lee, Y.; Yeom, K.H.; Kim, Y.K.; Jin, H.; Kim, V.N. The Drosha-DGCR8 complex in primary microRNA processing. *Genes Dev.* **2004**, *18*, 3016–27.

426. Bohnsack, M.T.; Czaplinski, K.; Görlich, D. Exportin 5 is a RanGTP-dependent dsRNA-binding protein that mediates nuclear export of pre-miRNAs. *RNA* **2004**, *10*, 185–91.

427. Kim, Y.; Kim, B.; Kim, V.N. Re-evaluation of the roles of DROSHA , Exportin 5 , and DICER in microRNA biogenesis. *Proc. Natl. Acad. Sci.* **2016**, *113*, E1881-9.

428. Grishok, A.; Pasquinelli, A.E.; Conte, D.; Li, N.; Parrish, S.; Ha, I.; Baillie, D.L.; Fire, A.; Ruvkun, G.; Mello, C.C. Genes and mechanisms related to RNA interference regulate expression of the small temporal RNAs that control C. elegans developmental timing. *Cell* **2001**, *106*, 23–34.

429. Ketting, R.F.; Fischer, S.E.J.; Bernstein, E.; Sijen, T.; Hannon, G.J.; Plasterk, R.H.A. Dicer functions in RNA interference and in synthesis of small RNA involved in developmental timing in C. elegans. *Genes Dev.* **2001**, *15*, 2654–9.

430. Ota, H.; Sakurai, M.; Gupta, R.; Valente, L.; Wulff, B.E.; Ariyoshi, K.; Iizasa, H.; Davuluri, R. V.;

Nishikura, K. ADAR1 forms a complex with dicer to promote MicroRNA processing and RNA-induced gene silencing. *Cell* **2013**, *153*, 575–89.

431. Jakob, L.; Treiber, T.; Treiber, N.; Gust, A.; Kramm, K.; Hansen, K.; Stotz, M.; Wankerl, L.; Herzog, F.; Hannus, S.; Grohmann, D.; Meister, G. Structural and functional insights into the fly microRNA biogenesis factor Loquacious. *RNA* **2016**, *22*, 383–96.

432. Khvorova, A.; Reynolds, A.; Jayasena, S.D. Functional siRNAs and miRNAs exhibit strand bias. *Cell* **2003**, *115*, 209–16.

433. Yoda, M.; Kawamata, T.; Paroo, Z.; Ye, X.; Iwasaki, S.; Liu, Q.; Tomari, Y. ATP-dependent human RISC assembly pathways. *Nat. Struct. Mol. Biol.* **2010**, *17*, 17–23.

434. Liu, J.; Carmell, M.A.; Rivas, F. V.; Marsden, C.G.; Thomson, J.M.; Song, J.J.; Hammond, S.M.; Joshua-Tor, L.; Hannon, G.J. Argonaute2 is the catalytic engine of mammalian RNAi. *Science (80-.).* **2004**, *305*, 1437–41.

435. Ruby, J.G.; Jan, C.H.; Bartel, D.P. Intronic microRNA precursors that bypass Drosha processing. *Nature* **2007**, *448*, 83–6.

436. Cifuentes, D.; Xue, H.; Taylor, D.W.; Patnode, H.; Mishima, Y.; Cheloufi, S.; Ma, E.; Mane, S.; Hannon, G.J.; Lawson, N.D.; Wolfe, S.A.; Giraldez, A.J. A novel miRNA processing pathway independent of dicer requires argonaute2 catalytic activity. *Science (80-.).* **2010**, *328*, 1694–8.

437. Cheloufi, S.; Dos Santos, C.O.; Chong, M.M.W.; Hannon, G.J. A dicer-independent miRNA biogenesis pathway that requires Ago catalysis. *Nature* **2010**, *465*, 584–9.

438. Okamura, K.; Hagen, J.W.; Duan, H.; Tyler, D.M.; Lai, E.C. The mirtron pathway generates microRNA-class regulatory RNAs in drosophila. *Cell* **2007**, *130*, 89–100.

439. Grimson, A.; Farh, K.K.H.; Johnston, W.K.; Garrett-Engele, P.; Lim, L.P.; Bartel, D.P. MicroRNA targeting specificity in mammals: determinants beyond seed pairing. *Mol. Cell* **2007**.

440. Broughton, J.P.; Lovci, M.T.; Huang, J.L.; Yeo, G.W.; Pasquinelli, A.E. Pairing beyond the seed supports MicroRNA targeting specificity. *Mol. Cell* **2016**, *64*, 320–33.

441. Lewis, B.P.; Shih, I.; Jones-Rhoades, M.W.; Bartel, D.P.; Burge, C.B.; Grimson, A.; Farh, K.K.H.; Johnston, W.K.; Garrett-Engele, P.; Lim, L.P.; Bartel, D.P. Prediction of mammalian microRNA targets. *Cell* **2003**, *115*, 787–98.

442. Zeng, Y.; Yi, R.; Cullen, B.R. MicroRNAs and small interfering RNAs can inhibit mRNA expression by similar mechanisms. *Proc. Natl. Acad. Sci.* **2003**, *100*, 9779–84.

443. Djuranovic, S.; Nahvi, A.; Green, R. miRNA-mediated gene silencing by translational repression followed by mRNA deadenylation and decay. *Science (80-.).* **2012**, *336*, 237–40.

444. Bhattacharyya, S.N.; Habermacher, R.; Martine, U.; Closs, E.I.; Filipowicz, W. Relief of microRNA-mediated translational repression in human cells subjected to stress. *Cell* **2006**, *125*, 1111–24.

445. Kedde, M.; Strasser, M.J.; Boldajipour, B.; Vrielink, J.A.F.O.; Slanchev, K.; le Sage, C.; Nagel, R.; Voorhoeve, P.M.; van Duijse, J.; Ørom, U.A.; Lund, A.H.H.; Perrakis, A.; Raz, E.; Agami, R. RNA-binding protein Dnd1 inhibits microRNA access to target mRNA. *Cell* **2007**, *131*, 1273–86.

446. Vasudevan, S. Posttranscriptional upregulation by microRNAs. *Wiley Interdiscip. Rev. RNA* **2012**, *3*, 311–30.

447. Lagos-Quintana, M.; Rauhut, R.; Yalcin, A.; Meyer, J.; Lendeckel, W.; Tuschl, T. Identification of tissue-specific microRNAs from mouse. *Curr. Biol.* **2002**, *12*, 735–9.

448. Sempere, L.F.; Freemantle, S.; Pitha-Rowe, I.; Moss, E.; Dmitrovsky, E.; Ambros, V. Expression profiling of mammalian microRNAs uncovers a subset of brain-expressed microRNAs with possible roles in murine and human neuronal differentiation. *Genome Biol* **2004**, *5*, R13.

449. McCarthy, J.J. MicroRNA-206: The skeletal muscle-specific myomiR. *Biochim. Biophys. Acta - Gene Regul. Mech.* **2008**, *1779*, 682–91.

450. van Rooij, E.; Quiat, D.; Johnson, B.A.; Sutherland, L.B.; Qi, X.; Richardson, J.A.; Kelm, R.J.; Olson, E.N. A family of microRNAs encoded by myosin genes governs myosin expression and muscle performance. *Dev. Cell* **2009**, *17*, 662–73.

451. Kakimoto, Y.; Tanaka, M.; Kamiguchi, H.; Hayashi, H.; Ochiai, E.; Osawa, M. MicroRNA deep sequencing reveals chamber-specific miR-208 family expression patterns in the human heart. *Int. J. Cardiol.* **2016**, *211*, 43–8.

452. Wang, J.; Song, C.; Cao, X.; Li, H.; Cai, H.; Ma, Y.; Huang, Y.; Lan, X.; Lei, C.; Ma, Y.; Bai, Y.; Lin, F.; Chen, H. MiR-208b regulates cell cycle and promotes skeletal muscle cell proliferation by targeting CDKN1A. *J. Cell. Physiol.* **2018**, 1–10.

453. Liu, N.; Williams, A.H.; Kim, Y.; McAnally, J.; Bezprozvannaya, S.; Sutherland, L.B.; Richardson, J.A.; Bassel-Duby, R.; Olson, E.N. An intragenic MEF2-dependent enhancer directs muscle-specific expression of microRNAs 1 and 133. *Proc. Natl. Acad. Sci.* **2007**, *104*, 20844–9.

454. Kim, H.K.; Lee, Y.S.; Sivaprasad, U.; Malhotra, A.; Dutta, A.; Hak, K.K.; Yong, S.L.; Sivaprasad, U.; Malhotra, A.; Dutta, A. Muscle-specific microRNA miR-206 promotes muscle differentiation. *J. Cell Biol.* **2006**, *174*, 677–87.

455. Rao, P.K.; Kumar, R.M.; Farkhondeh, M.; Baskerville, S.; Lodish, H.F. Myogenic factors that regulate expression of muscle-specific microRNAs. *Proc. Natl. Acad. Sci.* **2006**, *103*, 8721–6.

456. Chen, J.F.; Mandel, E.M.; Thomson, J.M.; Wu, Q.; Callis, T.E.; Hammond, S.M.; Conlon, F.L.; Wang, D.Z. The role of microRNA-1 and microRNA-133 in skeletal muscle proliferation and differentiation. *Nat. Genet.* **2006**, *38*, 228–33.

457. Chen, J.F.; Tao, Y.; Li, J.; Deng, Z.; Yan, Z.; Xiao, X.; Wang, D.Z. microRNA-1 and microRNA-206 regulate skeletal muscle satellite cell proliferation and differentiation by repressing Pax7. *J. Cell Biol.* **2010**, *190*, 867–79.

458. Cai, R.; Qimuge, N.; Ma, M.; Wang, Y.; Tang, G.; Zhang, Q.; Sun, Y.; Chen, X.; Yu, T.; Dong, W.; Yang, G.; Pang, W. MicroRNA-664-5p promotes myoblast proliferation and inhibits myoblast differentiation by targeting serum response factor and Wnt1. *J. Biol. Chem.* **2018**, *293*, 19177–90.

459. Boon, R.A.; Iekushi, K.; Lechner, S.; Seeger, T.; Fischer, A.; Heydt, S.; Kaluza, D.; Tréguer, K.; Carmona, G.; Bonauer, A.; Horrevoets, A.J.G.; Didier, N.; Girmatsion, Z.; Biliczki, P.; Ehrlich, J.R.; Katus, H.A.; Müller, O.J.; Potente, M.; Zeiher, A.M.; Hermeking, H.; Dimmeler, S. MicroRNA-34a regulates cardiac ageing and function. *Nature* **2013**, *495*, 107–10.

460. Eulalio, A.; Mano, M.; Ferro, M.D.; Zentilin, L.; Sinagra, G.; Zacchigna, S.; Giacca, M. Functional screening identifies miRNAs inducing cardiac regeneration. *Nature* **2012**, *492*, 376–81.

461. Eisenberg, I.; Eran, A.; Nishino, I.; Moggio, M.; Lamperti, C.; Amato, A.A.; Lidov, H.G.; Kang, P.B.; North, K.N.; Mitrani-Rosenbaum, S.; Flanigan, K.M.; Neely, L.A.; Whitney, D.; Beggs, A.H.; Kohane, I.S.; Kunkel, L.M. Distinctive patterns of microRNA expression in primary muscular disorders. *Proc. Natl. Acad. Sci.* **2007**, *104*.

462. Greco, S.; De Simone, M.; Colussi, C.; Zaccagnini, G.; Fasanaro, P.; Pescatori, M.; Cardani, R.; Perbellini, R.; Isaia, E.; Sale, P.; Meola, G.; Capogrossi, M.C.; Gaetano, C.; Martelli, F. Common micro-RNA signature in skeletal muscle damage and regeneration induced by Duchenne muscular dystrophy and acute ischemia. *FASEB J.* **2009**, *23*, 3335–46.

463. Roberts, T.C.; Blomberg, K.E.M.; McClorey, G.; El Andaloussi, S.; Godfrey, C.; Betts, C.; Coursindel, T.; Gait, M.J.; Smith, C.E.I.E.; Wood, M.J.A. Expression analysis in multiple muscle groups and serum reveals complexity in the MicroRNA transcriptome of the mdx mouse with

implications for therapy. *Mol. Ther. Nucleic Acids* **2012**, *1*, e39.

464. Cacchiarelli, D.; Martone, J.; Girardi, E.; Cesana, M.; Incitti, T.; Morlando, M.; Nicoletti, C.; Santini, T.; Sthandier, O.; Barberi, L.; Auricchio, A.; Musar, A.; Bozzoni, I. MicroRNAs involved in molecular circuitries relevant for the duchenne muscular dystrophy pathogenesis are controlled by the dystrophin/nNOS pathway. *Cell Metab.* **2010**, *12*, 341–51.

465. Wang, L.; Zhou, L.; Jiang, P.; Lu, L.; Chen, X.; Lan, H.; Guttridge, D.C.; Sun, H.; Wang, H. Loss of miR-29 in myoblasts contributes to dystrophic muscle pathogenesis. *Mol. Ther.* **2012**, *20*, 1222–33.

466. Alexander, M.S.; Casar, J.C.; Motohashi, N.; Vieira, N.M.; Eisenberg, I.; Marshall, J.L.; Gasperini, M.J.; Lek, A.; Myers, J.A.; Estrella, E.A.; Kang, P.B.; Shapiro, F.; Rahimov, F.; Kawahara, G.; Widrick, J.J.; Kunkel, L.M. MicroRNA-486-dependent modulation of DOCK3/PTEN/AKT signaling pathways improves muscular dystrophy-associated symptoms. *J. Clin. Invest.* **2014**, *124*, 2651–67.

467. Cacchiarelli, D.; Incitti, T.; Martone, J.; Cesana, M.; Cazzella, V.; Santini, T.; Sthandier, O.; Bozzoni, I. MiR-31 modulates dystrophin expression: New implications for Duchenne muscular dystrophy therapy. *EMBO Rep.* **2011**, *12*, 136–41.

468. Zhou, J.; Gao, J.; Zhang, X.; Liu, Y.; Gu, S.; Zhang, X.; An, X.; Yan, J.; Xin, Y.; Su, P. microRNA-340-5p functions downstream of cardiotrophin-1 to regulate cardiac eccentric hypertrophy and heart failure via target gene dystrophin. *Int. Heart J.* **2015**, *56*, 454–8.

469. Prado, F.P.; Dos Santos, D.O.; Blefari, V.; Silva, C.A.; Machado, J.; Kettelhut, I.D.C.; Ramos, S.G.; Baruffi, M.D.; Salgado, H.C.; Prado, C.M. Early dystrophin loss is coincident with the transition of compensated cardiac hypertrophy to heart failure. *PLoS One* **2017**, *12*, e0189469.

470. Kyrychenko, S.; Kyrychenko, V.; Badr, M.A.; Ikeda, Y.; Sadoshima, J.; Shirokova, N. Pivotal role of miR-448 in the development of ROS-induced cardiomyopathy. *Cardiovasc. Res.* **2015**, *108*, 324–34.

471. Turchinovich, A.; Weiz, L.; Langheinz, A.; Burwinkel, B. Characterization of extracellular circulating microRNA. *Nucleic Acids Res.* **2011**, *39*, 7223–33.

472. Arroyo, J.D.; Chevillet, J.R.; Kroh, E.M.; Ruf, I.K.; Pritchard, C.C.; Gibson, D.F.; Mitchell, P.S.; Bennett, C.F.; Pogosova-Agadjanyan, E.L.; Stirewalt, D.L.; Tait, J.F.; Tewari, M. Argonaute2 complexes carry a population of circulating microRNAs independent of vesicles in human plasma. *Proc. Natl. Acad. Sci.* **2011**, *108*, 5003–8.

473. Vickers, K.C.; Palmisano, B.T.; Shoucri, B.M.; Shamburek, R.D.; Remaley, A.T. MicroRNAs are transported in plasma and delivered to recipient cells by high-density lipoproteins. *Nat. Cell Biol.* **2011**, *13*, 423–33.

474. Turchinovich, A.; Tonevitsky, A.G.; Burwinkel, B. Extracellular miRNA: A collision of two paradigms. *Trends Biochem. Sci.* **2016**, *41*, 883–92.

475. Forterre, A.; Jalabert, A.; Chikh, K.; Pesenti, S.; Euthine, V.; Granjon, A.; Errazuriz, E.; Lefai, E.; Vidal, H.; Rome, S. Myotube-derived exosomal miRNAs downregulate Sirtuin1 in myoblasts during muscle cell differentiation. *Cell Cycle* **2014**, *13*, 78–89.

476. Sverdlov, E.D. Amedeo Avogadro's cry: What is 1μg of exosomes? *BioEssays* **2012**, *34*, 873–5.

477. Coenen-stass, A.M.L.; Wood, M.J.A.; Roberts, T.C. Biomarker potential of extracellular miRNAs in Duchenne muscular dystrophy. *Trends Mol. Med.* **2017**, *23*, 989–1001.

478. Cacchiarelli, D.; Legnini, I.; Martone, J.; Cazzella, V.; D'Amico, A.; Bertini, E.; Bozzoni, I. miRNAs as serum biomarkers for Duchenne muscular dystrophy. *EMBO Mol Med* **2011**, *3*, 258–65.

479. Roberts, T.C.; Godfrey, C.; McClorey, G.; Vader, P.; Briggs, D.; Gardiner, C.; Aoki, Y.; Sargent, I.; Morgan, J.E.; Wood, M.J.A. Extracellular microRNAs are dynamic non-vesicular biomarkers of

muscle turnover. *Nucleic Acids Res.* **2013**, *41*, 9500–13.

480. Coenen-Stass, A.M.L.; Betts, C.A.; Lee, Y.F.; Mäger, I.; Turunen, M.P.; El Andaloussi, S.; Morgan, J.E.; Wood, M.J.A.; Roberts, T.C. Selective release of muscle-specific, extracellular microRNAs during myogenic differentiation. *Hum. Mol. Genet.* **2016**, *25*, 3960–74.

481. Zaharieva, I.T.I.T.; Calissano, M.; Scoto, M.; Preston, M.; Cirak, S.; Feng, L.; Collins, J.; Kole, R.; Guglieri, M.; Straub, V.; Bushby, K.; Ferlini, A.; Morgan, J.E.J.E.; Muntoni, F. Dystromirs as serum biomarkers for monitoring the disease severity in Duchenne muscular dystrophy. *PLoS One* **2013**, *8*, e80263.

482. Lu, Q.L.; Cirak, S.; Partridge, T. What can we learn from clinical trials of exon skipping for DMD? *Mol. Ther. - Nucleic Acids* **2014**, *3*, e152.

483. Beekman, C.; Janson, A.A.; Baghat, A.; van Deutekom, J.C.; Datson, N.A. Use of capillary Western immunoassay (Wes) for quantification of dystrophin levels in skeletal muscle of healthy controls and individuals with Becker and Duchenne muscular dystrophy. *PLoS One* **2018**, *13*, e0195850.

484. Zatz, M.; Rapaport, D.; Vainzof, M.; Passos-Bueno, M.R.; Bortolini, E.R.; Pavanello, R. de C.M.; Peres, C.A. Serum creatine-kinase (CK) and pyruvate-kinase (PK) activities in Duchenne (DMD) as compared with Becker (BMD) muscular dystrophy. *J. Neurol. Sci.* **1991**, *102*, 190–6.

485. Li, X.; Li, Y.; Zhao, L.; Zhang, D.; Yao, X.; Zhang, H.; Wang, Y.C.; Wang, X.Y.; Xia, H.; Yan, J.; Ying, H. Circulating muscle-specific miRNAs in duchenne muscular dystrophy patients. *Mol. Ther. - Nucleic Acids* **2014**, *3*, e177.

486. Becker, S.; Florian, A.; Patrascu, A.; Rösch, S.; Waltenberger, J.; Sechtem, U.; Schwab, M.; Schaeffeler, E.; Yilmaz, A. Identification of cardiomyopathy associated circulating miRNA biomarkers in patients with muscular dystrophy using a complementary cardiovascular magnetic resonance and plasma profiling approach. *J. Cardiovasc. Magn. Reson.* **2016**, *18*, 25.

487. Jeanson-Leh, L.; Lameth, J.; Krimi, S.; Buisset, J.; Amor, F.; Le Guiner, C.; Barthélémy, I.; Servais, L.; Blot, S.; Voit, T.; Israeli, D. Serum profiling identifies novel muscle miRNA and cardiomyopathy-related miRNA biomarkers in golden retriever muscular dystrophy dogs and duchenne muscular dystrophy patients. *Am. J. Pathol.* **2014**, *184*, 2885–98.

488. Catapano, F.; Domingos, J.; Perry, M.; Ricotti, V.; Phillips, L.; Servais, L.; Seferian, A.; Groot, I. De; Krom, Y.D.; Niks, E.H.; Verschuuren, J.J.G.M.; Straub, V.; Voit, T.; Morgan, J.; Muntoni, F. Downregulation of miRNA-29, -23 and -21 in urine of Duchenne muscular dystrophy patients. *Epigenomics* **2018**, *10*, 875–89.

489. Pfaffl, M.W. A new mathematical model for relative quantification in real-time RT-PCR. *Nucleic Acids Res.* **2001**, *29*, e45.

490. Ramakers, C.; Ruijter, J.M.; Lekanne Deprez, R.H.; Moorman, A.F.M. Assumption-free analysis of quantitative real-time polymerase chain reaction (PCR) data. *Neurosci. Lett.* **2003**, *339*, 62–6.

491. Tian, L.J.; Cao, J.H.; Deng, X.Q.; Zhang, C.L.; Qian, T.; Song, X.X.; Huang, B.S. Gene expression profiling of Duchenne muscular dystrophy reveals characteristics along disease progression. *Genet. Mol. Res.* **2014**, *13*, 1402–11.

492. Roberts, T.C.; Johansson, H.J.; McClorey, G.; Godfrey, C.; Blomberg, K.E.M.; Coursindel, T.; Gait, M.J.; Smith, C.I.E.; Lehtiö, J.; EL Andaloussi, S.; Wood, M.J. a. Multi-level omics analysis in a murine model of dystrophin loss and therapeutic restoration. *Hum. Mol. Genet.* **2015**, *24*, 6756–8.

493. Zhao, X.-S.; Gallardo, T.D.; Lin, L.; Schageman, J.J.; Shohet, R. V Transcriptional mapping and genomic analysis of the cardiac atria and ventricles. *Physiol. Genomics* **2002**, *12*, 53–60.

494. Barth, A.S.; Merk, S.; Arnoldi, E.; Zwermann, L.; Kloos, P.; Gebauer, M.; Steinmeyer, K.; Bleich, M.; Kääb, S.; Pfeufer, A.; Überfuhr, P.; Dugas, M.; Steinbeck, G.; Nabauer, M. Functional profiling of human atrial and ventricular gene expression. *Pflugers Arch. Eur. J. Physiol.* **2005**, *450*, 201–8.

495. Ng, S.Y.Y.S.Y.; Wong, C.K.C.K.; Tsang, S.Y.S.Y. Differential gene expressions in atrial and ventricular myocytes: insights into the road of applying embryonic stem cell-derived cardiomyocytes for future therapies. *Am. J. Physiol. Physiol.* **2010**, *299*, C1234–C1249.

496. Shimura, D.; Nakai, G.; Jiao, Q.; Osanai, K.; Kashikura, K.; Endo, K.; Soga, T.; Goda, N.; Minamisawa, S. Metabolomic profiling analysis reveals chamber-dependent metabolite patterns in the mouse heart. *Am. J. Physiol. Heart Circ. Physiol.* **2013**, *305*, H494-505.

497. Park, H.W.; Kim, Y.C.; Yu, B.; Moroishi, T.; Mo, J.S.; Plouffe, S.W.; Meng, Z.; Lin, K.C.; Yu, F.X.; Alexander, C.M.; Wang, C.Y.; Guan, K.L. Alternative Wnt signaling activates YAP/TAZ. *Cell* **2015**, *162*, 780–94.

498. Dawson, K.; Aflaki, M.; Nattel, S. Role of the Wnt-Frizzled system in cardiac pathophysiology: A rapidly developing, poorly understood area with enormous potential. *J. Physiol.* **2013**, *6*, 1409–32.

499. Pescatori, M.; Broccolini, A.; Minetti, C.; Bertini, E.; Bruno, C.; D'amico, A.; Bernardini, C.; Mirabella, M.; Silvestri, G.; Giglio, V.; Modoni, A.; Pedemonte, M.; Tasca, G.; Galluzzi, G.; Mercuri, E.; Tonali, P.A.; Ricci, E. Gene expression profiling in the early phases of DMD: a constant molecular signature characterizes DMD muscle from early postnatal life throughout disease progression. *FASEB J.* **2007**, *21*, 1210–26.

500. Liu, F.; Liang, Z.; Xu, J.; Li, W.; Zhao, D.; Zhao, Y.; Yan, C. Activation of the wnt/β-catenin signaling pathway in polymyositis, dermatomyositis and duchenne muscular dystrophy. *J. Clin. Neurol.* **2016**, *12*, 351–60.

501. von Maltzahn, J.; Renaud, J.-M.; Parise, G.; Rudnicki, M.A. Wnt7a treatment ameliorates muscular dystrophy. *Proc. Natl. Acad. Sci.* **2012**, *109*, 20614–9.

502. Alexander, M.S.; Kawahara, G.; Motohashi, N.; Casar, J.C.; Eisenberg, I.; Myers, J.A.; Gasperini, M.J.; Estrella, E.A.; Kho, A.T.; Mitsuhashi, S.; Shapiro, F.; Kang, P.B.; Kunkel, L.M. MicroRNA-199a is induced in dystrophic muscle and affects WNT signaling, cell proliferation, and myogenic differentiation. *Cell Death Differ.* **2013**, *20*, 1194–208.

503. Shang, Y.C.; Wang, S.H.; Xiong, F.; Peng, F.N.; Liu, Z.S.; Geng, J.; Zhang, C. Activation of Wnt3a signaling promotes myogenic differentiation of mesenchymal stem cells in mdx mice. *Acta Pharmacol. Sin.* **2016**, *37*, 873–81.

504. Oerlemans, M.I.F.J.; Goumans, M.J.; Van Middelaar, B.; Clevers, H.; Doevendans, P.A.; Sluijter, J.P.G. Active Wnt signaling in response to cardiac injury. *Basic Res. Cardiol.* **2010**, *105*, 631–41.

505. Aisagbonhi, O.; Rai, M.; Ryzhov, S.; Atria, N.; Feoktistov, I.; Hatzopoulos, A.K. Experimental myocardial infarction triggers canonical Wnt signaling and endothelial-to-mesenchymal transition. *Dis. Model. Mech.* **2011**, *4*, 469–83.

506. Chen, X.; Shevtsov, S.P.; Hsich, E.; Cui, L.; Haq, S.; Aronovitz, M.; Kerkela, R.; Molkentin, J.D.; Liao, R.; Salomon, R.N.; Patten, R.; Force, T. The beta-catenin/T-Cell factor/lymphocyte enhancer factor signaling pathway is required for normal and stress-induced cardiac hypertrophy. *Mol. Cell. Biol.* **2006**, *26*, 4462–73.

507. Hahn, J.Y.; Cho, H.J.; Bae, J.W.; Yuk, H.S.; Kim, K. Il; Park, K.W.; Koo, B.K.; Chae, I.H.; Shin, C.S.; Oh, B.H.; Choi, Y.S.; Park, Y.B.; Kim, H.S. β-catenin overexpression reduces myocardial infarct size through differential effects on cardiomyocytes and cardiac fibroblasts. *J. Biol. Chem.* **2006**, *281*, 30979–89.

508. Zhang, C.G.; Jia, Z.Q.; Li, B.H.; Zhang, H.; Liu, Y.N.; Chen, P.; Ma, K.T.; Zhou, C.Y. β-Catenin/TCF/LEF1 can directly regulate phenylephrine-induced cell hypertrophy and Anf transcription in cardiomyocytes. *Biochem. Biophys. Res. Commun.* **2009**, *390*, 258–62.

509. Hou, N.; Ye, B.; Li, X.; Margulies, K.B.; Xu, H.; Wang, X.; Li, F. Transcription factor 7-like 2 mediates canonical Wnt/β-catenin signaling and c-Myc upregulation in heart failure. *Circ. Hear. Fail.* **2016**, *9*, 1–9.

510. Morgan, J.E.; Beauchamp, J.R.; Pagel, C.N.; Peckham, M.; Ataliotis, P.; Jat, P.S.; Noble, M.D.; Farmer, K.; Partridge, T.A. Myogenic cell lines derived from transgenic mice carrying a thermolabile T antigen: A model system for the derivation of tissue-specific and mutation-specific cell lines. *Dev. Biol.* **1994**, *162*, 486–98.

511. Gentleman, R.C.; Carey, V.J.; Bates, D.M.; Bolstad, B.; Dettling, M.; Dudoit, S.; Ellis, B.; Gautier, L.; Ge, Y.; Gentry, J.; Hornik, K.; Hothorn, T.; Huber, W.; Iacus, S.; Irizarry, R.; Leisch, F.; Li, C.; Maechler, M.; Rossini, A.J.; Sawitzki, G.; Smith, C.; Smyth, G.; Tierney, L.; Yang, J.Y.H.; Zhang, J. Bioconductor: open software development for computational biology and bioinformatics. *GENOME Biol.* **2004**, *5*, R80.

512. Irizarry, R. Exploration, normalization, and summaries of high density oligonucleotide array probe level data. *Biostatistics* **2003**, *4*, 249–64.

513. Li, C.; Rabinovic, A.; Johnson, W.E.; Li, C.; Rabinovic, A. Adjusting batch effects in microarray expression data using empirical Bayes methods. *Biostatistics* **2007**, *8*, 118–27.

514. Ritchie, M.E.; Phipson, B.; Wu, D.; Hu, Y.; Law, C.W.; Shi, W.; Smyth, G.K. Limma powers differential expression analyses for RNA-sequencing and microarray studies. *Nucleic Acids Res.* **2015**, *43*, e47.

515. Alexa, A.; Rahnenfuhrer, J. topGO Available online: https://bioconductor.org/packages/release/bioc/html/topGO.html.

516. Supek, F.; Bošnjak, M.; Škunca, N.; Šmuc, T. Revigo summarizes and visualizes long lists of gene ontology terms. *PLoS One* **2011**, *6*, e21800.

517. Hopper, I.; Kotecha, D.; Chin, K.L.; Mentz, R.J.; von Lueder, T.G. Comorbidities in heart failure: Are there gender differences? *Curr. Heart Fail. Rep.* **2016**, *13*, 1–12.

518. Bostick, B.; Yue, Y.; Duan, D. Gender influences cardiac function in the mdx model of Duchenne cardiomyopathy. *Muscle and Nerve* **2010**, *42*, 600–3.

519. Quinlan, J.G.; Hahn, H.S.; Wong, B.L.; Lorenz, J.N.; Wenisch, A.S.; Levin, L.S. Evolution of the mdx mouse cardiomyopathy: Physiological and morphological findings. *Neuromuscul. Disord.* **2004**, *14*, 491–6.

520. Mavrogeni, S.I.; Markousis-Mavrogenis, G.; Papavasiliou, A.; Papadopoulos, G.; Kolovou, G. Cardiac involvement in duchenne muscular dystrophy and related dystrophinopathies. *Methods Mol. Biol.* **2018**, *1687*, 31–42.

521. Wang, H.-S.; Hung, S.-C.; Peng, S.-T.; Huang, C.-C.; Wei, H.-M.; Guo, Y.-J.; Fu, Y.-S.; Lai, M.-C.; Chen, C.-C. Mesenchymal stem cells in the Wharton's jelly of the human umbilical cord. *Stem Cells* **2004**, *22*, 1330–7.

522. Layland, J.; Solaro, R.J.; Shah, A.M. Regulation of cardiac contractile function by troponin I phosphorylation. *Cardiovasc. Res.* **2005**, *66*, 12–21.

523. Chiavegato, A.; Bollini, S.; Pozzobon, M.; Callegari, A.; Gasparotto, L.; Taiani, J.; Piccoli, M.; Lenzini, E.; Gerosa, G.; Vendramin, I.; Cozzi, E.; Angelini, A.; Iop, L.; Zanon, G.F.; Atala, A.; De Coppi, P.; Sartore, S. Human amniotic fluid-derived stem cells are rejected after transplantation in the myocardium of normal, ischemic, immuno-suppressed or immuno-deficient rat. *J. Mol. Cell. Cardiol.* **2007**, *42*, 746–59.

524. Stefanska, M.; Costa, G.; Lie-a-Ling, M.; Kouskoff, V.; Lacaud, G. Smooth muscle cells largely develop independently of functional hemogenic endothelium. *Stem Cell Res.* **2014**, *12*, 222–32.

525. Souders, C.A.; Bowers, S.L.K.; Baudino, T.A. Cardiac fibroblast: The renaissance cell. *Circ. Res.* **2009**, *105*, 1164–76.

526. Yovchev, M.I.; Dabeva, M.D.; Oertel, M. Isolation, characterization, and transplantation of adult liver progenitor cells. *Methods Mol. Biol.* **2013**, *976*, 37–51.

527. Iyer, D.; Gambardella, L.; Bernard, W.G.; Serrano, F.; Mascetti, V.L.; Pedersen, R.A.; Sinha, S.; Talasila, A. Robust derivation of epicardium and its differentiated smooth muscle cell progeny from human pluripotent stem cells. *Development* **2016**, *142*, 1528–41.

528. Pallante, B.A.; Giovannone, S.; Fang-Yu, L.; Zhang, J.; Liu, N.; Kang, G.; Dun, W.; Boyden, P.A.; Fishman, G.I. Contactin-2 expression in the cardiac Purkinje fiber network. *Circ. Arrhythmia Electrophysiol.* **2010**, *3*, 186–94.

529. Chong, J.M.; Üren, A.; Rubin, J.S.; Speicher, D.W. Disulfide bond assignments of secreted Frizzled-related protein-1 provide insights about Frizzled homology and netrin modules. *J. Biol. Chem.* **2002**, *277*, 5134–44.

530. Foulquier, S.; Daskalopoulos, E.P.; Lluri, G.; Hermans, K.C.M.; Deb, A.; Blankesteijn, W.M. WNT signaling in cardiac and vascular disease. *Pharmacol. Rev.* **2018**, *70*, 68–141.

531. Bovolenta, P.; Esteve, P.; Ruiz, J.M.; Cisneros, E.; Lopez-Rios, J. Beyond Wnt inhibition: new functions of secreted Frizzled-related proteins in development and disease. *J. Cell Sci.* **2008**, *121*, 737–46.

532. Schmeckpeper, J.; Verma, A.; Yin, L.; Beigi, F.; Zhang, L.; Payne, A.; Zhang, Z.; Pratt, R.E.; Dzau, V.J.; Mirotsou, M. Inhibition of Wnt6 by Sfrp2 regulates adult cardiac progenitor cell differentiation by differential modulation of Wnt pathways. *J. Mol. Cell. Cardiol.* **2015**, *85*, 215–25.

533. Lin, H.; Angeli, M.; Chung, K.J.; Ejimadu, C.; Rosa, A.R.; Lee, T.; Jin Chung, K.; Ejimadu, C.; Rivera Rosa, A.; Lee, T. sFRP2 activates Wnt/β-catenin signaling in cardiac fibroblasts: differential roles in cell growth, energy metabolism, and extracellular matrix remodeling. *Am. J. Physiol. Physiol.* **2016**, *311*, C710-9.

534. Hara, T.; Nakayama, Y.; Nara, N. [Regenerative medicine of skeletal muscle]. *Rinsho Shinkeigaku* **2005**, *45*, 880–2.

535. Hildyard, J.C.W.; Finch, A.M.; Wells, D.J. Identification of qPCR reference genes suitable for normalizing gene expression in the mdx mouse model of Duchenne muscular dystrophy. *PLoS One* **2019**, *14*, 1–28.

536. Malbon, Craig, C. Frizzleds: new members of the superfamily of G-protein-coupled receptors. *Front. Biosci.* **2004**, *9*, 1048–58.

537. Voloshanenko, O.; Gmach, P.; Winter, J.; Kranz, D.; Boutros, M. Mapping of Wnt-Frizzled interactions by multiplex CRISPR targeting of receptor gene families. *FASEB J.* **2017**, *31*, 4832–44.

538. Tissir, F.; Goffinet, A.M. Expression of planar cell polarity genes during development of the mouse CNS. *Eur. J. Neurosci.* **2006**, *23*, 597–607.

539. Zhang, Q.; Shi, X.E.; Song, C.; Sun, S.; Yang, G.; Li, X. BAMBI promotes C2C12 myogenic differentiation by enhancing Wnt/β-catenin signaling. *Int. J. Mol. Sci.* **2015**, *16*, 17734–45.

540. Brantjes, H. All Tcf HMG box transcription factors interact with Groucho-related co-repressors. *Nucleic Acids Res.* **2001**, *29*, 1410–9.

541. Dijksterhuis, J.P.; Petersen, J.; Schulte, G. WNT/Frizzled signalling: Receptor-ligand selectivity

with focus on FZD-G protein signalling and its physiological relevance: IUPHAR Review 3. *Br. J. Pharmacol.* **2014**, *171*, 1195–209.

542. Descamps, S.; Arzouk, H.; Bacou, F.; Bernardi, H.; Fedon, Y.; Gay, S.; Reyne, Y.; Rossano, B.; Levin, J. Inhibition of myoblast differentiation by Sfrp1 and Sfrp2. *Cell Tissue Res.* **2008**, *332*, 299–306.

543. Gang, E.J.; Jeong, J.A.; Hong, S.H.; Hwang, S.H.; Kim, S.W.; Yang, I.H.; Ahn, C.; Han, H.; Kim, H. Skeletal myogenic differentiation of mesenchymal stem cells isolated from human umbilical cord blood. *Stem Cells* **2004**, *22*, 617–24.

544. Ito, H.; Ueda, H.; Iwamoto, I.; Inaguma, Y.; Takizawa, T.; Asano, T.; Kato, K. Nordihydroguaiaretic acid (NDGA) blocks the differentiation of C2C12 myoblast cells. *J. Cell. Physiol.* **2005**, *202*, 874–9.

545. Benjamin, E.J.; Virani, S.S.; Callaway, C.W.; Chamberlain, A.M.; Chang, A.R.; Cheng, S.; Chiuve, S.E.; Cushman, M.; Delling, F.N.; Deo, R.; De Ferranti, S.D.; Ferguson, J.F.; Fornage, M.; Gillespie, C.; Isasi, C.R.; Jiménez, M.C.; Jordan, L.C.; Judd, S.E.; Lackland, D.; Lichtman, J.H.; Lisabeth, L.; Liu, S.; Longenecker, C.T.; Lutsey, P.L.; MacKey, J.S.; Matchar, D.B.; Matsushita, K.; Mussolino, M.E.; Nasir, K.; O'Flaherty, M.; Palaniappan, L.P.; Pandey, A.; Pandey, D.K.; Reeves, M.J.; Ritchey, M.D.; Rodriguez, C.J.; Roth, G.A.; Rosamond, W.D.; Sampson, U.K.A.; Satou, G.M.; Shah, S.H.; Spartano, N.L.; Tirschwell, D.L.; Tsao, C.W.; Voeks, J.H.; Willey, J.Z.; Wilkins, J.T.; Wu, J.H.Y.; Alger, H.M.; Wong, S.S.; Muntner, P. Heart disease and stroke statistics - 2018 update: A report from the American Heart Association. *Circulation* **2018**, *137*, e67-492.

546. Frey, N.; Katus, H.A.; Olson, E.N.; Hill, J.A. Hypertrophy of the heart: A new therapeutic target? *Circulation* **2004**, *109*, 1580–9.

547. Crisp, A.; Yin, H.F.; Goyenvalle, A.; Betts, C.; Moulton, H.M.; Seow, Y.; Babbs, A.; Merritt, T.; Saleh, A.F.; Gait, M.J.; Stuckey, D.J.; Clarke, K.; Davies, K.E.; Wood, M.J.A. Diaphragm rescue alone prevents heart dysfunction in dystrophic mice in vitro. *Hum. Mol. Genet.* **2011**, *20*, 413–21.

548. Barbin, I.C.C.; Pereira, J.A.; Bersan Rovere, M.; de Oliveira Moreira, D.; Marques, M.J.; Santo Neto, H. Diaphragm degeneration and cardiac structure in mdx mouse: Potential clinical implications for Duchenne muscular dystrophy. *J. Anat.* **2016**, *228*, 784–91.

549. Smythe, G.M.; Forwood, J.K. Altered mitogen-activated protein kinase signaling in dystrophic (mdx) muscle. *Muscle and Nerve* **2012**, *46*, 374–83.

550. Caloca, M.J.; Zugaza, J.L.; Vicente-Manzanares, M.; Sánchez-Madrid, F.; Bustelo, X.R. F-actin-dependent translocation of the Rap1 GDP/GTP exchange factor RasGRP2. *J. Biol. Chem.* **2004**, *279*, 20435–46.

551. Rybakova, I.N.; Ervasti, J.M. Dystrophin-glycoprotein complex is monomeric and stabilizes actin filaments in vitro through a lateral association. *J. Biol. Chem.* **1997**, *272*, 28771–8.

552. Champliaud, M.F.; Virtanen, I.; Tiger, C.F.; Korhonen, M.; Burgeson, R.; Gullberg, D. Posttranslational modifications and β/γ chain associations of human laminin α1 and laminin α5 chains: Purification of laminin-3 from placenta. *Exp. Cell Res.* **2000**, *259*, 326–35.

553. Hamill, K.J.; Kligys, K.; Hopkinson, S.B.; Jones, J.C.R. Laminin deposition in the extracellular matrix: a complex picture emerges. *J. Cell Sci.* **2009**, *122*, 4409–17.

554. Mirotsou, M.; Zhang, Z.; Deb, A.; Zhang, L.; Gnecchi, M.; Noiseux, N.; Mu, H.; Pachori, A.; Dzau, V. Secreted frizzled related protein 2 (Sfrp2) is the key Akt-mesenchymal stem cell-released paracrine factor mediating myocardial survival and repair. *Proc. Natl. Acad. Sci.* **2007**, *104*, 1643–8.

555. He, W.; Zhang, L.; Ni, A.; Zhang, Z.; Mirotsou, M.; Mao, L.; Pratt, R.E.; Dzau, V.J. Exogenously

administered secreted frizzled related protein 2 (Sfrp2) reduces fibrosis and improves cardiac function in a rat model of myocardial infarction. *Proc. Natl. Acad. Sci.* **2010**, *107*, 21110–5.

556. Kobayashi, K.; Luo, M.; Zhang, Y.; Wilkes, D.C.; Ge, G.; Grieskamp, T.; Yamada, C.; Liu, T.C.; Huang, G.; Basson, C.T.; Kispert, A.; Greenspan, D.S.D.S.; Sato, T.N. Secreted Frizzled-related protein 2 is a procollagen C proteinase enhancer with a role in fibrosis associated with myocardial infarction. *Nat. Cell Biol.* **2009**, *11*, 46–55.

557. Xin, M.; Olson, E.N.; Bassel-Duby, R. Mending broken hearts: cardiac development as a basis for adult heart regeneration and repair. *Nat. Publ. Gr.* **2013**, *14*, 529–41.

558. Courtwright, A.; Siamakpour-Reihani, S.; Arbiser, J.L.; Banet, N.; Hilliard, E.; Fried, L.; Livasy, C.; Ketelsen, D.; Nepal, D.B.; Perou, C.M.; Patterson, C.; Klauber-DeMore, N. Secreted frizzle-related protein 2 stimulates angiogenesis via a calcineurin/NFAT signaling pathway. *Cancer Res.* **2009**, *69*, 4621–8.

559. Xavier, C.P.; Melikova, M.; Chuman, Y.; Üren, A.; Baljinnyam, B.; Rubin, J.S. Secreted Frizzled-related protein potentiation versus inhibition of Wnt3a/β-catenin signaling. *Cell. Signal.* **2014**, *26*, 94–101.

560. Zeke, A.; Misheva, M.; Reményi, A.; Bogoyevitch, M.A. JNK signaling: Regulation and functions based on complex protein-protein partnerships. *Microbiol. Mol. Biol. Rev.* **2016**, *80*, 793–835.

561. Anthony, K.; Arechavala-Gomeza, V.; Taylor, L.E.; Vulin, A.; Kaminoh, Y.; Torelli, S.; Feng, L.; Janghra, N.; Bonne, G.; Beuvin, M.; Barresi, R.; Henderson, M.; Laval, S.; Lourbakos, A.; Campion, G.; Straub, V.; Voit, T.; Sewry, C.A.; Morgan, J.E.; Flanigan, K.M.; Muntoni, F. Dystrophin quantification: Biological and translational research implications. *Neurology* **2014**, *83*, 2062–9.

562. Gygi, S.P.; Rochon, Y.; Franza, B.R.; Aebersold, R. Correlation between Protein and mRNA Abundance in Yeast. *Mol. Cell. Biol.* **1999**, *19*, 1720–30.

563. Nie, L.; Wu, G.; Zhang, W. Correlation between mRNA and protein abundance in Desulfovibrio vulgaris: A multiple regression to identify sources of variations. *Biochem. Biophys. Res. Commun.* **2006**, *339*, 603–10.

564. De Sousa Abreu, R.; Penalva, L.O.; Marcotte, E.M.; Vogel, C. Global signatures of protein and mRNA expression levels. *Mol. Biosyst.* **2009**, *5*, 1512–26.

565. Gardan-Salmon, D.; Dixon, J.M.; Lonergan, S.M.; Selsby, J.T. Proteomic assessment of the acute phase of dystrophin deficiency in mdx mice. *Eur. J. Appl. Physiol.* **2011**, *111*, 2763–73.

566. Carberry, S.; Zweyer, M.; Swandulla, D.; Ohlendieck, K. Profiling of age-related changes in the tibialis anterior muscle proteome of the mdx mouse model of dystrophinopathy. *J. Biomed. Biotechnol.* **2012**, *2012*, 1–11.

567. Ohlendieck, K. Skeletal muscle proteomics: current approaches, technical challenges and emerging techniques. *Skelet. Muscle* **2011**, *1*, 6.

568. Muller, J.; Vayssiere, N.; Royuela, M.; Leger, M.E.; Muller, A.; Bacou, F.; Pons, F.; Hugon, G.; Mornet, D. Comparative evolution of muscular dystrophy in diaphragm, gastrocnemius and masseter muscles from old male mdx mice. *J. Muscle Res. Cell Motil.* **2001**, *22*, 133–9.

569. Fröhlich, T.; Kemter, E.; Flenkenthaler, F.; Klymiuk, N.; Otte, K.A.; Blutke, A.; Krause, S.; Walter, M.C.; Wanke, R.; Wolf, E.; Arnold, G.J. Progressive muscle proteome changes in a clinically relevant pig model of Duchenne muscular dystrophy. *Sci. Rep.* **2016**, *6*, 33362.

570. Dangain, J.; Vrbova, G. Muscle development in mdx mutant mice. *Muscle Nerve* **1984**, *7*, 700–4.

571. Turk, R.; Sterrenburg, E.; de Meijer, E.J.; van Ommen, G.-J.B.; den Dunnen, J.T.; 't Hoen, P.A.C. Muscle regeneration in dystrophin-deficient mdx mice studied by gene expression profiling.

BMC Genomics **2005**, *6*, 98.

572. Roig, M.; Roma, J.; Fargas, A.; Munell, F. Longitudinal pathologic study of the gastrocnemius muscle group in mdx mice. *Acta Neuropathol.* **2004**, *107*, 27–34.

573. Lefaucheur, J.P.; Pastoret, C.; Sebille, A. Phenotype of dystrophinopathy in old mdx mice. *Anat. Rec.* **1995**, *242*, 70–6.

574. The UMD-TREAT-NMD DMD Locus Specific Databases The UMD TREAT-NMD DMD mutations database Available online: http://umd.be/TREAT_DMD/.

575. Araki, E.; Nakamurab, K.; Nakaob, K.; Kameyac, S.; Kobayashid, O.; Nonakad, I.; Kobayashia, T.; Katsuki, M.; Araki, E.; Nakamura, K.; Nakao, K.; Kameya, S.; Kobayashi, O.; Nonaka, I.; Kobayashi, T. Targeted disruption of exon 52 in the mouse dystrophin gene induced muscle degeneration similar to that observed in Duchenne muscular dystrophy. *Biochem. Biophys. Res. Commun.* **1997**, *238*, 492–7.

576. Echigoya, Y.; Lee, J.; Rodrigues, M.; Nagata, T.; Tanihata, J.; Nozohourmehrabad, A.; Panesar, D.; Miskew, B.; Aoki, Y.; Yokota, T. Mutation types and aging differently affect revertant fiber expansion in dystrophic mdx and mdx52 mice. *PLoS One* **2013**, *8*, e69194.

577. Oliveros, J.C. Venny. An interactive tool for comparing lists with Venn's diagrams Available online: http://bioinfogp.cnb.csic.es/tools/venny/.

578. Mizuno, H.; Nakamura, A.; Aoki, Y.; Ito, N.; Kishi, S.; Yamamoto, K.; Sekiguchi, M.; Takeda, S.; Hashido, K. Identification of muscle-specific MicroRNAs in serum of muscular dystrophy animal models: Promising novel blood-based markers for muscular dystrophy. *PLoS One* **2011**, *6*, 14–9.

579. Goyenvalle, A.; Babbs, A.; Wright, J.; Wilkins, V.; Powell, D.; Garcia, L.; Davies, K.E. Rescue of severely affected dystrophin/utrophin-deficient mice through scAAV-U7snRNA-mediated exon skipping. *Hum. Mol. Genet.* **2012**, *21*, 2559–71.

580. Roberts, T.C.; Coenen-Stass, A.M.L.; Wood, M.J.A. Assessment of RT-qPCR normalization strategies for accurate quantification of extracellular microRNAs in murine Serum. *PLoS One* **2014**, *9*, e89237.

581. Branca, R.M.M.; Orre, L.M.; Johansson, H.J.; Granholm, V.; Huss, M.; Pérez-Bercoff, A.; Forshed, J.; Käll, L.; Lehtiö, J. HiRIEF LC-MS enables deep proteome coverage and unbiased proteogenomics. *Nat. Methods* **2014**, *11*, 59–62.

582. Ervasti, J.M.; Ohlendieck, K.; Kahl, S.D.; Gaver, M.G.; Campbell, K.P. Deficiency of glycoprotein component of the dystrophin complex in dystrophic muscle Deficiency of a glycoprotein component of the dystrophin complex in dystrophic muscle. *Nature* **1990**, *345*, 315–9.

583. Yu, K.; Yau, Y.H.; Sinha, A.; Tan, T.; Kickhoefer, V.A.; Rome, L.H.; Lee, H.; Shochat, S.G.; Lim, S. Modulation of the vault protein-protein interaction for tuning of molecular release. *Sci. Rep.* **2017**, *7*, 14816.

584. Xiang, Z.; Yuan, W.; Luo, N.; Wang, Y.; Tan, K.; Deng, Y.; Zhou, X.; Zhu, C.; Li, Y.; Liu, M.; Wu, X.; Li, Y. A novel human zinc finger protein ZNF540 interacts with MVP and inhibits transcriptional activities of the ERK signal pathway. *Biochem. Biophys. Res. Commun.* **2006**, *347*, 288–96.

585. Das, D.; Wang, Y.H.; Hsieh, C.Y.; Suzuki, Y.J. Major vault protein regulates cell growth/survival signaling through oxidative modifications. *Cell. Signal.* **2016**, *28*, 12–8.

586. Fanin, M.; Danieli, G.A.; Cadaldini, M.; Miorin, M.; Vitiello, L.; Angelini, C. Dystrophin-positive fibers in duchenne dystrophy: Origin and correlation to clinical course. *Muscle Nerve* **1995**, *18*, 1115–20.

587. Hoffman, E.P.; Fischbeck, K.H.; Brown, R.H.; Johnson, M.; Medori, R.; Loike, J.D.; Harris, J.B.; Waterston, R.; Brooke, M.; Specht, L.; Kupsky, W.; Chamberlain, J.; Caskey, T.; Shapiro, F.;

Kunkel, L.M. Characterization of dystrophin in muscle-biopsy specimens from patients with Duchenne's or Becker's muscular dystrophy. *N. Engl. J. Med.* **1988**, *318*, 1363–8.

588. Piñol-Jurado, P.; Gallardo, E.; de Luna, N.; Suárez-Calvet, X.; Sánchez-Riera, C.; Fernández-Simón, E.; Gomis, C.; Illa, I.; Díaz-Manera, J. Platelet-derived growth factor BB influences muscle regeneration in Duchenne muscle dystrophy. *Am. J. Pathol.* **2017**, *187*, 1814–27.

589. Fog, C.K.; Galli, G.G.; Lund, A.H. PRDM proteins: Important players in differentiation and disease. *BioEssays* **2012**, *34*, 50–60.

590. Rayavarapu, S.; Coley, W.; Cakir, E.; Jahnke, V.; Takeda, S.; Aoki, Y.; Grodish-Dressman, H.; Jaiswal, J.K.; Hoffman, E.P.; Brown, K.J.; Hathout, Y.; Nagaraju, K. Identification of disease specific pathways using in vivo SILAC proteomics in dystrophin deficient mdx mouse. *Mol. Cell. proteomics* **2013**, *12*, 1061–73.

591. Jiang, J.; Huang, L.; Yu, W.; Wu, X.; Zhou, P.; Li, X. Overexpression of HTRA1 leads to down-regulation of fibronectin and functional changes in RF/6A cells and HUVECs. *PLoS One* **2012**, *7*, e46115.

592. Traba, J.; Del Arco, A.; Duchen, M.R.; Szabadkai, G.; Satrústegui, J. SCaMC-1 promotes cancer cell survival by desensitizing mitochondrial permeability transition via ATP/ADP-mediated matrix Ca 2 buffering. *Cell Death Differ.* **2012**, *19*, 650–60.

593. Etienne-Manneville, S.; Hall, A. Rho GTPases in Cell Biology. *Nature* **2002**, *420*, 629–35.

594. Mu, X.; Usas, A.; Tang, Y.; Lu, A.; Wang, B.; Weiss, K.; Huard, J. RhoA mediates defective stem cell function and heterotopic ossification in dystrophic muscle of mice. *FASEB J.* **2013**, *27*, 3619–31.

595. Gauthier-Rouvière, C.; Bonet-Kerrache, A. RhoA leads to up-regulation and relocalization of utrophin in muscle fibers. *Biochem. Biophys. Res. Commun.* **2009**, *384*, 322–8.

596. Raith, M.; Valencia, R.G.; Fischer, I.; Orthofer, M.; Penninger, J.M.; Spuler, S.; Rezniczek, G.A.; Wiche, G. Linking cytoarchitecture to metabolism: sarcolemma-associated plectin affects glucose uptake by destabilizing microtubule networks in mdx myofibers. *Skelet. Muscle* **2013**, *3*, 14.

597. Stapleton, D.I.; Lau, X.; Flores, M.; Trieu, J.; Gehrig, S.M.; Chee, A.; Naim, T.; Lynch, G.S.; Koopman, R. Dysfunctional muscle and liver glycogen metabolism in mdx dystrophic mice. *PLoS One* **2014**, *9*, e91514.

598. Rodríguez-Cruz, M.; Sanchez, R.; Escobar, R.E.; Del Rocío Cruz-Guzmán, O.; López-Alarcón, M.; Bernabe García, M.; Coral-Vázquez, R.; Matute, G.; Velázquez Wong, A.C. Evidence of insulin resistance and other metabolic alterations in boys with duchenne or becker muscular dystrophy. *Int. J. Endocrinol.* **2015**, *2015*, 1–8.

599. Sarbassov, D.D. Phosphorylation and regulation of Akt/PKB by the Rictor-mTOR complex. *Science (80-.).* **2005**, *307*, 1098–1101.

600. Showkat, M.; Beigh, M.A.; Andrabi, K.I. mTOR signaling in protein translation regulation: Implications in cancer genesis and therapeutic interventions. *Mol. Biol. Int.* **2014**, *2014*, 1–14.

601. Shu, L.; Houghton, P.J. The mTORC2 complex regulates terminal differentiation of C2C12 myoblasts. *Mol. Cell. Biol.* **2009**, *29*, 4691–4700.

602. Dogra, C.; Changotra, H.; Wergedal, J.E.; Kumar, A. Regulation of phosphatidylinositol 3-kinase (PI3K)/Akt and nuclear factor-kappa B signaling pathways in dystrophin-deficient skeletal muscle in response to mechanical stretch. *J. Cell. Physiol.* **2006**, *208*, 575–85.

603. Gurpur, P.B.; Liu, J.; Burkin, D.J.; Kaufman, S.J. Valproic acid activates the PI3K/Akt/mTOR pathway in muscle and ameliorates pathology in a mouse model of Duchenne muscular dystrophy. *Am. J. Pathol.* **2009**, *174*, 999–1008.

604. Mouisel, E.; Vignaud, A.; Hourdé, C.; Butler-Browne, G.; Ferry, A. Muscle weakness and atrophy are associated with decreased regenerative capacity and changes in mtor signaling in skeletal muscles of venerable (18-24-month-old) dystrophic mdx mice. *Muscle and Nerve* **2010**, *41*, 809–18.

605. Risson, V.; Mazelin, L.; Roceri, M.; Sanchez, H.; Moncollin, V.; Corneloup, C.; Richard-Bulteau, H.; Vignaud, A.; Baas, D.; Defour, A.; Freyssenet, D.; Tanti, J.F.; Le-Marchand-Brustel, Y.; Ferrier, B.; Conjard-Duplany, A.; Romanino, K.; Bauché, S.; Hantaï, D.; Mueller, M.; Kozma, S.C.; Thomas, G.; Rüegg, M.A.; Ferry, A.; Pende, M.; Bigard, X.; Koulmann, N.; Schaeffer, L.; Gangloff, Y.G. Muscle inactivation of mTOR causes metabolic and dystrophin defects leading to severe myopathy. *J. Cell Biol.* **2009**, *187*, 859–74.

606. Kleinert, M.; Parker, B.L.; Fritzen, A.M.; Knudsen, J.R.; Jensen, T.E.; Kjøbsted, R.; Sylow, L.; Ruegg, M.; James, D.E.; Richter, E.A. mTORC2 regulates muscle glucose uptake during exercise in mice. *J. Physiol.* **2017**, *595*, 4845–55.

607. Lamming, D.W.; Ye, L.; Katajisto, P.; Goncalves, M.D.; Saitoh, M.; Stevens, D.M.; Davis, J.G.; Salmon, A.B.; Richardson, A.; Ahima, R.S.; Guertin, D.A.; Sabatini, D.M.; Baur, J.A. Rapamycin-induced insulin resistance is mediated by mTORC2 loss and uncoupled from longevity. *Science (80-.).* **2012**, *335*, 1638–43.

608. Repetto, S.; Bado, M.; Broda, P.; Lucania, G.; Masetti, E.; Sotgia, F.; Carbone, I.; Pavan, A.; Bonilla, E.; Cordone, G.; Lisanti, M.P.; Minetti, C. Increased number of caveolae and caveolin-3 overexpression in Duchenne muscular dystrophy. *Biochem. Biophys. Res. Commun.* **1999**, *261*, 547–50.

609. Sotgia, F.; Lee, J.K.; Das, K.; Bedford, M.; Petrucci, T.C.; Macioce, P.; Sargiacomo, M.; Bricarelli, F.D.; Minetti, C.; Sudol, M.; Lisantia, M.P. Caveolin-3 directly interacts with the C-terminal tail of β-dystroglycan. Identification of a central WW-like domain within caveolin family members. *J. Biol. Chem.* **2000**, *275*, 38048–58.

610. Galbiati, F.; Volonté, D.; Chu, J. Transgenic overexpression of caveolin-3 in skeletal muscle fibers induces a Duchenne-like muscular dystrophy phenotype. *Proc. Natl. Acad. Sci. U. S. A.* **2000**, *97*, 9689–94.

611. Mossink, M.H.; Van Zon, A.; Fränzel-Luiten, E.; Schoester, M.; Kickhoefer, V.A.; Scheffer, G.L.; Scheper, R.J.; Sonneveld, P.; Wiemer, E.A.C. Disruption of the murine major vault protein (MVP/LRP) gene does not induce hypersensitivity to cytostatics. *Cancer Res.* **2002**, *62*, 7298–304.

612. Muntoni, F.; Fletcher, S.; Wilton, S. Response to “Railroading at the FDA.” *Nat. Biotechnol.* **2017**, *35*, 207–9.

613. Neri, M.; Torelli, S.; Brown, S.; Ugo, I.; Sabatelli, P.; Merlini, L.; Spitali, P.; Rimessi, P.; Gualandi, F.; Sewry, C.; Ferlini, A.; Muntoni, F. Dystrophin levels as low as 30% are sufficient to avoid muscular dystrophy in the human. *Neuromuscul. Disord.* **2007**, *17*, 913–8.

614. Yue, Y.; Skimming, J.W.; Liu, M.; Strawn, T.; Duan, D. Full-length dystrophin expression in half of the heart cells ameliorates beta-isoproterenol-induced cardiomyopathy in mdx mice. *Hum. Mol. Genet.* **2004**, *13*, 1669–75.

615. Wasala, N.B.; Yue, Y.; Vance, J.; Duan, D. Uniform low-level dystrophin expression in the heart partially preserved cardiac function in an aged mouse model of Duchenne cardiomyopathy. *J. Mol. Cell. Cardiol.* **2017**, *102*, 45–52.

616. Godfrey, C.; Muses, S.; McClorey, G.; Wells, K.E.; Coursindel, T.; Terry, R.L.; Betts, C.; Hammond, S.; O’Donovan, L.; Hildyard, J.; El Andaloussi, S.; Gait, M.J.; Wood, M.J.; Wells, D.J. How much dystrophin is enough: the physiological consequences of different levels of dystrophin in the mdx mouse. *Hum. Mol. Genet.* **2015**, *24*, 4225–37.

617. Pegoraro, E.; Schimke, R.N.; Garcia, C.; Stern, H.; Cadaldini, M.; Angelini, C.; Barbosa, E.; Carroll, J.; Marks, W.A.; Neville, H.E.; Marks, H.; Appleton, S.; Toriello, H.; Wessel, H.B.; Donnelly, J.; Bernes, S.M.; Taber, J.W.; Weiss, L.; Hoffman, E.P. Genetic and biochemical normalization in female carriers of Duchenne muscular dystrophy: evidence for failure of dystrophin production in dystrophin-competent myonuclei. *Neurology* **1995**, *45*, 677–90.

618. Schmidt-Achert, M.; Fischer, P.; Müller-Felber, W.; Mudra, H.; Pongratz, D. Heterozygotic gene expression in endomyocardial biopsies: a new diagnostic tool confirms the Duchenne carrier status. *Clin. Investig.* **1993**, *71*, 247–53.

619. Azofeifa, J.; Voit, T.; Hübner, C.; Cremer, M. X-chromosome methylation in manifesting and healthy carriers of dystrophinopathies: concordance of activation ratios among first degree female relatives and skewed inactivation as cause of the affected phenotypes. *Hum. Genet.* **1995**, *96*, 167–76.

620. Wells, D.J.; Wells, K.E.; Asante, E.A.; Turner, G.; Sunada, Y.; Campbell, K.P.; Walsh, F.S.; Dickson, G. Expression of human full-length and minidystrophin in transgenic mdx mice: Implications for gene therapy of duchenne muscular dystrophy. *Hum. Mol. Genet.* **1995**, *4*, 1245–50.

621. Hauser, M.A.; Amalfitano, A.; Kumar-Singh, R.; Hauschka, S.D.; Chamberlain, J.S. Improved adenoviral vectors for gene therapy of Duchenne muscular dystrophy. *Neuromuscul. Disord.* **1997**, *7*, 277–83.

622. Kogelman, B.; Putker, K.; Hulsker, M.; Tanganyika-de Winter, C.; van der Weerd, L.; Aartsma-Rus, A.; van Putten, M. Voluntary exercise improves muscle function and does not exacerbate muscle and heart pathology in aged Duchenne muscular dystrophy mice. *J. Mol. Cell. Cardiol.* **2018**, *125*, 29–38.

623. Anaya-Segura, M.A.M.A.; Rangel-Villalobos, H.H.; Martínez-Cortés, G.; Gómez-Díaz, B.; Coral-Vázquez, R.; Zamora-González, E.; García, S.; López-Hernández, L.B. Serum levels of microRNA-206 and novel mini-STR assays for carrier detection in Duchenne muscular dystrophy. *Int. J. Mol. Sci.* **2016**, *17*, E1334.

624. Senner, C.E.; Brockdorff, N. Xist gene regulation at the onset of X inactivation. *Curr. Opin. Genet. Dev.* 2009, *19*, 122–6.

625. Newall, A.E.T.; Duthie, S.; Formstone, E.; Nesterova, T.B.; Alexiou, M.; Johnston, C.; Caparros, M.-L.L.; Brockdorff, N. Primary non-random X inactivation associated with disruption of Xist promoter regulation. *Hum Mol Genet* **2001**, *10*, 581–9.

626. van Putten, M.; Hulsker, M.; Nadarajah, V.D.; van Heiningen, S.H.; van Huizen, E.; van Iterson, M.; Admiraal, P.; Messemaker, T.; den Dunnen, J.T.; 't Hoen, P.A.C.; Aartsma-Rus, A. The effects of low levels of dystrophin on mouse muscle function and pathology. *PLoS One* **2012**, *7*, e31937.

627. Van Erp, C.; Loch, D.; Laws, N.; Trebbin, A.; Hoey, A.J. Timeline of cardiac dystrophy in 3-18-month-old mdx mice. *Muscle and Nerve* **2010**, *42*, 504–13.

628. Vignier, N.; Amor, F.; Fogel, P.; Duvallet, A.; Poupiot, J.; Charrier, S.; Arock, M.; Montus, M.; Nelson, I.; Richard, I.; Carrier, L.; Servais, L.; Voit, T.; Bonne, G.; Israeli, D. Distinctive serum miRNA profile in mouse models of striated muscular pathologies. *PLoS One* **2013**, *8*, e55281.

629. Blondal, T.; Jensby Nielsen, S.; Baker, A.; Andreasen, D.; Mouritzen, P.; Wrang Teilum, M.; Dahlsveen, I.K. Assessing sample and miRNA profile quality in serum and plasma or other biofluids. *Methods* 2013, *59*, 164–9.

630. Kozomara, A.; Griffiths-Jones, S. miRBase: Annotating high confidence microRNAs using deep sequencing data. *Nucleic Acids Res.* **2014**, *42*, D68-73.

631. Coenen-stass, A.M.L.; Sork, H.; Gatto, S.; Godfrey, C.; Bhomra, A.; Krjutškov, K.; Hart, J.R.;

Westholm, J.O.; O'Donovan, L.; Roos, A.; Lochmüller, H.; Puri, P.L.; El Andaloussi, S.; Wood, M.J.A.; Roberts, T.C.; Krjut, K.; Hart, J.R.; Westholm, J.O.; Donovan, L.O.; Roos, A.; Lochmüller, H.; Puri, P.L.; Andaloussi, S.E.L.; Wood, M.J.A.; Roberts, T.C. Comprehensive RNA sequencing analysis in serum and muscle reveals novel small RNA signatures with biomarker potential for Duchenne Muscular Dystrophy. *Mol. Ther. - Nucleic Acids* **2018**, *13*, 1–15.

632. Hourdé, C.; Joanne, P.; Noirez, P.; Agbulut, O.; Butler-Browne, G.; Ferry, A. Protective effect of female gender-related factors on muscle force-generating capacity and fragility in the dystrophic mdx mouse. *Muscle Nerve* **2013**, *48*, 68–75.

633. Salimena, M.C.; Lagrota-Candido, J.; Quírico-Santos, T. Gender dimorphism influences extracellular matrix expression and regeneration of muscular tissue in mdx dystrophic mice. *Histochem. Cell Biol.* **2004**, *122*, 435–44.

634. Monleau, M.; Bonnel, S.; Gostan, T.; Blanchard, D.; Courgnaud, V.; Lecellier, C.-H. Comparison of different extraction techniques to profile microRNAs from human sera and peripheral blood mononuclear cells. *BMC Genomics* **2014**, *15*, 395.

635. Brown, R.A.M.; Epis, M.R.; Horsham, J.L.; Kabir, T.D.; Richardson, K.L.; Leedman, P.J. Total RNA extraction from tissues for microRNA and target gene expression analysis: not all kits are created equal. *BMC Biotechnol.* **2018**, *18*, 16.

636. Watkins, S.C.; Hoffman, E.P.; Slayter, H.S.; Kunkel, L.M.; Hoffman, P.; Slayter, H.S.; Kunkel, L.M. Dystrophin distribution in heterozygote mdx mice. *Muscle Nerve* **1989**, *12*, 861–8.

637. Karpati, G.; Zubrzycka-Gaarn, E.E.; Carpenter, S.; Bulman, D.E.; Ray, P.N.; Worton, R.G. Age-related conversion of dystrophin-negative to -positive fiber segments of skeletal but not cardiac muscle fibers in heterozygote mdx mice. *J. Neuropathol. Exp. Neurol.* **1990**, *49*, 96–105.

638. Bittner, R.E.; Popoff, I.; Shorny, S.; Höger, H.; Wachtler, F. Dystrophin expression in heterazygous mdx/+ mice indicates imprinting of X chromosome inactivation by parent-of-origin-, tissue-, strain- and position-dependent factors. *Anat. Embryol. (Berl).* **1997**, *195*, 175–82.

639. Van Putten, M.; Van der Pijl, E.M.; Hulsker, M.; Verhaart, I.E.C.; Nadarajah, V.D.; van der Weerd, L.; Aartsma-Rus, A. Low dystrophin levels in heart can delay heart failure in mdx mice. *J. Mol. Cell. Cardiol.* **2014**, *69*, 17–23.

640. Van Putten, M.; Hulsker, M.; Young, C.; Nadarajah, V.D.; Heemskerk, H.; Van Der Weerd, L.; 'T Hoen, P.A.C.; Van Ommen, G.J.B.; Aartsma-Rus, A.M. Low dystrophin levels increase survival and improve muscle pathology and function in dystrophin/utrophin double-knockout mice. *FASEB J.* **2013**, *27*, 2484–95.

641. Kuwabara, Y.; Ono, K.; Horie, T.; Nishi, H.; Nagao, K.; Kinoshita, M.; Watanabe, S.; Baba, O.; Kojima, Y.; Shizuta, S.; Imai, M.; Tamura, T.; Kita, T.; Kimura, T. Increased microRNA-1 and microRNA-133a levels in serum of patients with cardiovascular disease indicate myocardial damage. *Circ. Cardiovasc. Genet.* **2011**, *4*, 446–54.

642. Hermes, T. de A.; Kido, L.A.; Macedo, A.B.; Mizobuti, D.S.; Moraes, L.H.R.; Somazz, M.C.; Cagnon, V.H.A.; Minatel, E. Sex influences diaphragm muscle response in exercised mdx mice. *Cell Biol. Int.* **2018**, *42*, 1611–21.

643. Matsakas, A.; Yadav, V.; Lorca, S.; Narkar, V. Muscle ERRγ mitigates Duchenne muscular dystrophy via metabolic and angiogenic reprogramming. *FASEB J.* **2013**, *27*, 4004–16.

644. Nielsen, S.; Hvid, T.; Kelly, M.; Lindegaard, B.; Dethlefsen, C.; Winding, K.; Mathur, N.; Scheele, C.; Pedersen, B.K.; Laye, M.J. Muscle specific miRNAs are induced by testosterone and independently upregulated by age. *Front. Physiol.* **2014**, *4*, 394.

645. Hall, Z.W.; Ralston, E. Nuclear domains in muscle cells. *Cell* **1989**, *59*, 771–2.

646. Pavlath, G.K.; Rich, K.; Webster, S.G.; Blau, H.M. Localization of muscle gene products in nuclear domains. *Nature* **1989**, *337*, 570–3.

647. Phelps, S.F.; Hauser, M.A.; Cole, N.M.; Rafael, J.A.; Hinkle, R.T.; Faulkner, J.A.; Chamberlain, J.S. Expression of full-length and truncated dystrophin mini-genes in transgenic mdx mice. *Hum. Mol. Genet.* **1995**, *4*, 1251–8.

648. Hauschka, S.D.; Ramos, J.N.; Hollinger, K.; Chamberlain, J.S.; Allen, J.M.; Bengtsson, N.E. Development of novel micro-dystrophins with enhanced functionality. *Mol. Ther.* **2019**, *27*, 1–13.

649. Davies, K.E.; Guiraud, S. Micro-dystrophin genes bring hope of an effective therapy for Duchenne muscular dystrophy. *Mol. Ther.* **2019**, *27*, 1–3.

650. Simhadri, V.L.; McGill, J.; McMahon, S.; Wang, J.; Jiang, H.; Sauna, Z.E. Prevalence of pre-existing antibodies to CRISPR-associated nuclease Cas9 in the USA population. *Mol. Ther. Methods Clin. Dev.* **2018**, *10*, 105–12.

651. Leborgne, C.; Latournerie, V.; Boutin, S.; Desgue, D.; Quéré, A.; Pignot, E.; Collaud, F.; Charles, S.; Simon Sola, M.; Masat, E.; Jouen, F.; Boyer, O.; Masurier, C.; Mingozzi, F.; Veron, P. Prevalence and long-term monitoring of humoral immunity against adeno-associated virus in Duchenne Muscular Dystrophy patients. *Cell. Immunol.* **2018**, *8749*, 30114.

652. Maggio, I.; Chen, X.; Gonçalves, M.A.F. V. The emerging role of viral vectors as vehicles for DMD gene editing. *Genome Med.* **2016**, *8*, 59.

653. Morandi, L.; Mora, M.; Confalonieri, V.; Barresi, R.; Di Blasi, C.; Brugnoni, R.; Bernasconi, P.; Mantegazza, R.; Dworzak, F.; Antozzi, C. Dystrophin characterization in BMD patients: correlation of abnormal protein with clinical phenotype. *J. Neurol. Sci.* **1995**, *132*, 146–55.

654. Guiraud, S.; Edwards, B.; Squire, S.E.; Moir, L.; Berg, A.; Babbs, A.; Ramadan, N.; Wood, M.J.; Davies, K.E. Embryonic myosin is a regeneration marker to monitor utrophin-based therapies for DMD. *Hum. Mol. Genet.* **2019**, *28*, 307–19.

655. Maier, T.; Güell, M.; Serrano, L. Correlation of mRNA and protein in complex biological samples. *FEBS Lett.* **2009**, *583*, 3966–73.

656. Hathout, Y.; Marathi, R.L.; Rayavarapu, S.; Zhang, A.; Brown, K.J.; Seol, H.; Gordish-Dressman, H.; Cirak, S.; Bello, L.; Nagaraju, K.; Partridge, T.; Hoffman, E.P.; Takeda, S.; Mah, J.K.; Henricson, E.; McDonald, C. Discovery of serum protein biomarkers in the mdx mouse model and cross-species comparison to Duchenne muscular dystrophy patients. *Hum. Mol. Genet.* **2014**, *23*, 6458–69.

657. Coenen-Stass, A.M.L.L.; Mcclorey, G.; Manzano, R.; Betts, C.A.; Blain, A.; Saleh, A.F.; Gait, M.J.; Lochmüller, H.; Wood, M.J.A.A.; Roberts, T.C. Identification of novel, therapy-responsive protein biomarkers in a mouse model of Duchenne muscular dystrophy by aptamer-based serum proteomics. *Sci. Rep.* **2015**, *5*, 17014.

658. Hathout, Y.; Brody, E.; Clemens, P.R.; Cripe, L.; DeLisle, R.K.; Furlong, P.; Gordish-Dressman, H.; Hache, L.; Henricson, E.; Hoffman, E.P.; Kobayashi, Y.M.; Lorts, A.; Mah, J.K.; McDonald, C.; Mehler, B.; Nelson, S.; Nikrad, M.; Singer, B.; Steele, F.; Sterling, D.; Sweeney, H.L.; Williams, S.; Gold, L. Large-scale serum protein biomarker discovery in Duchenne muscular dystrophy. *Proc. Natl. Acad. Sci.* **2015**, *112*, 7153–8.

659. Hoffman, E.P.; Brown, R.H.; Kunkel, L.M. Dystrophin: the protein product of the Duchene muscular dystrophy locus. 1987. *Cell* **1987**, *51*, 919–28.

8. Appendix

8.1 Differentially expressed *Fzd* receptors, *Sfrp* and *Wnt* ligands in all anatomical areas of the heart at all ages.

Gene	FC	*P*-value	Adjusted *P*-value
RA 10 weeks			
Sfrp5	0.302684	0.024226	0.858613
RA 24 weeks			
Sfrp2	3.772416	1.55E-06	0.016109
Wnt6	1.44129	0.003397	0.938916
Wnt9a	0.701023	0.022117	0.938916
RA 52 weeks			
Sfrp2	1.763498	0.008086	0.725395
Sfrp5	0.129217	0.003154	0.721568
Wnt1	0.705397	0.008921	0.725395
RV 10 weeks			
Fzd2	1.727409	0.045442	0.71132
Fzd3	1.682706	0.047546	0.716834
Fzd9	0.640038	0.011926	0.601651
Sfrp2	3.255054	0.001075	0.422665
Wnt1	0.622624	0.047568	0.716834
Wnt10a	0.575921	0.002857	0.530038
RV 24 weeks			
Sfrp2	2.529215	4.88E-06	0.045549
Wnt8a	0.69536	0.015481	0.5429
RV 52 weeks			
Fzd1	1.478703	0.023719	0.525502
Sfrp2	3.876184	0.003079	0.433078
Wnt2b	1.463689	0.033972	0.551819
Wnt7b	1.443848	0.042974	0.570598
LV 10 weeks			
Sfrp2	2.105365	0.008445	0.721046
Wnt7a	0.676695	0.045289	0.748813
LV 24 weeks			
Sfrp2	2.869325	8.29E-05	0.167298
LV 52 weeks			
Fzd1	1.614977	0.016141	0.797912
Sfrp2	2.655427	0.018096	0.797912
Wnt9a	1.531493	0.032161	0.816541

8.2 Selected miRNAs for initial FirePlex screen

#	miRNA	Sequence	Justification
1	mmu-miR-1-3p	UGGAAUGUAAAGAAGUAUGUAU	MyomiR - Classical
2	mmu-miR-133a-1-3p	UUUGGUCCCCUUCAACCAGCUG	MyomiR - Classical
3	mmu-miR-133b-3p	UUUGGUCCCCUUCAACCAGCUA	MyomiR - Classical
4	mmu-miR-206-3p	UGGAAUGUAAGGAAGUGUGUGG	MyomiR - Classical
1	mmu-miR-193b-3p	AACUGGCCCACAAAGUCCCGCU	MyomiR - Novel
2	mmu-miR-22-3p	AAGCUGCCAGUUGAAGAACUGU	MyomiR - Novel
3	mmu-miR-30a-5p	UGUAAACAUCCUCGACUGGAAG	MyomiR - Novel
4	mmu-miR-378a-3p	ACUGGACUUGGAGUCAGAAGG	MyomiR - Novel
5	mmu-miR-483-3p	UCACUCCUCCCCUCCCGUCUU	MyomiR - Novel
1	mmu-miR-101a-3p	UACAGUACUGUGAUAACUGAA	Cardiac-associated
2	mmu-miR-103-3p	AGCAGCAUUGUACAGGGCUAUGA	Cardiac-associated
3	mmu-miR-106b-5p	UAAAGUGCUGACAGUGCAGAU	Cardiac-associated
4	mmu-miR-122-5p	UGGAGUGUGACAAUGGUGUUUG	Cardiac-associated
5	mmu-miR-124-3p	UAAGGCACGCGGUGAAUGCC	Cardiac-associated
6	mmu-miR-125a-5p	UCCCUGAGACCCUUUAACCUGUGA	Cardiac-associated
7	mmu-miR-125b-5p	UCCCUGAGACCCUAACUUGUGA	Cardiac-associated
8	mmu-miR-126a-3p	UCGUACCGUGAGUAAUAAUGCG	Cardiac-associated
9	mmu-miR-132-3p	UAACAGUCUACAGCCAUGGUCG	Cardiac-associated
10	mmu-miR-140-3p	UACCACAGGGUAGAACCACGG	Cardiac-associated
11	mmu-miR-142a-3p	UGUAGUGUUUCCUACUUUAUGGA	Cardiac-associated
12	mmu-miR-144-5p	GGAUAUCAUCAUAUACUGUAAGU	Cardiac-associated
13	mmu-miR-145a-5p	GUCCAGUUUUCCCAGGAAUCCCU	Cardiac-associated
14	mmu-miR-146a-5p	UGAGAACUGAAUUCCAUGGGUU	Cardiac-associated
15	mmu-miR-150-5p	UCUCCCAACCCUUGUACCAGUG	Cardiac-associated
16	mmu-miR-155-5p	UUAAUGCUAAUUGUGAUAGGGGU	Cardiac-associated
17	mmu-miR-15b-5p	UAGCAGCACAUCAUGGUUUACA	Cardiac-associated
18	mmu-miR-18a-5p	UAAGGUGCAUCUAGUGCAGAUAG	Cardiac-associated
19	mmu-miR-181b-5p	AACAUUCAUUGCUGUCGGUGGGU	Cardiac-associated
20	mmu-miR-192-5p	CUGACCUAUGAAUUGACAGCC	Cardiac-associated
21	mmu-miR-194-5p	UGUAACAGCAACUCCAUGUGGA	Cardiac-associated
22	mmu-miR-195a-5p	UAGCAGCACAGAAAUAUUGGC	Cardiac-associated
23	mmu-miR-199a-3p	ACAGUAGUCUGCACAUUGGUUA	Cardiac-associated
24	mmu-miR-199a-5p	CCCAGUGUUCAGACUACCUGUUC	Cardiac-associated
25	mmu-miR-19a-3p	UGUGCAAAUCUAUGCAAAACUGA	Cardiac-associated
26	mmu-miR-20b-5p	CAAAGUGCUCAUAGUGCAGGUAG	Cardiac-associated
27	mmu-miR-208a-3p	AUAAGACGAGCAAAAAGCUUGU	Cardiac-associated
28	mmu-miR-208b-3p	AUAAGACGAACAAAAGGUUUGU	Cardiac-associated
29	mmu-miR-210-3p	CUGUGCGUGUGACAGCGGCUGA	Cardiac-associated

30	mmu-miR-214-3p	ACAGCAGGCACAGACAGGCAGU	Cardiac-associated
31	mmu-miR-219a-5p	UGAUUGUCCAAACGCAAUUCU	Cardiac-associated
32	mmu-miR-21a-5p	UAGCUUAUCAGACUGAUGUUGA	Cardiac-associated
33	mmu-miR-222-3p	AGCUACAUCUGGCUACUGGGU	Cardiac-associated
34	mmu-miR-223-3p	UGUCAGUUUGUCAAAUACCCCA	Cardiac-associated
35	mmu-miR-25-3p	CAUUGCACUUGUCUCGGUCUGA	Cardiac-associated
36	mmu-miR-26a-5p	UUCAAGUAAUCCAGGAUAGGCU	Cardiac-associated
37	mmu-miR-28a-5p	AAGGAGCUCACAGUCUAUUGAG	Cardiac-associated
38	mmu-miR-29a-3p	UAGCACCAUCUGAAAUCGGUUA	Cardiac-associated
39	mmu-miR-31-5p	AGGCAAGAUGCUGGCAUAGCUG	Cardiac-associated
40	mmu-miR-328-3p	CUGGCCCUCUCUGCCCUUCCGU	Cardiac-associated
41	mmu-miR-337-5p	CGGCGUCAUGCAGGAGUUGAUU	Cardiac-associated
42	mmu-miR-342-3p	UCUCACACAGAAAUCGCACCCGU	Cardiac-associated
43	mmu-miR-34a-5p	UGGCAGUGUCUUAGCUGGUUGU	Cardiac-associated
44	mmu-miR-370-3p	GCCUGCUGGGGUGGAACCUGGU	Cardiac-associated
45	mmu-miR-375-3p	UUUGUUCGUUCGGCUCGCGUGA	Cardiac-associated
46	mmu-miR-423-5p	UGAGGGGCAGAGAGCGAGACUUU	Cardiac-associated
47	mmu-miR-433-3p	AUCAUGAUGGGCUCCUCGGUGU	Cardiac-associated
48	mmu-miR-486a-5p	UCCUGUACUGAGCUGCCCCGAG	Cardiac-associated
49	mmu-miR-499-5p	UUAAGACUUGCAGUGAUGUUU	Cardiac-associated
50	mmu-miR-505-5p	GGGAGCCAGGAAGUAUUGAUGUU	Cardiac-associated
51	mmu-miR-532-5p	CAUGCCUUGAGUGUAGGACCGU	Cardiac-associated
52	mmu-miR-539-5p	GGAGAAAUUAUCCUUGGUGUGU	Cardiac-associated
53	mmu-miR-590-5p	GAGCUUAUUCAUAAAAGUGCAG	Cardiac-associated
54	mmu-mir-93-5p	CAAAGUGCUGUUCGUGCAGGUAG	Cardiac-associated
1	mmu-miR-16-5p	UAGCAGCACGUAAAUAUUGGCG	Quality control
2	mmu-miR-17-5p	CAAAGUGCUUACAGUGCAGGUAG	Quality control
3	mmu-miR-23a-3p	AUCACAUUGCCAGGGAUUUCC	Quality control
4	mmu-miR-451a	AAACCGUUACCAUUACUGAGUU	Quality control
5	mmu-miR-92a-3p	UAUUGCACUUGUCCCGGCCUG	Quality control

8.3 Selected miRNAs for longitudinal FirePlex analysis

#	miRNA	Sequence	Justification
1	mmu-miR-1-3p	UGGAAUGUAAAGAAGUAUGUAU	MyomiR - Classical
2	mmu-miR-133a-1-3p	UUUGGUCCCCUUCAACCAGCUG	MyomiR - Classical
3	mmu-miR-133b-3p	UUUGGUCCCCUUCAACCAGCUA	MyomiR - Classical
4	mmu-miR-206-3p	UGGAAUGUAAGGAAGUGUGUGG	MyomiR - Classical
1	mmu-miR-193b-3p	AACUGGCCCACAAAGUCCCGCU	MyomiR - Novel
2	mmu-miR-22-3p	AAGCUGCCAGUUGAAGAACUGU	MyomiR - Novel
3	mmu-miR-30a-5p	UGUAAACAUCCUCGACUGGAAG	MyomiR - Novel
4	mmu-miR-378a-3p	ACUGGACUUGGAGUCAGAAGG	MyomiR - Novel
5	mmu-miR-483-3p	UCACUCCUCCCCUCCCGUCUU	MyomiR - Novel
1	mmu-miR-208a-3p	AUAAGACGAGCAAAAAGCUUGU	Cardiac-associated
2	mmu-miR-370-3p	GCCUGCUGGGGUGGAACCUGGU	Cardiac-associated
3	mmu-miR-539-5p	GGAGAAAUUAUCCUUGGUGUGU	Cardiac-associated
1	mmu-miR-16-5p	UAGCAGCACGUAAAUAUUGGCG	Quality control
2	mmu-miR-17-5p	CAAAGUGCUUACAGUGCAGGUAG	Quality control
3	mmu-miR-23a-3p	AUCACAUUGCCAGGGAUUUCC	Quality control
4	mmu-miR-451a	AAACCGUUACCAUUACUGAGUU	Quality control
5	mmu-miR-92a-3p	UAUUGCACUUGUCCCGGCCUG	Quality control

8.4 Publications

8.4.1 First author publications

1. **van Westering TLE**, Betts CA, Wood MJ (2015). Current understanding of molecular pathology and treatment of cardiomyopathy in Duchenne muscular dystrophy. *Molecules* **20**(5):8832-8855.

8.4.2 Co-authored publications

2. Betts CA, McClorey G, Healicon R, Hammond SM, Manzano R, Muses S, Ball V, Godfrey C, Meritt TM, **van Westering T**, O'Donovan L, Wells KE, Gait MJ, Wells DJ, Tyler D, Wood MJ (2018). Cmah-dystrophin deficient mdx mice display an accelerated cardiac phenotype that is improved following peptide-PMO exon skipping treatment. *Human Molecular Genetics* doi: 10.1093/hmg/ddy346

3. Walter LM, Koch CE, Betts CA, Ahlskog N, Meijboom KE, **van Westering TLE**, Hazell G, Bhomra A, Claus P, Oster H, Wood MJA, Bowerman M (2018). Light modulation ameliorates expression of circadian genes and disease progression in spinal muscular atrophy mice. *Human Molecular Genetics* **27**(20): 3582-3597

4. Walter LM, Deguise MO, Meijboom KE, Betts CA, Ahlskog N, **van Westering TLE**, Hazell G, McFall E, Kordala A, Hammond SM, Abendroth F, Murray LM, Shorrock HK, Prosdocimo DA, Haldar SM, Jain MK, Gillingwater TH, Claus P, Kothary R, Wood MJA, Bowerman M (2018). Interventions Targeting Glucocorticoid-Krüppel-like Factor 15-Branched-Chain Amino Acid Signaling Improve Disease Phenotypes in Spinal Muscular Atrophy Mice. *EBioMedicine* **31**: 226-242